University of Alberta
Department of Civil Engineering

Structural Engineering Report No. 96

Dynamic Response of Bridge Piers to Ice Forces

by

E. W. Gordon

and

C. J. Montgomery

April, 1981

DYNAMIC RESPONSE OF BRIDGE PIERS TO ICE FORCES

by

E. W. GORDON

and

C. J. MONTGOMERY

DEPARTMENT OF CIVIL ENGINEERING

THE UNIVERSITY OF ALBERTA

EDMONTON, ALBERTA

MAY 1981

ABSTRACT

The dynamic response of bridge piers to time-varying ice loads is investigated. Measured ice load histories, recorded at two bridge piers, are used in the study.

For the purpose of analysis, bridge piers are modelled by single-degree-of-freedom systems. The maximum dynamic response of a range of piers to each of the load histories is evaluated. The results are summarized in the form of mean response spectra and curves of coefficients of variation in the maximum response. The mean spectra show that dynamic effects can be significant and that the response of bridge piers depends on the time-varying characteristics of the load histories.

Dynamic effects of ice-structure interaction are not accounted for in the current Canadian standard. It is shown how the mean response spectra and curves of coefficients of variation developed in this study, can be used in design procedures which account for dynamic effects.

The results of a design example demonstrate that where dynamic effects are significant, the present code procedures may underestimate the effective ice load.

ACKNOWLEDGEMENTS

This report is based on the thesis of E. W. Gordon submitted to the Faculty of Graduate Studies and Research at the University of Alberta in partial fulfilment of the requirements for the degree of Master of Science in Civil Engineering.

The authors extend their appreciation to A. W. Lipsett, Transportation and Surface Water Engineering Division of the Alberta Research Council for comments and assistance during the course of the study.

The digitized ice load records used in the study, Figs. 2.1 and 2.2, and Plates 2.1 and 2.2 were supplied by the Transportation and Surface Water Engineering Division of the Alberta Research Council.

Table of Contents

Chapter Page

1. INTRODUCTION 1
   1.1 Introductory Remarks 1
   1.2 Background Information 2
   1.3 Purpose and Scope 6
2. ICE LOAD HISTORIES 7
   2.1 Introduction 7
   2.2 Test Piers 8
      2.2.1 Hondo 8
      2.2.2 Pembridge 9
   2.3 Types of Ice Load Histories 11
      2.3.1 Introductory Remarks 11
      2.3.2 Bending Failure Load Histories 11
      2.3.3 Crushing Failure Load Histories 13
      2.3.4 Splitting Failure Load Histories 14
      2.3.5 Classification of Load Histories 15
3. DYNAMIC RESPONSE OF BRIDGE PIERS 25
   3.1 Introduction 25
   3.2 Single-Degree-of-Freedom System 26
      3.2.1 Dynamic Properties 26
      3.2.2 Response to Harmonic Loading 28
      3.2.3 Response to a Rectangular Impulse 30
      3.2.4 Response to an Ice Load History 31
   3.3 Hondo Response Spectra 33
      3.3.1 Bending Failure Response Spectra 33

3.3.2 Crushing Failure Response Spectra 36
3.3.3 Splitting Failure Response Spectra 38
3.4 Pembridge Response Spectra 40
4. DESIGN APPLICATION 53
4.1 Introduction 53
4.2 Current Design Practice 53
4.3 Response Spectra and Design 55
4.4 Design Equation 57
4.4.1 Direct Approach 57
4.4.2 Limit States Design Approach 58
4.4.3 Derivation of Load Factor, λ_i 60
4.5 Design Example 64
4.5.1 Introductory Remarks 64
4.5.2 Code Procedure 65
4.5.3 Direct Approach 65
4.5.4 Limit States Design Approach 67
4.5.5 Discussion of Results 69
4.6 General 71
4.6.1 Design of Slender Piles 71
4.6.2 Scope of Results 72
4.6.3 Implications of Dynamic Effects on the Design Process 74
5. SUMMARY AND CONCLUSIONS 82
BIBLIOGRAPHY 84
APPENDIX A 89
APPENDIX B 105

List of Tables

Table		Page
4.1	Hondo Design Results	77
4.2	Pembridge Design Results	77

List of Figures

Figure		Page
2.1	Schematic View of Hondo Pier Showing Test Set-up.	17
2.2	Schematic View of Pembridge Pier Showing Test Set-up.	18
2.3	Bending Failure Load History - Hondo.	19
2.4	Crushing Failure Load Histories - Hondo and Pembridge.	20
2.5	Splitting Failure Load Histories - Hondo and Pembridge.	21
2.6	Hybrid Load History - Bending with Crushing.	22
2.7	Hybrid Load History - Crushing with Bending.	23
3.1	Single-Degree-of-Freedom System.	43
3.2	Build up of Resonant Response.	44
3.3	Maximum Response to Harmonic Loading.	44
3.4	Rectangular Impulse.	45
3.5	Maximum Response to Rectangular Impulse.	45
3.6	Bending Failure Response Spectra - Hondo.	46
3.7	Mean Bending Failure Response Spectra - Hondo.	47
3.8	Variation in Bending Failure Response - Hondo.	47
3.9	Crushing Failure Response Spectra - Hondo.	48
3.10	Mean Crushing Failure Response Spectra - Hondo.	49
3.11	Variation in Crushing Failure Response - Hondo.	49
3.12	Splitting Failure Response Spectra - Hondo.	50
3.13	Mean Splitting Failure Response Spectra - Hondo.	51
3.14	Variation in Splitting Failure Response - Hondo.	51
3.15	Mean Response Spectra - Pembridge.	52
3.16	Variation in Response - Pembridge.	52

Figure Page

4.1 Distribution in Bending Failure Response - Hondo. .78

4.2 Distribution in Crushing Failure Response - Hondo. 79

4.3 Distribution in Splitting Failure Response - Hondo. 80

4.4 Distribution in Response - Pembridge. 81

List of Plates

Plate		Page
2.1	Bending Failure Event	24
2.2	Crushing Failure Event	24

List of Symbols

b	pier width.
c, c_s	damping coefficients.
C_n	coefficient for nose inclination.
E	factor accounting for uncertainty in estimating load effect.
$\bar{E}$	mean value of E.
F_e	effective ice force.
F_{ni}	specified ice force using code procedure.
F'_{ni}	specified ice force using proposed direct approach.
F''_{ni}	specified ice force using proposed limit states design approach.
F_s	specified 'static' component of ice force.
$F(t)$	time-varying ice force.
F_{max}	maximum value of F(t).
$F_n(t)$	ice force of n-th. normal mode.
g	integer
h	ice thickness.
$H_n(\bar{\omega})$	complex frequency response function in n-th. normal mode.
k	spring constant.
m	mass.
$\bar{m}$	mass/unit length.
M_n	generalized mass of n-th. normal mode.

$N(t)$	time-varying reaction.
p	effective ice strength.
$Q(t)$	time-varying shear.
Q_{max}	maximum value of $Q(t)$.
$R(t)$	response ratio.
R_{max}	maximum value of $R(t)$.
$\overline{R}_{max}$	mean value of R_{max}.
S	structural strength.
S_n	nominal value of S.
s	distance.
t	time.
T	natural period.
T_p	event duration.
$T(\overline{\omega})$	transfer function.
U	total load.
U_n	nominal value of U.
V_E	coefficient of variation of E.
V_F	coefficient of variation of F_{max}.
V_R	coefficient of variation of R_{max}.
V_S	coefficient of variation of S.
V_U	coefficient of variation of U.
x	displacement.
Y_n	generalized displacement of n-th. normal mode.
α, α_1	separation functions.
β	safety index.
β_n	frequency ratio in n-th. normal mode.

γ	ratio of mean to nominal force.
λ, λ_i	load factors.
ξ	damping ratio.
ξ_n	damping ratio in n-th. normal mode.
ϕ	resistance factor.
Φ_n	shape function in n-th. normal mode.
ω	natural circular frequency.
ω_n	natural circular frequency in n-th. normal mode.
$\overline{\omega}$	circular frequency of forcing function.

1. INTRODUCTION

1.1 Introductory Remarks

Ice forces are a major consideration in the design of structures in cold regions. Bridge piers are, perhaps, the most common type of structure that must be considered when dealing with the effects of ice loads.

The forces caused by moving ice sheets striking a pier, during spring break-up, are dynamic in nature in that rapid changes in force magnitude occur over short periods of time. In some cases, the structural properties of the pier are such that significant dynamic interaction may occur between the pier and ice sheet. As a result, the maximum response of the pier may differ markedly from that caused by a static application of the maximum ice force. This study investigates the magnification in response that may occur as a result of dynamic effects.

In Canada, the design of bridge piers subjected to dynamic ice loads is carried out in accordance with the CSA Standard CAN3-S6-M78 (CSA, 1978). The specified ice force, which is a function of the geometrical properties of the pier and the physical properties of the ice, does not account for any dynamic effects. In the case of slender and flexible piers only, the code recognizes that dynamic effects may be significant and should be investigated further. However, no procedures are presented to assist the designer in this respect. The need for further research in

this area, with particular emphasis on the development of appropriate design procedures, is therefore apparent.

1.2 Background Information

Design engineers have been concerned with the forces caused by moving ice impinging on structures since the 19th. century. The results of most of the major research into ice forces have been summarized by Michel (1978). Past studies have, by and large, been directed towards determining the magnitude of maximum ice forces.

More recently, engineers have recognized the importance of the time-varying characteristics of ice forces. Peyton (1966) has discussed the form of the force oscillations recorded at a test pile in Cook Inlet, Alaska. The magnitude of the force was found to vary considerably with time and in some cases the variations were almost periodic. As the force history was determined directly from the measured reaction on the pile, it probably contains significant effects caused by the filtering process of the measuring system. Although the observed rate of force fluctuations corresponded closely to the natural frequency of the structure, Peyton concluded that the fluctuations were caused by a characteristic failure frequency of the ice. Records from the same site were presented by Blenkarn (1970) who suggested that the periodicity in the measured forces resulted from the structural response to random ice loads.

The most extensive program to record ice forces on bridge piers has been conducted in Alberta, Canada, over the past 14 years. The results of the program have been reported by Sanden and Neill (1968), and Neill (1970,1972 and 1976). The results showed that the magnitude of the ice force at spring break-up changes rapidly with time. Gerard (1978) extended the analysis of the Alberta records by relating the type of failure of the ice to the form of the ice load histories. The results of this experimental program were also discussed by Watts and Podolny (1978), with particular reference to code recommendations for bridge pier design. Although specific recommendations were not made, both Gerard and Watts and Podolny recognized that the time-varying characteristics of ice forces are an important design consideration.

The effect of dynamic interaction between structure and ice was described by Englebrektson (1977). He investigated the heavy vibrations felt by the staff at a Swedish lighthouse which was subjected to the action of moving ice. In this case, the ice load was derived from the measured response of the structure. Määttänen (1975) studied very severe vibrations of a flexible steel lighthouse in the Gulf of Bothnia and concluded that structural resonance occurred with the ice force oscillations. In 1978, Määttänen developed a mathematical model that relates structural response to ice forces and accounts for the effect of loading rate on ice strength. Määttänen (1979) further

investigated the dependence of ice force on loading rate by conducting laboratory tests on dynamic ice-structure interaction. The effects of the measuring system on the recorded ice force were eliminated by using a transfer function approach.

Matlock *et al.* (1971) assumed that a cantilever pile subjected to ice forces responds primarily in the fundamental mode of vibration. Accordingly, they analyzed the pile as a single-degree-of-freedom system subjected to an ice force modelled by a deterministic 'saw-tooth' type function.

Sundararajan and Reddy (1973) recognized the stochastic nature of ice loads and used frequency domain analysis to study the random response of a single-degree-of-freedom system to an actual ice force hisory. The analysis was extended to a multi-degree-of-freedom system by Reddy and Cheema (1974). Only one record, that reported by Blenkarn, was considered in the analysis. Sundararajan and Reddy (1977) noticed significant differences between the power spectral density curves for three sections of the force record. They recommended that, in the absence of more data, an envelope power spectral density curve be used when applying the method of analysis.

In an attempt to increase the ice force data base, Swamidas *et al.* (1977) have generated artifical ice force records with characteristics similar to Blenkarn's measured record. By investigating the response of an offshore tower

to these artifical records, they have shown that dynamic interaction can cause significant magnifications over static response.

Reddy *et al.* (1975) have used the concept of response spectra to evaluate the response of offshore structures to ice forces. This concept, which is used extensively in the area of earthquake engineering, will be explained in detail in Chapter 3. Blenkarn's force record was again used to develop the response spectra.

As an extension of the testing progam on bridge piers in Alberta, referred to previously, Montgomery *et al.* (1980) have studied the problem of dynamic ice-pier interaction. From field tests, they found that some types of bridge piers respond to ice forces primarily in a single mode of vibration. They evaluated the response of a range of single degree-of-freedom systems to three ice load histories, recorded at a test pier, and presented their results in the form of response spectra. Each of the load histories corresponded to a particular type of ice failure, as distinguished by Gerard (1978). The results showed that dynamic effects can be significant for a wide range of bridge piers.

The above investigations demonstrate that the response of structures to ice forces can be significantly influenced by dynamic effects. Although theoretical methods of analysis are demonstrated, much of the past research has not been directed specifically toward bridge piers or design

applications. In addition, where results have been presented in a form applicable to design, their use is restricted by the small amount or dubious quality of ice force data considered.

1.3 Purpose and Scope

The purpose of this study is to evaluate the maximum response of a range of bridge piers to dynamic ice loads and to present the results in a form which enables dynamic effects to be easily incorporated into the design procedure. Extensive ice force records from two bridge piers in Alberta have been considered. Design curves have been developed which enable dynamic effects to be accounted for in the current code format. An alternative design format, based on the concepts of limit states design, is also presented.

The scope of the study has been restricted to the dynamic nature of ice loads and the response of structures to dynamic ice forces. While the investigation is concerned with bridge piers, the analytical procedure can be applied to any structure which can be modelled by the simple dynamic systems considered herein. Although the results are only directly applicable to piers which experience the same flow conditions as the Alberta test structures, they can be applied as an approximation to estimate the dynamic effects for piers in other locations.

2. ICE LOAD HISTORIES

2.1 Introduction

To investigate the problem of dynamic interaction, both load and structure must be represented by an appropriate model. This chapter is devoted to a description of the ice force records considered in this study.

Over the past 14 years, the Alberta Research Council has been carrying out full scale ice force measurements, during spring break-up, at two test piers in the province. One of the test piers, located at Hondo on the Athabasca River, is a massive structure with an inclined nose. The other pier, at Pembridge on the Pembina River, is slender and vertical. In this chapter, the test set-up at both piers is described and it is shown how the raw data, originally recorded on magnetic tape at the piers, has been reduced to the form of digitized ice force time histories.

The way in which ice fails on impact with a pier influences the time-varying characteristics of the ice force history. Several failure types have been distinguished and these are discussed in detail in this chapter.

In subsequent chapters, it is shown how a bridge pier may be modelled by a single-degree-of-freedom system. The ice load histories, developed and grouped in this chapter, are applied to the structural model and the resulting dynamic interaction is evaluated and analyzed.

2.2 Test Piers

2.2.1 Hondo

A detailed description of the load measurement installations at both the Hondo and Pembridge locations is given by Lipsett and Gerard (1980). The test set-up at the massive, concrete Hondo pier is shown in Fig. 2.1. The nose of the pier, semicircular in plan, is inclined at 23° to the vertical. It has been fitted with a moveable section, pinned at the base and supported by a load cell at the top. As the moving ice sheets strike this moveable section, the load cell measures the upper reaction, which is recorded on magnetic tape. The displacements of the pier are assumed to be small relative to the displacements of the ice and hence any movement of the pier does not affect the measured reactions.

In general, for a load measuring system, the time-varying ice force may be related to the measured reaction by a transfer function. This function, depending on the dynamic characteristics of the load and the load measuring system, may be derived from simple statics or alternatively, may be required to account for dynamic effects. In the latter case, the dynamic interaction between load and system causes the measured reaction to be different from the corresponding static reaction. In the case of the Hondo pier, calculations indicate that dynamic effects are not significant because of the relatively high natural frequency of the measuring system. The estimated

natural frequency is 57 Hz while the significant frequency components in the ice force are less than 25 Hz. Accordingly, the transfer function relating the measured reaction to the applied load has been derived from static relationships alone.

Data from the Hondo tapes have been processed, in digitized form, to produce the records of the ice load histories considered herein. Significant ice runs occurred during the springs of 1976, 1977 and 1979. The data from 1977 has been digitized at 125 Hz and filtered above 50 Hz to eliminate the possibility of aliasing. The data from 1976 and 1979 have been digitized at 250 Hz enabling frequency components up to 125 Hz to be uniquely defined. Above 125 Hz the frequency components are not significant and therefore aliasing is not a problem.

2.2.2 Pembridge

The test set-up used to measure the ice forces at Pembridge is shown in Fig. 2.2. In this case, the floes strike a specially constructed vertical steel pile, the top of which is enclosed in a steel collar. The pile is filled with concrete. A load cell at the top measures the resulting reaction parallel to the flow direction and the reaction is recorded on magnetic tape. Similar to the Hondo case, it is assumed that the displacements of the pier are relatively small and that, in effect, the pier provides a rigid support to the load measuring system.

The results of vibration tests show that the fundamental frequency of the pile is between 12 and 14 Hz and that the damping ratio is 0.04 (Lipsett, 1980). Calculations based on the procedures presented by Michel (1978) show that, for the flow conditions experienced at Pembridge, the ice loads may have significant frequency components in the range of 5 to 30 Hz. The effect of the test pile is to magnify the frequency components which are close to the fundamental frequency of vibration of the pile. Hence, in this case, the transfer function between load and reaction cannot be derived from statics alone, as the dynamic characteristics of the pile significantly influence the measured reactions.

As discussed in detail in Appendix A, if the ice force and the measured reaction are expressed in terms of harmonic components, the transfer function between reaction and force, for each component, can be conveniently developed. To develop the function, the test pile has been modelled by a simply supported beam with distributed mass and elasticity. The steps in calculating the ice force from the measured reaction were as follows:

(1) Express the time history of the reaction response in terms of harmonic components, using a Fourier transform.

(2) Evaluate the amplitudes of the harmonic components of the ice force from the components of the reaction using the transfer function.

(3) Evaluate the time history of the ice force from the

harmonic components using the inverse Fourier transform.

In order to define the complete range of significant frequency components in the ice force and to eliminate the problem of aliasing, the Pembridge data were digitized at 250 Hz. The digitized data were then processed according to the above procedures. Significant ice runs occurred only in the spring of 1974 and these load histories have been used in this report.

2.3 Types of Ice Load Histories

2.3.1 Introductory Remarks

At Hondo, ice sheets may fail by simply crushing against the pier and eventually splitting, or alternatively, by riding up the pier nose and failing in flexure. Since the Pembridge test pile is vertical, the ice sheets fail mainly by crushing and splitting. Accordingly, the ice force time histories considered in this study were grouped under three main headings, depending on the primary mode of failure: crushing, bending or splitting. Examples of ice force time histories from each group are described below. The entire set of load records is presented in Appendix B.

2.3.2 Bending Failure Load Histories

At Hondo, bending failures result because the inclined nose of the pier provides a vertical reaction component to the impinging ice sheet. This reaction component causes the sheet to rise up the pier nose and fail as flexural cracks

form. Plate 2.1 shows a typical bending failure event. Larger ice sheets are more prone to fail by bending as they have the necessary momentum to rise up the pier nose. Also, bending failure occurs in preference to crushing if the strength of the ice sheet is such that the ultimate bending moment is reached before the contact force induces crushing across the entire contact area.

Figure 2.3 shows the repetitive series of large amplitude force fluctuations that characterize a typical bending ice force history. Each force fluctuation is caused by the 'rise up and bend' action of the ice sheet as it is forced against the pier. The initial increase in load corresponds to the floe moving up the nose. The force then drops off as the sheet breaks around the pier. The process is repeated until all of the floe has been forced past the pier, or alternatively, until bending ceases to be the failure mode. The load history of Fig. 2.3 also shows higher frequency, small amplitude force variations superimposed on those caused by bending. As discussed in the following section, these are characteristic of local crushing of the ice which occurs as the sheet goes through the bending process.

The frequency of the bending force fluctuations depends on a number of factors. The 'rise up and bend' action of fast flowing ice occurs at a greater rate than for slow flowing ice. Also, the rate is dependent on the ice strength and thickness. For the years under consideration

at Hondo, the frequencies associated with bending failure were found to be between 0.2 and 2 Hz.

2.3.3 Crushing Failure Load Histories

Plate 2.2 shows an ice sheet undergoing crushing failure at the Hondo pier. As the ice floe strikes the pier, local crushing of the ice occurs across the entire contact area. This crushing process is restricted to a zone around the pier from which the crushed ice is continually cleared by the movement of the ice. As the pier continues to cut through the moving sheet, the stresses induce cracks which propagate from the pier into the moving ice. If the size of the floe is small, these cracks completely split the sheet into smaller parts. This type of failure also occurs at Pembridge.

Figures 2.4 (a) and (b) show typical crushing failure load histories from Hondo and Pembridge, respectively. The initial impact of the ice sheet on the pier causes a sudden increase in load. The force then remains at an almost constant average level, with high frequency small amplitude oscillations occurring throughout the crushing process. The rate at which these force oscillations occur depends on a number of factors. As suggested by Michel (1978) and Montgomery *et al.* (1980), the ice velocity and thickness should be of particular significance, higher frequencies being associated with faster, less thick floes. For the years under consideration at Hondo, the floe velocities and

thicknesses were of the order of 1m/s and 1m, respectively, and the crushing frequencies were in the 15 to 20 Hz range. At Pembridge, however, the respective values were 2m/s and 0.6m and the corresponding crushing fequencies were in the region of 35 Hz.

The duration of the loading event depends on the size of the ice sheet. Crushing may continue until the complete floe has been forced past the pier. Alternatively, if the stress cracks which occur simultaneously with crushing completely split the sheet, the force drops off as the now smaller floes move past the pier.

2.3.4 Splitting Failure Load Histories

In splitting failure, the initial impact between sheet and pier is followed by local crushing and the formation of stress cracks. When the size of the floe is comparatively small, these cracks completely split the sheet in a relatively short time and the event is then complete. Although the successive occurrence of impact, crushing and cracking is also associated with crushing events, splitting events differ in that the duration of the event is much shorter. Splitting events have been observed at both test locations.

A splitting failure load history from the Hondo data is shown in Fig. 2.5(a). The initial sudden rise or 'step' in force corresponding to the impact between sheet and pier, is characteristic of both splitting and crushing events. It

differs from the slightly more gradual rise in force caused by a bending failure. The rise in force is followed, for a short time by high frequency force fluctuation owing to local crushing of the ice. Finally, the sheet splits and the load suddenly drops.

Load histories of similar duration as splitting events, but which differ in detail, are also grouped under this heading. Since the load in each case is a short impulse, the dynamic response of a pier to each type is essentially the same. For example, a small floe may strike the pier and move past the side, with very little crushing involved. In this case, an impact event results and the rise and fall in force is almost instantaneous. An example of such a load history, recorded at Hondo, is shown in Fig. 2.5(b). Alternatively, if the sheet is not completely split by the formation of cracks, crushing continues until the floe has been forced past the pier. The decrease in force is not as sudden as for a true splitting event, but more gradual, as shown in the Pembridge example of Fig. 2.5 (c).

2.3.5 Classification of Load Histories

Although the Hondo data has been grouped into crushing, bending and splitting load histories, in practice, any particular loading event may not be composed entirely of a single ice failure type, but rather of a combination of types. In cases where more than one type of failure occurred, the force history was grouped by considering not

only the failure type but also the predominant frequency components contained in the record.

The load history shown in Fig. 2.6, for example, consists of force variations caused by bending in addition to crushing events of short duration. Hence, it has the characteristic low and high frequency components of a bending failure load history and was categorized accordingly. The load history in Fig. 2.7 shows a crushing failure event. However, low frequency force fluctuations about the almost constant force level are also apparent. These may be caused by partial bending of the ice sheet as it crushes against the pier. In this case, crushing characteristics as regards both failure type and component frequencies were considered to be predominant and the load history was classified as such.

Because only one year of good data was available for the Pembridge site, definite distinctions could not be made between the load histories on the basis of failure types. Records corresponding to crushing and splitting events seemed to predominate. However, load histories composed of a series of splitting events in close succession have also been recorded and these would warrant a distinct category. Because of insufficient data, the Pembridge force histories have been considered in a single group.

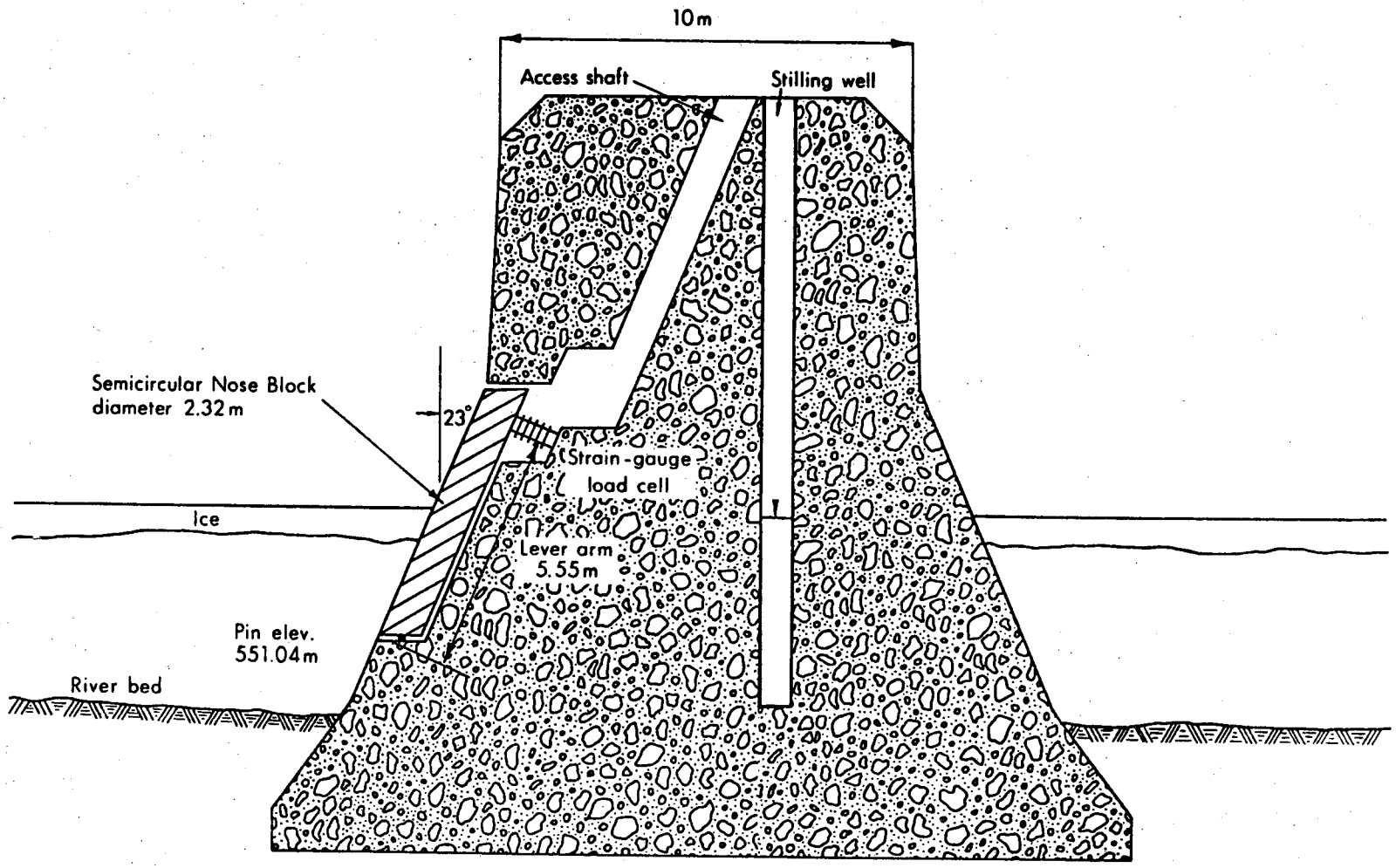

FIGURE 2.1 SCHEMATIC VIEW OF HONDO PIER SHOWING TEST SET-UP.

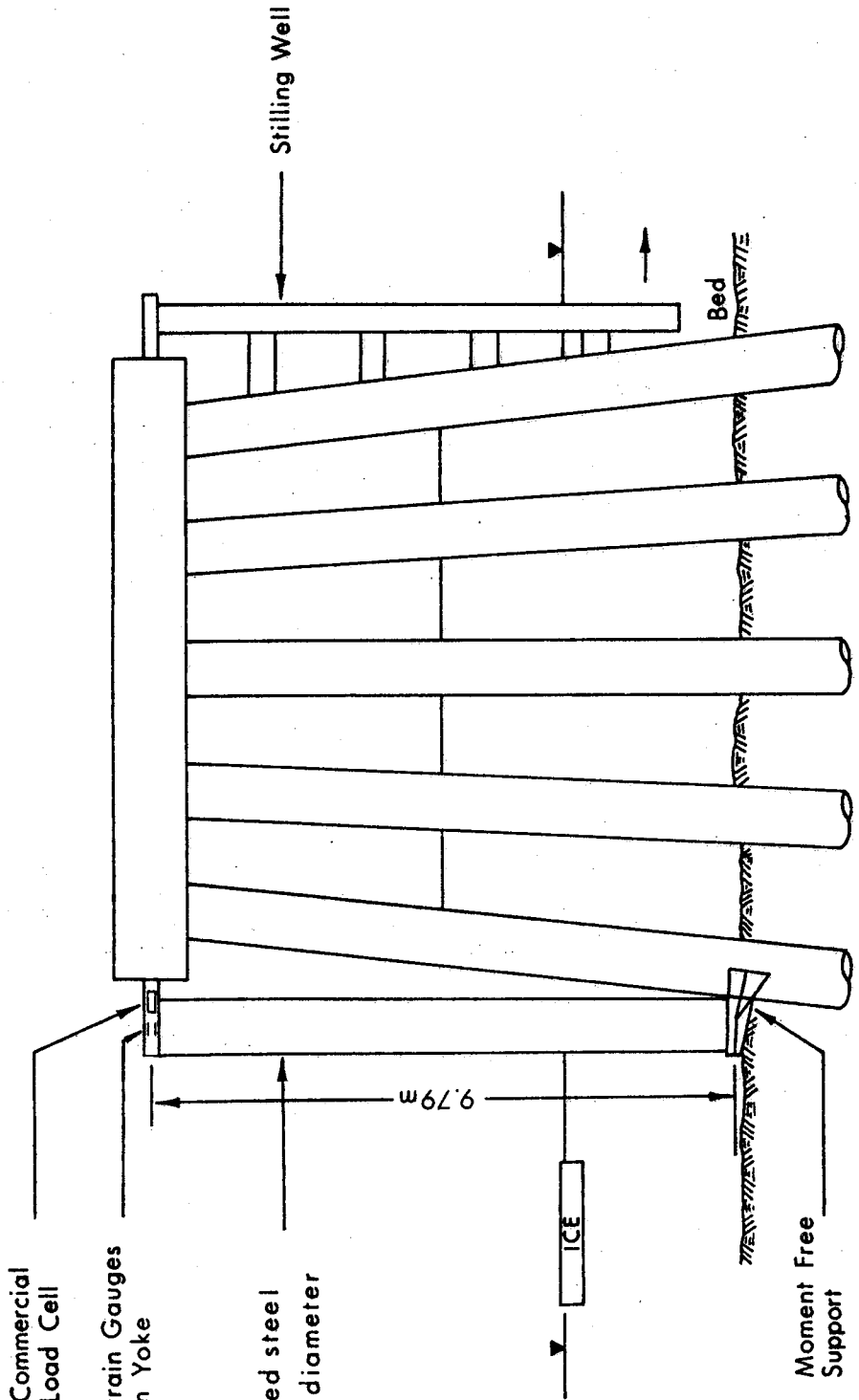

FIGURE 2.2 SCHEMATIC VIEW OF PEMBRIDGE PILE SHOWING TEST SET-UP.

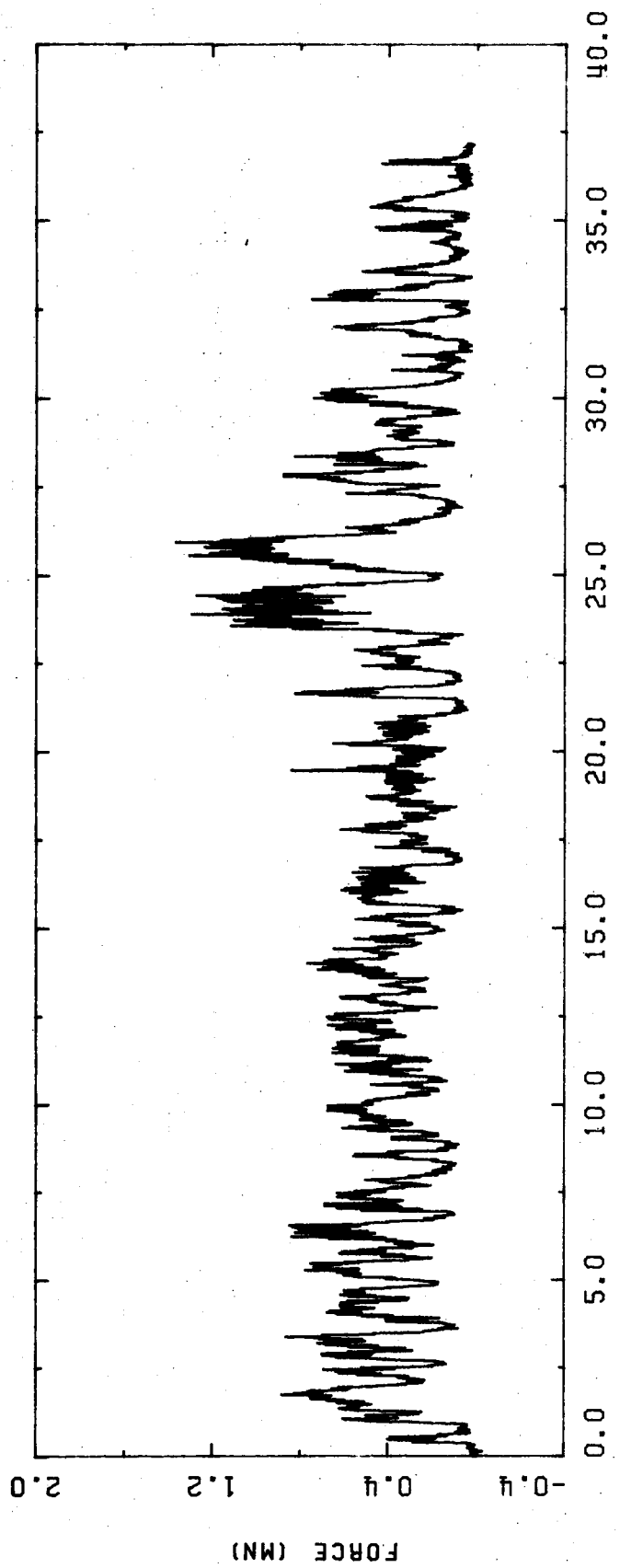

FIGURE 2.3 BENDING FAILURE LOAD HISTORY - HONDO.

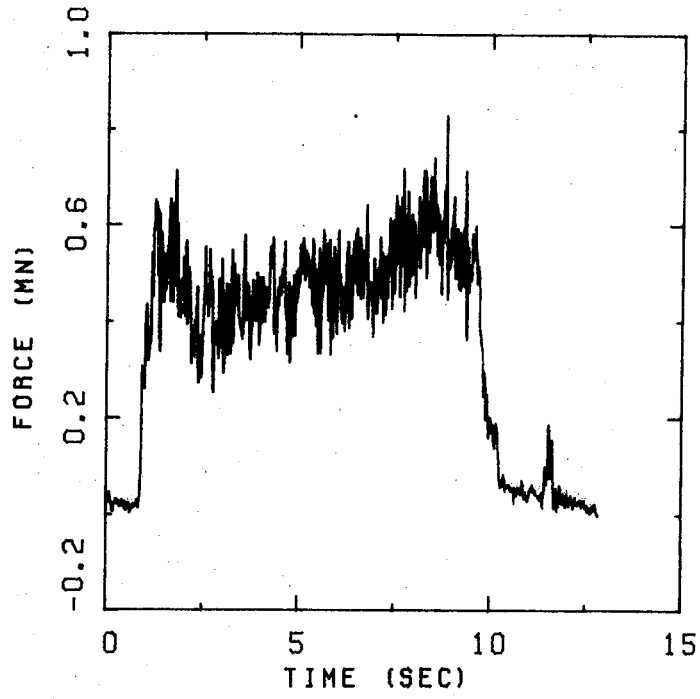

(a)

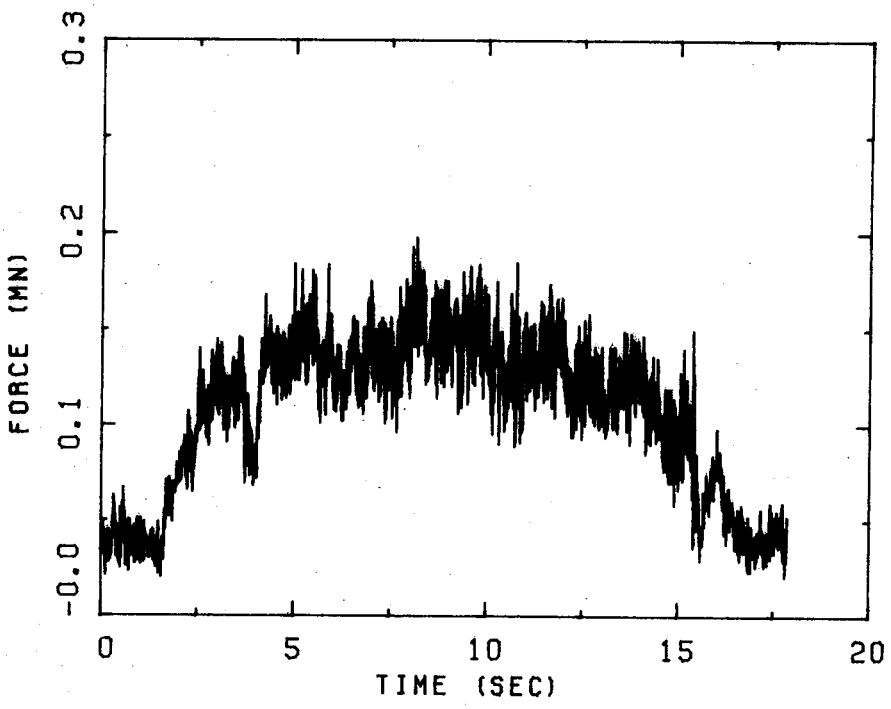

(b)

FIGURE 2.4 CRUSHING FAILURE LOAD HISTORIES.

(a) HONDO, (b) PEMRIDGE

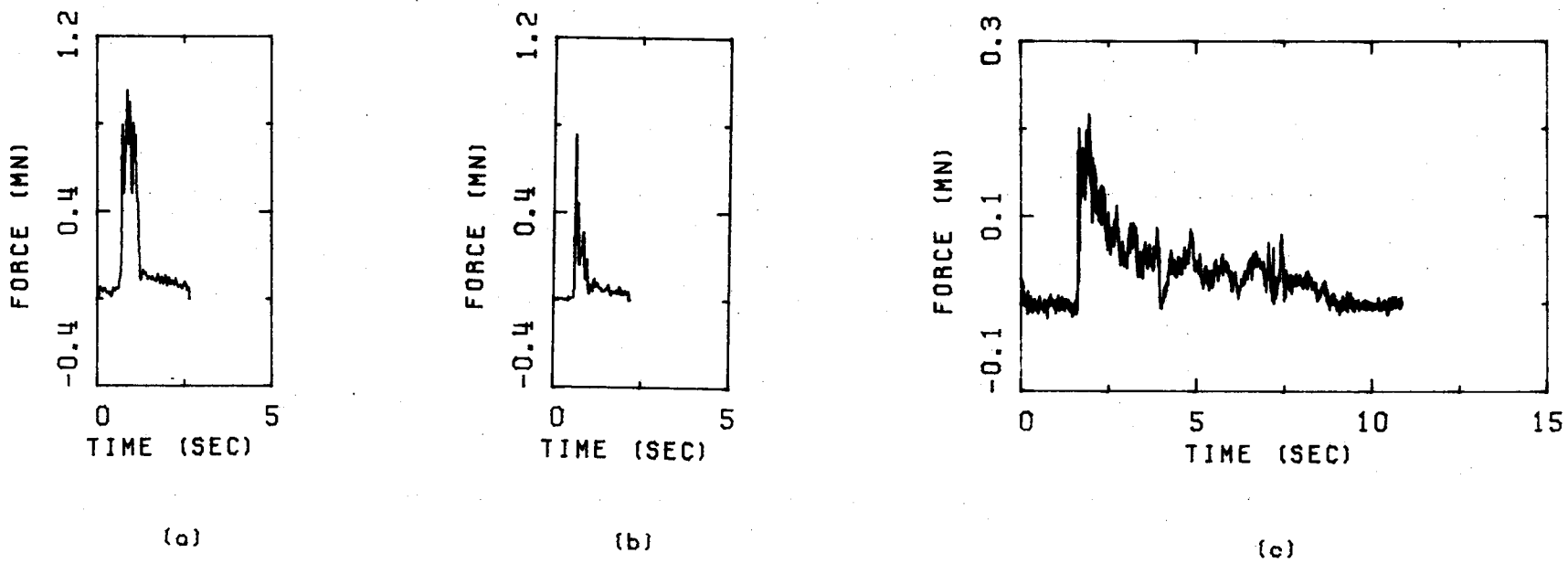

FIGURE 2.5 SPLITTING FAILURE LOAD HISTORIES. (a), (b) HONDO. (c) PEMBRIDGE.

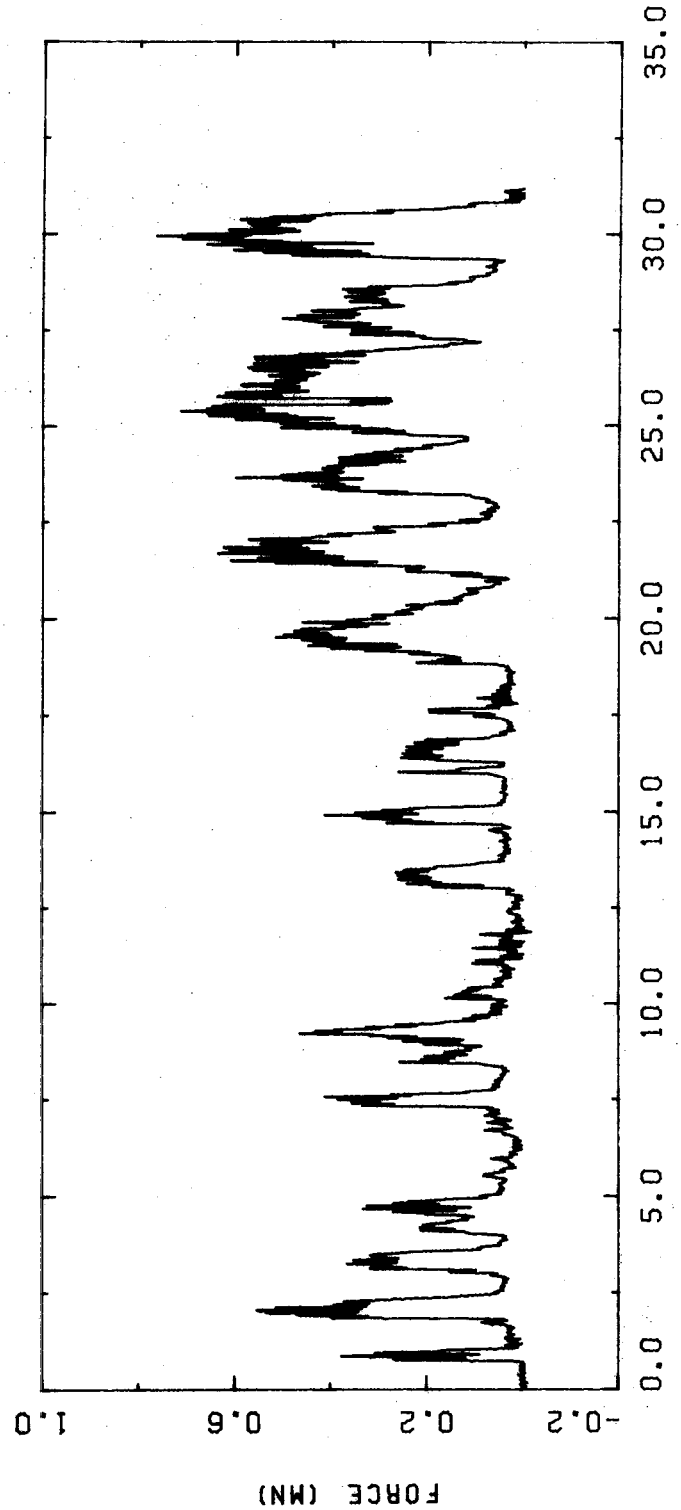

FIGURE 2.6 HYBRID LOAD HISTORY - BENDING WITH CRUSHING.

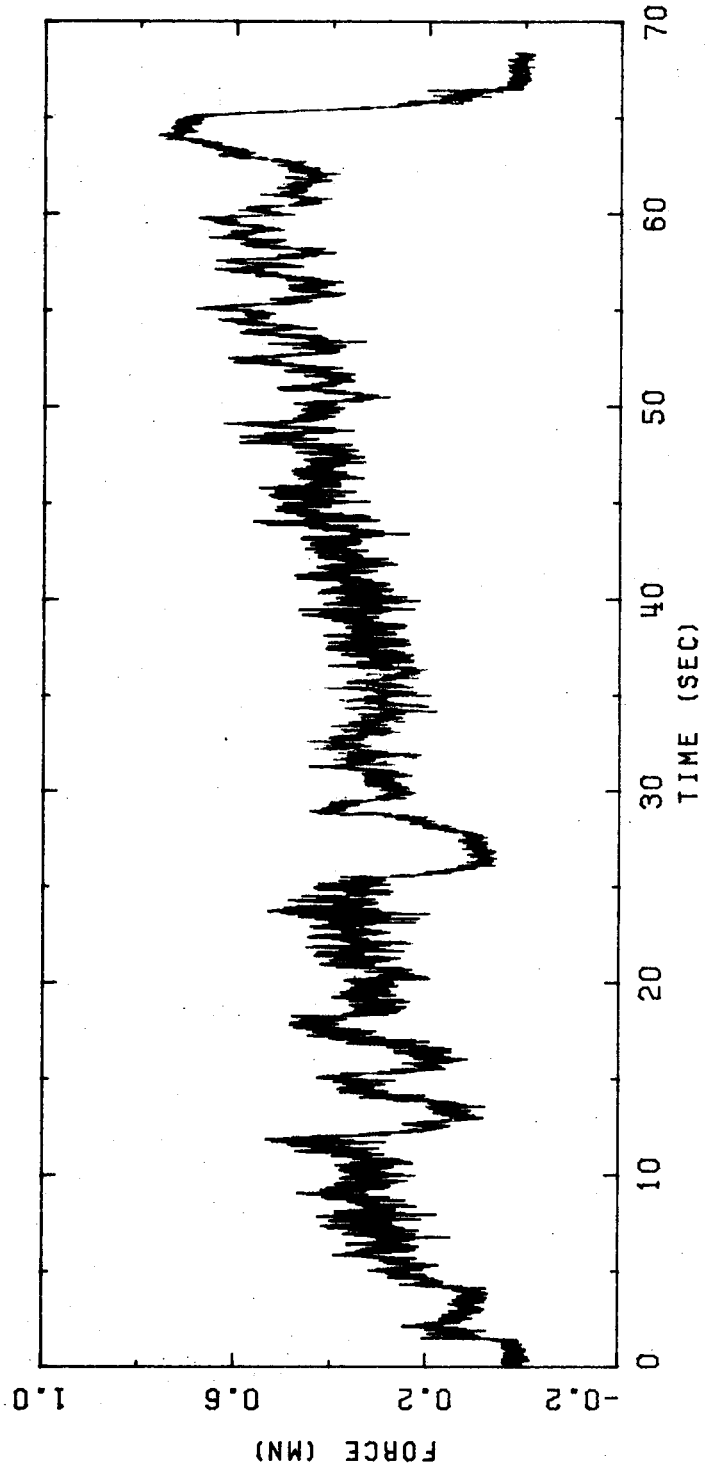

FIGURE 2.7 HYBRID LOAD HISTORY - CRUSHING WITH BENDING.

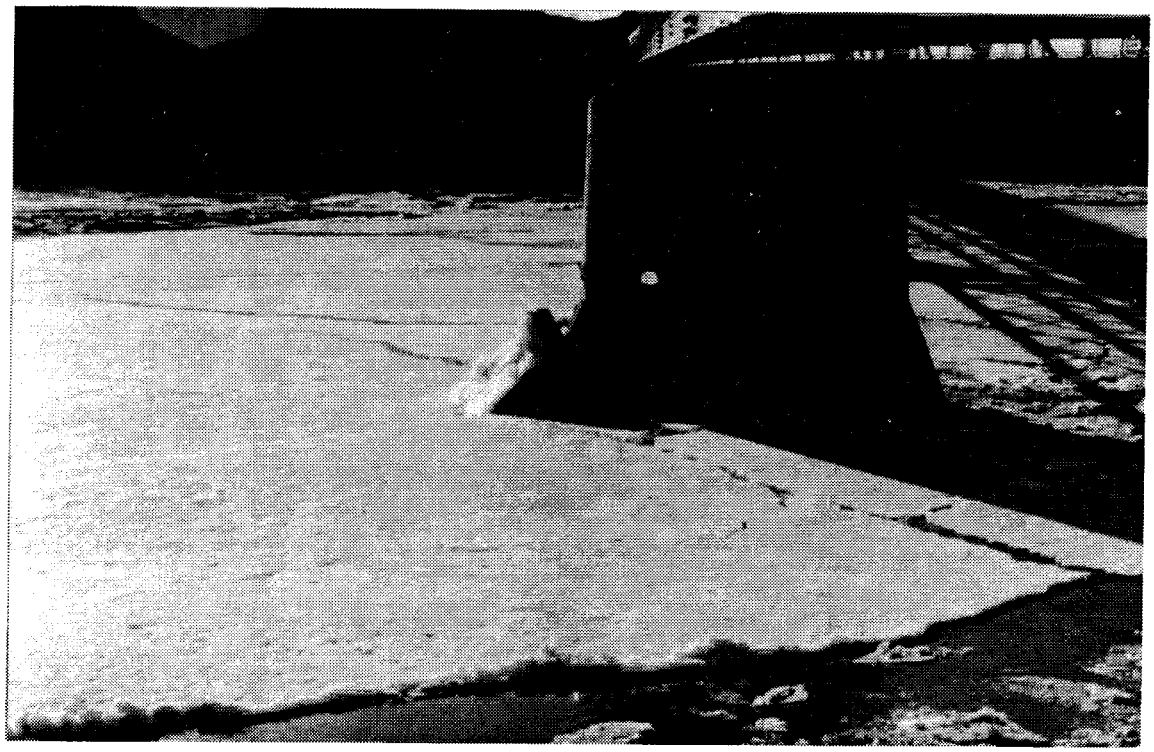

PLATE 2.1 BENDING FAILURE EVENT.

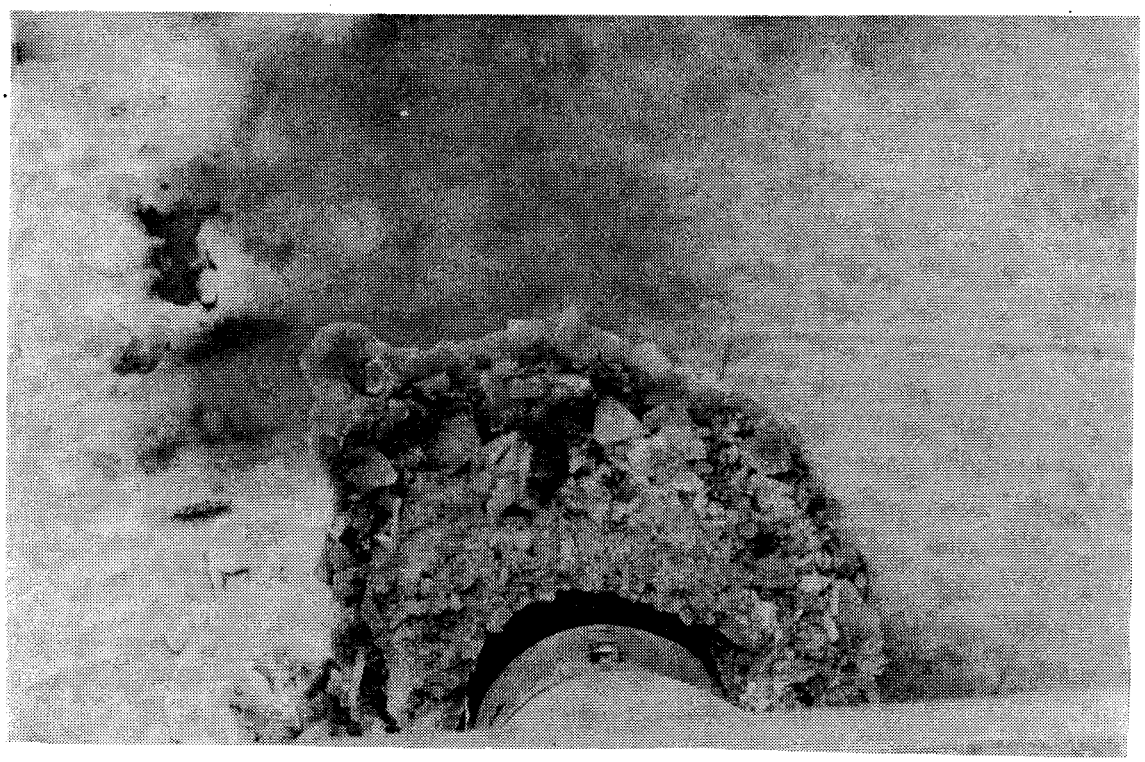

PLATE 2.2 CRUSHING FAILURE EVENT.

3. DYNAMIC RESPONSE OF BRIDGE PIERS

3.1 Introduction

When a time-varying ice load is applied to a bridge pier, the dynamic characteristics of the pier influence the way in which it responds to the load. Dynamic characteristics may result in a magnification or reduction in response when compared to the response that would occur if the load was applied statically. Hence, the dynamic properties of both load and pier should be taken into account when considering ice-pier interaction.

In this study, it is assumed that the dynamic characteristics of bridge piers can be represented by a single-degree-of-freedom oscillator. Accordingly, this chapter contains a review of the theory of vibration for single-degree-of-freedom systems. The theory is illustrated by evaluating the response of piers to idealized and actual ice loadings. For convenience, the maximum response of a range of piers to a given loading is presented in the form of response spectra.

Response spectra have been evaluated for each of the ice load histories considered in this study. In this chapter, the results of these calculations are summarized in terms of mean response spectra for crushing, bending and splitting load histories at Hondo and for the Pembridge load histories. Curves of coefficients of variation of maximum response are also presented for each category of load

history. It is shown that the form of the mean response spectra depends on the predominant frequency components and dynamic characteristics of the load histories.

The next chapter contains a discussion of the use of the mean response spectra and curves of coefficients of variation in a design procedure which includes dynamic effects.

3.2 Single-Degree-of-Freedom System

3.2.1 Dynamic Properties

The single-degree-of-freedom system shown in Fig. 3.1 is composed of a single mass, m, a linear spring, k, and a viscous dashpot with damping constant, c. The position of the mass at any time, t, is defined by the single co-ordinate, $x(t)$. When a time-varying ice force, $F(t)$, is applied to the system, the equation of motion of the system may be expressed by

$$m\ddot{x}(t) + c\dot{x}(t) + kx(t) = F(t) \qquad 3.1$$

In Eqn. 3.1, a dot above the variable $x(t)$ represents one differentiation with respect to time. Dividing Eqn. 3.1 by the mass, m, results in an equation of the form

$$\ddot{x}(t) + 2\xi\omega\dot{x}(t) + \omega^2 x(t) = F(t)/m \qquad 3.2$$

When the undamped system is vibrating freely, with no

applied load, it oscillates sinusoidally with a natural circular frequency, ω, given by

$$\omega = \sqrt{k/m} \qquad 3.3$$

The period, T, and natural frequency, f, of these free oscillations are given by

$$T = 2\pi/\omega \qquad 3.4$$

$$f = 1/T = \omega/2\pi \qquad 3.5$$

If damping is present in the system, in general, the free vibration response attenuates with time and the period of vibration is altered slightly. It is convenient to express the amount of damping associated with the system as a ratio of the critical damping value, $2m\omega$, the value of damping for which the free vibration response of the system becomes non-oscillatory. Accordingly, the damping ratio, ξ, is defined by

$$\xi = c/2m\omega \qquad 3.6$$

The response of a pier to an ice force history, which is essentially an arbitrary load, must be evaluated by numerical means. However, as discussed in Sec. 2.3, depending on the type of failure of the ice, certain

frequency components become predominant. Hence, comparisions can be made with the response of a pier to an idealized force oscillating at a single frequency. In addition, the initial step in the load, characteristic of splitting and crushing events, may be represented by a simple rectangular force. The response to these two idealized loads will be investigated prior to considering actual ice force histories.

3.2.2 Response to Harmonic Loading

An idealized ice force, $F(t)$, which varies harmonically at the circular frequency, $\bar{\omega}$, with amplitude, F_{max}, may be expressed as

$$F(t) = F_{max} \text{ Sin } \bar{\omega}t \qquad 3.7$$

The steady state solution for this particular forcing function (Clough and Penzien, 1975) is

$$x(t) = G \text{ Sin}(\bar{\omega}t - \alpha) \qquad 3.8$$

where the response amplitude, G, has the form

$$G = (F_{max}/k) \frac{\omega^2}{[(\omega^2 - \bar{\omega}^2)^2 + (2\xi\omega\bar{\omega})^2]^{\frac{1}{2}}} \qquad 3.9$$

and α is a phase angle.

It is convenient to normalize the displacement response

by the displacement that would be produced if the maximum value of the load was applied statically. The resulting function is known as the response ratio, R(t). For the load under consideration the response ratio is given by

$$R(t) = \frac{x(t)}{F_{max}/k} \qquad 3.10$$

From Eqns. 3.8, 3.9 and 3.10, the maximum value of the response ratio, R_{max}, is

$$R_{max} = \frac{\omega^2}{[(\omega^2 - \bar{\omega}^2)^2 + (2\xi\omega\bar{\omega})^2]^{\frac{1}{2}}} \qquad 3.11$$

When the frequency of the applied loading is close to the natural frequency of the pier, the denominator in Eqn. 3.11 becomes relatively small and for piers with zero damping the amplitude of the forced vibrations tends toward infinity. In this case, the pier is said to resonate with the applied loading. In practice, the presence of damping reduces the resonant maximum response ratio to approximately $1/2\xi$. The time required to attain this maximum response ratio depends on the amount of damping present in the system. The build up of resonant response from rest is demonstrated by Fig. 3.2, which shows the largest response ratio attained for a given number of cycles of oscillation.

In Fig. 3.3, the maximum response ratio has been plotted against system frequency for harmonic loads oscillating at two particular cyclic frequencies, $\bar{f} = \bar{\omega}/2\pi$.

These curves show the relatively large resonant response that occurs when the natural frequency of the pier is close to that of the applied load. As the pier frequency decreases from the resonant frequency, the maximum response ratio tends toward zero. This indicates that lower frequency piers do not respond in full to the higher frequency force oscillations. Alternatively, as the system frequency increases from the point of resonance, the maximum response ratio approaches unity. In this case the dynamic magnification of response is progressively reduced until the system responds statically to the fluctuating load.

3.2.3 Response to a Rectangular Impulse

A rectangular impulsive load is shown in Fig. 3.4. The sudden rise and fall in force is a characteristic of crushing and splitting ice load histories. (see Figs. 2.4(a) and 2.5(a)). The maximum response of an undamped pier to a rectangular pulse occurs during the loading stage if the natural frequency of the pier is greater than or equal to 0.5 divided by the pulse duration, T_p. In this case, at least half a cycle of vibration occurs before the load is removed. When the natural frequency of the pier is less than 0.5 divided by the pulse duration, the maximum response occurs during the free vibration following the loading stage. The maximum response ratios for these cases are given by

$$R_{max} = 2 \qquad (f \geq 0.5/T_p) \qquad 3.12$$

$$R_{max} = 2\ Sin(\pi f T_p) \qquad (f < 0.5/T_p) \qquad 3.13$$

These equations have been plotted against system frequency in Fig. 3.5 for a pulse of one second duration. Note that the lower frequency systems with $f < 0.5$ Hz do not complete the necessary half cycle of vibration during the load application to attain the constant maximum response ratio of 2, given by Eqn. 3.12.

3.2.4 Response to an Ice Load History

In evaluating the response of bridge piers to digitized ice force histories, the response history was divided into a number of small time increments. The method of Newmark (1959) was used to transform the differential equation of motion (Eqn. 3.2) into an incremental algebraic equation. The resulting algebraic equation was used to calculate the change in response during each time increment. Calculations advanced in a step by step manner to build up the complete time history response.

In the analysis, the response was evaluated at each time increment and also at each discontinuity in the slope of the forcing function. To ensure accuracy and stability of the solution, the time step used in the calculations was always less than or equal to 1/20 of the period of the system. Linear acceleration of the mass was assumed during

each time interval and the system was assumed to be initially at rest.

For the purpose of design, it is the maximum response to an ice load history, rather than the response with time, that is of particular interest. Accordingly, it is convenient to represent the maximum response of a wide range of bridge piers to a particular forcing function, by using response spectra. These are plots of the maximum response ratio against system natural frequency. Curves of this type have already been presented in Figs. 3.3 and 3.5 for a harmonic loading and a rectangular impulse, respectively. Since the maximum response ratio gives the ratio of maximum dynamic to maximum static displacement and since other response quantities such as stresses and moments are proportional to displacement for elastic systems, the maximum response ratio may be applied to any static response quantity to obtain the corresponding maximum dynamic response.

The response spectra calculated for each of the ice loading events measured at Hondo and Pembridge are presented in Appendix B. These response spectra have been obtained for systems with natural frequencies between 0.1 and 50 Hz and with damping ratios between 0 and 20%. The form of the spectra for the various types of load history is discussed below.

3.3 Hondo Response Spectra

3.3.1 Bending Failure Response Spectra

Examples of response spectra corresponding to bending ice load histories recorded at Hondo are shown in Figs. 3.6 (a) and (b). These response spectra correspond to the bending load histories discussed in Chapter 2 (Figs. 2.3 and 2.6, respectively). Both spectra show that relatively high maximum response ratios occur at system frequencies around 0.5 and 15 Hz, with reduced responses occurring between these limits. Differences in detail, caused by peculiarities in the individual loads, are also apparent.

The peculiarities in the response spectra can be eliminated by developing curves which reflect the average response to bending failure records. For this purpose, the average maximum response ratio was evaluated at each system frequency, for all the bending response spectra. These values were then plotted to obtain the mean response spectra shown in Fig. 3.7. The averaging procedure has resulted in a smoothed set of curves, more representative of the response to the major characteristics in the load histories.

In describing the response spectra in this report, three different frequency ranges are referred to: a low frequency range corresponding to pier frequencies between 0.1 and 1 Hz, a medium range corresponding to frequencies between 1 and 10 Hz and a high frequency range including piers between 10 and 50 Hz. The mean response spectra (Fig. 3.7) show that the maximum response ratio rises to a peak in

both the low and high frequency ranges. The magnification of static response is similar in both regions, reaching a magnitude of about 1.8 for a damping ratio of 2%. Higher damping significantly diminishes the response at each system frequency, the peak values for a 20% damping ratio being reduced to about 1.0. The maximum response ratio remains almost constant throughout the medium frequency range, with values of approximately 1.3 and 1.0 for damping ratios of 2 and 20%, respectively.

As discussed in Chapter 2, bending failure load histories have significant low and high frequency components, resulting from flexural failure and local crushing of the ice, respectively. When discussing the form of the mean response spectra, comparisons can be made to the response spectra presented previously in Fig. 3.3 for the case of harmonic loads. Fig. 3.3 has been plotted for harmonic loads oscillating at the predominant frequencies for flexural failure and local crushing of ice at the Hondo pier.

By analogy to Fig. 3.3, the mean bending spectra of Fig. 3.7 indicate that low frequency piers resonate with the slow force fluctuations associated with bending failure. This causes the peak response at approximately 0.5 Hz. Similarly, high frequency piers resonate with the crushing component of the load, causing the peak response at 15 Hz.

At the lower end of the low frequency range, the maximum response ratios are less than unity. Comparison

with Fig. 3.3 indicates that these piers, with very low natural frequencies, do not respond fully to the higher frequency force fluctuations associated with bending or crushing failure of the ice. In the medium frequency range, the response is also reduced, but not below unity. The piers in this range respond statically to the slower force fluctuations of bending failure, but do not respond fully to the higher frequency crushing fluctuations. In contrast, piers at the upper limit of the high frequency range respond fully to all the frequency components in the load. The corresponding maximum response ratio tends to unity, indicating that no magnification of static effect occurs.

From consideration of the response spectra for each bending event, the ratios of standard deviation to mean value, or coefficients of variation of the maximum response ratio, have been evaluated at each system frequency. The resulting curves are shown in Fig. 3.8. These curves represent the variation in response between the individual spectra.

The highest coefficients of variation occur in the low frequency range. In this region, system response depends primarily on the frequency of bending failures which is in turn a function of several variable factors such as flow velocity, thickness and strength of the ice. As a result, the resonant peak response in the individual spectra occur anywhere between 0.2 and 2 Hz. In the high frequency range, the coefficients of variation are smaller. This indicates,

perhaps, that the frequency of crushing failure is less variable than the frequency for bending, at the Hondo site. Finally, since systems with smaller damping ratios respond more readily to the individual frequency characteristics in each load history, the curves show a greater variability in response for the lighter damped systems.

3.3.2 Crushing Failure Response Spectra

Examples of crushing failure response spectra, corresponding to the load histories discussed in Chapter 2 (Figs. 2.4(a) and 2.7) are shown in Figs. 3.9(a) and (b). Characteristic of the crushing case, both these spectra exhibit a peak in response in the high frequency range. However, in addition to the high frequency crushing component, the response spectra also reflect the individual peculiarities present in the load histories. To eliminate peculiarities, the mean response spectra shown in Fig. 3.10 have been developed for crushing failure load histories at Hondo.

Fig. 3.10 shows that the maximum response ratio remains almost constant throughout the low and medium frequency ranges. In these regions, the maximum static response of piers with a 2% damping ratio is magnified by about 1.3 However, no significant magnifications occur for piers with a damping ratio of 20%. A peak in response occurs in the high frequency region. The maximum values, occurring at 15 Hz, range from 1.7 to 1.1 for various damping ratios between

2 and 20%, respectively.

By analogy to the response spectrum given in Fig. 3.3 for a harmonic load oscillating at 15 Hz, the peak responses in the high frequency region of the mean spectra (Fig. 3.10) are largely due to resonance with the high frequency crushing component of the load histories. Interestingly, this resonant response is similar in magnitude to, and occurs at the same frequency as, the high frequency resonant response for the bending spectra (Fig. 3.7). For both the crushing and bending cases, resonant response is caused by local crushing of the ice.

In the low and medium frequency ranges of the mean spectra, the maximum response is caused, primarily, by the initial sudden 'step' in load, characteristic of crushing load histories. The maximum response is therefore similar to that given by Eqns. 3.12 and 3.13, for a rectangular impulse. These equations imply a constant maximum response ratio of 2 for undamped piers with natural frequencies greater than 0.5 divided by the event duration. This is shown in Fig. 3.5 for an impulse with a duration of one second. For the relatively long duration crushing events, most of the piers considered have natural frequencies larger than the limit implied by Eqn. 3.12. Consequently, the maximum response ratio reaches a constant value in the low and medium frequency ranges.

The coefficients of variation in the maximum response ratios for the crushing failure spectra are shown in Fig.

3.11. The variations are relatively high in the low frequency range, are reduced for medium frequencies, but increase again in the high frequency region. Individual crushing load histories at Hondo may exhibit particular characteristics such as slow force fluctuations caused by partial bending of the ice. These peculiarities contribute to the high variations at low frequencies. The variations are slightly less, however, than those corresponding to bending failure (Fig. 3.8).

In the high frequency region, the sensitivity of system response to any variations in the predominant crushing component of the load causes relatively high coefficients of variation (Fig. 3.11). The variations are reduced throughout the entire frequency range by increased amounts of damping.

3.3.3 Splitting Failure Response Spectra

Examples of response spectra corresponding to the Hondo splitting load histories are shown in Figs. 3.12 (a) and (b). Both of these response spectra show relatively high maximum response ratios occurring in the high frequency region. In addition, these example spectra, which correspond to the load histories discussed in Chapter 2 (Figs. 2.5 (a) and (b)) also reflect the differences between the individual cases. Hence, in order to discuss the major characteristics of splitting failure spectra, mean curves have been developed and are presented in Fig. 3.13.

Figure 3.13 shows that the maximum response ratio rises steadily within the limits of the low frequency range from values around 0.3, to values between 1.0 and 1.3, depending on the amount of damping. It levels off in the medium frequency region. A significant peak in response occurs in the high frequency range at 15 Hz where the maximum response ratios vary from 1.8 to 1.1 for damping ratios between 2 and 20%, respectively.

The range in response between the damping ratios considered is less than in the previous cases, especially for lower frequency systems. This may be explained with reference to Fig. 3.2 which shows that the number of cycles completed by these systems, during short duration splitting events, is insufficient for the build up of full resonant response.

In contrast, resonance with the crushing forces in splitting load histories causes the high frequency peak response. As demonstrated by Fig. 3.2, for damped high frequency piers an event duration of just a couple of seconds is sufficient for build up of resonant response. Consequently, the magnifications for these piers are similar to those resulting from bending and crushing failures.

Similar to the crushing case, the maximum response of low and medium frequency systems to a splitting failure load history is caused mainly by the sudden application of load. By analogy to the response for an impulsive load given by Eqns. 3.12 and 3.13 and shown by Fig. 3.5, in the splitting

case only systems in the medium frequency range respond fully to the short duration events. Low frequency systems do not respond fully to the impulsive load.

Plots of coefficients of variation in the maximum response ratios of the splitting failure spectra are shown in Fig. 3.14. As the event duration determines the frequency at which full response to the impulsive load is attained, the variation in this value causes higher coefficients of variation in the low frequency range. The relatively low mean values of maximum response ratio, in this region, also contribute to the higher coefficients. Significant variations again occur in the high frequency range where the systems are sensitive to the crushing component in the load.

3.4 Pembridge Response Spectra

At Pembridge the ice fails by local crushing against the vertical pile. Although load histories corresponding to crushing, splitting and also repeated splitting events have been observed, the smaller amount of data available for the Pembridge location were considered as a single group. Mean response spectra and curves of coefficients of variation for the Pembridge data are presented in Figs. 3.15 and 3.16, respectively.

Fig. 3.15 shows that the maximum response ratio increases within the limits of the low frequency range from values around 0.7 to values between 1.0 and 1.4, depending

on the damping ratio. It remains constant in the medium frequency region. In the high frequency range, a peak in response occurs at 35 Hz. At this frequency, the maximum response ratios vary from 2.0 to 1.2 for damping ratios between 2 and 20%, respectively. As for the cases previously discussed, damping attenuates the response throughout the spectra.

The crushing failure of the ice at Pembridge results in spectra that are similar in form to those for crushing and splitting at Hondo (Figs. 3.10 and 3.13). In the low and medium frequency regions, the pier responds primarily to the initial impact of the ice. The resulting response is comparable to the response for an impulse load (see Eqns. 3.12 and 3.13 and Fig. 3.5).

The peak in the high frequency range is caused by resonance with the crushing force fluctuations. In contrast to Hondo, for which the crushing resonant response occurs at about 15 Hz, at Pembridge, the corresponding peak occurs at 35 Hz. This reflects the variation in flow conditions between the two locations. In particular, the floes at Pembridge are thinner and have higher velocities.

The curves of coefficients of variation shown in Fig. 3.16 are similar to the Hondo cases in that the higher values occur in the low and high frequency ranges. For Pembridge, however, the different response of low frequency systems to crushing, splitting and repeated splitting events, contributes to these high coefficients. In the high

frequency range, the largest coefficients of variation occur at 35 Hz, as these systems are most sensitive to the crushing component in each of the load histories. Damping lowers the variation in response throughout the entire frequency range.

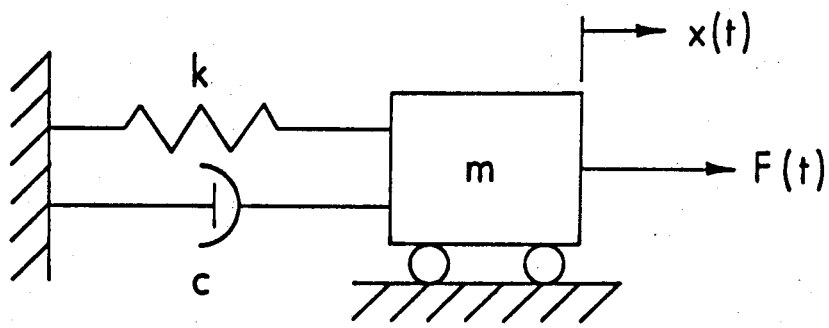

FIGURE 3.1 SINGLE-DEGREE-OF-FREEDOM SYSTEM

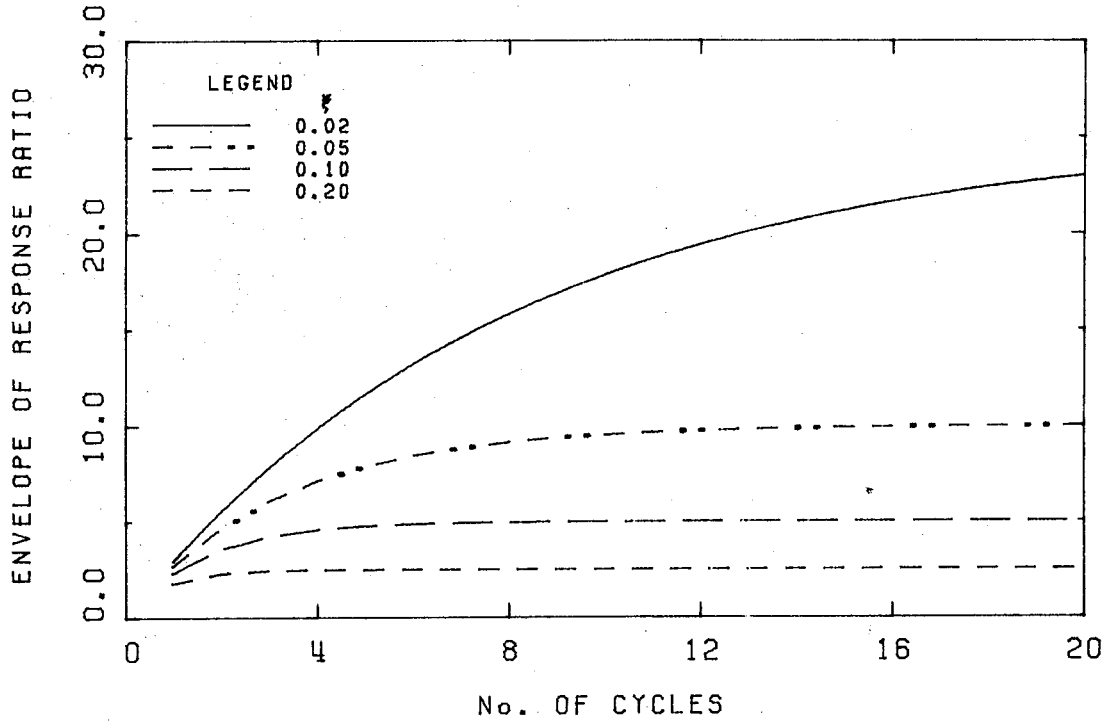

FIGURE 3.2 BUILD UP OF RESONANT RESPONSE

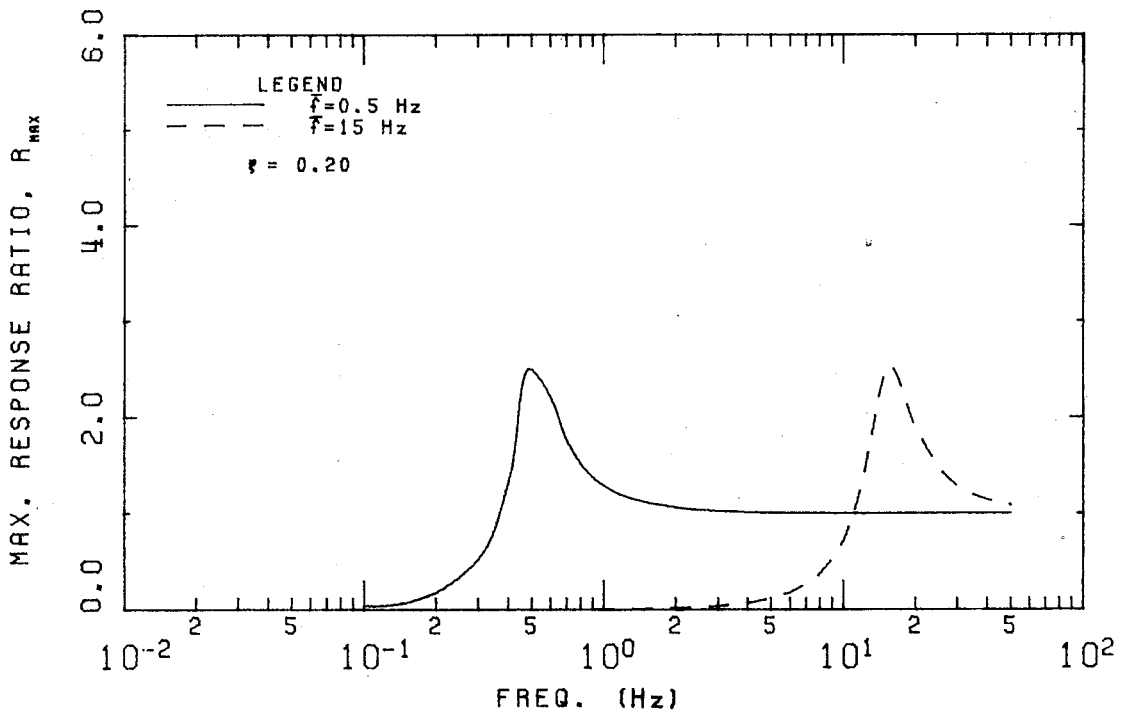

FIGURE 3.3 MAXIMUM RESPONSE TO HARMONIC LOADING.

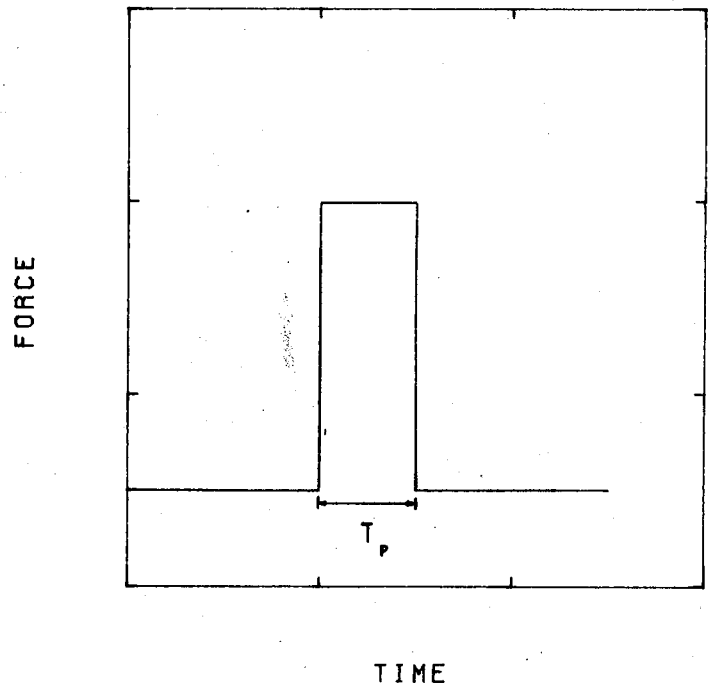

FIGURE 3.4 RECTANGULAR IMPULSE.

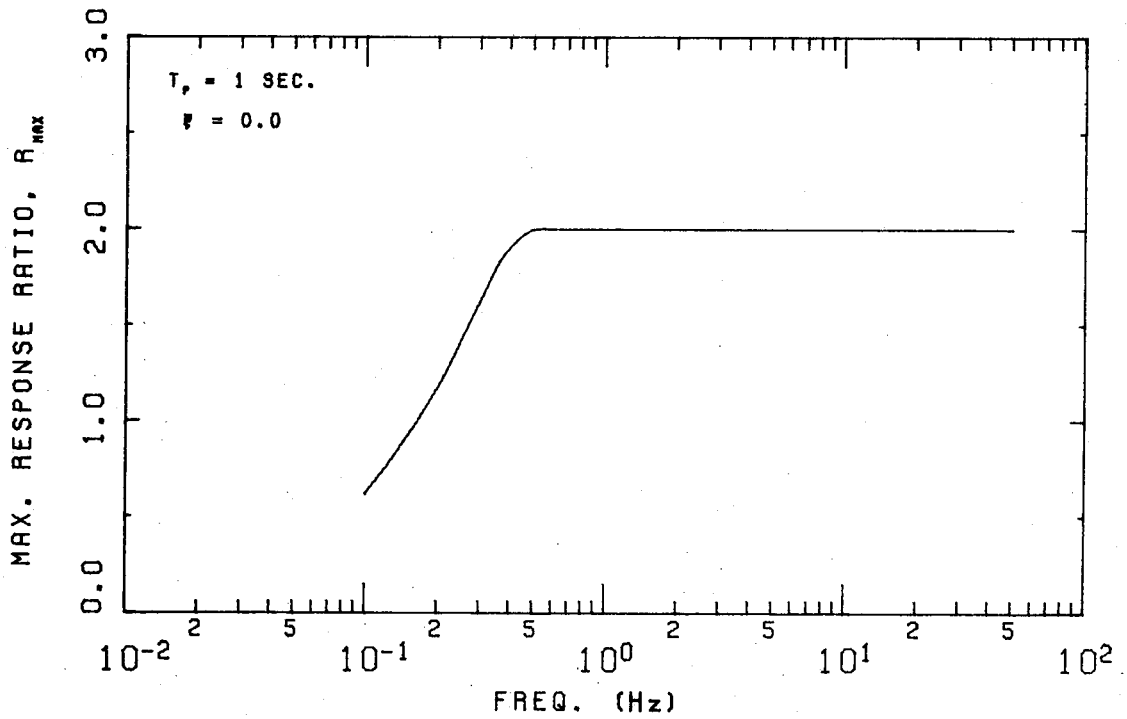

FIGURE 3.5 MAXIMUM RESPONSE TO RECTANGULAR IMPULSE

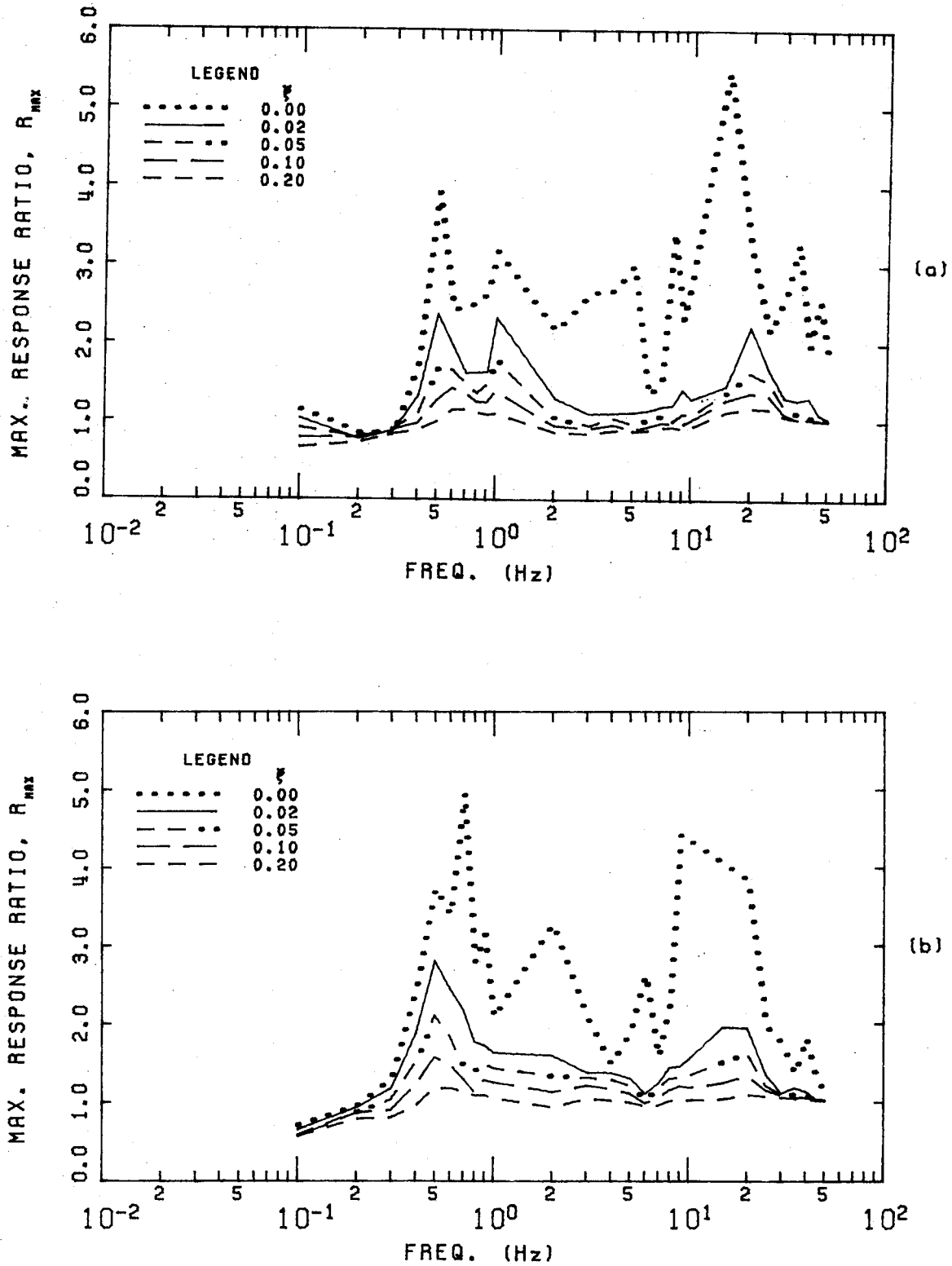

FIGURE 3.6 (a) and (b), BENDING FAILURE RESPONSE SPECTRA - HONDO.

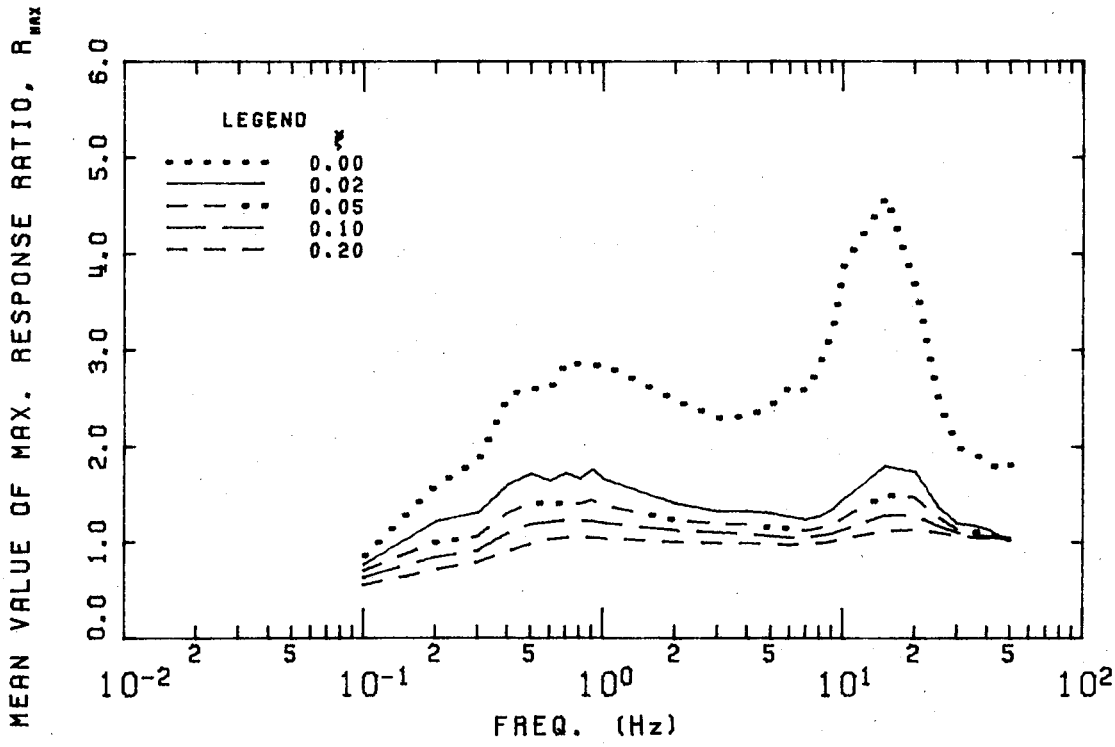

FIGURE 3.7 MEAN BENDING FAILURE RESPONSE SPECTRA - HONDO

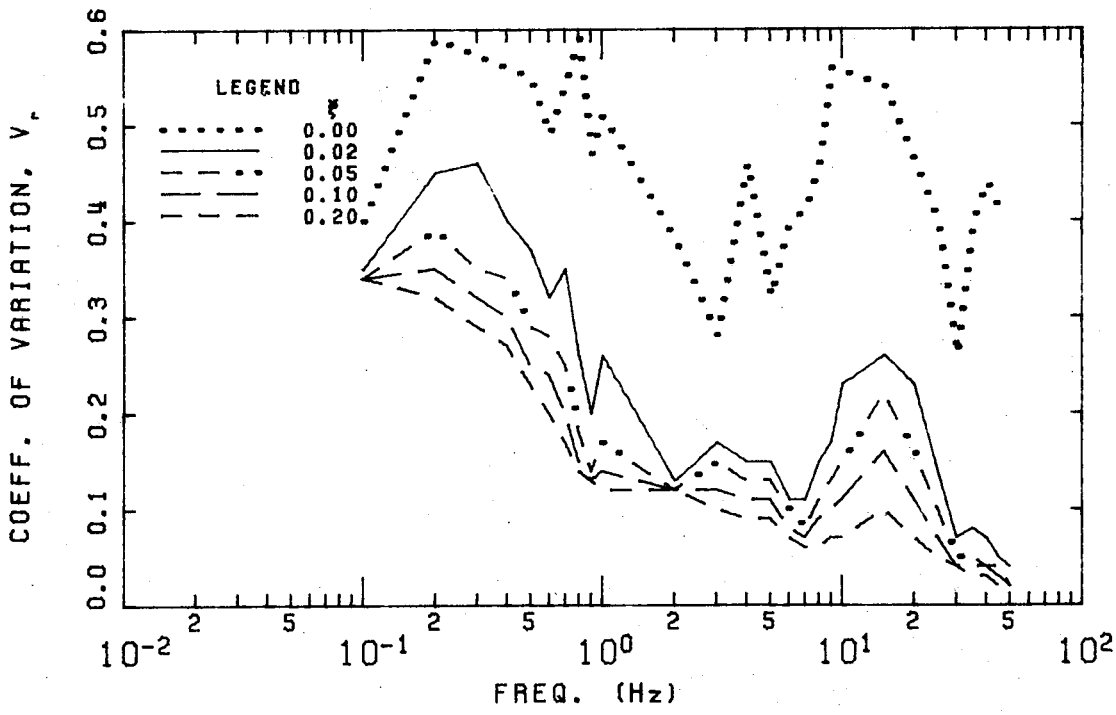

FIGURE 3.8 VARIATION IN BENDING FAILURE RESPONSE - HONDO

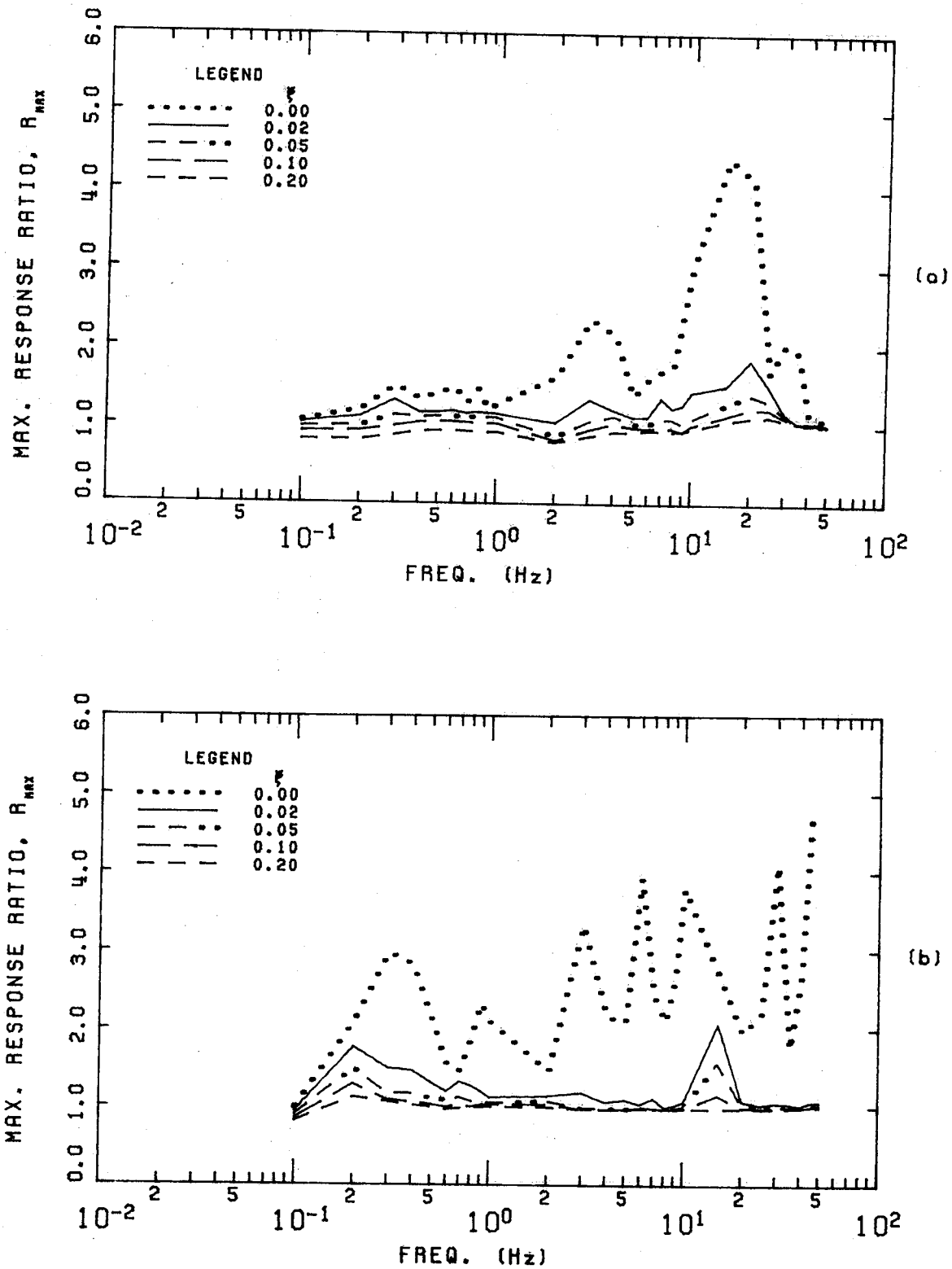

FIGURE 3.9 (a) and (b), CRUSHING FAILURE RESPONSE SPECTRA - HONDO.

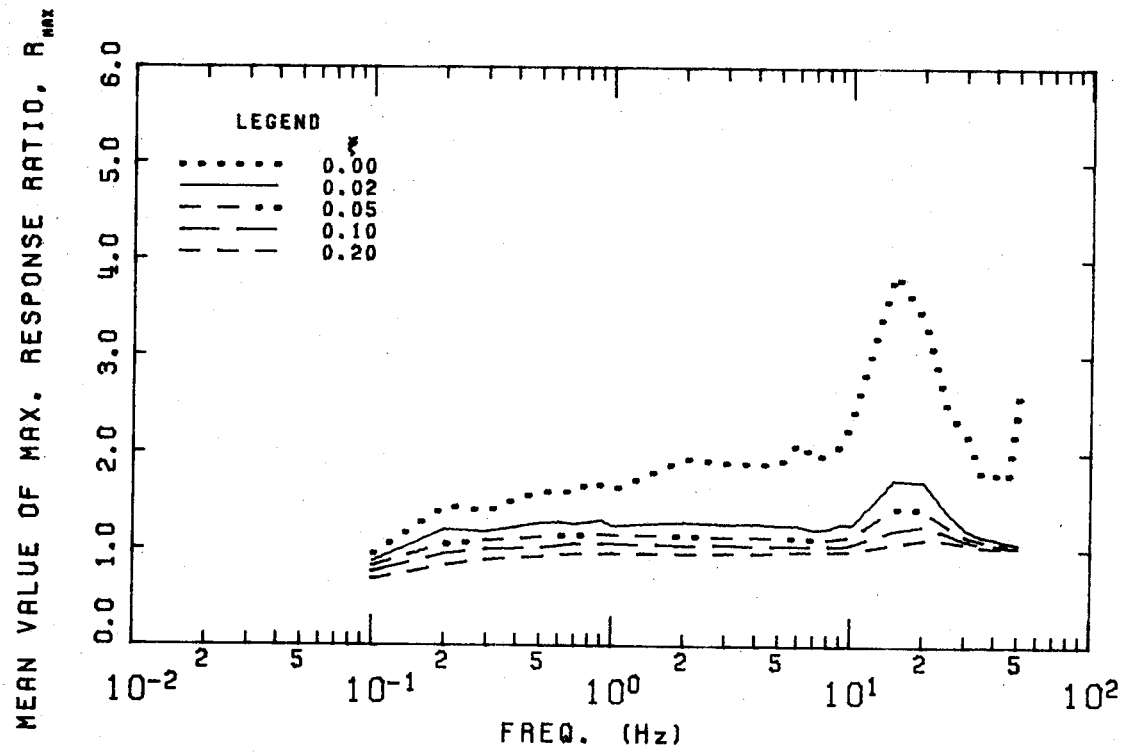

FIGURE 3.10 MEAN CRUSHING FAILURE RESPONSE SPECTRA - HONDO

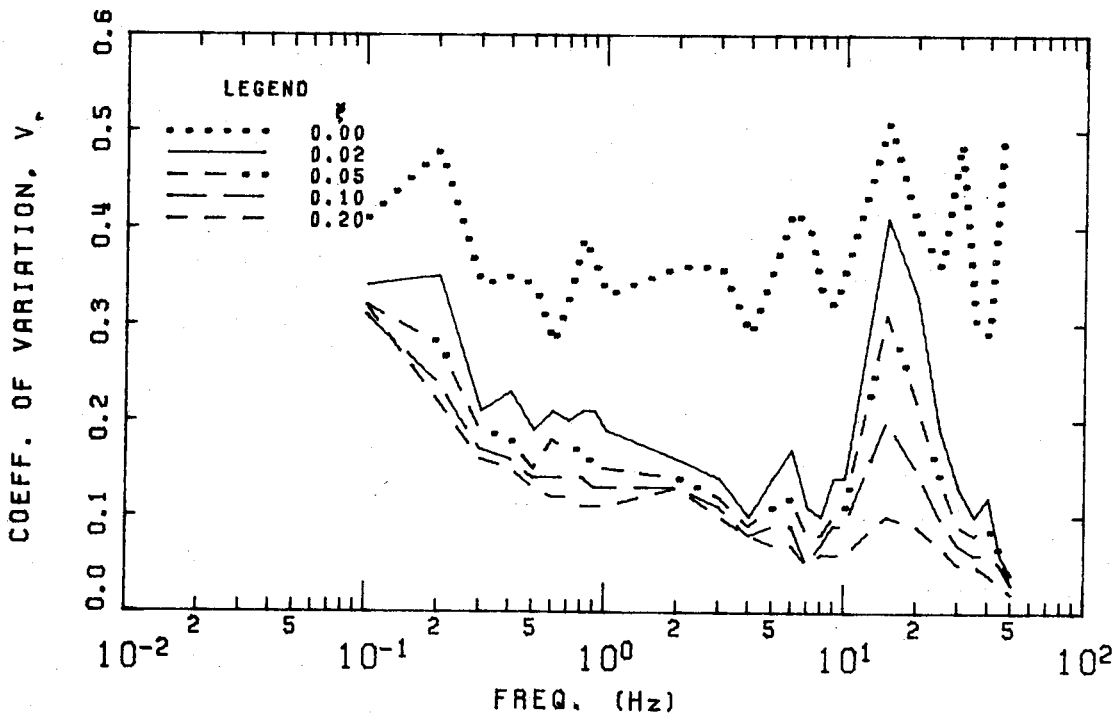

FIGURE 3.11 VARIATION IN CRUSHING FAILURE RESPONSE - HONDO

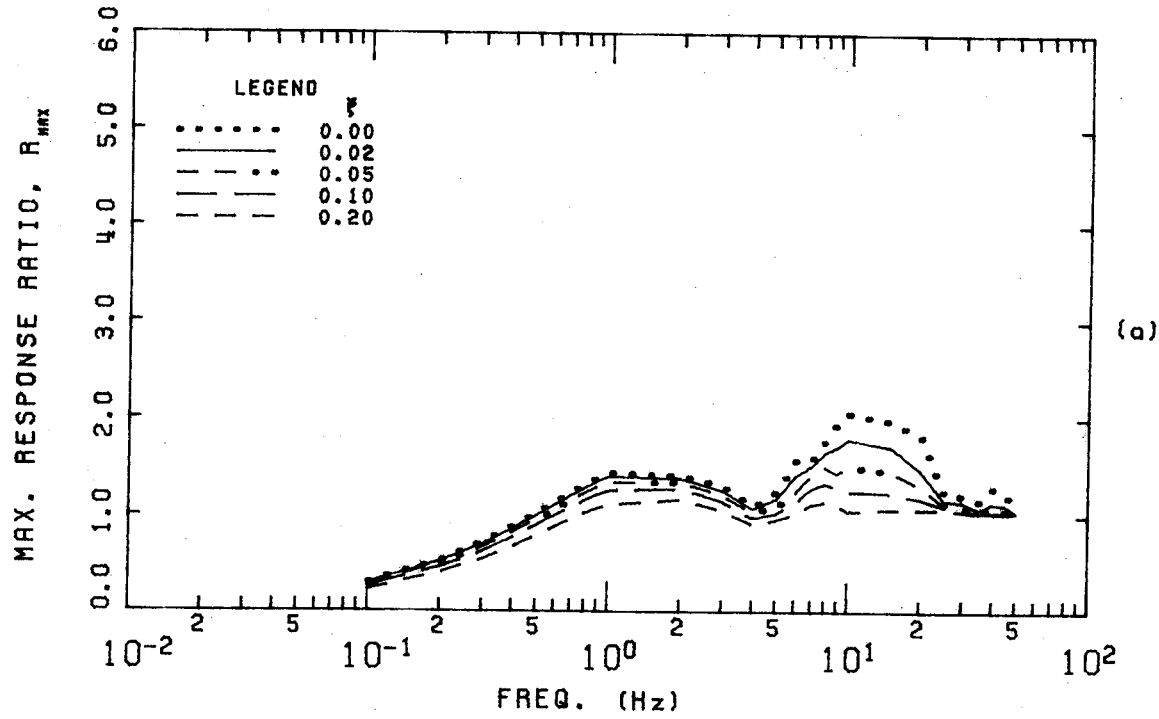

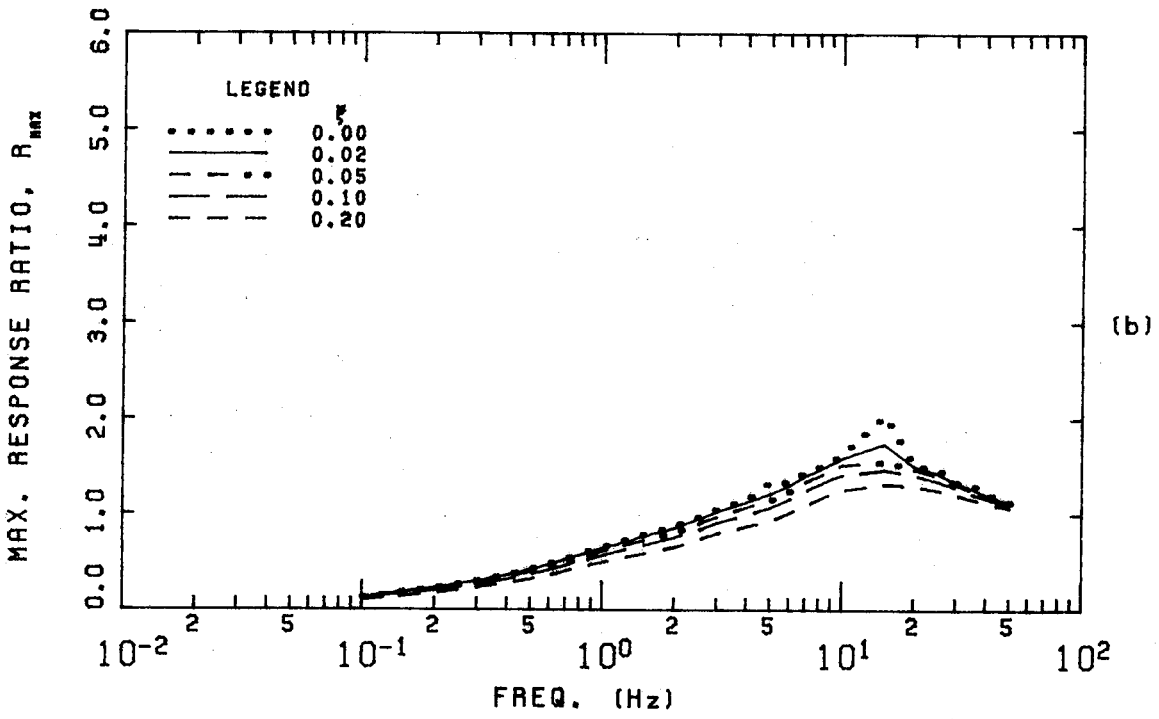

FIGURE 3.12 (a) and (b), SPLITTING FAILURE RESPONSE SPECTRA - HONDO.

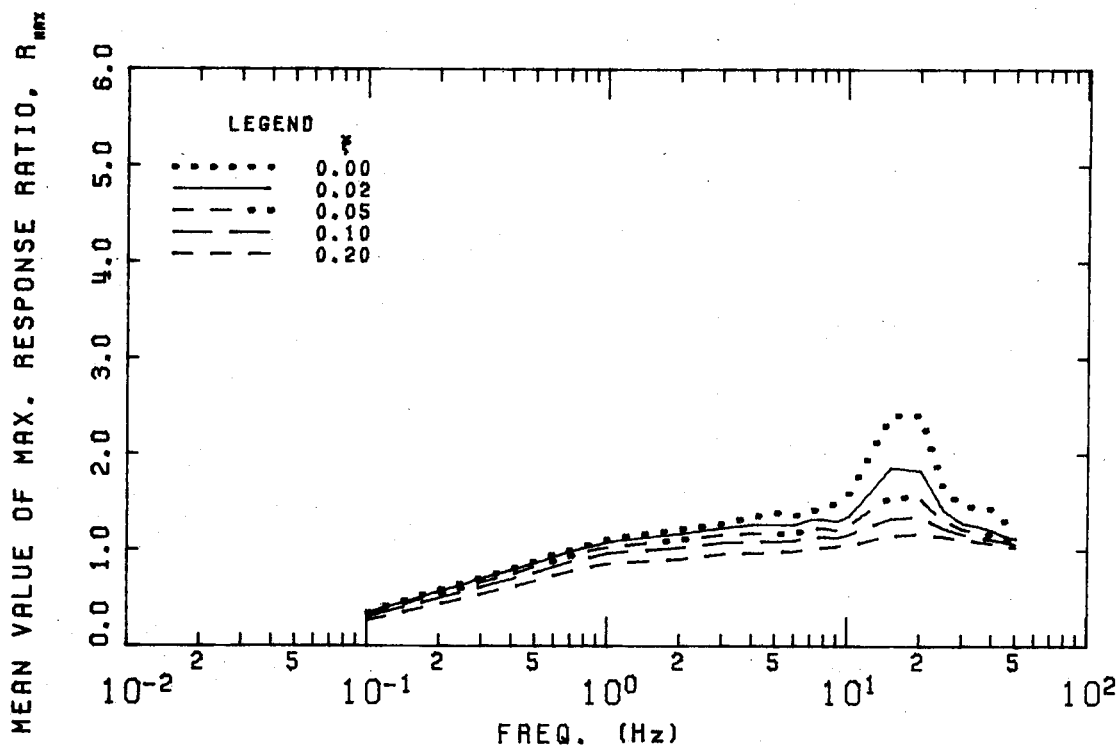

FIGURE 3.13 MEAN SPLITTING FAILURE RESPONSE SPECTRA - HONDO

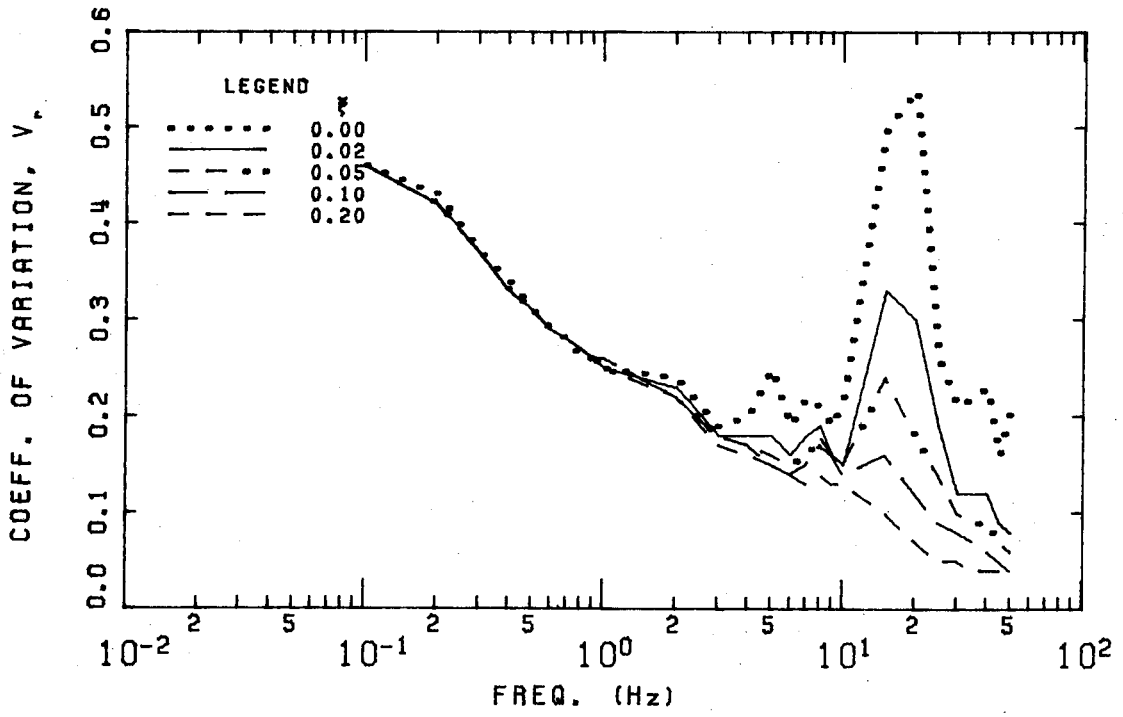

FIGURE 3.14 VARIATION IN SPLITTING FAILURE RESPONSE - HONDO

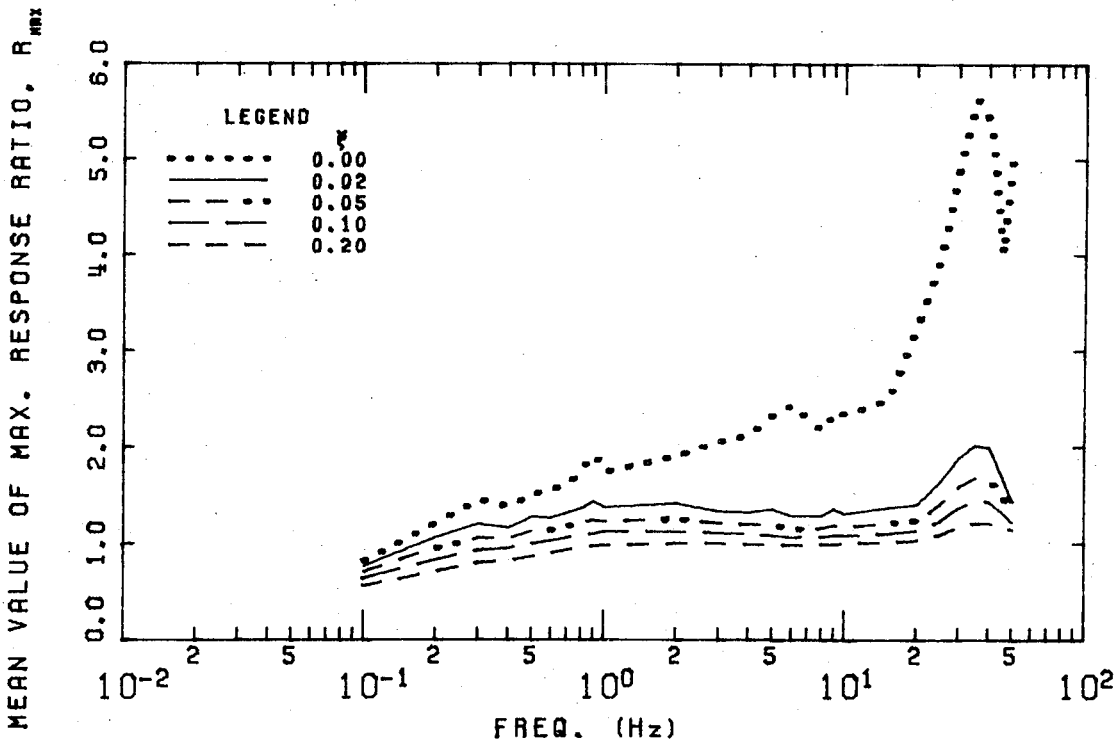

FIGURE 3.15 MEAN RESPONSE SPECTRA - PEMBRIDGE

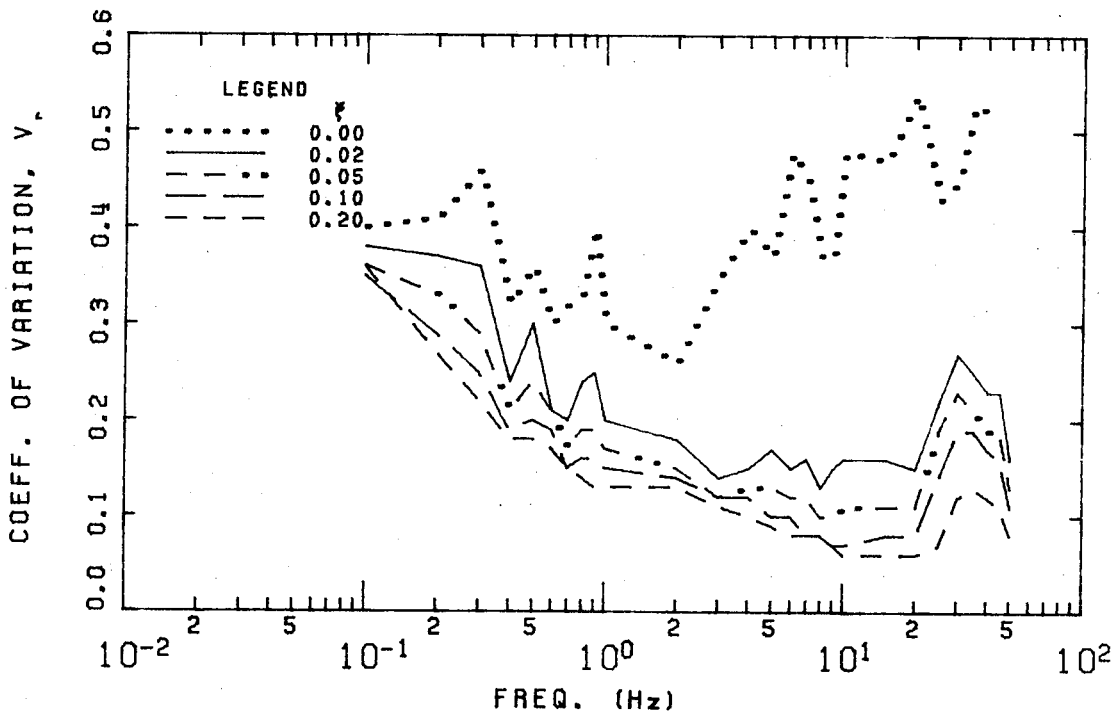

FIGURE 3.16 VARIATION IN RESPONSE - PEMBRIDGE

4. DESIGN APPLICATION

4.1 Introduction

The current CSA Standard (CSA, 1978) for the design of bridge piers subjected to ice forces indicates that the design engineer should investigate the possibility of structural resonance caused by ice-structure interaction. However, no procedures are presented to enable the designer to quantify these effects and include them in the design process.

This chapter briefly reviews the design method used in the code. Alternative procedures which incorporate the effects of dynamic interaction are then presented. These procedures require the use of the mean response spectra and curves of coefficients of variation presented in the previous chapter. Finally, the general implications of the proposed procedures are discussed.

4.2 Current Design Practice

In Canada, the design of bridge piers subjected to dynamic ice pressure caused by moving ice sheets, is carried out in accordance with the CSA Standard CAN3-S6-M78. The specified horizontal ice force, F_{ni}, is given by

$$F_{ni} = C_n pbh \qquad 4.1$$

where C_n is the coefficient for nose inclination, p is the

effective ice strength, h is the ice thickness and b is the pier width. The coefficient C_n accounts for the reduction in horizontal force as the angle of nose inclination with the vertical is increased. It ranges from 1.0, for inclinations of 0 to 15°, to 0.5 for angles of 30 to 45°.

The effective ice strength, p, is obtained by multiplying the specified ice strength by a pier coefficient that depends on the pier width to ice thickness ratio. The specified strength, ranging from 700 to 2800 kPa, depends on the temperature and the condition of the ice at break-up. The pier coefficient ranges from 1.8 to 0.8 for increasing pier width to ice thickness ratios.

The specified ice force, F_{ni}, determined by Eqn. 4.1, is an estimation of the maximum horizontal load applied to the pier by an impinging ice sheet. As such, when related to a particular load history, F_{ni} corresponds to F_{max}, the maximum ice force which occurs during the event. The specified force does not account for any dynamic effects resulting from ice-pier interaction.

The code recognizes the possibility of significant dynamic effects, in some cases, when it states

> "In the case of slender and flexible piers, consideration should be given to the vibrating nature of dynamic ice forces and the possibility of high momentary pressures and structural resonance".

However, no indication is given of how these effects should be evaluated, this being left to the judgement of the

individual designer.

In addition, consistent with the procedures of limit states design, the code proposes several loading combinations for which the pier should be proportioned. The ice load, F_{ni} , is included in two of these groupings which, in general, may be written in the form

$$\text{Total Factored Load} = \lambda [F_{n1} + F_{n2} + \ldots + F_{nk} + F_{ni}] \qquad 4.2$$

The load factor, λ, has the value 1.3 or 1.2, depending on the load combination and, F_{n1} to F_{nk} , are nominal or specified loads corresponding to, for example, dead or live loading. The code suggests that the load factors may be 'revised' if the engineer considers the 'predictability of the loads ' to be different than anticipated by the code itself.

The remainder of this chapter is concerned with formulating procedures which enable the engineer to incorporate the dynamic nature of the ice-pier interaction problem into design.

4.3 Response Spectra and Design

Response spectra are a basic tool employed in several design procedures concerned with time-varying loads, such as procedures for blast, earthquake and impact. The concept may be easily applied to the design of bridge piers, for which it provides a direct and rational approach to

incorporate dynamic effects.

As explained previously (Sec. 3.2.4) the maximum value of the response ratio quantifies the magnification or reduction in static response caused by the dynamic characteristics of both load and pier. Hence, the magnitude of the effective static force, F_e, which produces the same maximum response effect as a dynamically applied load with maximum value, F_{max}, is given by

$$F_e = R_{max} F_{max} \qquad 4.3$$

where R_{max} is the maximum response ratio for the particular load history and bridge pier.

The maximum response ratio and the maximum value of the dynamically applied load are dependent on the properties of the particular pier under consideration. For a given design application, however, R_{max} and F_{max} are random variables and can only be estimated by appropriate values based on statistical distributions.

The statistical characteristics of the maximum response ratio, R_{max}, have been investigated for each load category considered in this study. As demonstrated by sample cases shown in Figs. 4.1 to 4.4, the maximum response ratios for a particular pier frequency and damping value plot as a straight line on normal probability paper. Accordingly, the normal distribution is an acceptable model and the statistical variation in the maximum response ratio can be

determined from the mean value, $\bar{R}_{max}$, and the coefficient of variation, V_R.

The statistical characteristics of the maximum value of the dynamically applied load, F_{max}, are beyond the scope of this study. Estimates of this load can be made by using the current code expression (Eqn. 4.1) or alternatively by using expressions proposed by Lipsett and Gerard (1980), which take account of the type of failure of the ice. The equations of Lipsett and Gerard are presented in a subsequent example. In order to avoid confusion between measured and estimated quantities, the estimated maximum value of the dynamically applied load will be denoted by F_s and will be referred to as the 'static' component of the load in the remainder of the study.

In the next section, the form of Eqn. 4.3 is modified by probabilistic considerations so that it can be used for practical design situations. Two forms are presented. The first enables dynamic effects to be directly included in the current code format. As an alternative code format, the second enables the ice load to be evaluated according to the principles of limit states design.

4.4 Design Equation

4.4.1 Direct Approach

Under current code procedures, the specified ice load, F_{ni}, is included in two load combinations given, in general, by Eqn. 4.2. Dynamic effects and the uncertainty in their

estimation can be incorporated into this format by replacing the specified ice load by a modified value, F'_{ni} , evaluated from an expression of the form

$$F'_{ni} = (1 + gV_R)\overline{R}_{max}F_s \qquad 4.4$$

The mean maximum response ratio, $\overline{R}_{max}$, and the coefficient of variation of the maximum response ratio, V_R, for use in this equation are obtained from the design curves presented in Chapter 3 and the static component of the load, F_s, is evaluated using Eqn. 4.1. The symbol g is the number of standard deviations above the mean value by which $\overline{R}_{max}$ should be incremented to give a sufficiently low probability of exceedance. As R_{max} is normally distributed, g may be obtained from standard statistical tables.

The detailed application of Eqn. 4.4 will be demonstrated in a subsequent example.

4.4.2 Limit States Design Approach

According to the principles of limit states design, a single load factor, λ, should be applied to each specified load. The load factor reflects the uncertainties inherent in the evaluation of the load effect. In conjunction with a resistance factor, ϕ, applied to the estimated strength of the structure, the load factor ensures that an adequate safety margin exists against the structure reaching certain limits of usefulness. These limit states are termed

'Ultimate', as in the case of complete failure or collapse, or 'Serviceability', when, for example, excessive deflections occur.

In the direct approach discussed above, dynamic effects were incorporated into the design process by applying a simple modification to the current code format. The uncertainties associated with estimating both the dynamic effects and the static load were accounted for separately. The load factor currently employed in the code was assumed to account for the variability in the static component. However, using the concepts of limits states design, the uncertainties associated with both components can be incorporated in a single load factor.

By the limit states design approach, the factored ice load for use in design is given by

$$\text{Factored Ice Load} = \lambda_i F''_{ni} \qquad 4.5(a)$$

where

$$\lambda_i = 1.22(1 + V_R) \qquad 4.5(b)$$

and

$$F''_{ni} = \bar{R}_{max} F_s \qquad 4.5(c)$$

The expression for λ_i (Eqn. 4.5 (b)) applies to the ultimate limit state and is derived in the following section. It is based on an assumed coefficient of variation in the static ice load, F_s, and accounts for the overall uncertainty in estimating the effective ice load by the specified value

F''_{ni}.

4.4.3 Derivation of Load Factor, λ_i

If the random variables S and U represent structural strength and total load, respectively, then for a given structure the requirements of limit states design are satisfied if

$$\phi S_n \geq \lambda U_n \qquad 4.6$$

In this equation, S_n and U_n are the nominal or specified values of S and U, respectively.

In this approach to design, probability concepts are employed to determine values for the resistance factor, ϕ, and load factor, λ. The method most commonly used is the 'second moment probabilistic method', in which the random nature of each variable is accounted for by two parameters, the mean and coefficient of variation.

A variable associated with the success or failure of the structure is used to formulate a failure criterion. The one most commonly used (Galambos and Ravindra, 1973) states that for failure to occur

$$\ln S - \ln U = \ln(S/U) < 0 \qquad 4.7$$

The probability of failure may then be expressed as the probability that the random variable ln (S/U) is less than

zero. The failure limit can then be characterized by the safety index, β, which is the number of standard deviations the mean of ln (S/U) (i.e. $\overline{\ln (S/U)}$) is above the failure limit of zero. It can be shown (Galambos and Ravindra, 1973) that β may be approximated by

$$\beta = \frac{\ln(\overline{S}/\overline{U})}{\sqrt{V_S^2 + V_U^2}} \qquad 4.8$$

where $\overline{S}$ and $\overline{U}$ are the mean values of strength and load, respectively, and V_S and V_U are the corresponding coefficients of variation.

The design criterion, in the form of Eqn. 4.6, can now be developed directly from Eqn. 4.8. However, as explained previously, it is desireable to break up the total load into individual load components, with a separate load factor applied to each. The total load effect may be written in the form

$$U = E(F_1 + F_2 + \ldots + F_k + F_i) \qquad 4.9$$

The factor, E, is a random variable with mean, $\overline{E}$, and coefficient of variation, V_E, which accounts for the transformation of load into load effect. The variation in E reflects the uncertainty in this calculation. F_1 to F_k and F_i are the true values of the loads referred to previously, and V_1 to V_k and V_i, are the corresponding coefficients of variation.

Galambos and Ravindra (1973) have shown that the total load can be separated into individual components by linearizing Eqn. 4.8 and using a separation function, α. The error involved in this approximation has been found to be acceptable in the case of a dead, live and wind load combination. This combination of loads, with low to high variabilities, is similar to the case in question and the approximation will be employed here. Hence, using this procedure, Eqn. 4.8 can be written in the form

$$\gamma_s e^{-\alpha\beta V_s} S_n \geq \bar{E} e^{\alpha\beta V_E} [\gamma_1 (1+\alpha\beta V_1) F_{n1} + .. + \gamma_i (1+\alpha\beta V_i) F''_{ni}] \quad 4.10$$

where $\bar{E}$ and V_E are the mean and coefficient of variation of the errors introduced in the structural analysis. In Eqn. 4.10, the γ factors account for the fact that loads specified by design equations are not necessarily mean values. Accordingly, the γ values are simply the ratio of mean to specified loads. From Eqn. 4.10 the load factor, λ_i, applied to the specified ice load, F''_{ni}, is given by

$$\lambda_i = \gamma_i (\bar{E} e^{\alpha\beta V_E})(1 + \alpha\beta V_i) \quad 4.11$$

The coefficient of variation in the ice load, V_i, can be written in the form

$$V_i = \sqrt{V_F^2 + V_R^2} = \alpha_I V_F + \alpha_I V_R \quad 4.12$$

where V_F is the coefficient of variation in the maximum value of the dynamically applied load, V_R is the coefficient of variation in the maximum reponse ratio and α_I is a separation factor. In this study, the value of the separation factor is taken to be 0.75 (Lind 1971). If Eqn. 4.12 is substituted into Eqn. 4.11, the expression for the load factor λ_i can be written in the form

$$\lambda_i = \gamma_i (\bar{E} e^{\alpha \beta V_E})(1 + \alpha\beta\alpha_I V_F + \alpha\beta\alpha_I V_R) \qquad 4.13$$

Equation 4.13 can be simplified to a design expression by appropriate numerical substitutions. By analogy to the values proposed by Nowak and Lind (1979) for the calibration of the Ontario Highway Bridge Design Code, it is assumed that $\bar{E} = 1.0$, $V_E = 0.06$ and $\beta = 3.5$. From consideration of the available data for the maximum static ice loads recorded at the test locations, it is apparent that the equations proposed by Lipsett and Gerard (1980) overestimate the mean values. Based on these data, conservative values of 0.75 for γ_i and 0.3 for V_F have been chosen. With a greater amount of data, more exact estimates of these values could be developed. Finally, using the value $\alpha = 0.55$, determined by Galambos and Ravindra (1973), Eqn. 4.13 reduces to

$$\lambda_i = 1.22(1 + .V_R) \qquad 4.14$$

4.5 Design Example

4.5.1 Introductory Remarks

The dynamic properties of the Hondo and Pembridge test piers have been measured and hence these piers will be considered in the following examples. The factored design ice loads are evaluated by the present code procedure and also by the proposed procedures as presented in Secs. 4.4.1 and 4.4.2.

The direct approach is used in conjunction with the code estimate of static load. Since the code does not distinguish between ice failure types, the spectra relating to all the relevant failure types are consulted to determine the worst dynamic effects.

The load factor for use in the limit states design approach has been based on considerations of Lipsett and Gerard's (Lipsett and Gerard, 1980) estimate of the static ice load. Accordingly, this procedure is demonstrated using Lipsett and Gerard's equations to determine the static load and failure type. This approach could also be implemented, with similar results, using the code estimate of static load. However, the value of the ratio of mean to specified load, γ_i, in Eqn. 4.11 would have to be reevaluated.

Two equations have been proposed by Lipsett and Gerard, depending on whether the ice fails by bending or crushing. If both failure types are possible, the lower value is taken to be the load at which actual failure occurs. A static load caused by splitting failure is not considered to govern

in a design situation as it can always be exceeded by the load from a bigger ice sheet which crushes against the pier. Lipsett and Gerard's equations attempt to predict this larger load. When the static force and failure type have been determined, the corresponding spectra are consulted to determine the appropriate maximum response ratio.

4.5.2 Code Procedure

The specified ice load for which a pier should be proportioned using the code procedure is given by Eqn. 4.1. For the pier and flow conditions at Hondo

C_n = .75 p = 2100 kPa Pier coefficient = 1.0

h = 1 m b = 2.32 m

Hence, the specified ice load is

$$F_{ni} = 3.65 \text{ MN}$$

and the larger factored load (λ = 1.3) is given by

$$\lambda F_{ni} = 4.75 \text{ MN}$$

For the pier and flow conditions at Pembridge

C_n = 1.0 p = 2100 kPa Pier coefficient=1.1

h = 0.61 m b = 0.86 m

Hence, the specified ice load is

$$F_{ni} = 1.21 \text{ MN}$$

and the factored load (λ = 1.3) is

$$\lambda F_{ni} = 1.57 \text{ MN}$$

4.5.3 Direct Approach

In this method, the code estimates of the static ice

load, F_s, are used. These are simply the specified values, F_{ni}, evaluated above. In the proposed procedures, the dynamic properties of both load and pier are taken into account. The Hondo pier has a natural frequency of 8.9 Hz and damping ratio of 0.19 (Montgomery *et al.*, 1980). The respective values for the Pembridge pile are 12 Hz and 0.04 (Lipsett, 1980).

In the direct approach of Sec. 4.4.1, the effective ice load is calculated using Eqn. 4.4. A 1% probability of exceedance, corresponding to g = 2.33, is commonly used in design and will be assumed in this example. However, if in a particular case, the designer feels that the direct approach gives results which are too conservative a lower probability of exceedance may be adopted.

In the case of the Hondo pier, therefore, bending, crushing and splitting are possible failure types and reference to the mean spectra and curves of coefficients of variation show that the worst case is for splitting (Figs. 3.13 and 3.14) with

$$\bar{R}_{max} = 1.0 \qquad V_R = 0.13$$

In addition, from Sec. 4.5.2 we have

$$F_s = 3.65 \text{ MN}$$

By making the necessary substitions into Eqn. 4.4, the specified ice load is

$$F'_{ni} = 4.75 \text{ MN}$$

This value is then factored by the code load factor of 1.3 to account for the uncertainty in estimating the static load

component. The final factored design ice load is then given by

$$\lambda F'_{ni} = 6.18 \text{ MN}$$

The mean response spectra and curves of coefficients of variation for Pembridge (Figs. 3.15 and 3.16) give

$$\bar{R}_{max} = 1.25 \qquad V_R = 0.13$$

From Sec. 4.5.2 we have

$$F_s = 1.21 \text{ MN}$$

and therefore, Eqn. 4.4 gives a specified ice load of

$$F'_{ni} = 1.97 \text{ MN}$$

The code load factor of 1.3 is now applied to give

$$\lambda F'_{ni} = 2.56 \text{ MN}$$

4.5.4 Limit States Design Approach

In this method, the expressions proposed by Lipsett and Gerard (1980) are used to estimate the static ice load, F_s. These are

$$F_{sb} = k_b \sigma_t h^2 \qquad F_{sc} = k_c \sigma_c bh$$

F_{sb} and F_{sc} are the static loads caused by bending and crushing failure, respectively. The other terms are defined as follows:

k_b = coefficient relating to the characteristics of a bending failure,

k_c = coefficient relating to the characteristics of a crushing failure,

σ_c = crushing strength of ice,

σ_t = tensile strength of ice,

b = pier width,

h = ice thickness.

At Hondo, the ice fails by both bending and crushing and Lipsett and Gerard's equations give

$$F_{sb} = 2.62 \text{ MN} \qquad F_{sc} = 4.33 \text{ MN}$$

The static load used in design is taken as the lower of these values. Therefore, in the governing design situation, the ice fails by bending and the static load is

$$F_s = F_{sb} = 2.62 \text{ MN}.$$

For Pembridge, the ice can only crush against the pile. Therefore, we have

$$F_s = F_{sc} = 1.17 \text{ MN}.$$

These static loads can now be used in the proposed procedures. Firstly, however, the dynamic effects for the Hondo pier must be reevaluated as bending has been specified to be the critical ice failure type. The design curves for bending failure (Figs. 3.7 and 3.8) give,

$$\overline{R}_{max} = 1.0 \qquad V_R = 0.08$$

In the limit states design approach of Sec. 4.4.2, the factored ice load is evaluated using Eqns. 4.5. For the Hondo case, these give

$$F''_{ni} = (1.0)(2.62) = 2.62$$

$$\lambda_i = 1.22(1 + 0.08) = 1.32$$

and therefore

$$\lambda_i F''_{ni} = 3.46 \text{ MN}.$$

For the Pembridge case, Eqns. 4.5 give

$$F''_{ni} = (1.25)(1.17) = 1.46$$

$$\lambda_i = 1.22(1 + 0.13) = 1.38$$

and therefore

$$\lambda_i F''_{ni} = 2.01 \text{ MN.}$$

The results of the above design examples are summarized in Tables 4.1 and 4.2.

4.5.5 Discussion of Results

With reference to Tables 4.1 and 4.2, the maximum response ratios indicate that dynamic effects are significant for the Pembridge pile, but that no magnification of static response occurs for the Hondo pier. For Hondo, Lipsett and Gerard's lower estimate of static force, used in the limit states design approach, contributes to the factored load being less than the values determined by the code and direct approaches. However, the inclusion of dynamic effects in the direct approach, results in a factored ice load which is significantly greater than the code value. For the Pembridge pile, the significant dynamic effects incorporated in the proposed procedures cause both factored loads to be greater than the code estimate.

A comparison of the code and Lipsett and Gerard's estimates for the static load, shows that the values predicted by the latter are consistently lower. Lipsett and Gerard's estimates are thought to be preferable to the code estimates since they account for the type of failure of the ice.

Lipsett and Gerard neglect the splitting failure case,

which proved to produce the governing dynamic effects when considering all possible failure types for the Hondo pier. This is probably acceptable, nevertheless, as the maximum response ratios for splitting failure never significantly exceeded the corresponding crushing values. Therefore, it is unlikely that dynamic effects, resulting from a lower splitting load, would be critical in design.

A comparison of the results of the direct and limit states design approaches shows that lower factored loads are predicted by the latter procedure. In addition to the smaller estimates of static load used, the limit states load factors also reflect a more accurate representation of the uncertainties inherent in estimating the effective ice load. The direct approach, in accounting separately for the variability in dynamic and static effects, produces results which are unnecessarily conservative. As expected, the derived load factors are slightly greater than the code value as they reflect the uncertainty in estimating both dynamic and static effects.

In summary, therefore, the limit states design approach, as demonstrated, should be considered the preferable procedure. The factored ice load predicted for the Hondo pier, for which dynamic effects are not significant, is lower than the code estimate. For the Pembridge pile, however, dynamic effects cause a magnification of response and the factored design ice load is nearly 30% greater than the code value.

4.6 General

4.6.1 Design of Slender Piles

For slender piles, as opposed to massive piers, several modes of vibration may make a significant contribution to the response. However, the proposed design ice load has been based on a static force which produces the same maximum displacement response as the dynamic load when applied to a single-degree-of-freedom system. This model accurately represents the displacement response of the pile. However, for the higher order response quantities, the contribution of the higher modes may be significant. In particular, the maximum shear on the pile may be underestimated by direct static application of the design ice load.

In this case, a better estimate of the maximum dynamic shear in the pile is given by Biggs (1964). The improved estimate is based on the dynamic equilibrium of the total inertia force for the pile and the load when the pile is modelled by an equivalent single-degree-of-freedom system. The dynamic properties of the equivalent system are determined from the properties of the real system by a set of transformation factors. For a simply supported pile subjected to an ice load, F(t), at mid-height, the maximum shear, Q_{max}, given by Biggs is

$$Q_{max} = 0.78F_e - 0.28F \qquad 4.14$$

where the effective static load, F_e, is defined in Eqn. 4.3

and F, is the magnitude of the ice load at the time of maximum response.

In a general design situation the latter value is unknown. However, a conservative estimate of the shear can be obtained by neglecting F in Eqn. 4.14. In addition, F_e, should be estimated by the factored ice load, preferably by the limit states design force, $\lambda_i F''_{ni}$, determined for the dynamic properties of the particular pile under design. Hence, the maximum shear on the pile should be evaluated from

$$Q_{max} = 0.78\lambda_i F''_{ni} \qquad 4.15$$

The direct static application of the factored ice load at mid-height of the pile would, of course, give a much smaller value of $0.5\lambda_i F''_{ni}$ for the maximum shear.

4.6.2 Scope of Results

Certain restrictions apply to the direct application of the mean response spectra developed in this study. The form of the curves depends, to some extent, on the ice and flow conditions at the test locations. For example, the characteristic frequency of crushing failure is from 15 to 20 Hz at Hondo, but about 35 Hz at Pembridge. The Pembridge pile, with a natural frequency of 12 Hz, would experience greater dynamic effects if subjected to the Hondo flow conditions.

It has been suggested, (Montgomery *et al.*, 1980), that ice thickness and velocity are the significant flow parameters which affect the characteristic ice failure frequencies. These researchers have proposed that the response spectra may be generalized, for any flow conditions, in terms of a non-dimensional quantity formed by the product of system frequency with the ratio of ice thickness to flow velocity. Relatively crude estimates of these values have been recorded for the Hondo pier only and their application to the individual Hondo response spectra does not produce consistent generalizations. However, 1 and 2m/s are approximate estimates of the flow velocities for Hondo and Pembridge, respectively, and estimates of the respective ice thicknesses are 1 and 0.6m. When applied to the respective crushing frequencies of 15 and 35 Hz, the velocity to ice thickness ratios give non-dimensional frequencies of 15 and 10.5. The comparable magnitudes of these non-dimensional quantities suggest that this approach would be worthy of further investigation with more accurate ice flow data.

In addition, a certain component of the response reflected in the mean response spectra is related to the hybrid load histories considered in the load categories. The effect of generalizing this component to other locations is uncertain. Nevertheless, it is felt that the mean response spectra will give a good estimate of dynamic effects when applied to other locations. The hybrid load

histories correspond to actual loading events and therefore warrant consideration in the analysis.

For each location and load category, the coefficients of variation of the maximum response ratio have been determined by considering the data in a single group. Ideally, if data were available for a large number of years the coefficients of variation should be based on the largest maximum response ratios which occur in each year. However, the amount of data available for this study is insufficient to give statistically significant results by this approach.

4.6.3 Implications of Dynamic Effects on the Design Process

The results of the design example above show that dynamic effects can cause a significant increase in the design ice load above the code value. Attention to the dynamic properties of the pier during the design process, can result in these effects being minimized.

For inclined piers, similar to Hondo, the natural frequency should be such that resonance does not occur with either low frequency bending or high frequency crushing force fluctuations. Hence, for practical purposes, a natural frequency in the medium frequency range should be aimed at in design. The Hondo pier falls into this preferred region. It should be noted, however, that the mean response spectra indicate that this structure should be designed for at least the full static effect. As mentioned by Montgomery *et al.* (1980), this is contrary to the

proposals of some engineers who have suggested, with particular reference to short duration events, that massive structures can be designed for reduced loads.

For vertical piers, such as the Pembridge pile, natural frequencies in the high frequency range, which result in resonance with the crushing component in both splitting and crushing failure load histories, should be avoided. In addition, while the mean spectra for Pembridge indicate that dynamic effects are lower in the low and medium frequency ranges, the individual curves corresponding to repeated splitting load histories indicate that dynamic effects may be significant in the low frequency region. The slow rate of repeated splitting loads can cause resonance with these systems. Hence, for vertical piers also, natural frequencies in the medium frequency range are preferable.

The above considerations can be used as a guide when applying the mean response spectra, developed herein, to approximate the dynamic effects for piers subjected to more general flow conditions. For this purpose, the natural frequency of the pier should be considered in relation to the characteristic failure frequencies of the ice at the location under consideration.

The crushing frequency, for given flow conditions, can be estimated using the procedures presented by Michel (1978). The frequencies associated with repeated splitting events are more difficult to predict. For the conditions at Pembridge, ice floes 0.6 m thick with a velocity of 2m/s,

resulted in repeated splitting loads with frequencies up to 1 Hz. The frequencies for repeated bending failures can be estimated by using the flow conditions at Hondo as a reference. At Hondo, ice floes 1m thick with a velocity of 1m/s caused resonance at frequencies up to 1 Hz.

The above discussion of design requirements has been based throughout on choosing appropriate values for the pier's natural frequency. This indicates the important need for devising procedures to predict the natural frequencies of piers under design. These methods can only be reliably developed by correlation with the results of actual field tests. Hence, the need for extensive dynamic tests on piers, such as those performed at Hondo and Pembridge, is apparent.

TABLE 4.1 HONDO DESIGN RESULTS

Procedure	Code	Direct	Limit states design
Static ice load (MN)	3.65	3.65	2.62
Max. Response Ratio	-	1.0	1.0
Specified Ice Load (MN)	3.65	4.75	2.62
Load Factor	1.3	1.3	1.32
Factored Ice Load (MN)	4.75	6.18	3.46

TABLE 4.2 PEMBRIDGE DESIGN RESULTS

Procedure	Code	Direct	Limit States Design
Static Ice Load (MN)	1.21	1.21	1.17
Max. Response Ratio	-	1.25	1.25
Specified Ice Load (MN)	1.21	1.97	1.46
Load Factor	1.3	1.3	1.38
Factored Ice Load (MN)	1.57	2.56	2.01

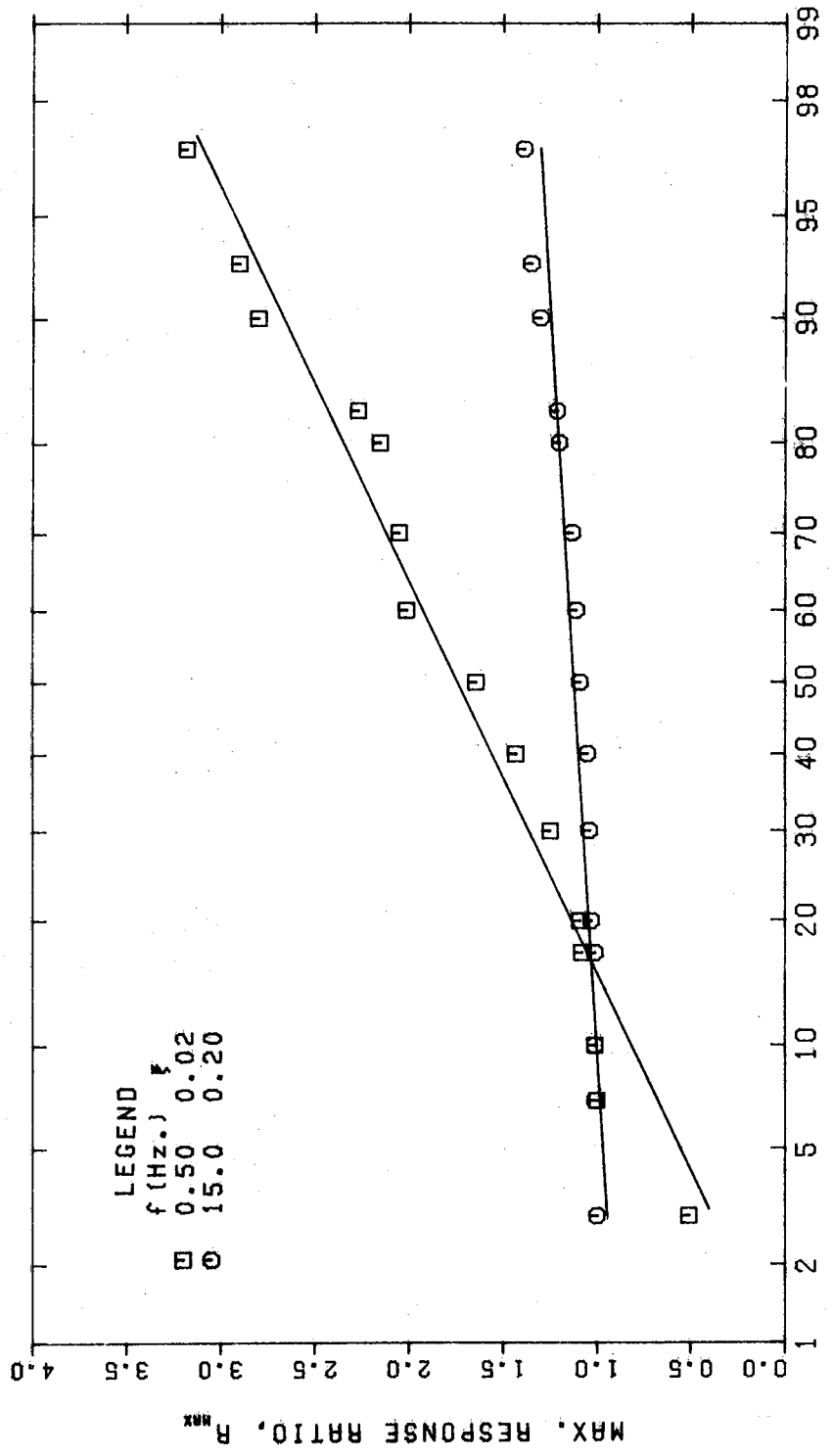

FIGURE 4.1 DISTRIBUTION IN BENDING FAILURE RESPONSE - HONDO

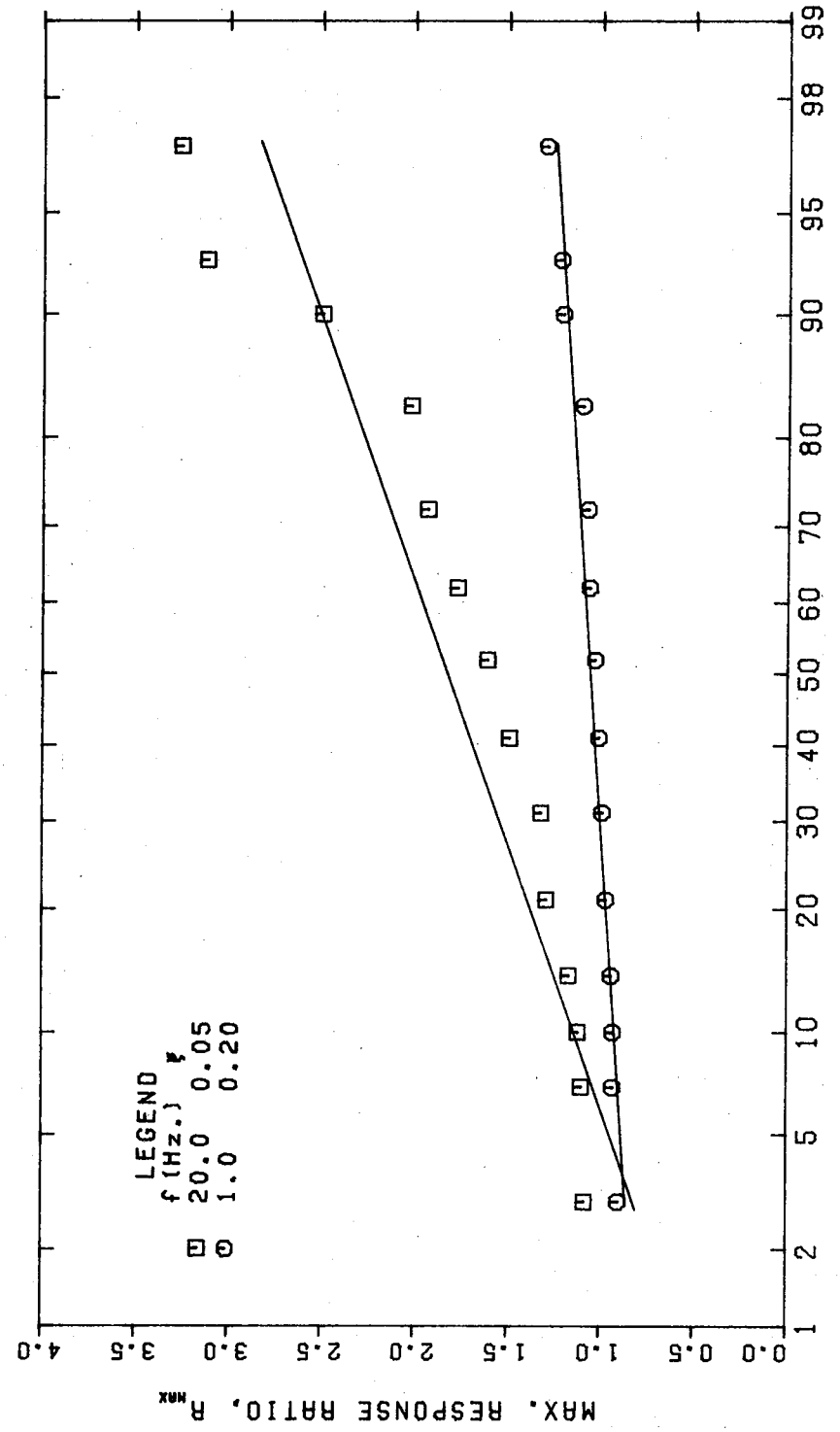

FIGURE 4.2 DISTRIBUTION IN CRUSHING FAILURE RESPONSE - HONDO

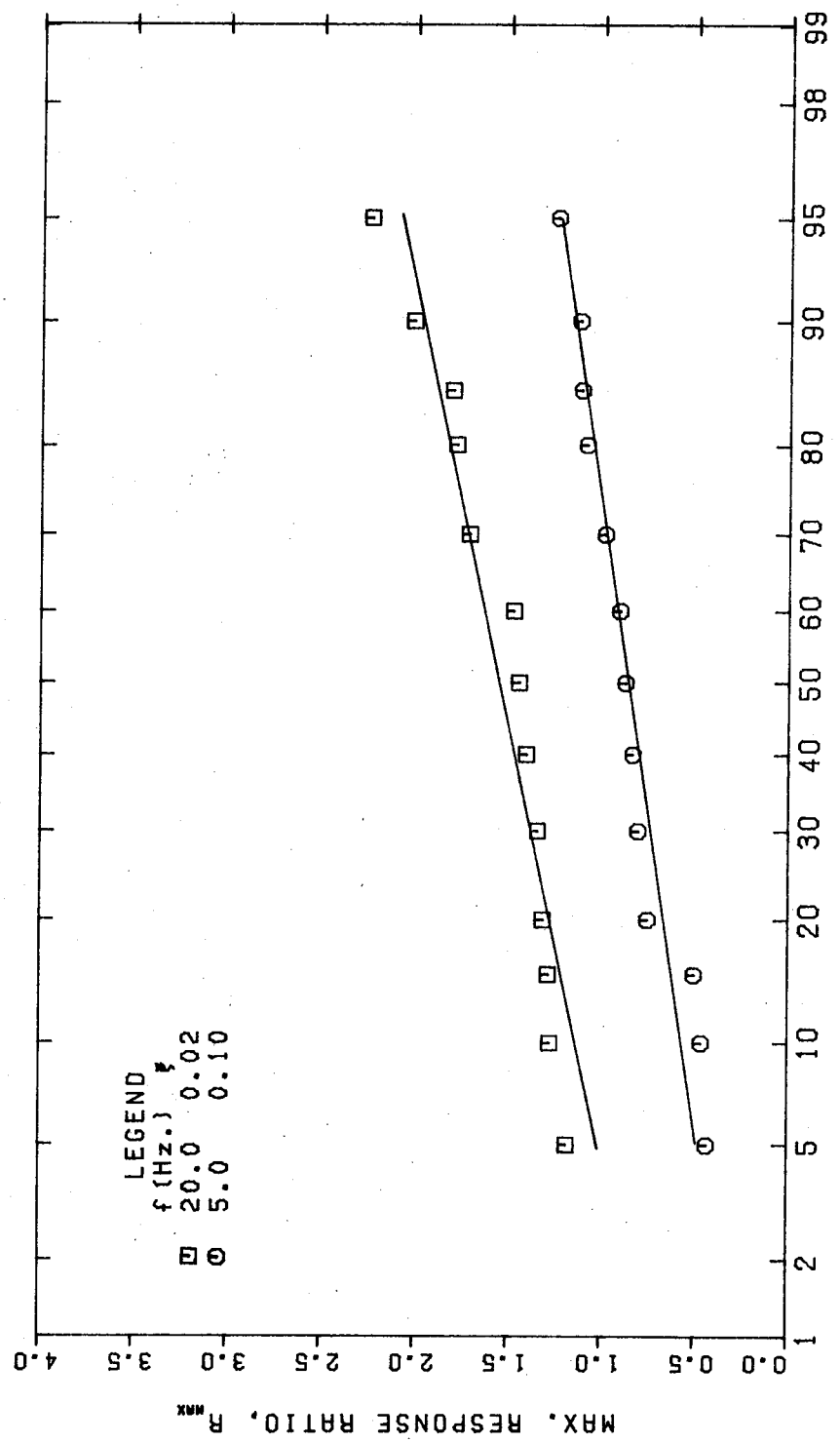

FIGURE 4.3 DISTRIBUTION IN SPLITTING FAILURE RESPONSE - HONDO

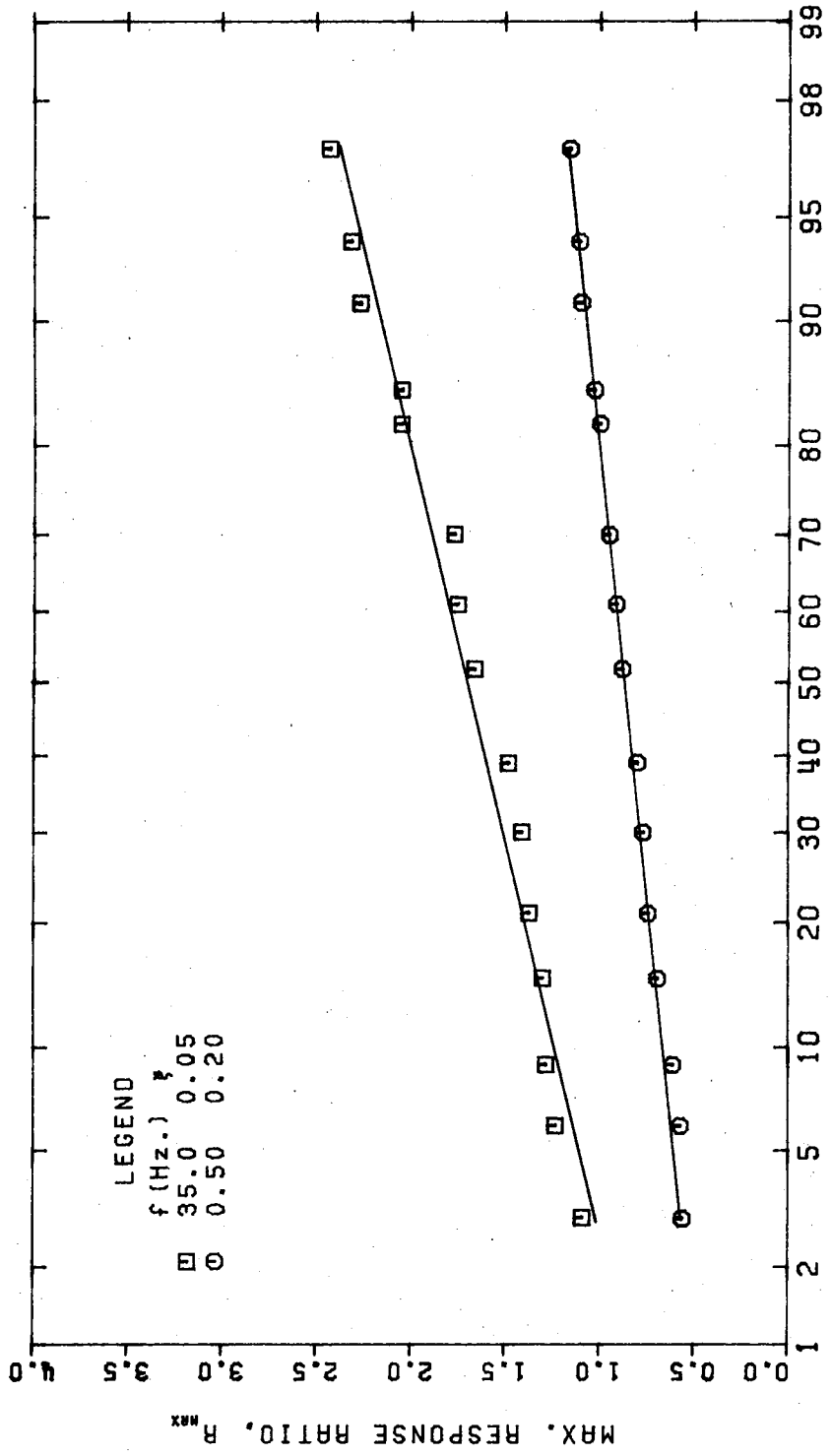

FIGURE 4.4 DISTRIBUTION IN RESPONSE - PEMBRIDGE.

5. SUMMARY AND CONCLUSIONS

This study has been devoted to the effect of dynamic interaction between bridge piers and time-varying ice loads. Extensive ice force data, recorded at two bridge piers in Alberta, Canada, have been used in the analysis. The time-varying characteristics of the ice force data have been discussed with reference to the way in which the ice fails on impact with the pier. For the data recorded at the massive Hondo pier, classifications have been made on the basis of the predominant failure type. Since only a small amount of data were available for the slender pile at Pembridge, the ice force histories recorded at this location have been considered in a single group.

For the purpose of dynamic analysis, bridge piers have been modelled by single-degree-of-freedom systems. The maximum response ratios of a range of these simple oscillators to each of the ice load histories have been evaluated and the results presented in the form of response spectra. Mean response spectra have been developed for each of the load categories considered. These mean curves reflect the response to the major dynamic characteristics in the load type and show that dynamic interaction can cause magnifications of almost twice the corresponding static effect. The greatest magnification occurs when the natural frequency of the pier is close to a characteristic failure frequency of the ice. Curves of coefficients of variation in the maximum response ratios have been used to discuss the

variation in response within each load group.

The present design procedure of the CSA Standard (CSA, 1978) neglects the effect of dynamic interaction between pier and load. Two approaches, which use the mean response spectra and curves of coefficients of variation developed in this study, are suggested for accounting for the dynamic effects. The first, or direct approach, enables dynamic effects to be incorporated into the current code format. In the second approach, the concepts of limits states design have been used to develop an expression for a single factored ice load which includes dynamic effects.

A design example has been used to demonstrate that the current code procedure may underestimate the effective ice load in the case of piers where dynamic effects are significant. In other cases, the proposed limit states design approach, which uses an improved estimate of static ice load proposed by Lipsett and Gerard (1980), shows that the design load given by the code may be conservative. In addition, while attention to the dynamic properties of a pier under design can enable dynamic effects to be minimized, all piers should be proportioned to withstand at least the full static effect of the load.

BIBLIOGRAPHY

Biggs, J.M. 1964. Introduction to structural dynamics. McGraw-Hill Inc., New York, N.Y.

Blenkarn, K.A. 1970. Measurements and analysis of ice forces on Cook Inlet structures. Proceedings 2nd. Offshore Technology Conference, Houston, TX., Vol. 11, pp. 365-378.

Canadian Standards Association. 1978. Design of highway bridges. CSA, Rexdale, Ont., Standard CAN3-S6-M78, pp. 34-36.

Clough, R.W. and Penzien, J. 1975. Dynamics of structures. McGraw-Hill Inc., New York, N.Y.

Englebrektson, A. 1977. Dynamic ice loads on a lighthouse structure. Proceedings of the 4th. International Conference on Port and Ocean Engineering under Arctic Conditions. Memorial University, St. Johns, Newfoundland, pp. 654-663.

Gerard, R. 1978. Mode of failure and the analysis of ice loads on bridge piers. Proceedings 4th. Symposium on Ice Problems, International Association For Hydraulic Research, Lulea, Sweden, pp. 335-348.

Galambos, T.V. and Ravindra, M.K. 1973. Tentative load and resistance factor design criteria for steel buildings. Research Report No.18, Civil Environmental Engineering Department, Washington University, St. Louis, Mo.

Lind, N.C. 1971. Consistent partial safety factors. A.S.C.E. Journal of the Structural Division, 97(ST6),

pp. 1651-1670.

Lipsett, A.W. 1980. Personal communication. Alberta Research Council.

Lipsett, A.W. and Gerard, R. 1980. Field measurements of ice forces on bridge piers, 1973-1979. Alberta Research Council, Transportation and Surface Water Engineering Division. Internal Report SWE-80/03.

Määttänen, M. 1975. Experiences of ice forces against a steel lighthouse mounted on the seabed and proposed constructional refinements. Proceedings 3rd. International Conference on Port and Ocean Engineering under Arctic Conditions, Fairbanks, Alaska, Vol. 11, pp. 857-869.

Määttänen, M. 1978. On conditions for the rise of self-excited ice-induced autonomous oscillations in slender marine pile structures. Finnish Board of Navigation, Winter Navigation Research Board, Research Report No.25.

Määttänen, M. 1979. Laboratory tests for dynamic ice-structure interaction. Proceedings 5th. International Conference on Port and Ocean Engineering under Arctic Conditions, at the Norwegian Institute of Technology, Vol. 11, pp. 1139-1153.

Matlock, H., Dawkins, N.P. and Panak, J.J. 1971. Analytical model for ice-structure interaction. A.S.C.E. Journal of the Engineering Mechanics Division, 97(EM4), pp. 1083-1092.

Michel, B. 1978. Ice mechanics. Les Presses de L'Université Laval, Quebec, Que.

Montgomery, C.J., Gerard, R. and Lipsett, A.W. 1980. Dynamic response of bridge piers to ice forces. Canadian Journal of Civil Engineering, Vol. 7, pp. 345-356.

Neill, C.R. 1970. Ice pressure on bridge piers in Alberta, Canada. Proceedings 1st. Symposium on Ice Problems, International Association for Hydraulic Research, pp. 6.1.1-6.1.8.

Neill, C.R. 1972. Force fluctuations during ice flow impact on piers. Proceedings 2nd. Symposium on Ice Problems, International Association for Hydraulic Research, Lenningrad, U.S.S.R.

Neill, C.R. 1976. Dynamic ice forces on piers and piles. An assesement of design guidelines in the light of recent research. Canadian Journal of Civil Engineering, Vol. 3, pp. 305-341.

Newmark, N.M. 1959. A method of computation for structural dynamics. A.S.C.E. Journal of the Engineering Mechanics Division, 85(EM3), pp. 67-94.

Nowak, A.S. and Lind, N.C. 1979. Practical Bridge Code Calibration. A.S.C.E. Journal of the Structural Division, 105(ST12), pp. 2497-2510.

Peyton, H.R. 1966. Sea ice strength. Report No. UAGR-182. Final report prepared for the Department of the Navy, Office of Naval Research, by Geophysical Institute,

University of Alaska.

Reddy, D.V. and Cheema, P.S. 1974. Response of an offshore structure to random ice forces. Proceedings International Conference on Engineering in the Ocean Environment, Halifax, Vol. 1, pp.84-88.

Reddy, D.V., Swamidas, A.S.J. and Cheema, P.S. 1975. Ice force response spectrum modal analysis of offshore towers. Proceedings 3rd. International Conference on Port and Ocean Engineering under Arctic Conditions, Fairbanks, Alaska, Vol. 11, pp. 887-910.

Sanden, E.J. and Neill, C.R. 1968. Determination of actual forces on bridge piers due to moving ice. Proceedings 1968 Convention, Canadian Good Roads Association, pp. 405-420.

Sundararajan, C. and Reddy, D.V. 1973. Stochastic analysis of ice-structure interaction. Proceedings 2nd. International Conference on Port and Ocean Engineering under Arctic Conditions, Reykjavik, Iceland, pp. 345-353.

Sundararajan, C. and Reddy, D.V. 1977. Probabilistic analysis of ice offshore structure interaction using enveloping step function power spectral densities. Canadian Journal of Civil Engineering, Vol. 4, pp. 455-461.

Swamidas, A.S.J., Reddy, D.V. and Purcell, G. 1977. Ice-structure interaction with artifically generated force records. Journal of Glaciology, 19(81), pp.

265-283.

Watts, F.J. and Podolny, W. 1978. Ice loads on bridge piers. Public Roads, 42(2), pp. 63-70.

APPENDIX A

A.1 Introduction

The ice load reaction recorded at the Pembridge pile during ice runs at spring break-up is related to the ice load by a transfer function. Because of the dynamic characteristics of the pile, the transfer function cannot be derived from statics alone. In particular, the pile magnifies frequency components in the load which are close to the fundamental natural frequency of the pile.

The purpose of this appendix is to show how the Pembridge load histories have been evaluated from the recorded ice force reactions. The transfer function which accounts for the dynamic characteristics of the pile is derived, and the analysis procedure developed is demonstrated with reference to example data.

A.2 Dynamic Model

In this section, an expression is derived which relates the time history of the reaction for the vertical pile at Pembridge to the components of the reaction associated with each mode of vibration.

In the derivation, the pile has been modelled by a simple beam of length, L, and mass per unit length, $\bar{m}$, (Fig. A.1.) In general, a horizontal ice load, F(s,t), may vary with position, s, along the beam and time, t. The resultant transverse displacement response, x(s,t), is also a function

of these variables. For each loading event, the ice force is assumed to act at a constant level, distance aL, from the lower support. The upper reaction at s = L is denoted by N(t).

Under the assumption that the pile is a distributed parameter system, the displacement response may be written as (Clough and Penzien, 1975)

$$x(s,t) = \sum_{n=1}^{\infty} \Phi_n(s)\, Y_n(t) \qquad \text{A.1}$$

This equation states that the total response is the sum of the responses in an infinite number of modes. The response in the n-th. mode consists of a constant shape, Φ_n, the amplitude of which varies with time according to the normalized displacement, Y_n. For the assumed simple end conditions, the shape function, Φ_n, is given by

$$\Phi_n(s) = \sin(n\pi s/L), \quad n=1,2,..\infty \qquad \text{A.2}$$

The time-varying component in the response, Y_n, is given by

$$\ddot{Y}_n(t) + 2\xi_n \omega_n \dot{Y}_n(t) + \omega_n^2 Y_n(t) = F_n(t)/M_n \qquad \text{A.3}$$

where a dot above Y_n represents one differentiation with respect to time.

The generalized mass of the beam, M_n, may be evaluated from

$$M_n = \int_0^L \Phi_n^2(s)\,\bar{m}\,ds \qquad \text{A.4}$$

which, using Eqn. A.2, reduces to

$$M_n = \bar{m}L/2 \qquad \text{A.5}$$

Similarly, the generalized load, $F_n(t)$, is defined by

$$F_n(t) = \int_0^L \Phi_n(s)\,F(s,t)\,ds \qquad \text{A.6}$$

which in this particular case reduces to

$$F_n(t) = Sin(n\pi a)\,F(t) \qquad \text{A.7}$$

In Eqn. A.3, ζ_n, is the damping ratio in the n-th. mode and ω_n, is the corresponding circular frequency of vibration. The latter may be evaluated from

$$\omega_n^2 = n^2\pi^2\sqrt{EI/\bar{m}L^4}\ , \quad n = 1, 2 \ldots \infty \qquad \text{A.8}$$

where the flexural rigidity of the beam is denoted by EI.

The shear on the beam corresponding to a given deflected shape is proportional to the third derivative of the displacement, x, with respect to position, s. In addition, assuming that the stresses produced by the internal damping are proportional to the rate of change of strain with time, the shear on the beam, Q(s,t), for any

position and time is given by

$$Q(s,t) = EI \frac{\partial^3 x(s,t)}{\partial s^3} + c_s I \frac{\partial^4 x(s,t)}{\partial s^3 \partial t} \qquad A.9$$

where c_s represents the internal damping, and is the constant of proportionality between stress and strain rate. By using Eqn. A.1, the shear may be written in the form

$$Q(s,t) = \sum_{n=1}^{\infty} EI \frac{d^3 \Phi_n(s)}{ds^3} Y_n(t) + \sum_{n=1}^{\infty} c_s I \frac{d^3 \Phi_n(s)}{ds^3} \dot{Y}_n(t) \qquad A.10$$

The reaction N(t), which is simply the shear when s = L, may be evaluated from

$$N(t) = Q(L,t) \qquad A.11$$

Accordingly, if Eqn. A.2 is substituted into Eqn. A.10, and the result is substituted into Eqn. A.11, we can write,

$$N(t) = -\sum_{n=1}^{\infty} EI \left(\frac{n\pi}{L}\right)^3 \cos n\pi \, Y_n(t) - \sum_{n=1}^{\infty} c_s I \left(\frac{n\pi}{L}\right)^3 \cos n\pi \, \dot{Y}_n(t) \qquad A.12$$

Eqn. A.12 relates the time history of the reaction to the time-varying component of the response, Y_n. By making appropriate substitutions in Eqn. A.12, the required relationship between reaction and load can be derived.

A.3 Derivation of Transfer Function

The dynamic effects of the system on the recorded reaction can be conveniently accounted for in the frequency domain. In this section, the transfer function, $T(\bar{\omega})$, is derived such that

$$F(\bar{\omega}) = T(\bar{\omega})\, N(\bar{\omega}) \qquad \text{A.13}$$

where $F(\bar{\omega})$ is the ice load and $N(\bar{\omega})$ is the reaction, both expressed as functions of circular frequency, $\bar{\omega}$.

The variables involved in the analysis can be transformed from the time to the frequency domain using Fourier transforms, (FT). A general function of time, P(t), composed of a range of frequency components has a Fourier transform, $P(\bar{\omega})$, defined by

$$FT[P(t)] = P(\bar{\omega}) = \int_{t=-\infty}^{+\infty} P(t)\, e^{-i\bar{\omega}t}\, dt \qquad \text{A.14}$$

The values of $P(\bar{\omega})$ reflect the magnitude and phase of all the harmonics contained in the complete time history. The following relationships can also be shown

$$FT[\dot{P}(t)] = i\bar{\omega}\, P(\bar{\omega}) \qquad \text{A.15(a)}$$

$$FT[\ddot{P}(t)] = -\bar{\omega}^2\, P(\bar{\omega}) \qquad \text{A.15(b)}$$

In addition, the inverse Fourier transform, (IFT), given by

$$IFT[P(\bar{\omega})] = P(t) = (1/2\pi)\int_{\bar{\omega}=-\infty}^{+\infty} P(\bar{\omega})\, e^{i\bar{\omega}t}\, d\bar{\omega} \qquad \text{A.16}$$

maps functions from the frequency to the time domain.

By taking the Fourier transform of both sides of Eqn. A.3, the governing equation of motion for the pile can be written as

$$-\bar{\omega}^2 Y_n(\bar{\omega}) + 2\xi_n \omega_n i\bar{\omega}\, Y_n(\bar{\omega}) + \omega_n^2\, Y_n(\bar{\omega}) = F_n(\bar{\omega})/M_n \qquad \text{A.17}$$

or

$$Y_n(\bar{\omega}) = H_n(\bar{\omega})\, F_n(\bar{\omega}) \qquad \text{A.18}$$

where

$$H_n(\bar{\omega}) = 1/[M_n \omega_n^2 (1 - \beta_n^2 + i 2\xi_n \beta_n)] \qquad \text{A.19}$$

and

$$\beta_n = \bar{\omega}/\omega_n \qquad \text{A.20}$$

The function, $H_n(\bar{\omega})$, called the modal complex frequency response, relates the frequency components in the response, $Y_n(\bar{\omega})$, to those in the modal generalized load, $F_n(\bar{\omega})$.

In the same way, the frequency components in the response, $Y_n(\bar{\omega})$, and reaction, $N(\bar{\omega})$, may be related by taking the Fourier transform of the time functions in Eqn. A.12. This gives

$$N(\bar{\omega}) = -\sum_{n=1}^{\infty} \left(\frac{n\pi}{L}\right)^3 \cos n\pi\, (EI + i\bar{\omega} C_s I)\, Y_n(\bar{\omega}) \qquad \text{A.21}$$

Further, the modal generalized load, $F_n(t)$, can be related to the ice load, $F(t)$, in the frequency domain, by using Eqn. A.7. This gives

$$F_n(\bar{\omega}) = Sin(n\pi a).F(\bar{\omega}) \qquad A.22$$

Substituting Eqns. A.18 and A.22 into A.21, results in the following expression for $N(\bar{\omega})$

$$N(\bar{\omega}) = \sum_{n=1}^{\infty} -\left(\frac{n\pi}{L}\right)^3 Cos\, n\pi\, (EI + i\bar{\omega} C_s I) H_n(\bar{\omega})\, Sin(n\pi a)\, F(\bar{\omega}) \qquad A.23$$

By using Eqns. A.19, A.5 and A.8, Eqn. A.23 can be written in the form

$$N(\bar{\omega}) = \sum_{n=1}^{\infty} -\frac{2}{\pi} \frac{Cos\, n\pi\, Sin\, n\pi a}{n} \frac{(1 + i\bar{\omega} C_s/E)}{(1 - \beta_n^2 + i2\xi_n \beta_n)}\, F(\bar{\omega}) \qquad A.24$$

If the damping is assumed to be stiffness proportional, then for orthogonality conditions to be satisfied, the damping term, c_s/E, is also given by $2\xi_n/\omega_n$ (Clough and Penzien, 1975). Therefore, with $Cos(n\pi) = (-1)^n$, Eqn. A.24 can be rearranged to give

$$F(\bar{\omega}) = \left\{ 1 \Big/ \left[\sum_{n=1}^{\infty} -\frac{2}{\pi} (-1)^n \frac{Sin\, n\pi a}{n} \frac{(1 + i2\xi_n \beta_n)}{(1 - \beta_n^2 + i2\xi_n \beta_n)} \right] \right\} N(\bar{\omega}) \qquad A.25$$

which is similar in form to Eqn. A.13, if the transfer function, relating the frequency components of the load and reaction is defined by

$$T(\bar{\omega}) = 1/\left[\sum_{n=1}^{\infty} \frac{-2}{\pi} (-1)^n \frac{\sin n\pi a}{n} \frac{(1+i2\xi_n\beta_n)}{(1-\beta_n^2+i2\xi_n\beta_n)}\right] \qquad \text{A.26}$$

A.4 Application

In this study a computer program was written to develop the ice force time history from the measured reaction time history. The program is listed on pp.104. The major steps involved are presented below, with reference to an example set of data. In the following, for convenience, functions of circular frequency, $\bar{\omega}$, are referred to in terms of cyclic frequency, $\bar{f} = \bar{\omega}/2\pi$.

(1) Read in reaction time history, N(t).

Fig. A.2 shows a typical reaction time history recorded at Pembridge.

(2) Transform N(t) to the frequency domain.

For numerical analysis of the digitized reaction time histories, the Fourier transform of Eqn. A.14 is replaced by the discrete equivalent and evaluated using fast Fourier transform (FFT) algorithims. Hence,

$$FFT[N(t)] = N(\bar{f})$$

Accordingly, the harmonic coefficients $N(\bar{f})$ are evaluatated at discrete frequencies, $\bar{f}$.

A plot of $N(\bar{f})$ is shown in Fig. A.3 for the time history of Fig. A.2. Consistent with the procedure presented by Michel (1978) which relates the crushing

frequency of the ice to the ice velocity and thickness, it has been assumed that all significant frequency components in the load are less than 50 Hz. The coefficients corresponding to higher frequencies are set equal to zero. The plot shows that the harmonic components in the region of 12 Hz are relatively large. Resonance of the pile in the fundamental mode amplifies the response of these frequency components.

(3) Evaluate the transfer function, $T(\bar{f})$.

In general, the transfer function is given by Eqn. A.26. For practical analysis, it is sufficient to consider only those modal components which provide significant contributions to the response. In this case, consideration of the first ten modes has been assumed to give sufficiently accurate results. In addition, due to the high frequencies of oscillation associated with the higher modes, the contribution to the response of the fourth and higher modes is essentially a static effect. This is indicated, mathematically, by the term β_n^2 in Eqn. A.26 approaching zero. Therefore, in the calculations, $T(\bar{f})$ has been approximated by,

$$T(\bar{f}) = 1 \Big/ \left[\sum_{n=1}^{3} \frac{-2}{\pi} (-1)^n \frac{\sin n\pi a}{n} \frac{(1 + i2\xi_n\beta_n)}{(1-\beta_n^2 + i2\xi_n\beta_n)} + \sum_{n=4}^{10} \frac{-2}{\pi} (-1)^n \frac{\sin n\pi a}{n} \right]$$

The plot of the transfer function, $T(\bar{f})$, in Fig. A.4 shows that, for low frequency components, $T(\bar{f})$ is

approximately 2.5. This is simply the static relationship between load and reaction, as for the force history under consideration the water level corresponded to a value for aL of about 0.4L. Since the dynamic characteristics of the pier magnify the frequency components of the load near the natural frequency of vibration for the pier, the values of the transfer function are significantly reduced at 12 Hz.

(4) Evaluate the ice load, $F(\bar{f})$.

Each harmonic component of the reaction, $N(\bar{f})$, is multiplied by its transfer function, $T(\bar{f})$, to give the corresponding harmonic component of the ice load, $F(\bar{f})$. Figure A.5 shows a plot of $F(\bar{f})$, derived from the reaction of Fig. A.3. The dynamic effects of the pile have been eliminated as indicated by the absence of relatively large components at 12 Hz.

(5) Evaluate the ice load time history, $F(t)$, from $F(\bar{f})$.

This is achieved by using the inverse fast Fourier transform (IFFT) algorithims. Hence,

$$F(t) = IFFT[F(\bar{f})]$$

The corrected ice load time history, $F(t)$, is shown in Fig. A.6. The function is independent of any characteristic of the load measuring system. As can be seen from Fig. A.6, it is similar in overall form to the reaction time history of Fig. A.2. with, however, significantly different frequency components.

The above procedures have been applied to each of the reaction time histories to give the ice loads on the Pembridge pile. The ice load time histories are presented in full in Appendix B.

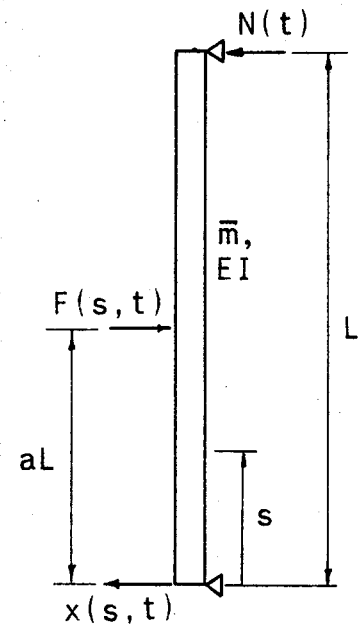

FIGURE A.1 SIMPLY SUPPORTED BEAM,
DISTRIBUTED PARAMETER SYSTEM.

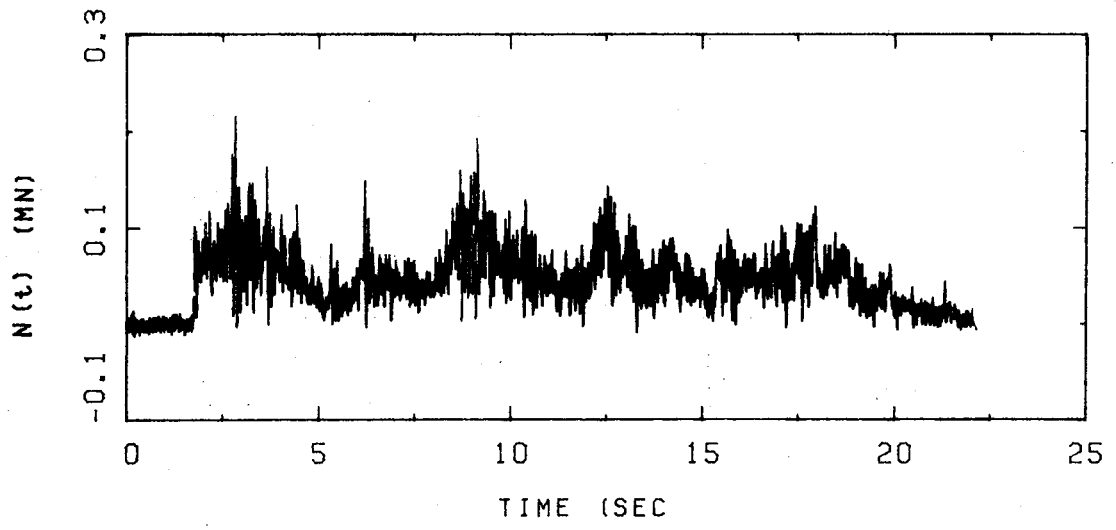

FIGURE A.2 REACTION TIME HISTORY

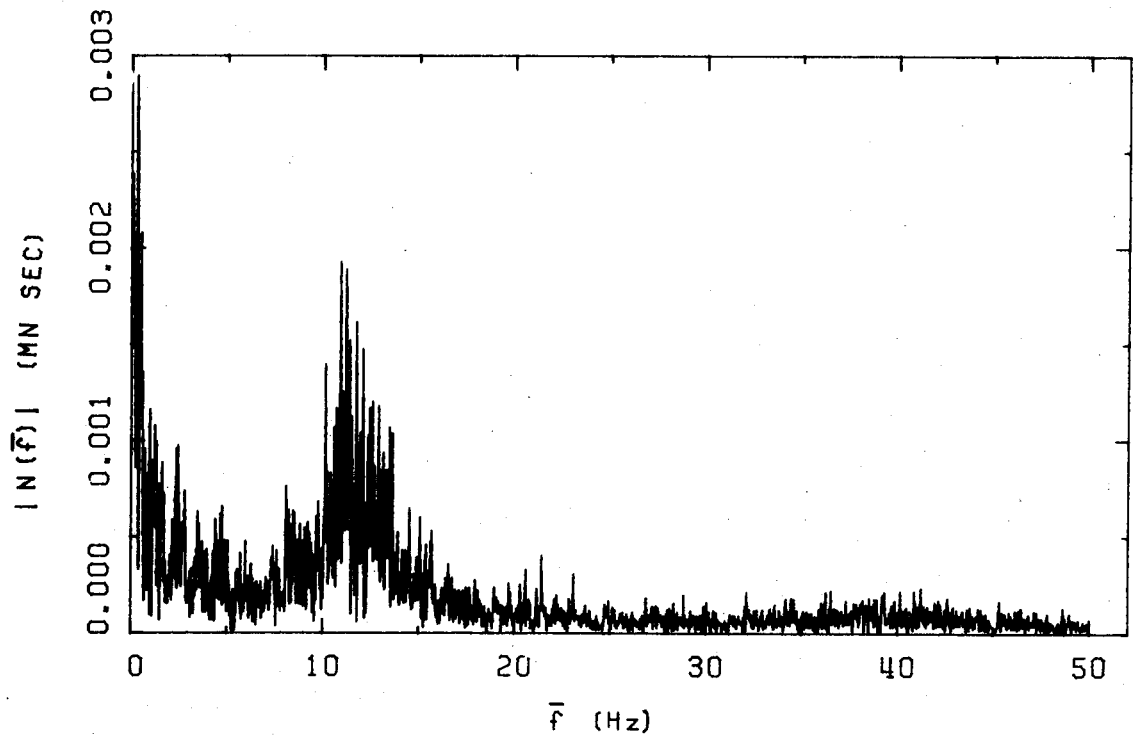

FIGURE A.3 FOURIER TRANSFORM OF REACTION

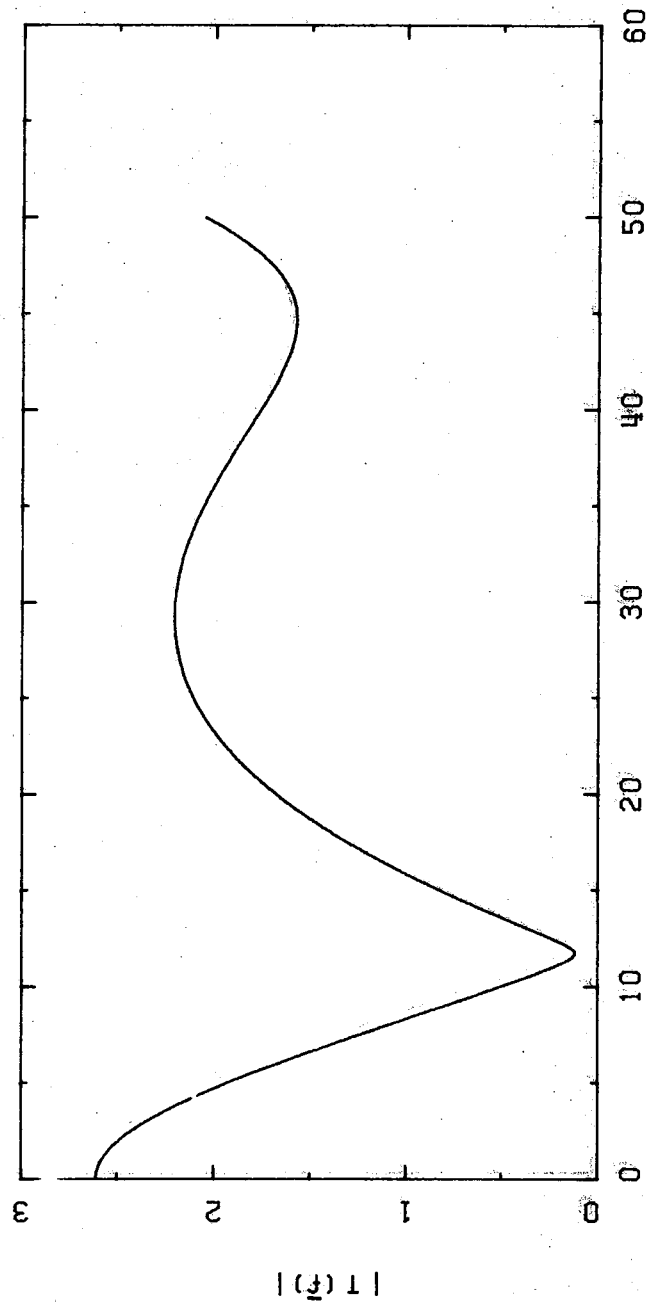

FIGURE A.4 TRANSFER FUNCTION

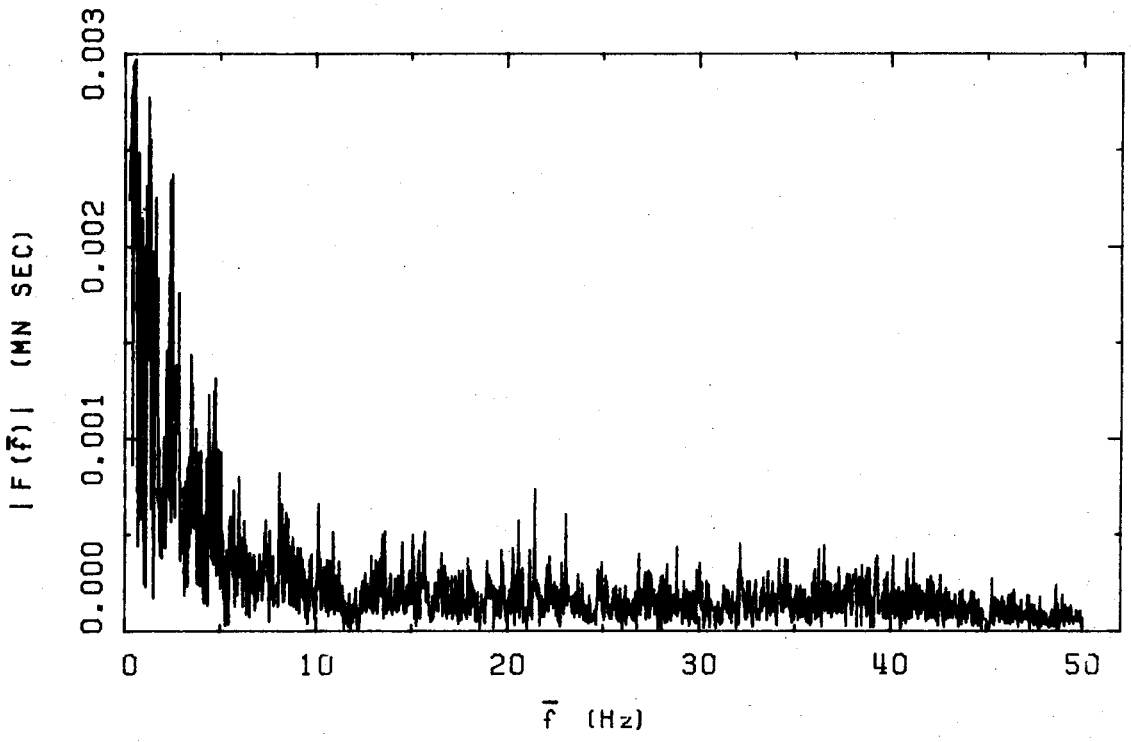

FIGURE A.5 FOURIER TRANSFORM OF ICE FORCE

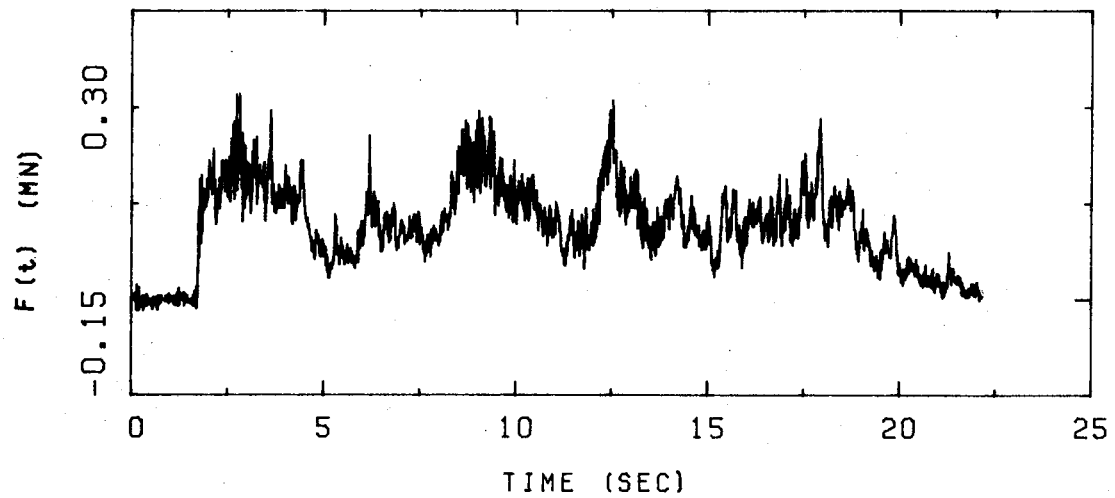

FIGURE A.6 ICE FORCE TIME HISTORY

```
C
C     PROGRAM TO DETERMINE ICE LOAD HISTOY, F(t), FROM
C     RECORDED REACTION, N(t), ON A SIMPLY SUPPORTED PILE.
C
C
C     PRINCIPAL VARIABLES
C
C     F    Ice Force.
C     RN    Reaction.
C     X    Fourier Transform of Reaction and
C          corrected Fourier Transform of Load.
C     T    Transfer Function.
C     H    Inverse of Transfer Function.
C     C    Fraction Reaction is of Load.
C     W    Frequency Increment.
C     WF   Frequency of Load Harmonic.
C     TP   Record Duration
C     NL   Number of lines in Reaction File.
C     K    Total No. of Data Points.
C     K50 No. of Data Points up to 50 Hz.
C
C
      IMPLICIT REAL*8(A - H,O - Z)
      COMPLEX*16 B, X(35000), T, H
      COMMON /BLK1/ RN(35000), F(35000)
      COMMON /BLK2/ WK(100000)
      DATA NWKSIZ /100000/
      CALL FTNCMD('EQUATE 96=SERCOM;')
C
C     Read in reaction time history
C
      READ (5,150) (NL,C,K)
      NL = NL + 10
      DO 10 I = 1, 150
      RN(I) = 0.0D0
   10 CONTINUE
      DO 20 I = 11, NL
      L = (I - 1) * 15
      READ (5,160) (RN(L + J),J=1,15)
   20 CONTINUE
C
C     Add zeros to RN
C
      J = 15 * NL + 1
      DO 30 I = J, K
      RN(I) = 0.0D0
   30 CONTINUE
C
C     Calculate FT of RN and store in X
C
      CALL FFTRC(RN, K, X, WK, WK)
      M = K / 2 + 1
      DO 40 I = 1, M
      X(I) = DCONJG(X(I)) / K
   40 CONTINUE
C
C     Evaluate K50, (time step = .004),
C     Record duration and freq. increment.
C
      K50 = 50 * K * .004
   50 TP = K * .004D0
      W = 2 * 3.1415D0 / TP
C
C     Evaluate transfer function and
C     corrected Fourier transform.
C
      DO 100 L = 1, K50
      WP = (L - 1) * W
      ZE = 1.002D-3 * WP
      H = DCMPLX(0.0D0,0.0D0)
      DO 90 I = 1, 10
      A = -0.63662D0 *
     P DSIN(C*I*3.14159D0) / I * (-1) ** I
      IF (I .GT. 3) GO TO 70
   60 B = DCMPLX(1.0D0,ZE) /
     P DCMPLX(1.0D0-((WP/(73.83D0*I**2))**2),ZE)
      GO TO 80
   70 B = DCMPLX(1.0D0,0.0D0)
   80 H = H + A * B
   90 CONTINUE
      T = DCMPLX(1.D0,0.D0) / H
      X(L) = C * X(L) * T
  100 CONTINUE
C
C     Array X now contains FT of forcing function.
C
C     Zero components above 50 Hz.
C
  110 L = K50 + 1
      DO 120 I = L, M
      X(I) = DCMPLX(0.D0,0.D0)
  120 CONTINUE
C
C     Expand X over complete frequency range.
C
      L = K / 2
      DO 130 I = 2, L
      X(K + 2 - I) = DCONJG(X(I))
  130 CONTINUE
C
C     Evaluate force history using IFT.
C
      CALL FFTCC(X, K, WK, WK)
C
C     Write force history
C
      DO 140 I = 1, K
      F(I) = REAL(X(I)) / 1000.D0
  140 CONTINUE
      WRITE (11,190) (F(I),I=1,K)
C
C
  150 FORMAT (I4, F5.2, I6)
  160 FORMAT (15F8.3)
  190 FORMAT (15F8.3)
  200 STOP
      END
```

APPENDIX B

B.1 Introductory remarks

The complete set of ice load histories and response spectra, used in the study, are presented in this appendix. The Hondo data are grouped under 3 headings: bending, crushing and splitting failure. The Pembridge data are presented in a single group.

In the following, the load history/response spectra combinations are presented in pairs (i.e. 2 load histories followed by the corresponding spectra). The plots are labelled according to the date and time when the maximum force in the loading event was measured in the field.

B.2 Bending Failure Load Histories and Response Spectra - Hondo

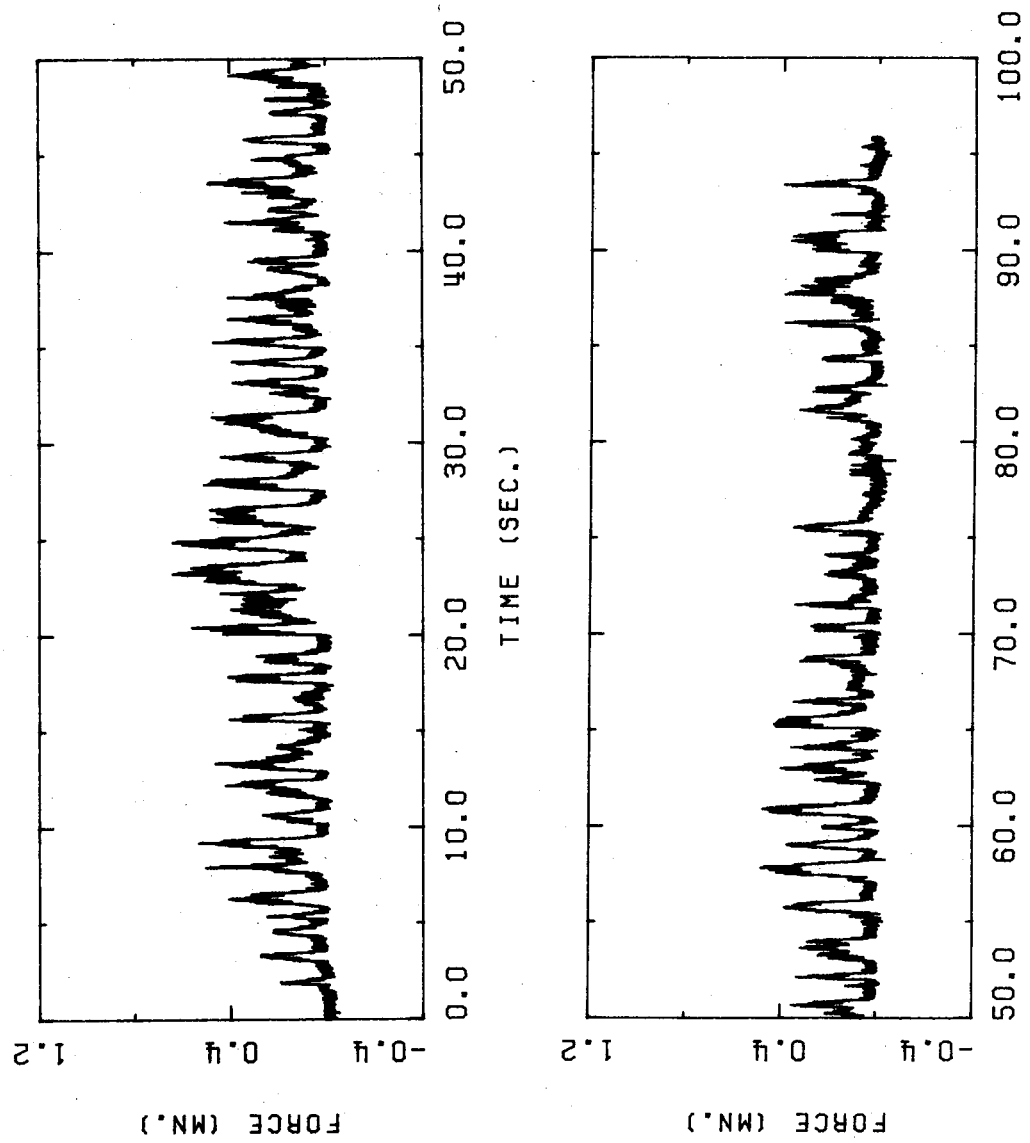

FIGURE B.1 HONDO 10 APRIL 1976 20H 27M 47S

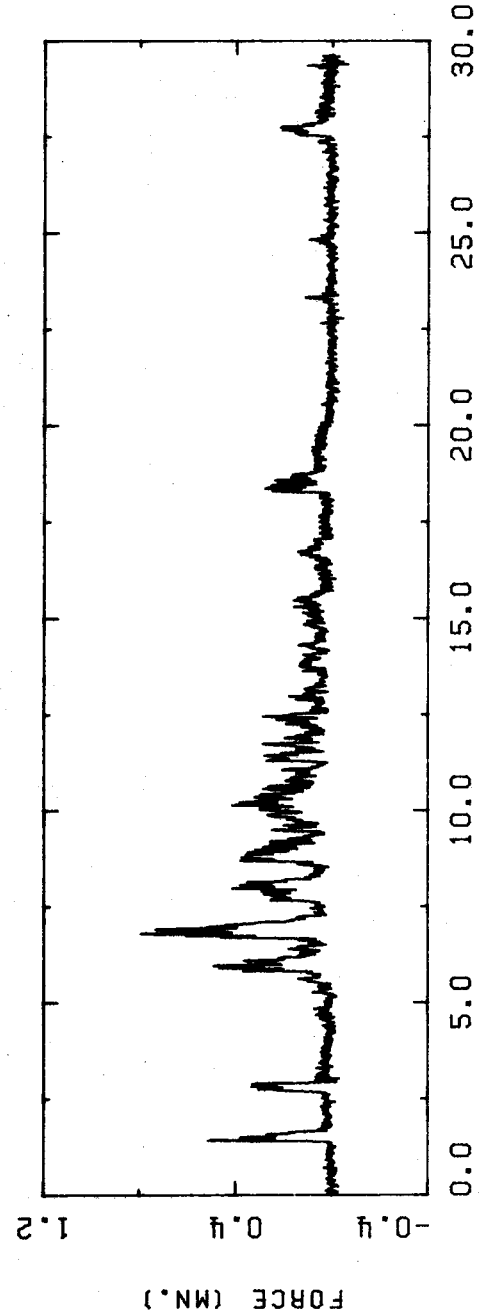

FIGURE B.2 HONDO 12 APRIL 1976 15H 45M 44S

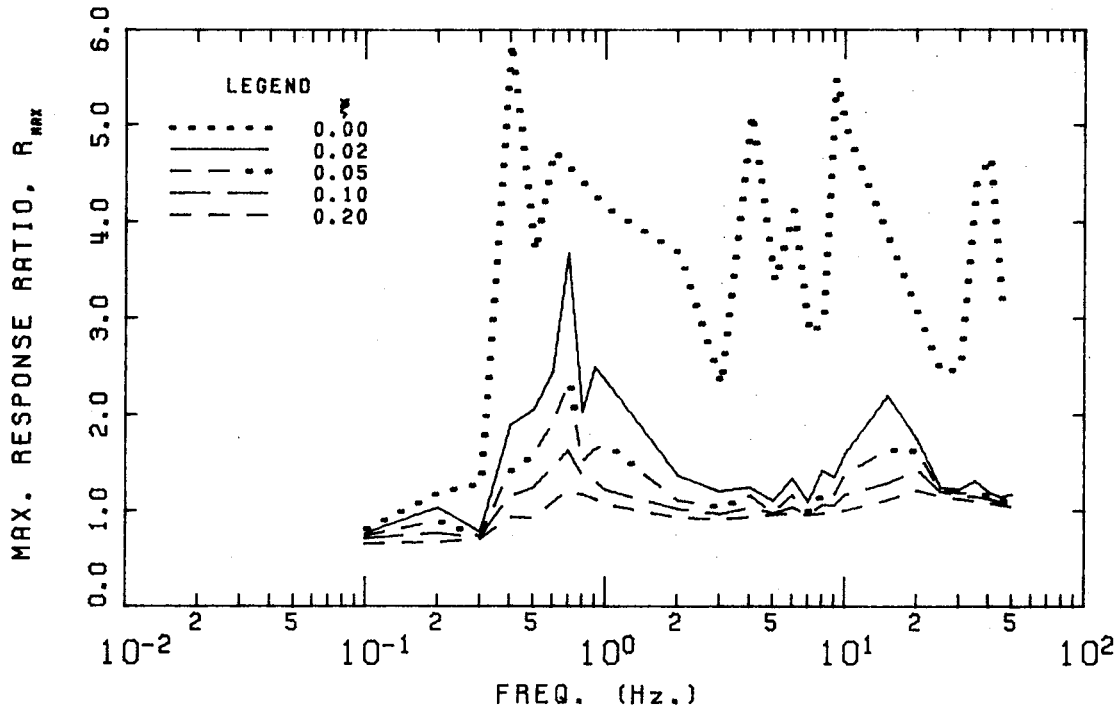

FIGURE B.3 HONDO 10 APRIL 1976 20H 27M 47S

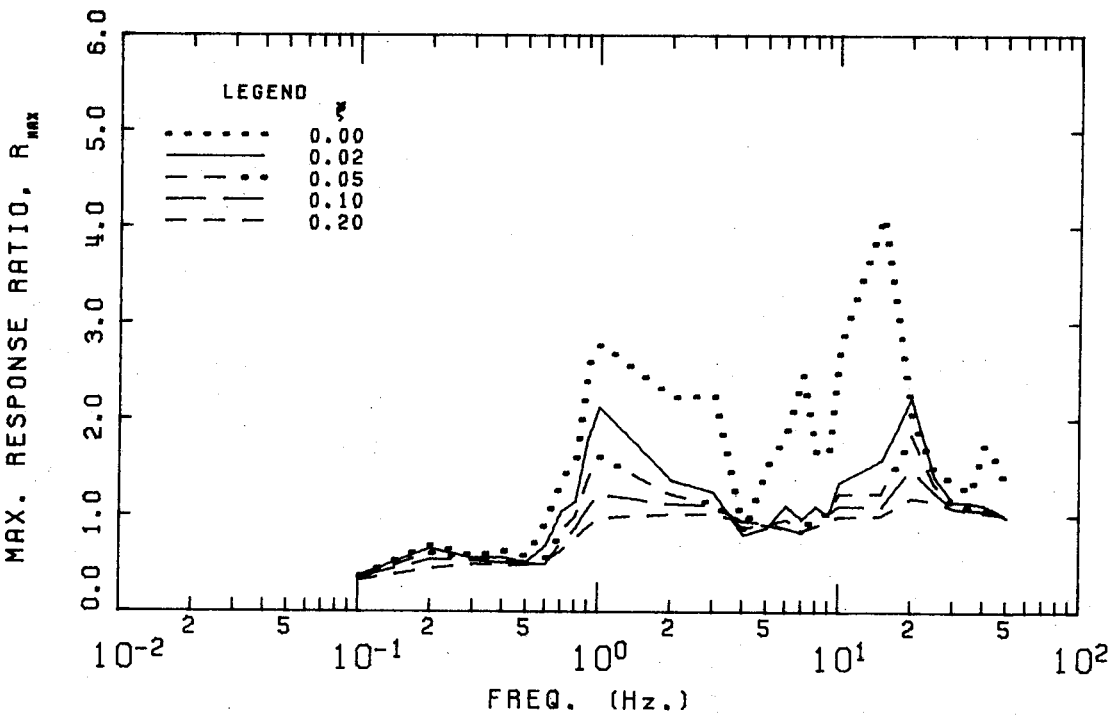

FIGURE B.4 HONDO 12 APRIL 1976 15H 45M 44S

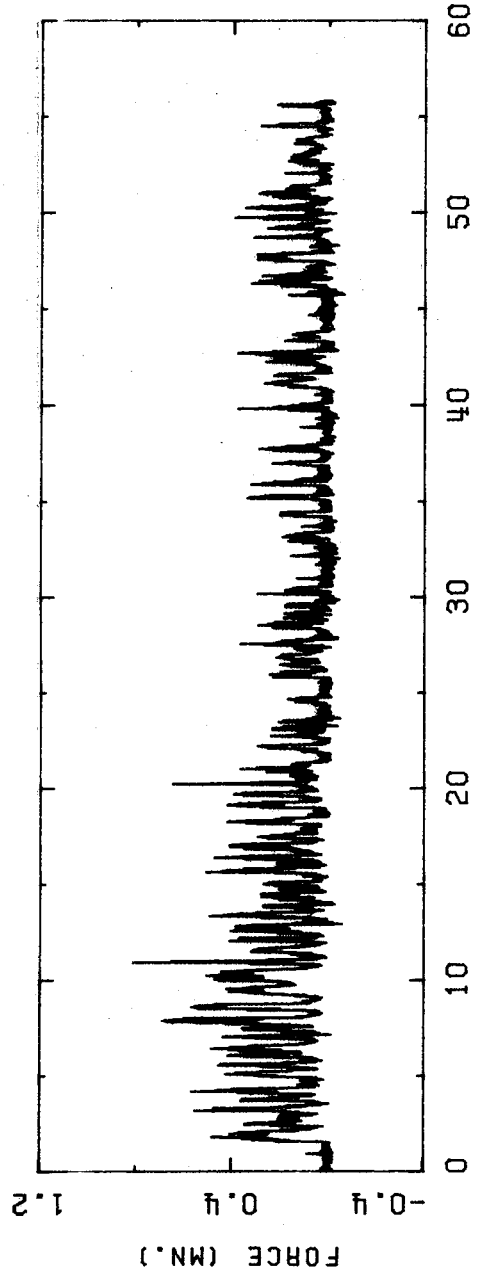

FIGURE B.5 HONDO 12 APRIL 1976 15H 46M 52S

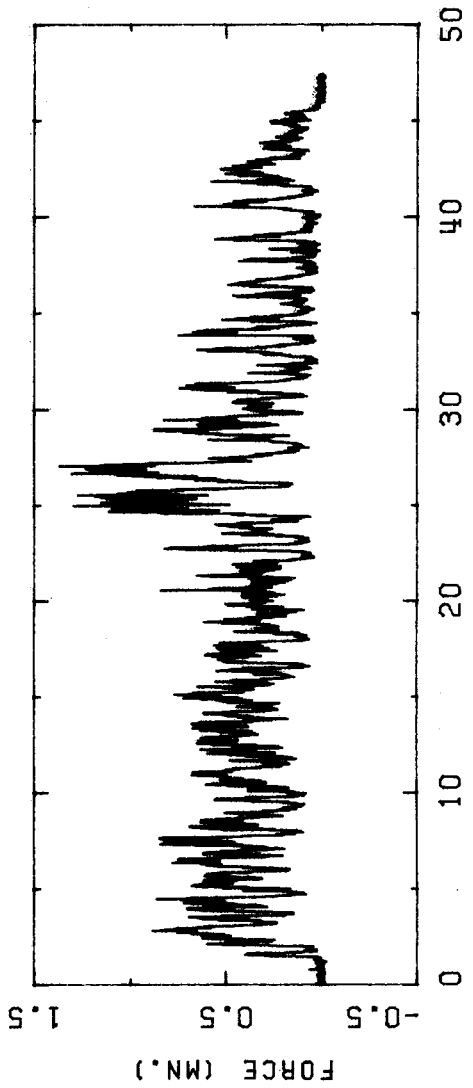

FIGURE B.6 HONDO 12 APRIL 1976 15H 50M 25S

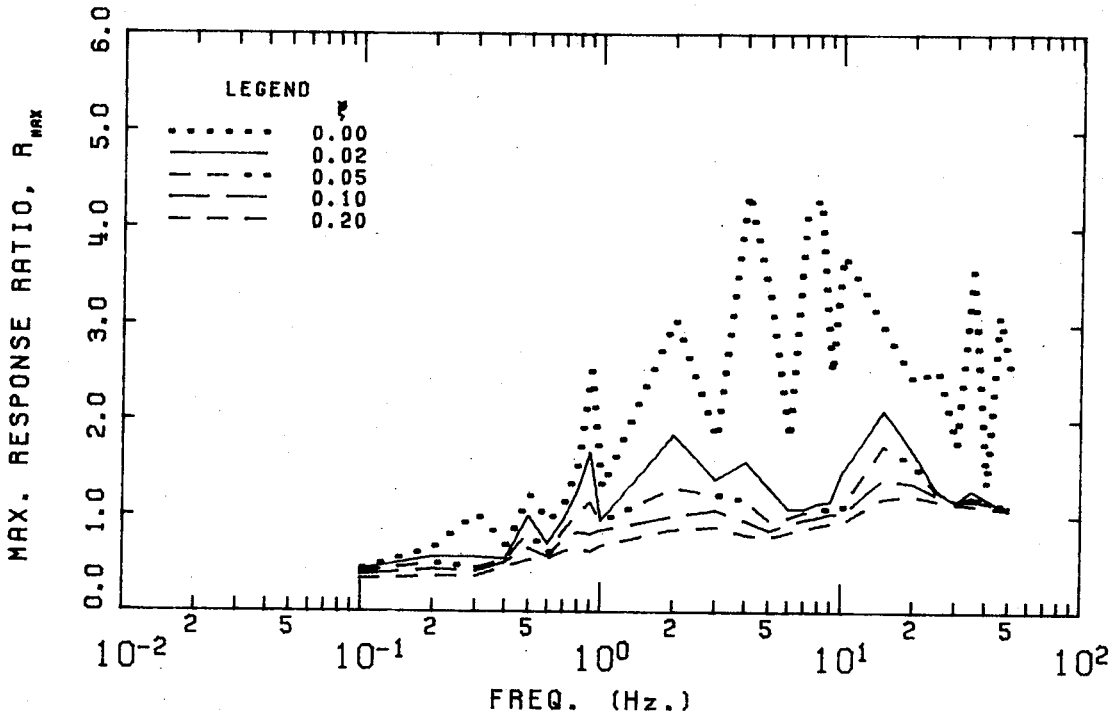

FIGURE B.7 HONDO 12 APRIL 1976 15H 46M 52S

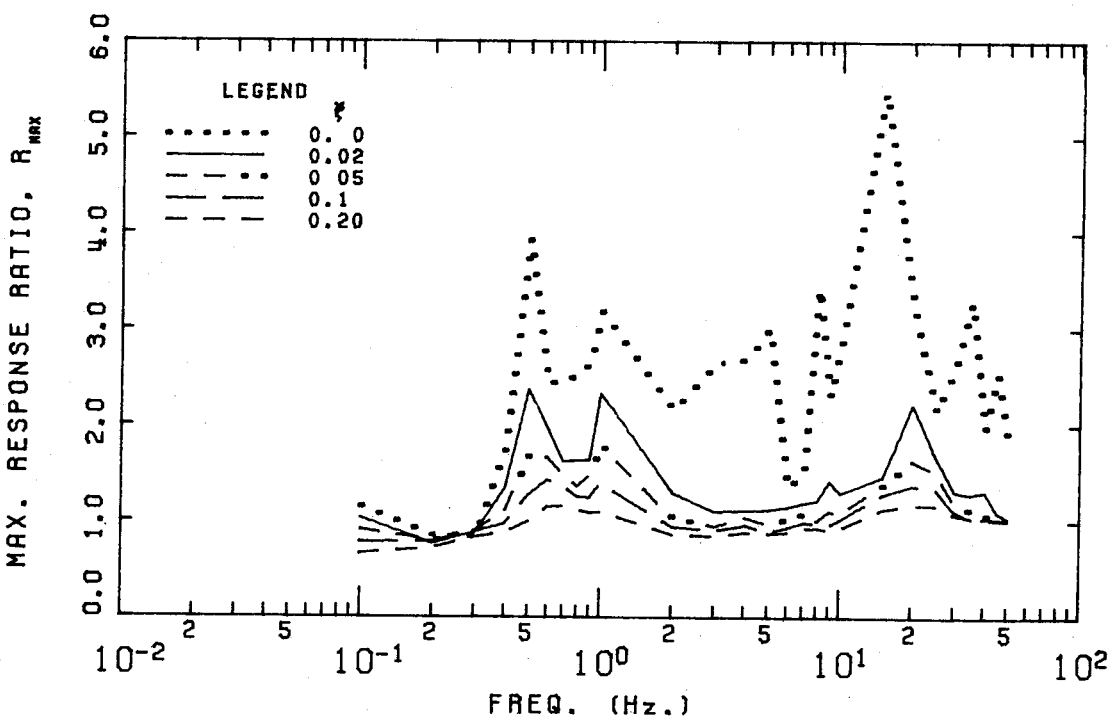

FIGURE B.8 HONDO 12 APRIL 1976 15H 50M 25S

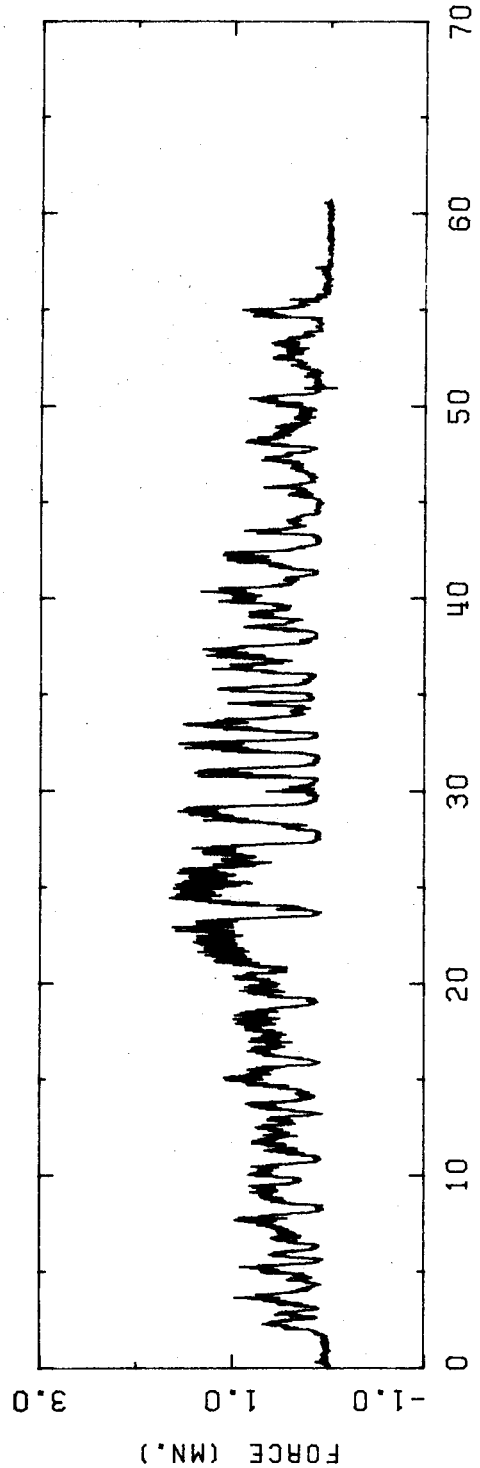

FIGURE B.9 HONDO 12 APRIL 1976 15H 52M 24S

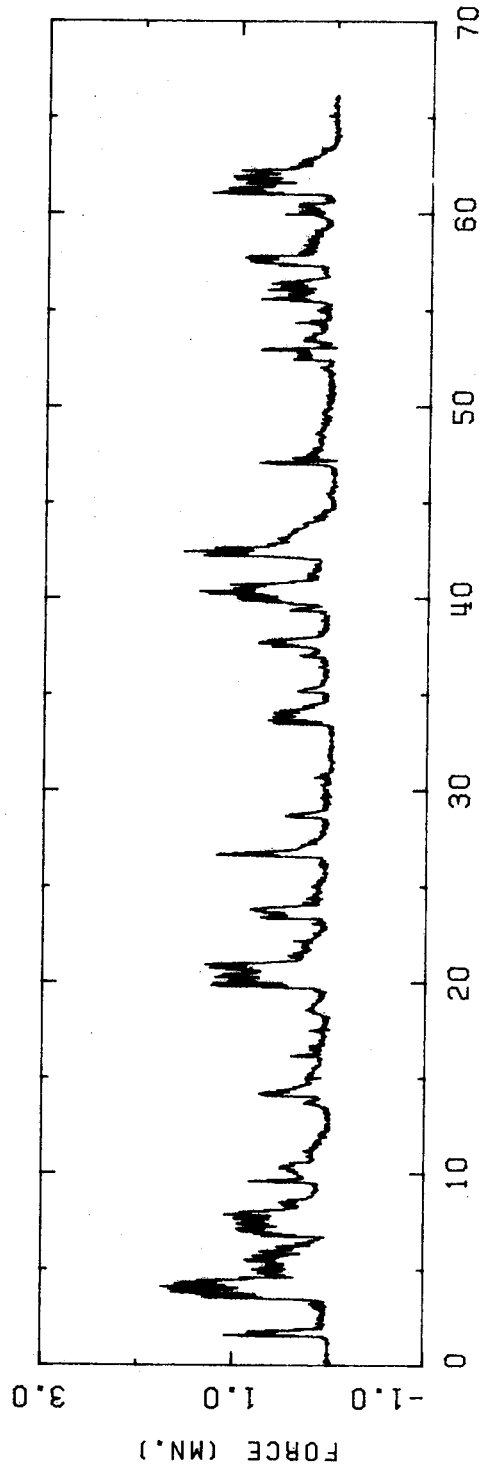

FIGURE B.10 HONDO 12 APRIL 1976 16H 03M 53S

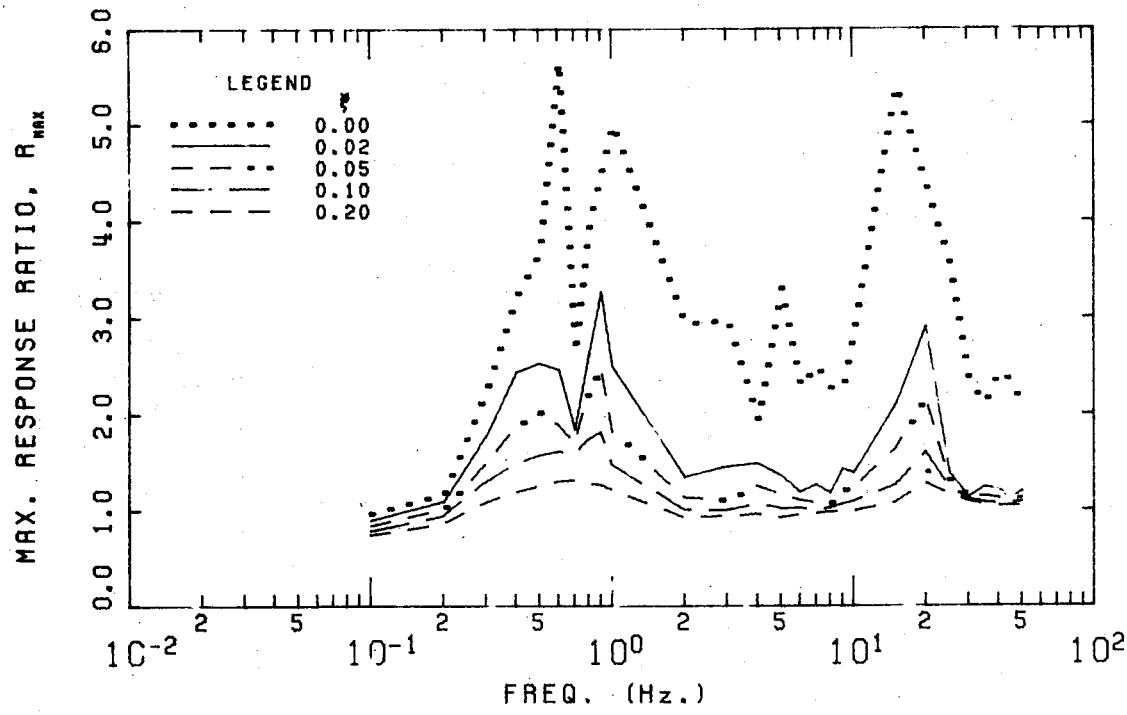

FIGURE B.11 HONDO 12 APRIL 1976 15H 52M 24S

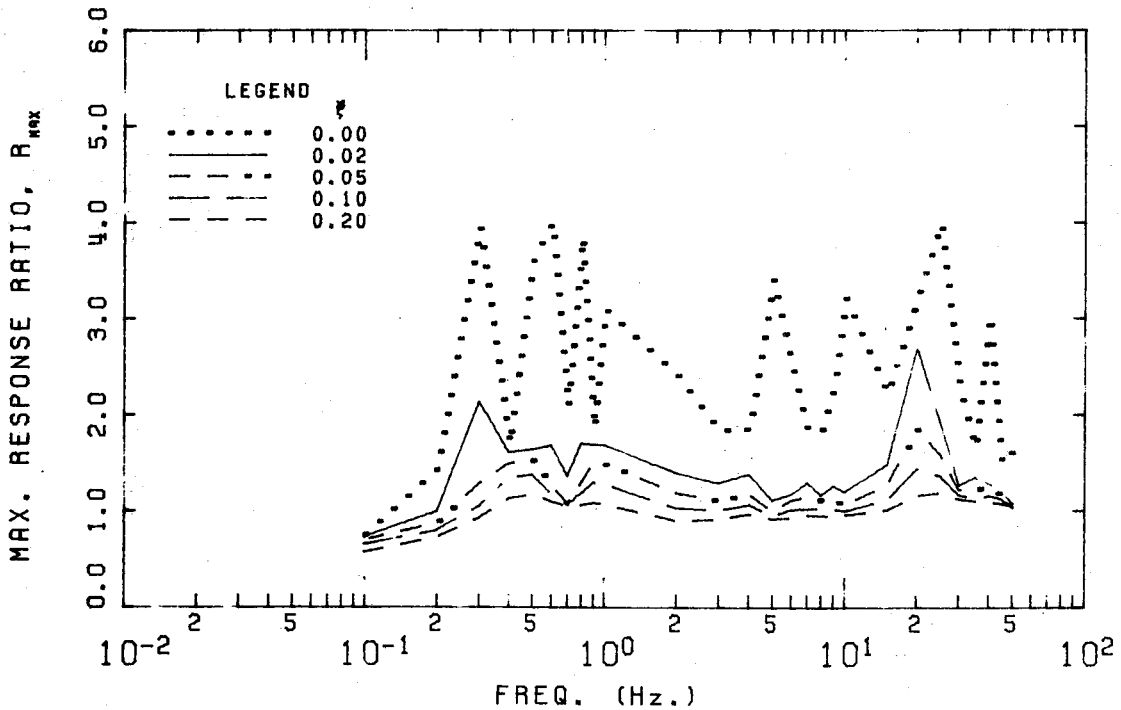

FIGURE B.12 HONDO 12 APRIL 1976 16H 03M 53S

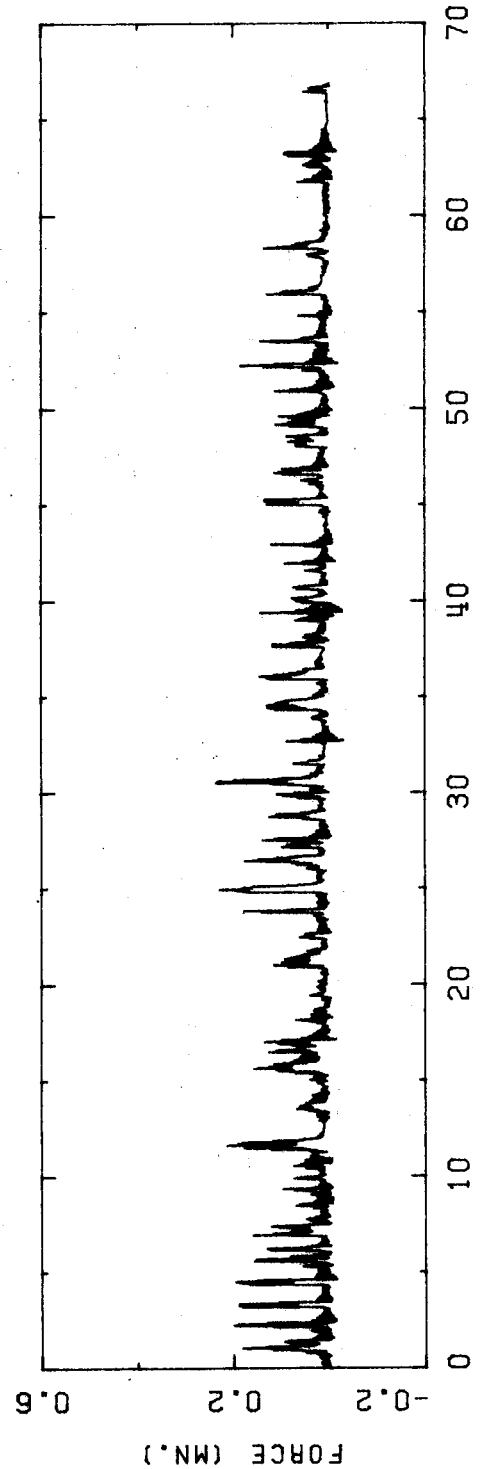

FIGURE B.13 HONDO 11 APRIL 1977 17H 22M 57S

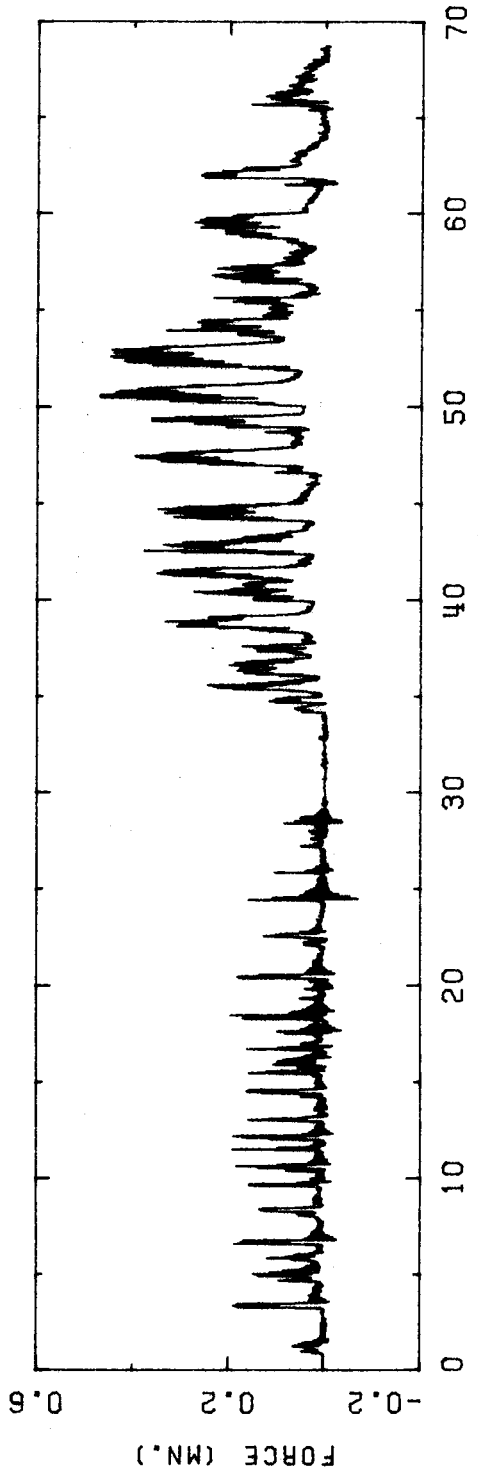

FIGURE B.14 HONDO 11 APRIL 1977 17H 23M 55S

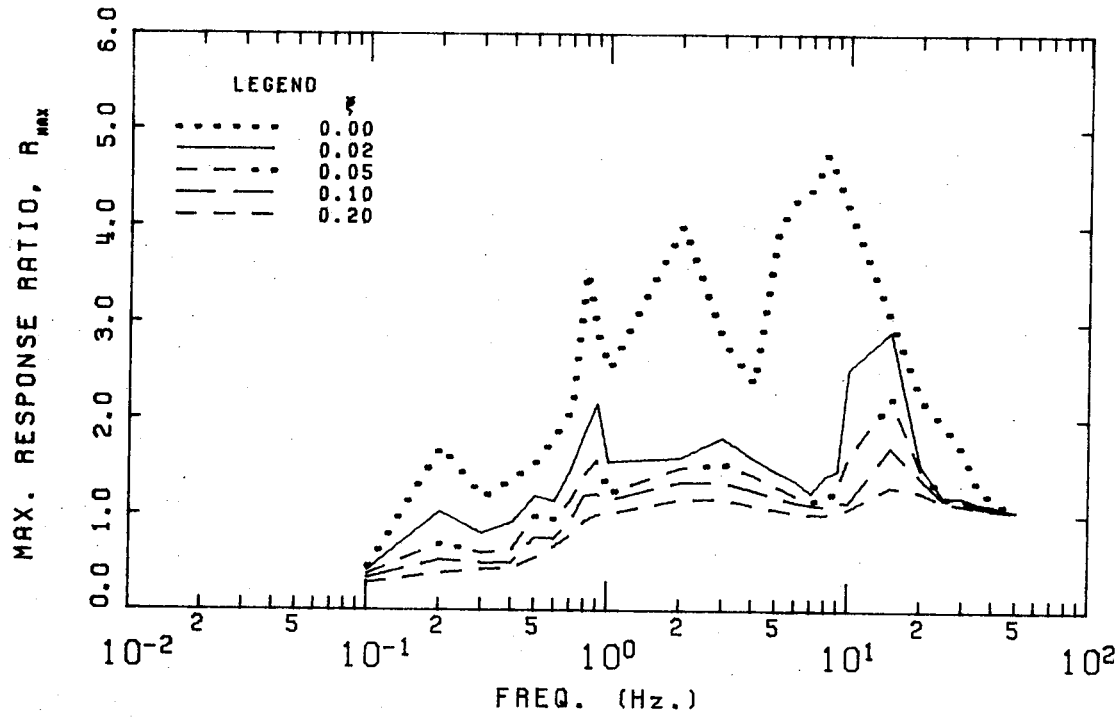

FIGURE B.15 HONDO 11 APRIL 1977 17H 22M 57S

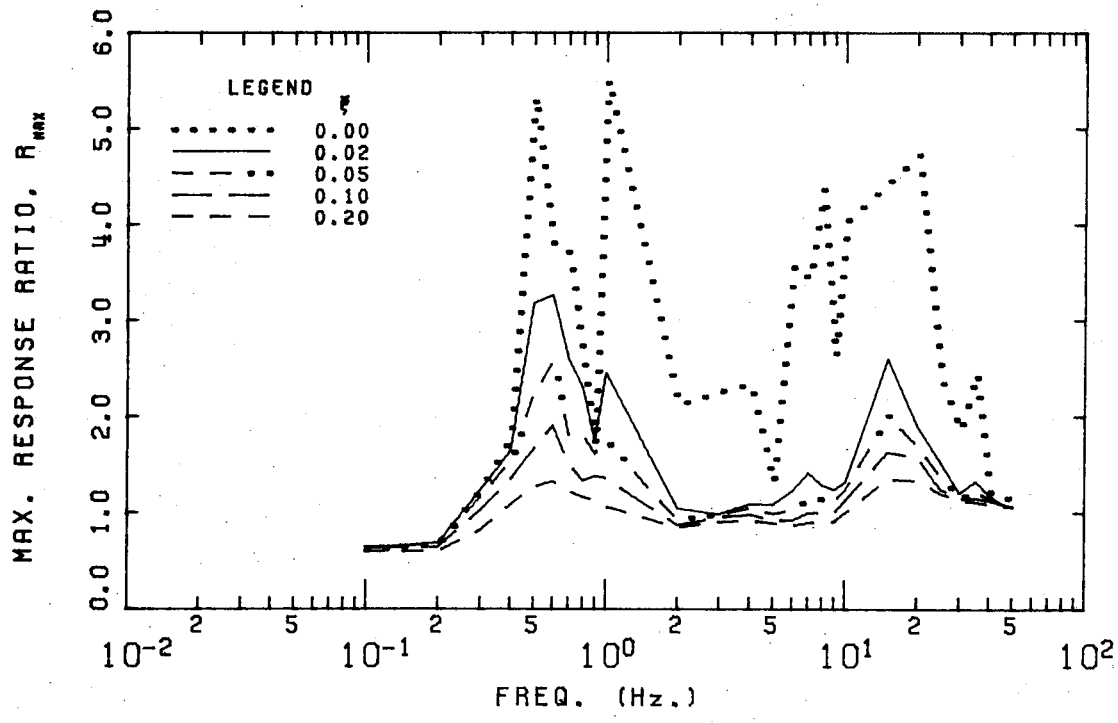

FIGURE B.16 HONDO 11 APRIL 1977 17H 23M 55S

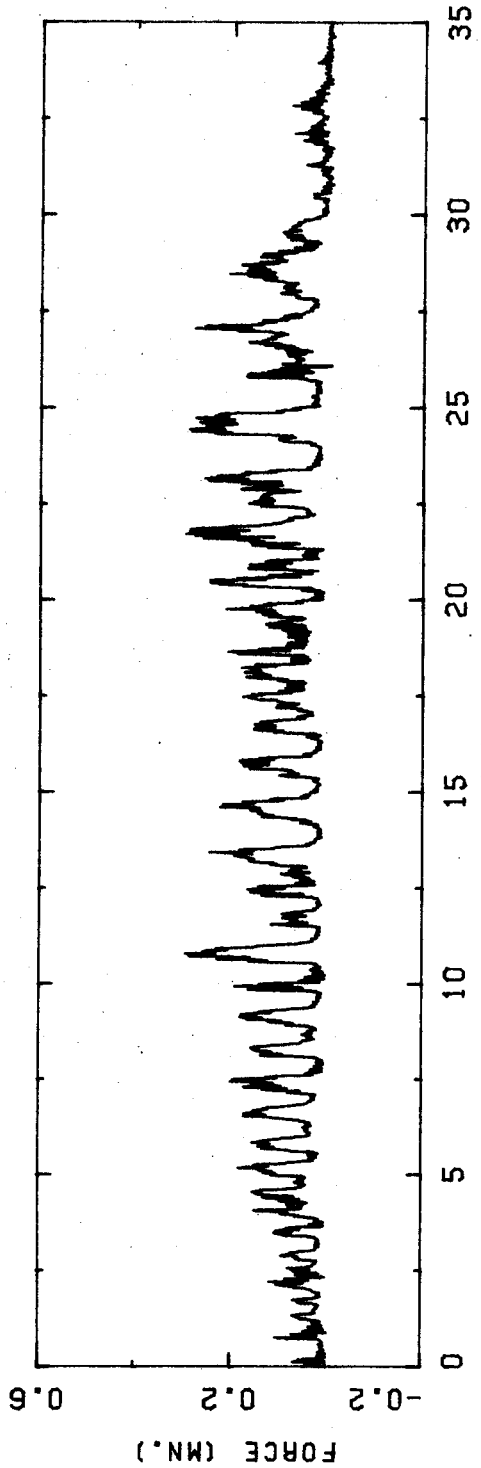

FIGURE B.17 HONDO 11 APRIL 1977 17H 41M 28S

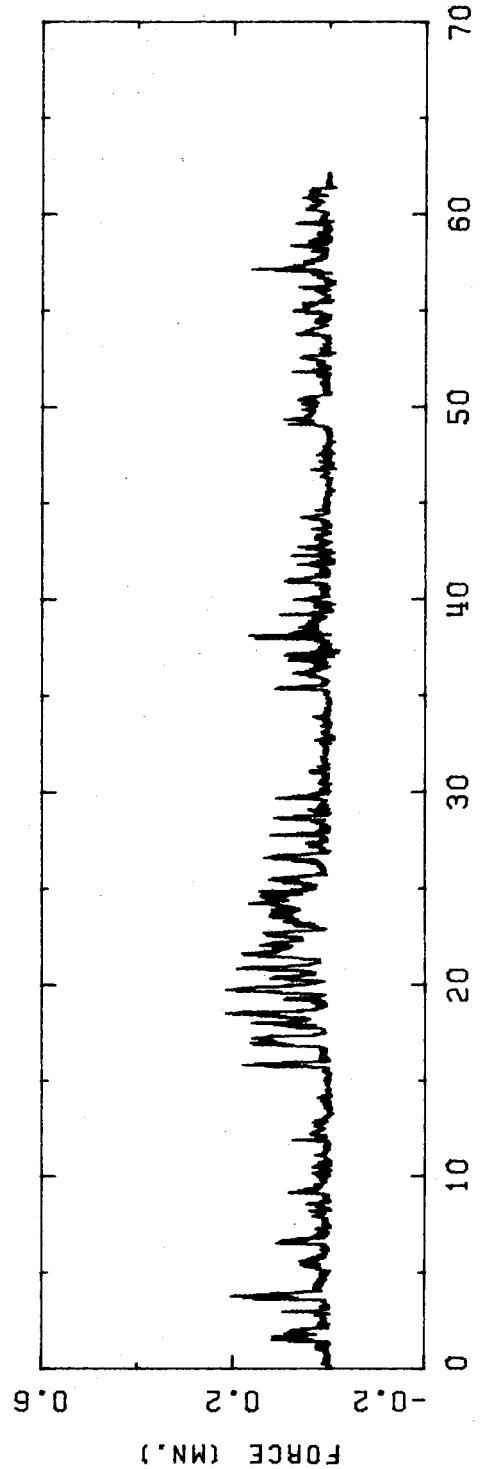

FIGURE B.18 HONDO 11 APRIL 1977 17H 42M 11S

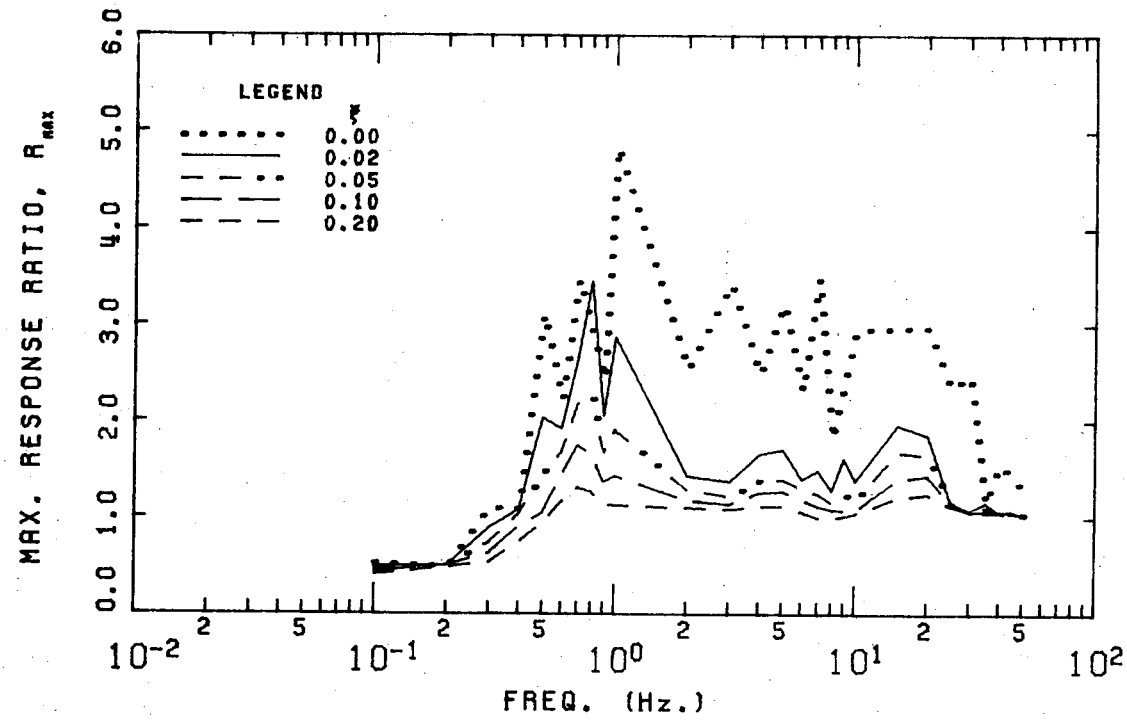

FIGURE B.19 HONDO 11 APRIL 1977 17H 41M 28S

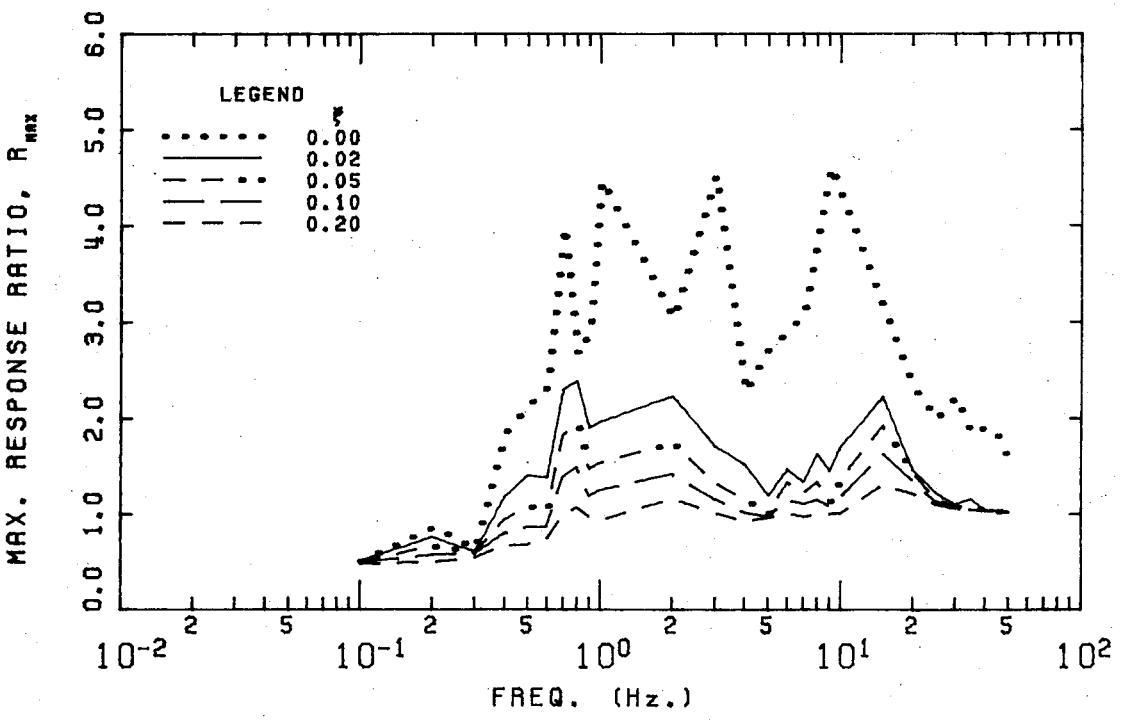

FIGURE B.20 HONDO 11 APRIL 1977 17H 42M 11S

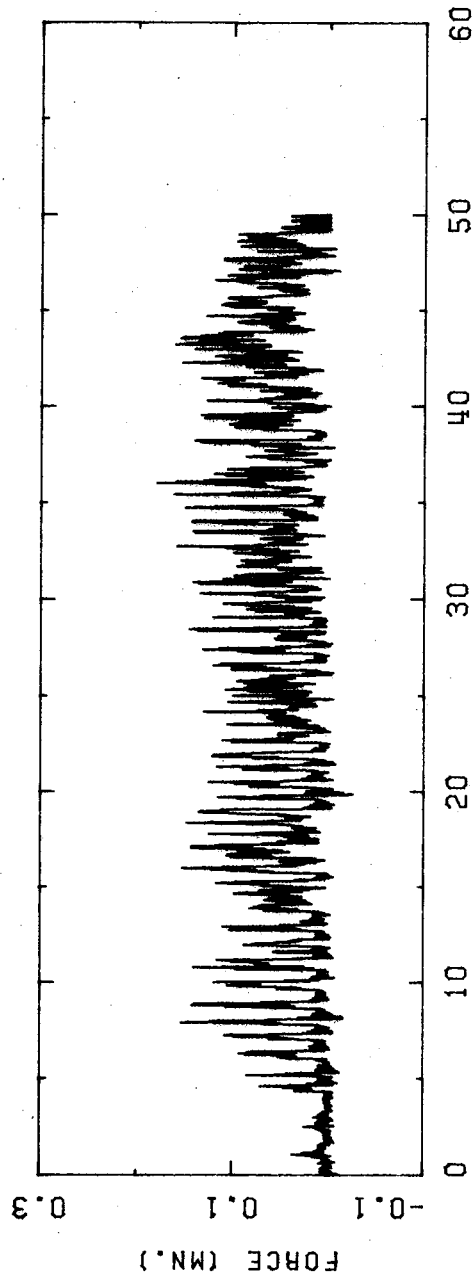

FIGURE B.21 HONDO 11 APRIL 1977 17H 44M 14S

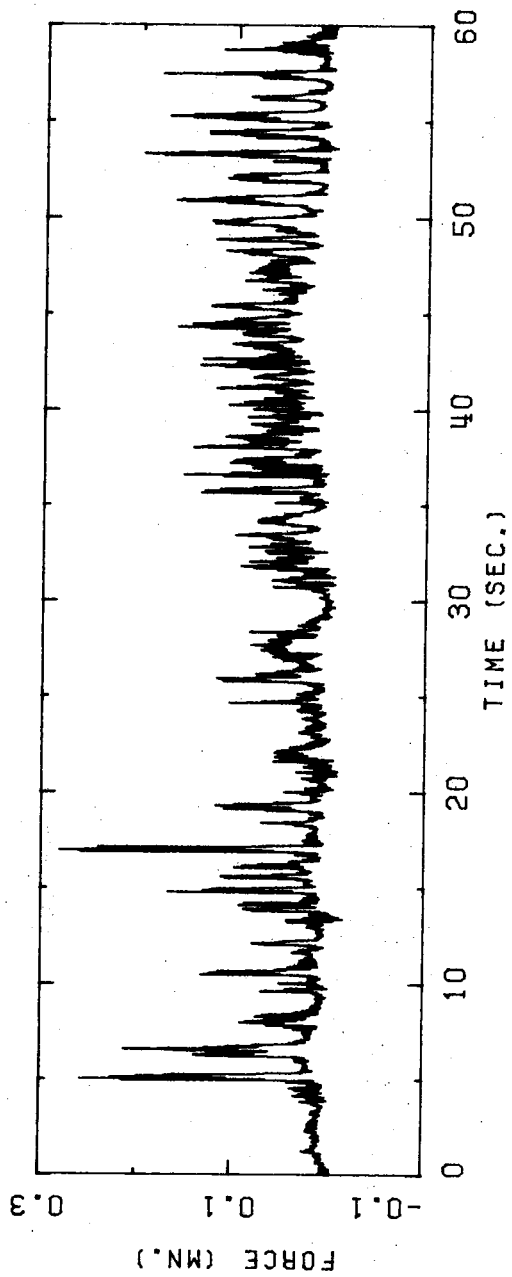

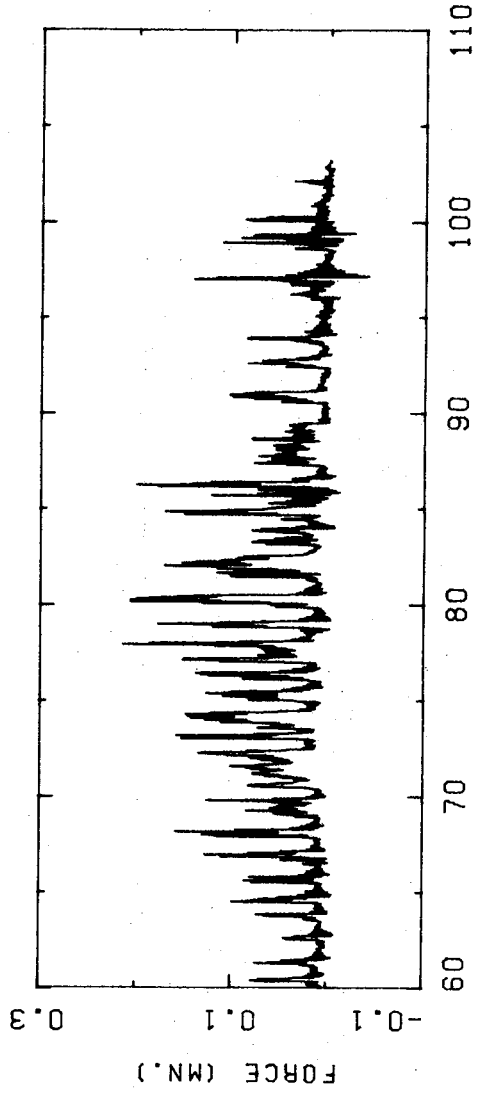

FIGURE B.22 HONDO 11 APRIL 1977 17H 48M 55S

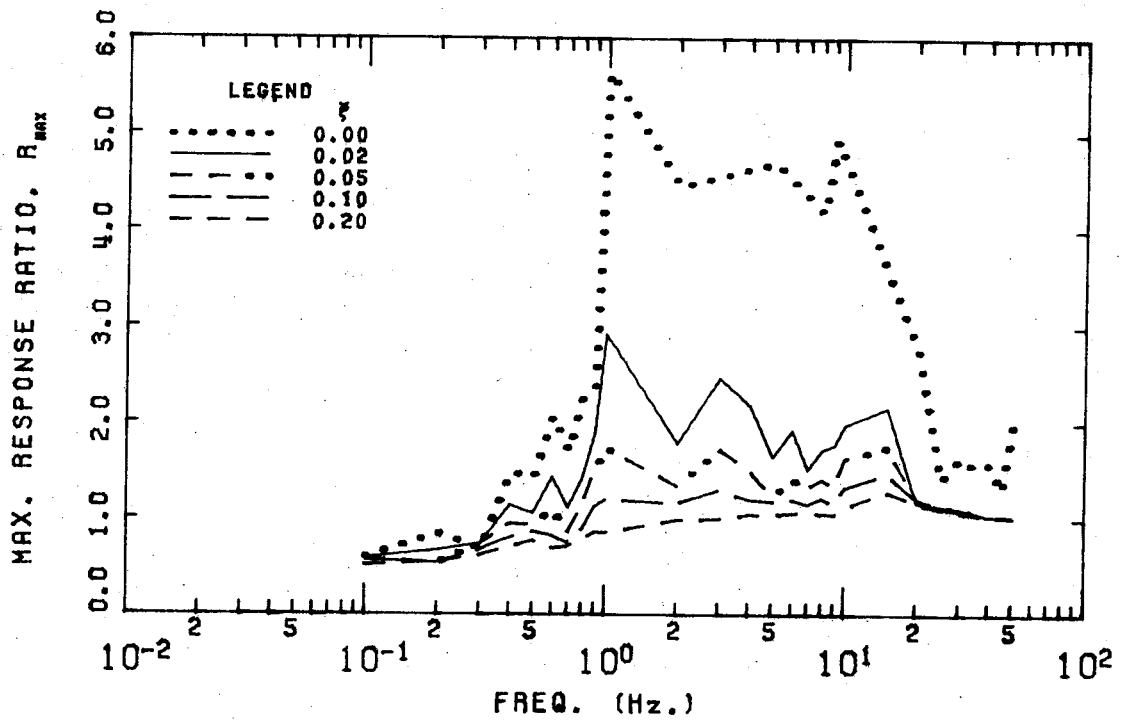

FIGURE B.23 HONDO 11 APRIL 1977 17H 44M 14S

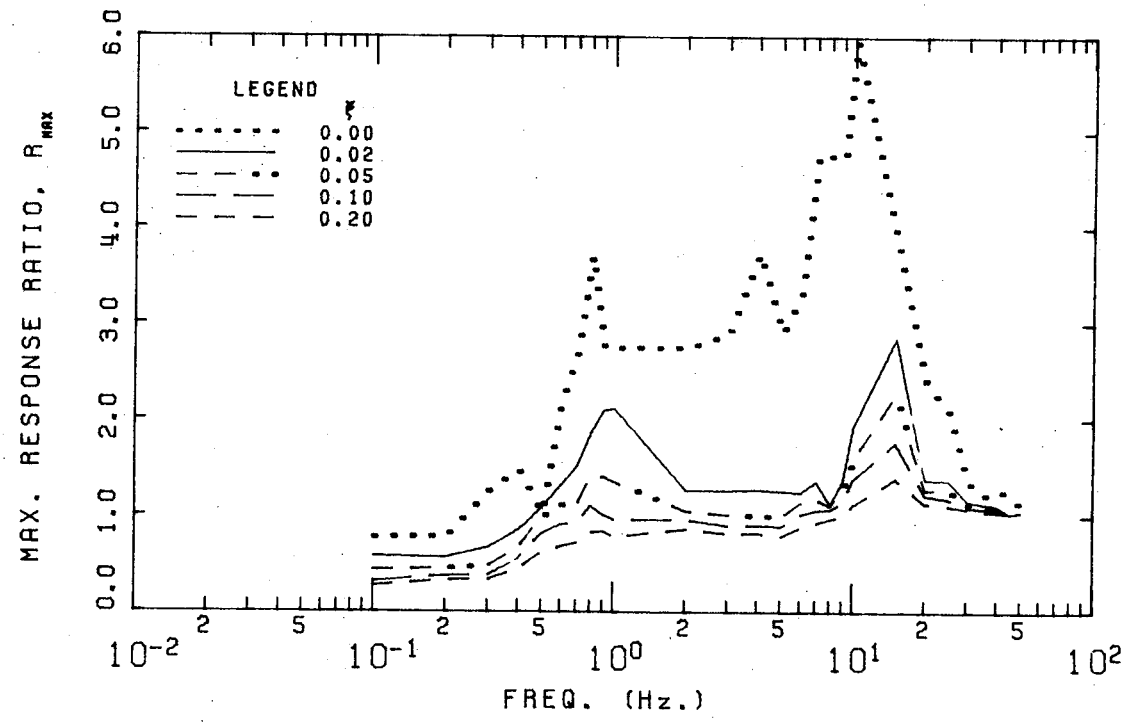

FIGURE B.24 HONDO 11 APRIL 1977 17H 48H 55S

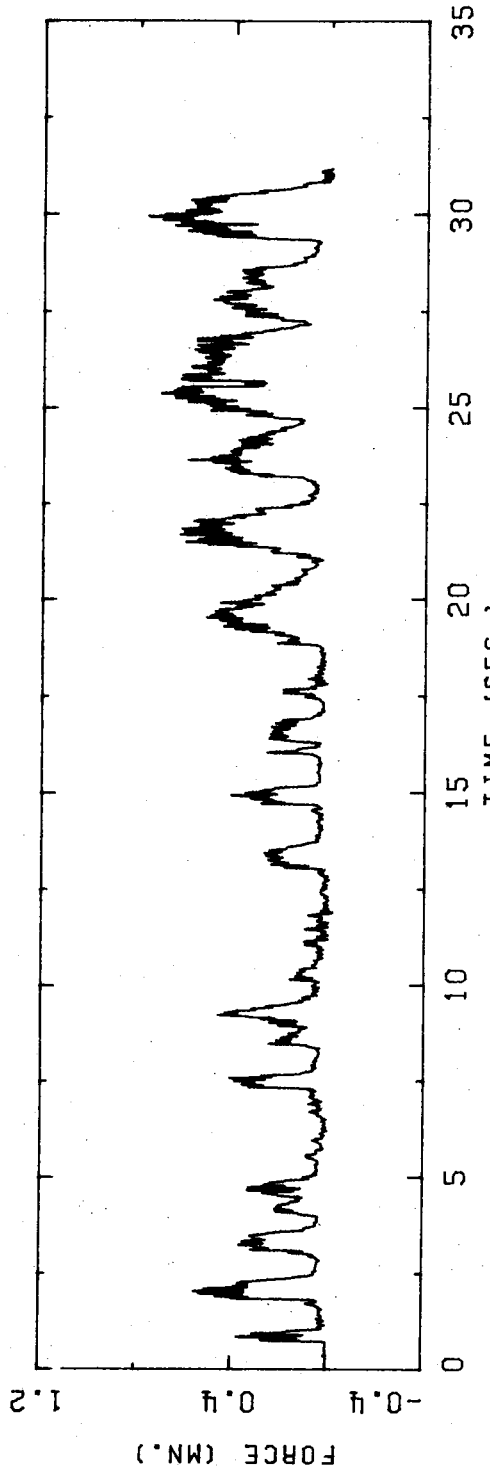

FIGURE B.25 HONDO 12 APRIL 1977 03H 46M 05S

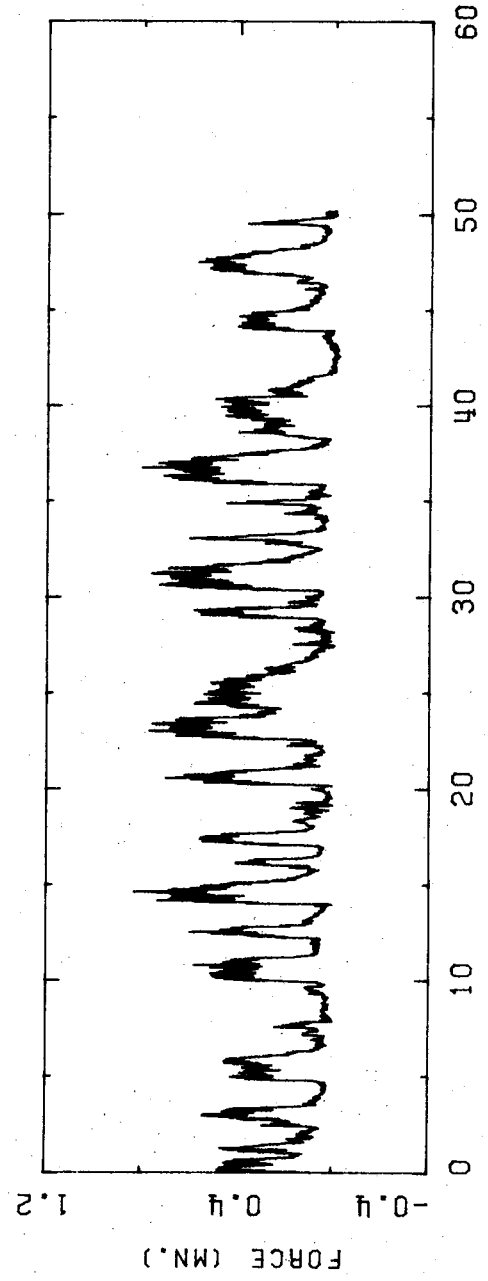

FIGURE B.26 HONDO 12 APRIL 1977 03H 46M 33S

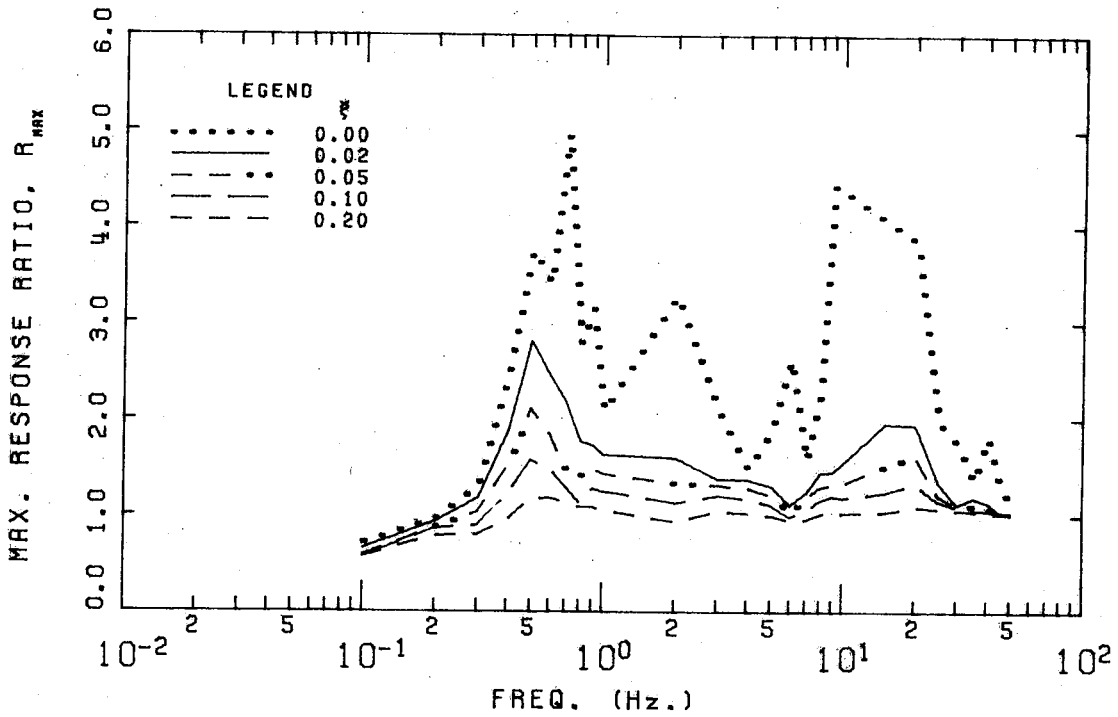

FIGURE B.27 HONDO 12 APRIL 1977 03H 46H 05S

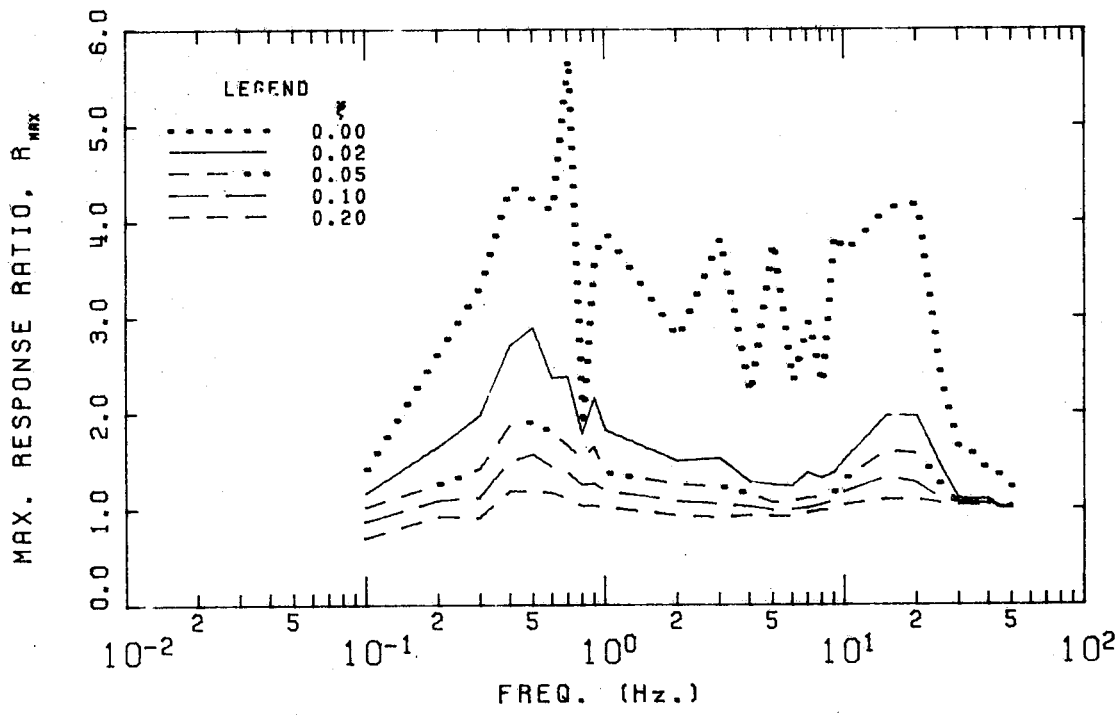

FIGURE B.28 HONDO 12 APRIL 1977 03H 46H 33S

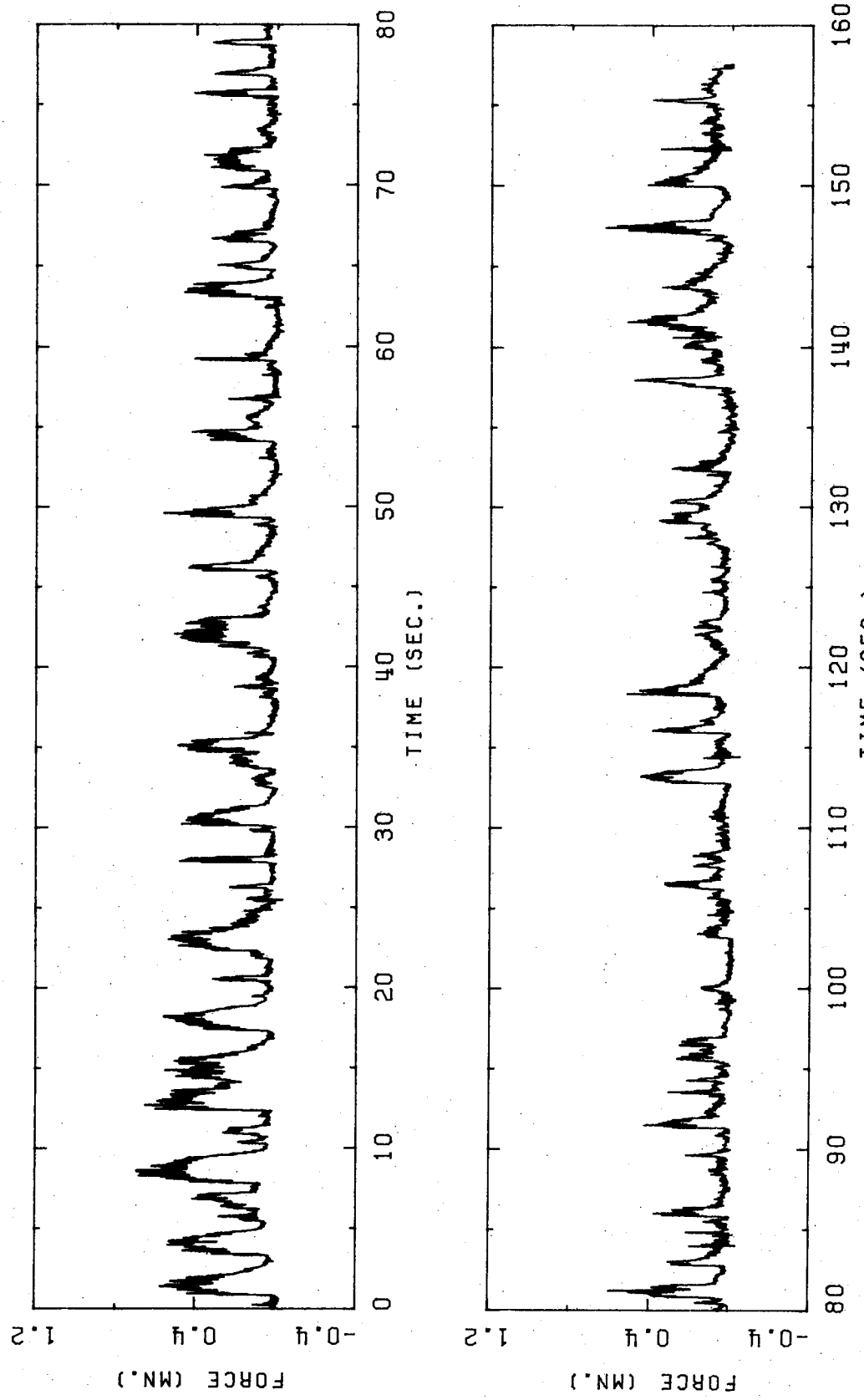

FIGURE B.29 HONDO 12 APRIL 1977 03H 47M 28S

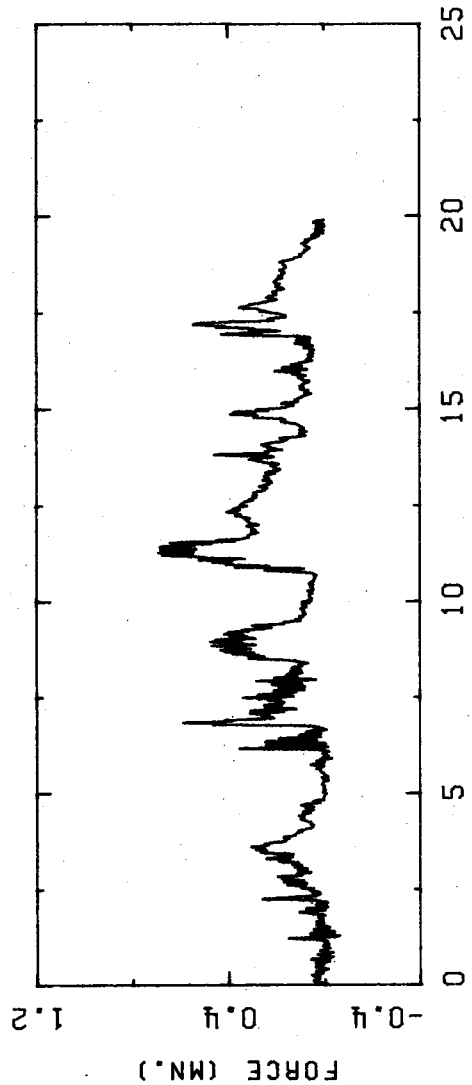

FIGURE B.30 HONDO 12 APRIL 1977 03H 50M 41S

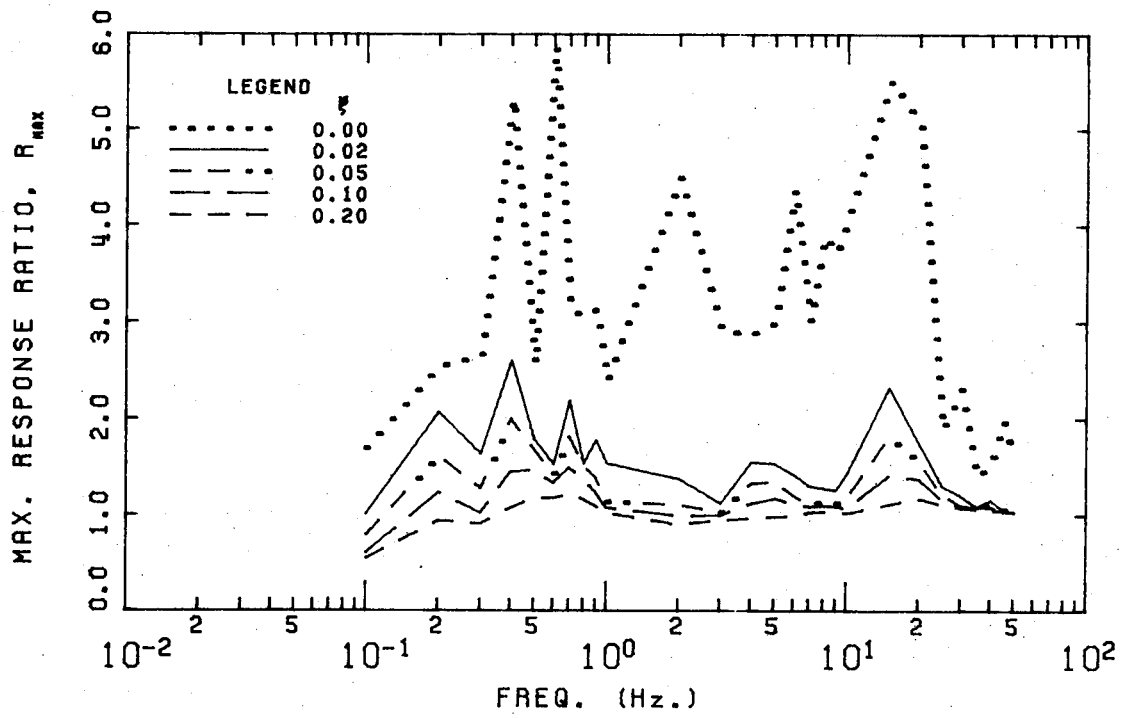

FIGURE B.31 HONDO 12 APRIL 1977 03H 47H 28S

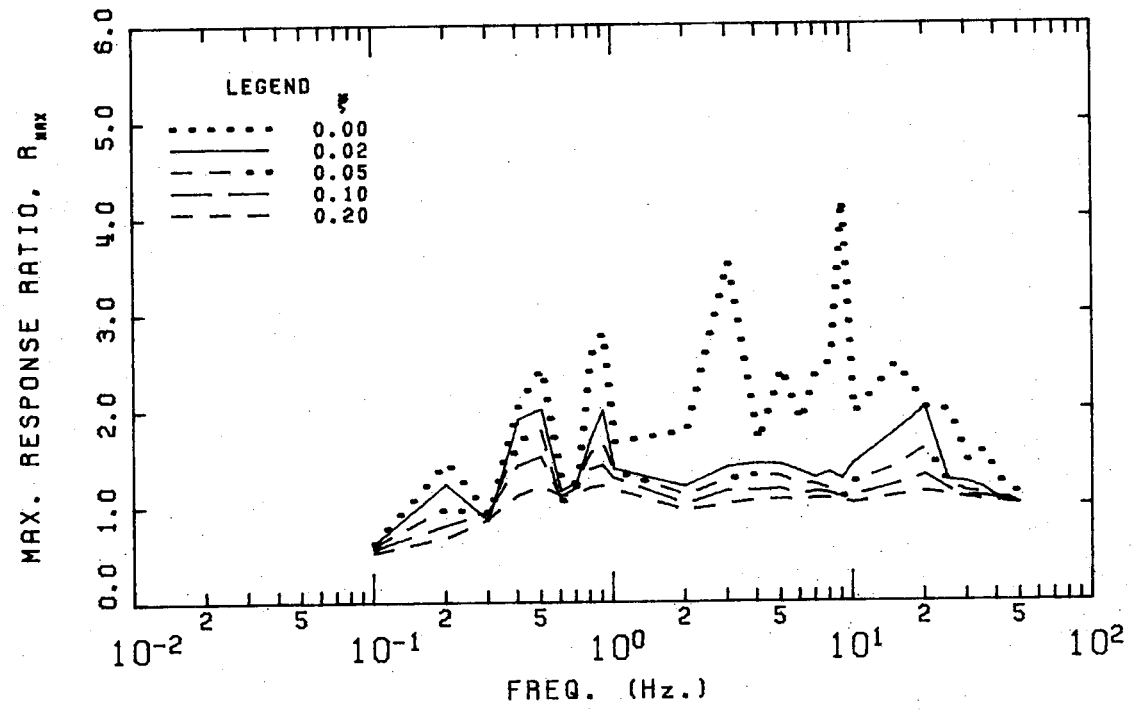

FIGURE B.32 HONDO 12 APRIL 1977 03H 50H 41S

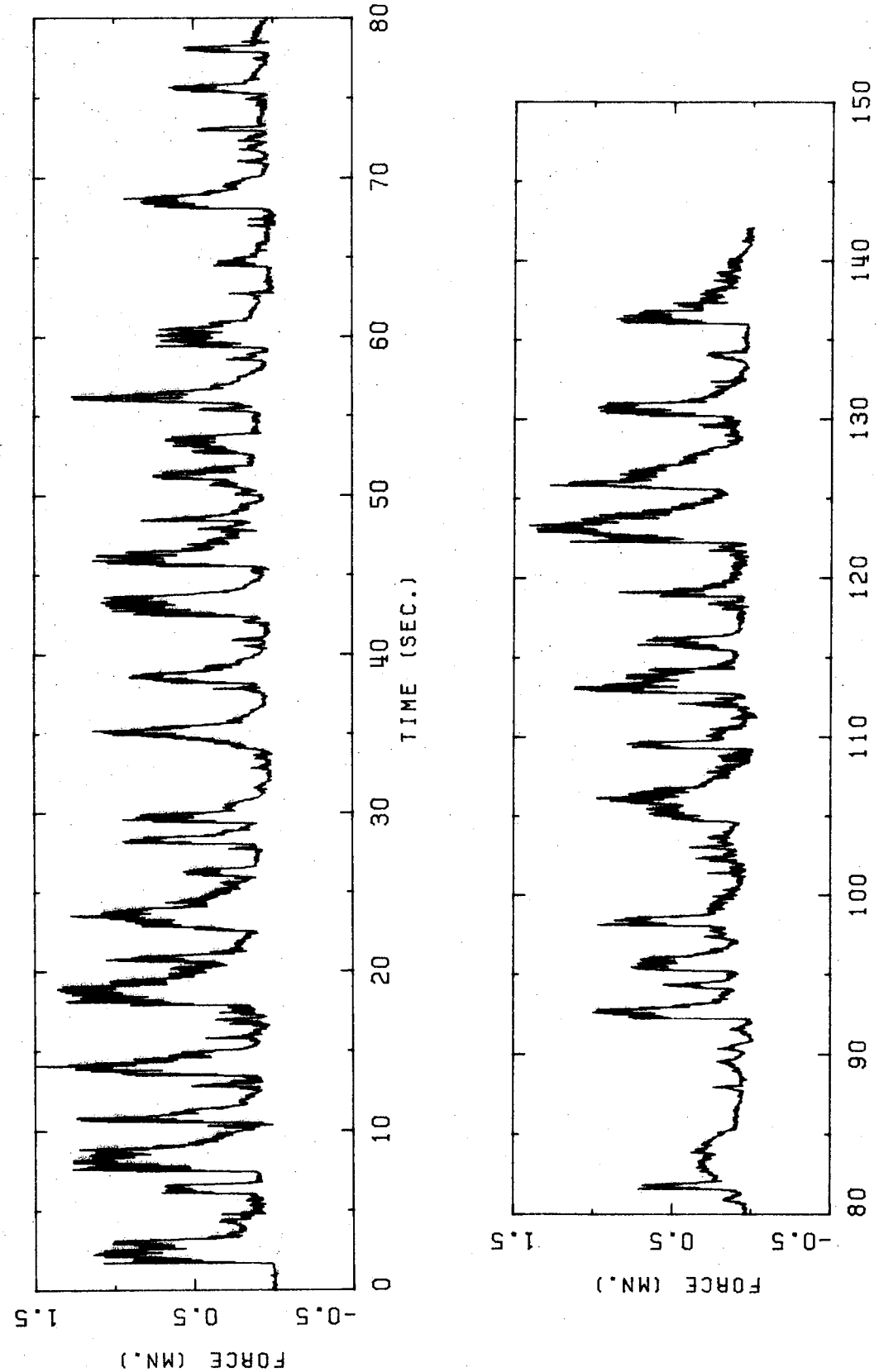

FIGURE B.33 HONDO 12 APRIL 1977 03H 54M 37S

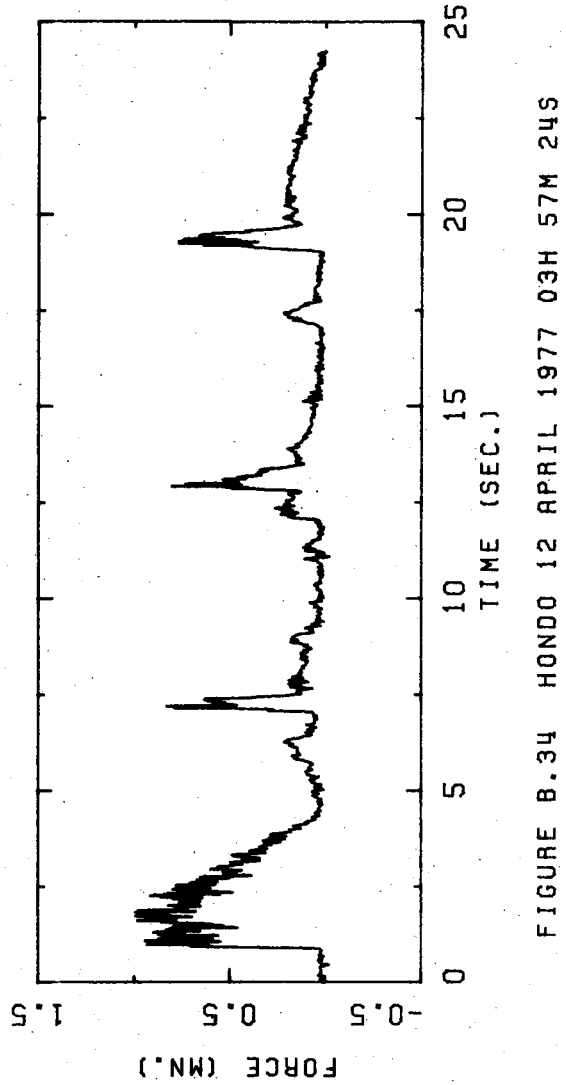

FIGURE B.34 HONDO 12 APRIL 1977 03H 57M 24S

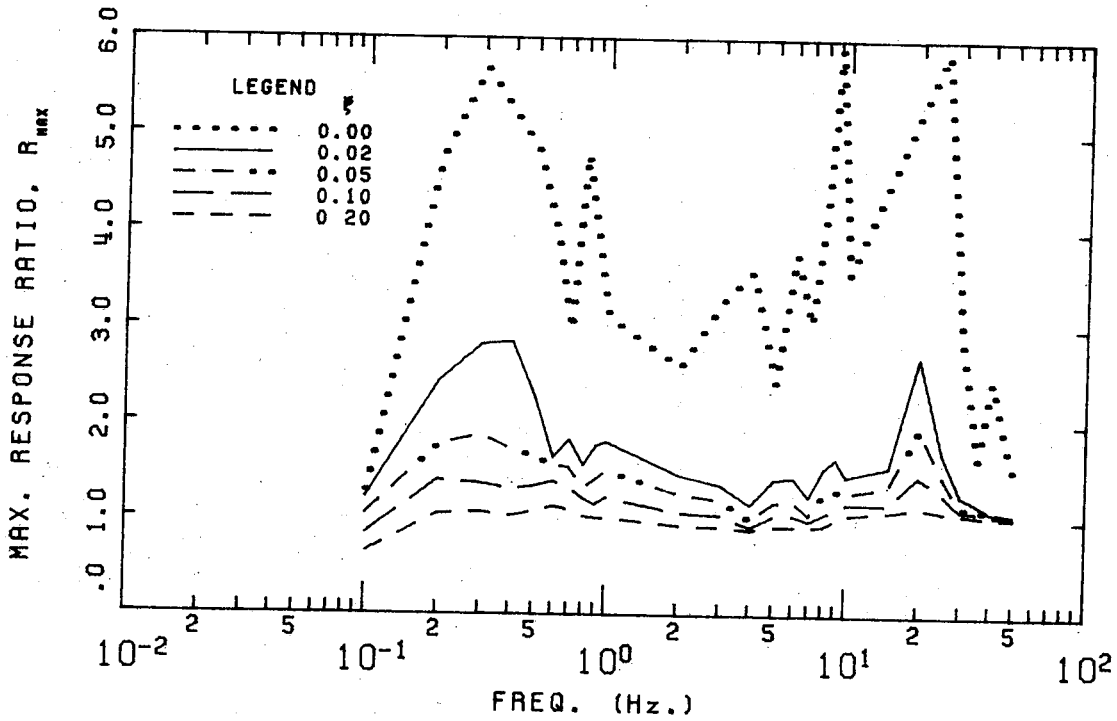

FIGURE B.35 HONDO 12 APRIL 1977 03H 54H 37S

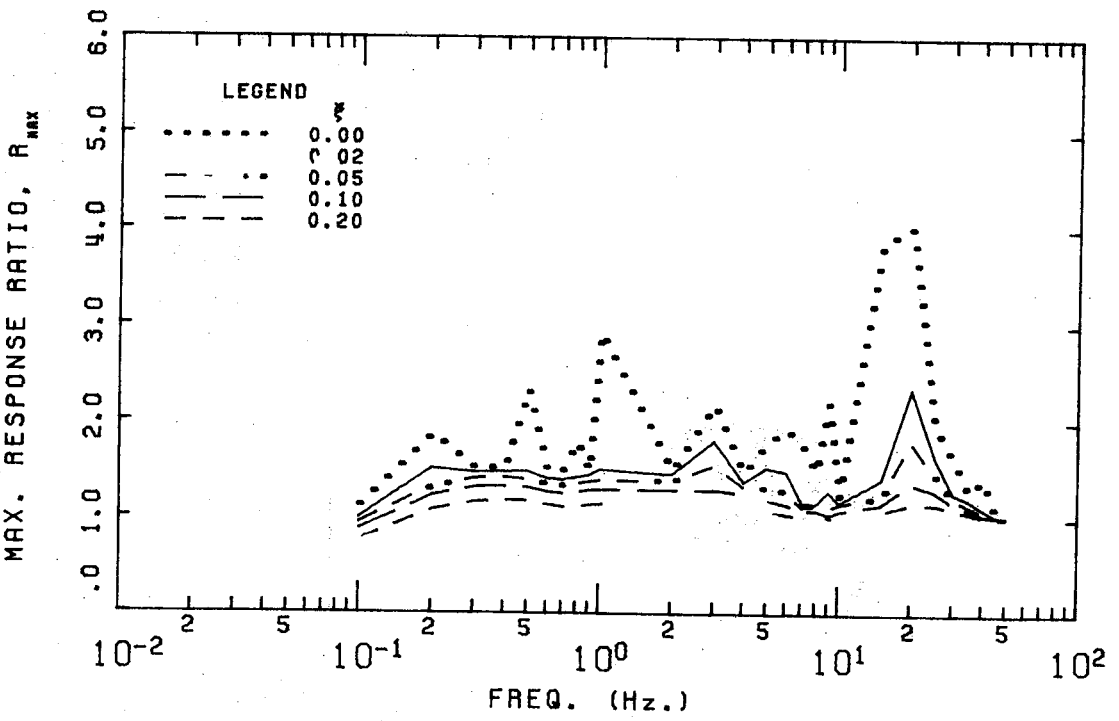

FIGURE B.36 HONDO 12 APRIL 1977 03H 57H 24S

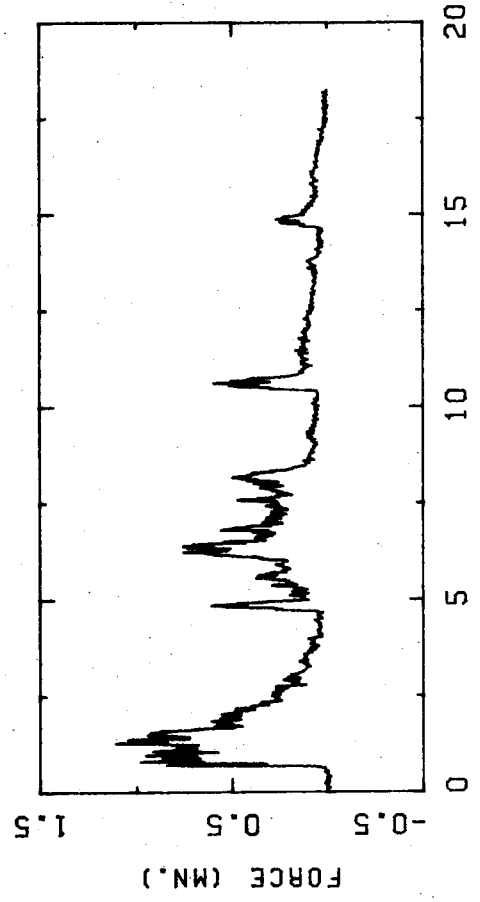

FIGURE B.37 HONDO 12 APRIL 1977 04H 05M 08S

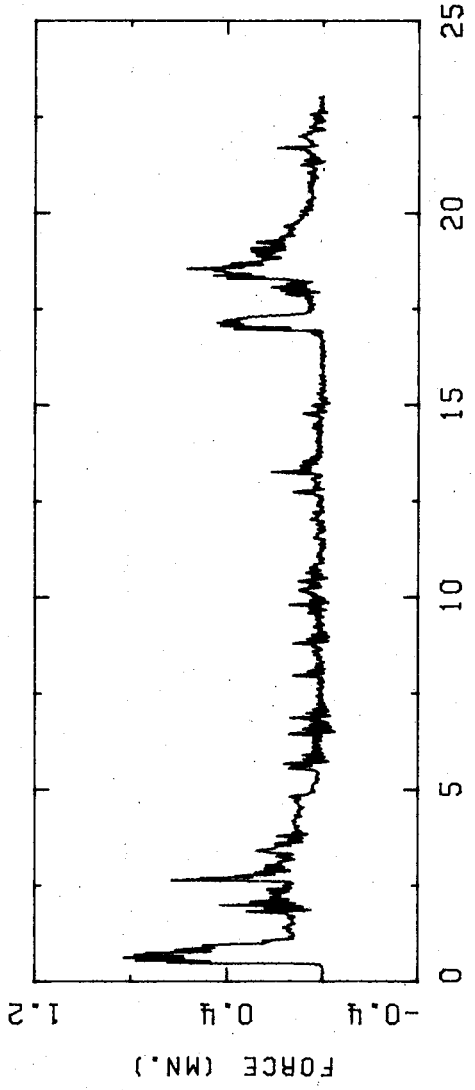

FIGURE B.38 HONDO 12 APRIL 1977 06H 18M 50S

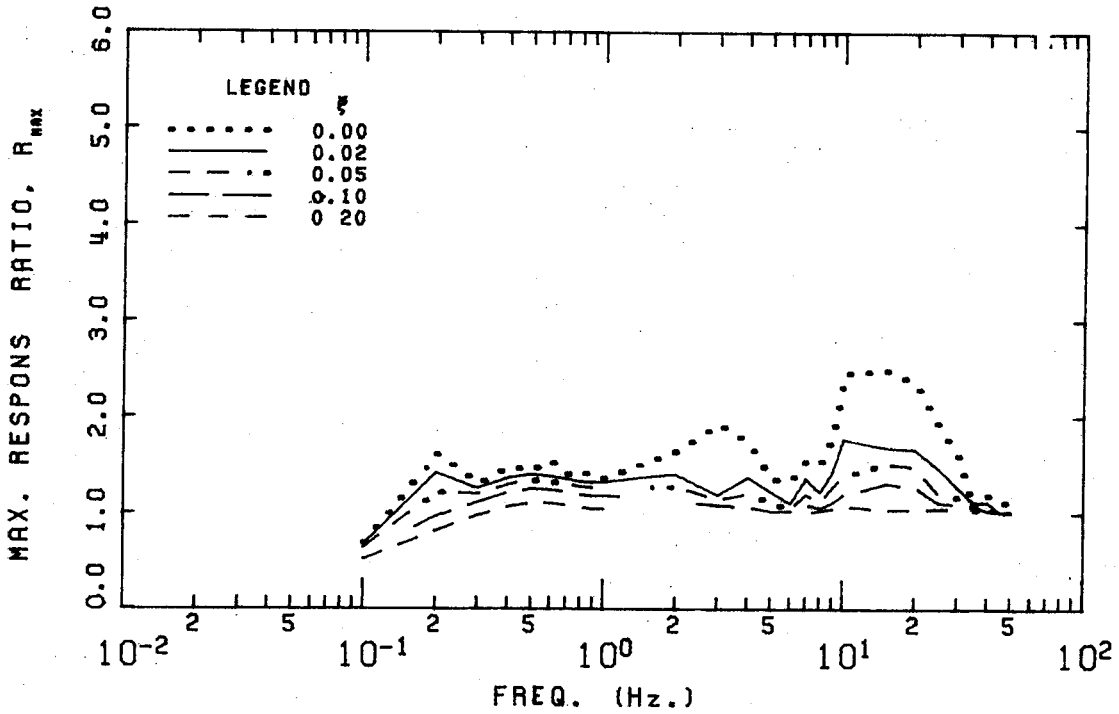

FIGURE B.39 HONDO 12 APRIL 1977 04H 05H 08S

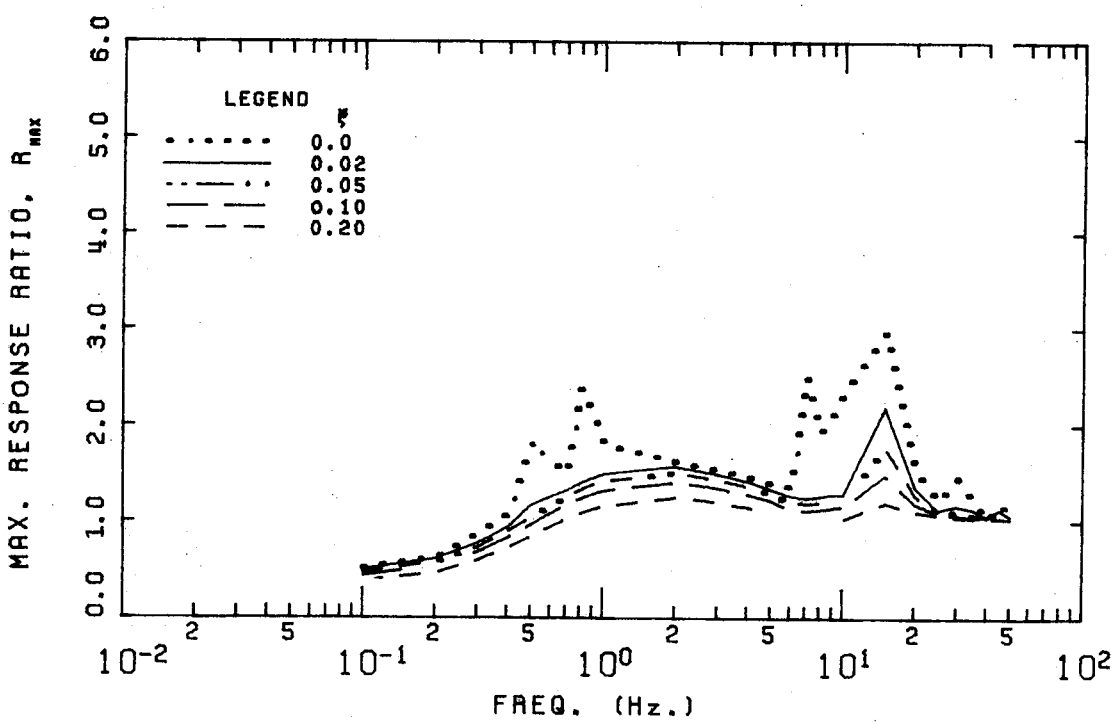

FIGURE B.40 HONDO 12 APRIL 1977 06H 18H 50S

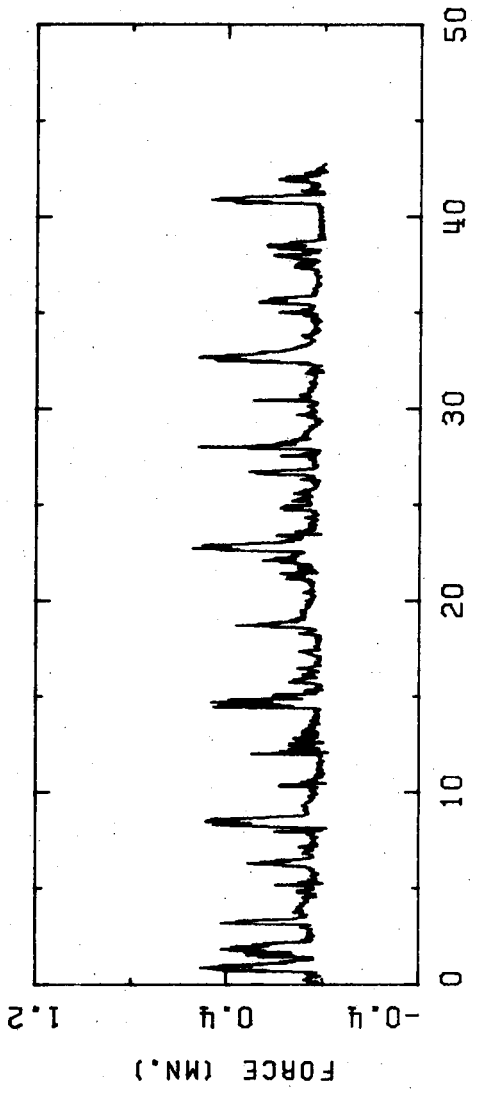

FIGURE B.41 HONDO 12 APRIL 1977 06H 31M 11S

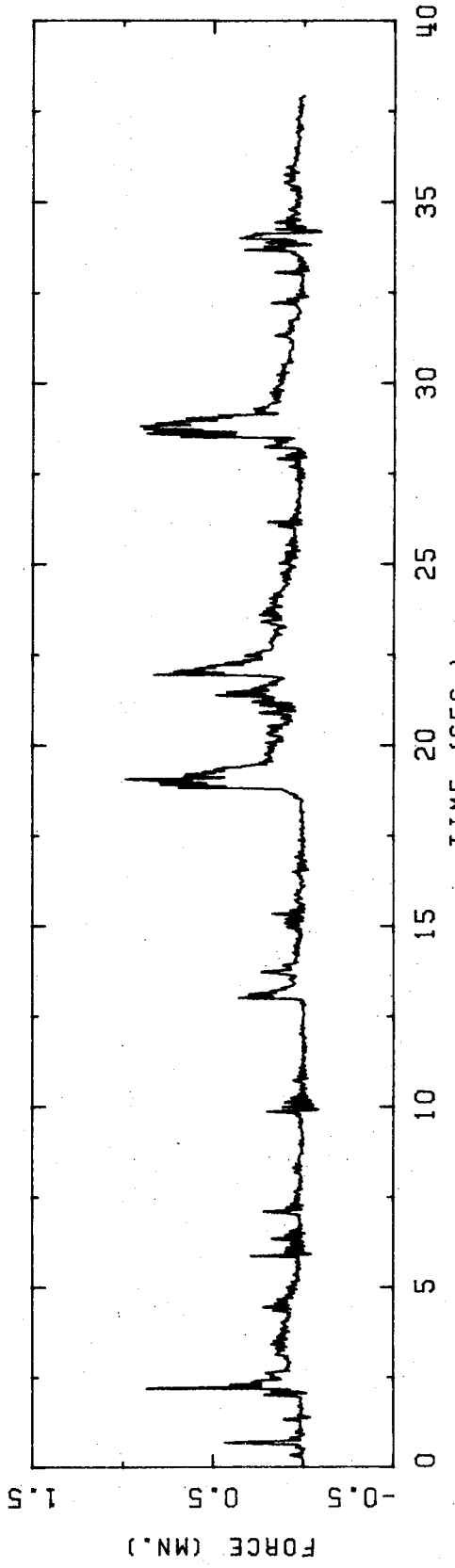

FIGURE B.42 HONDO 12 APRIL 1977 06H 43M 17S

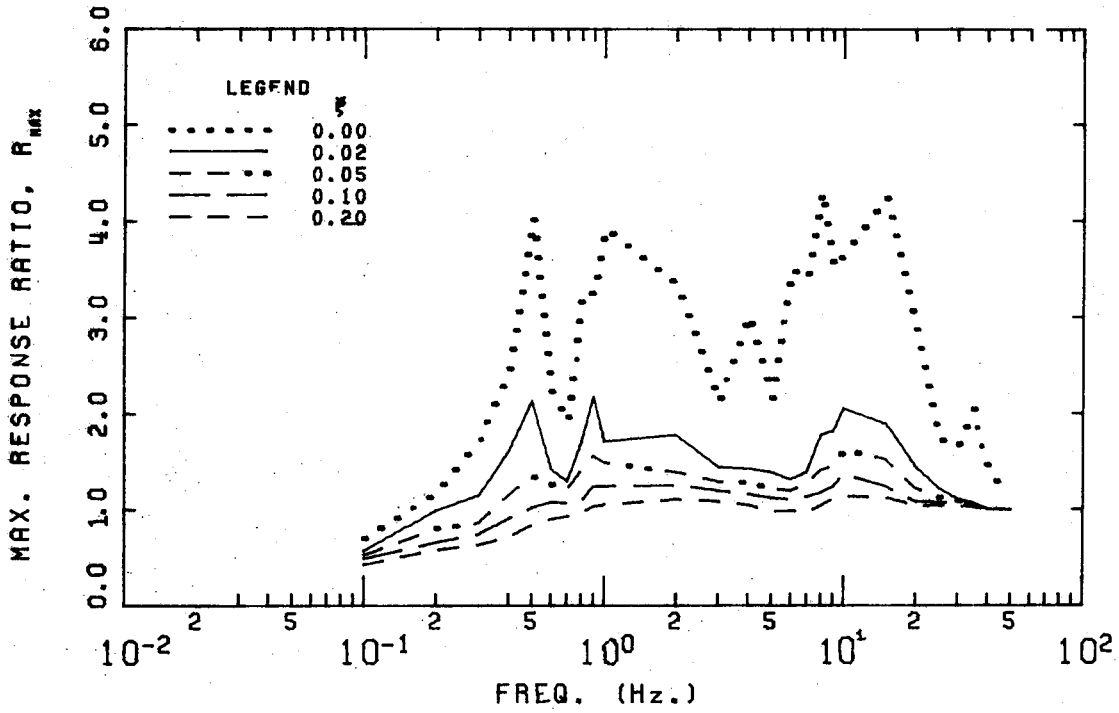

FIGURE B.43 HUNDO 12 APRIL 1977 06H 31H 11S

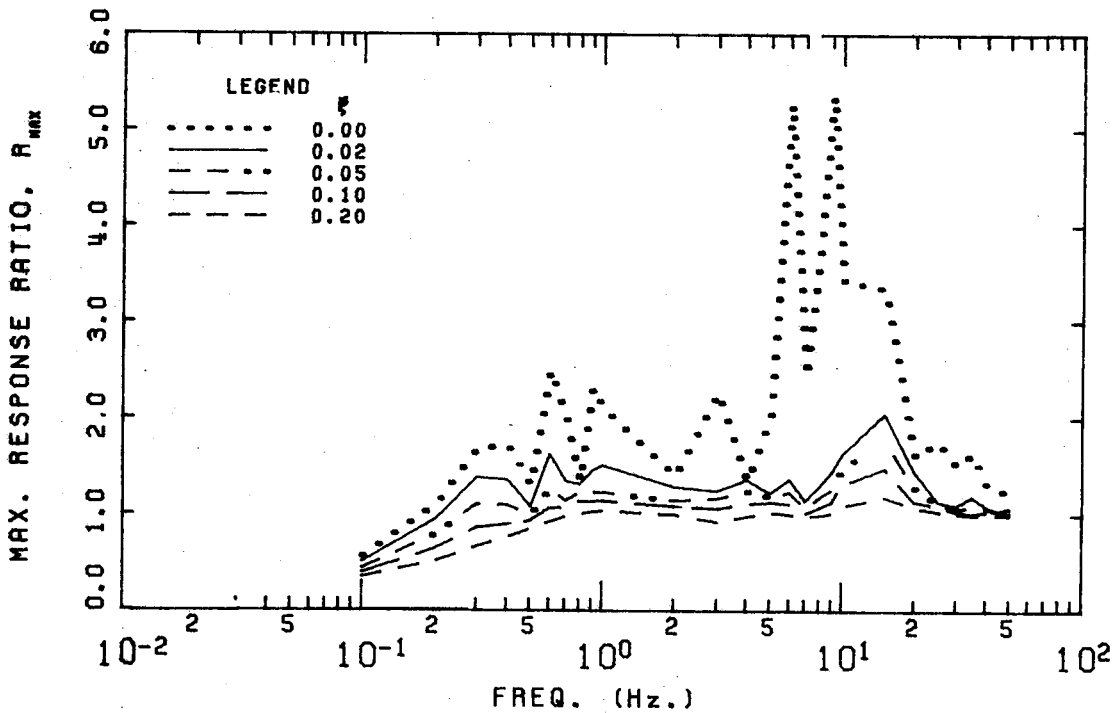

FIGURE B.44 HONDO 12 APRIL 1977 06H 43H 17S

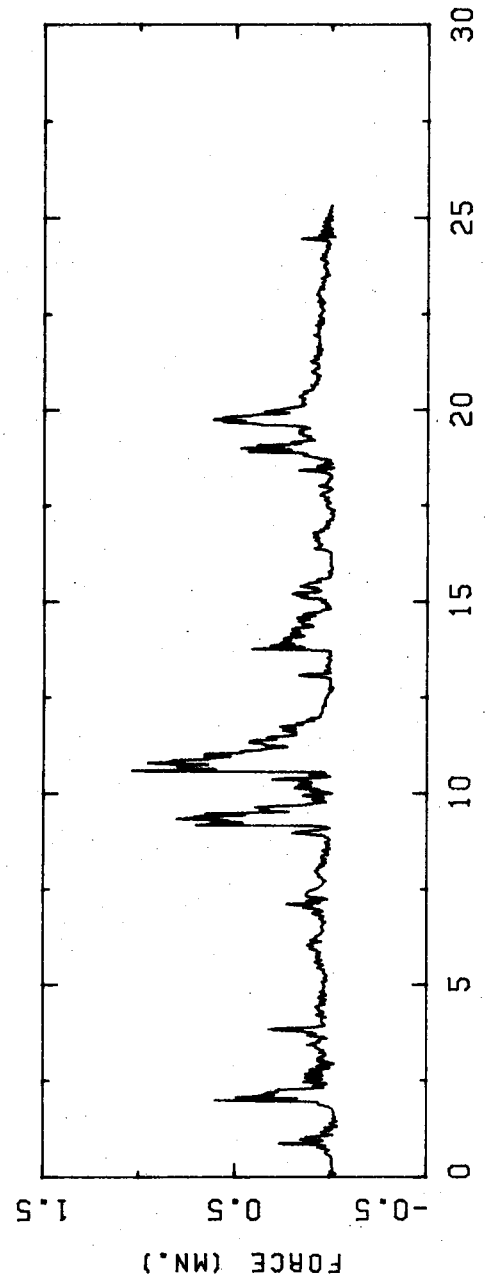

FIGURE B.45 HONDO 12 APRIL 1977 06H 44M 29S

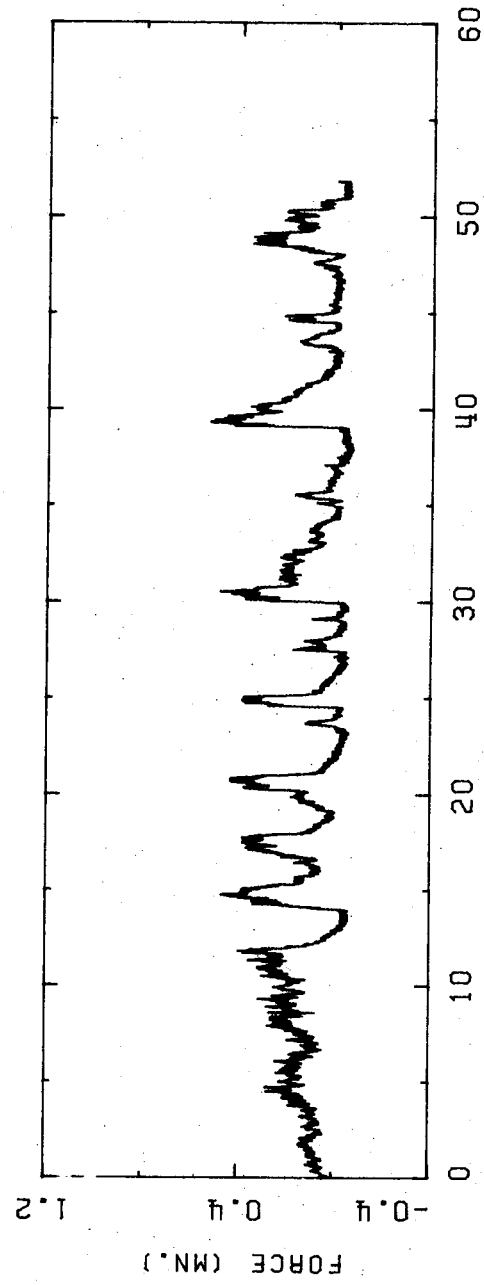

FIGURE B.46 HONDO 25 APRIL 1979 15H 05M 57S

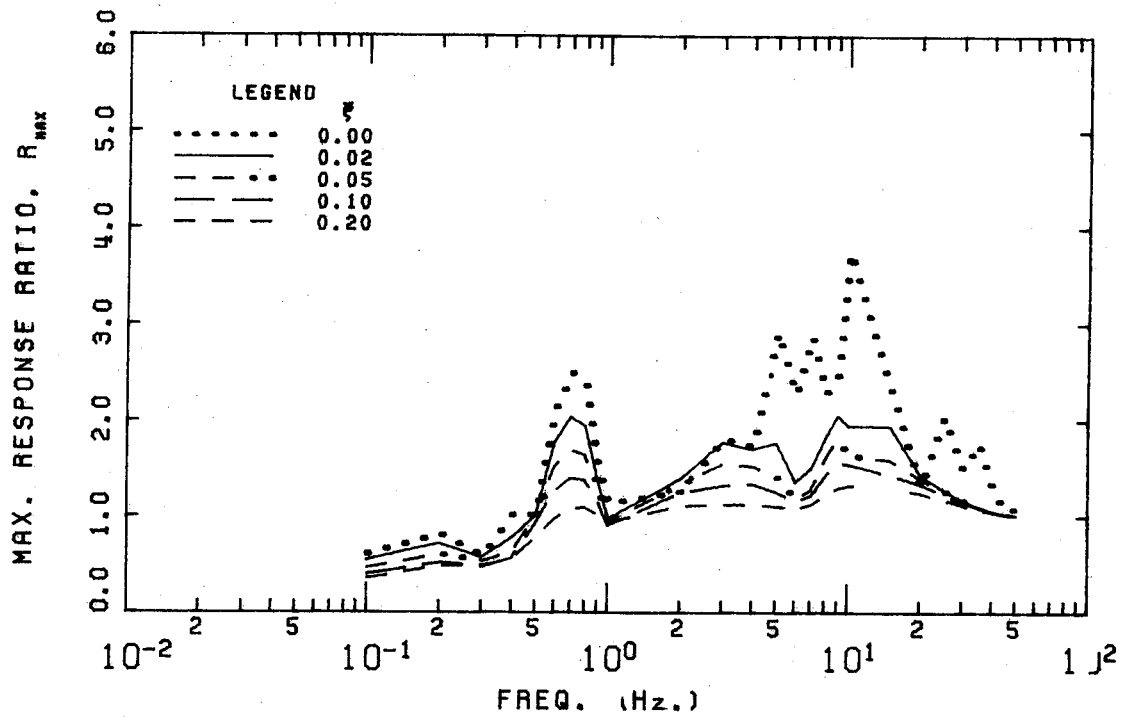

FIGURE B.47 HONDO 12 APRIL 1977 06H 44M 29S

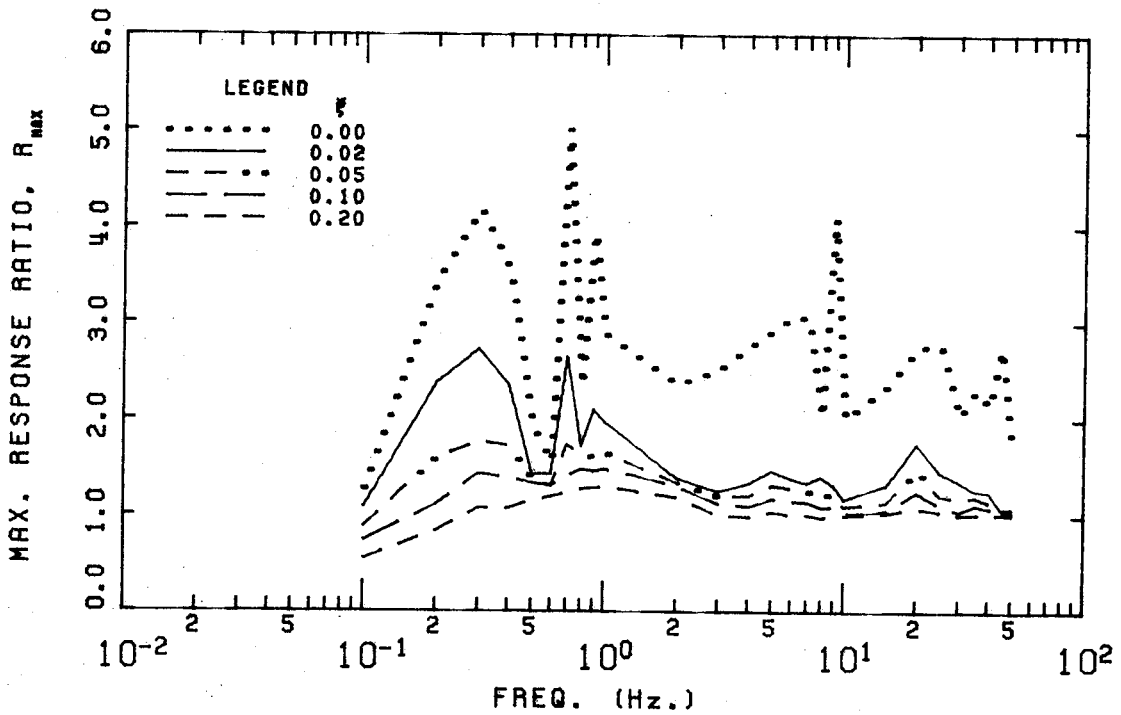

FIGURE B.48 HONDO 25 APRIL 1979 15H 05M 57S

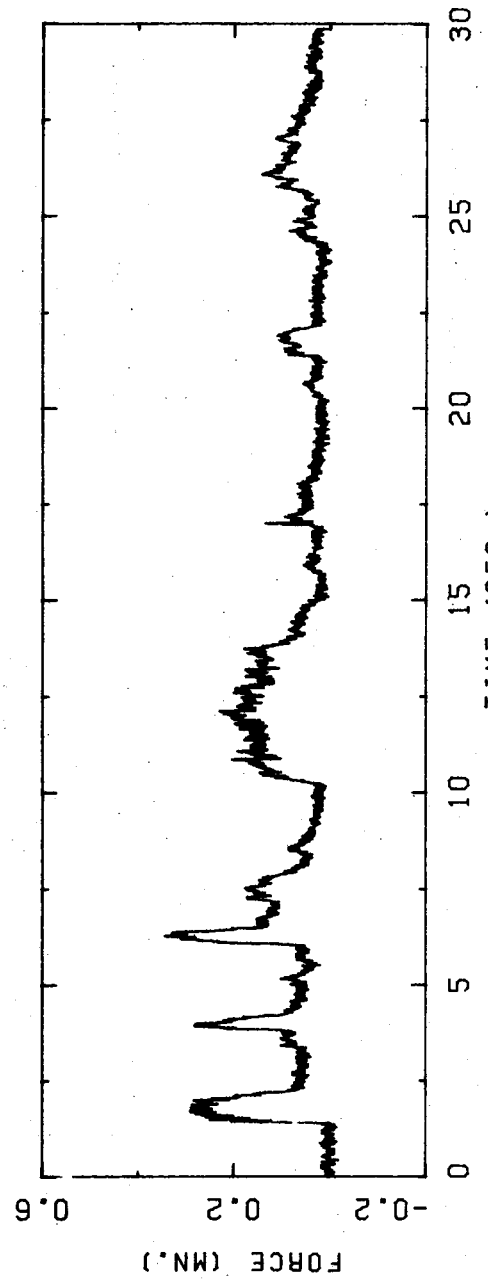

FIGURE B.49 HONDO 25 APRIL 1979 17H 54M 49S

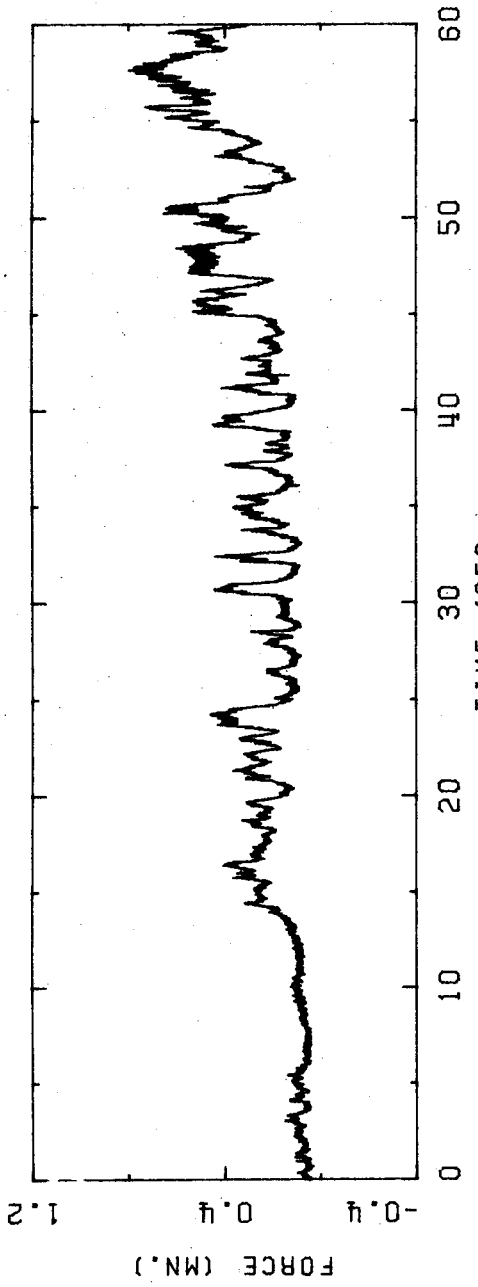

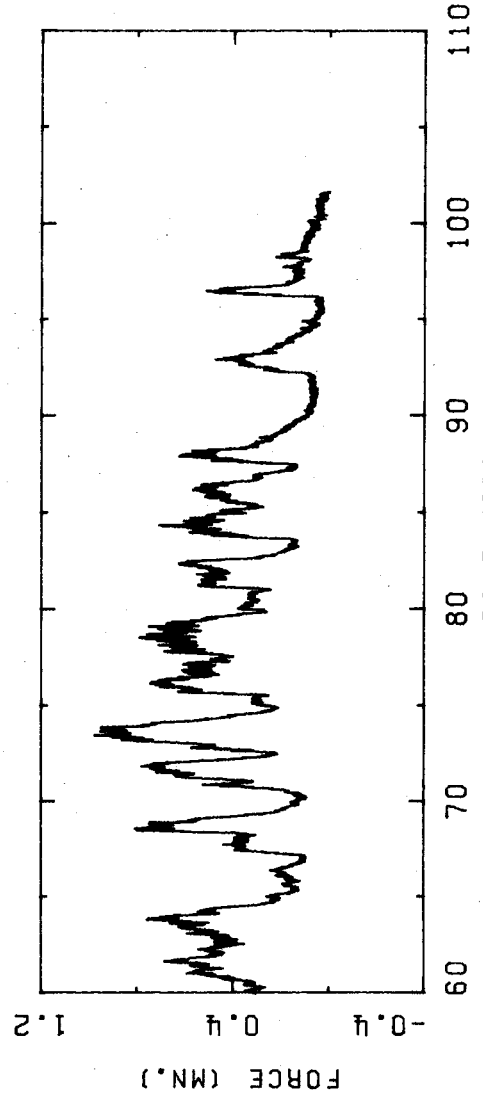

FIGURE B.50 HONDO 26 APRIL 1979 16H 47M 59S

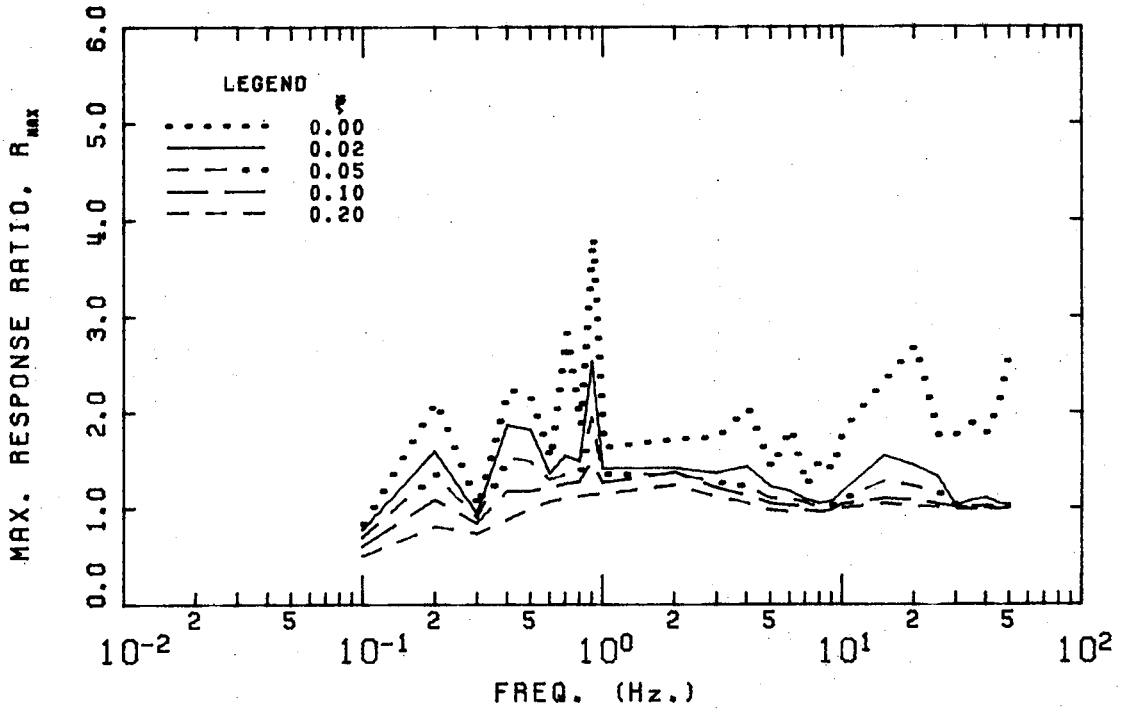

FIGURE B.51 HONDO 25 APRIL 1979 17H 54M 49S

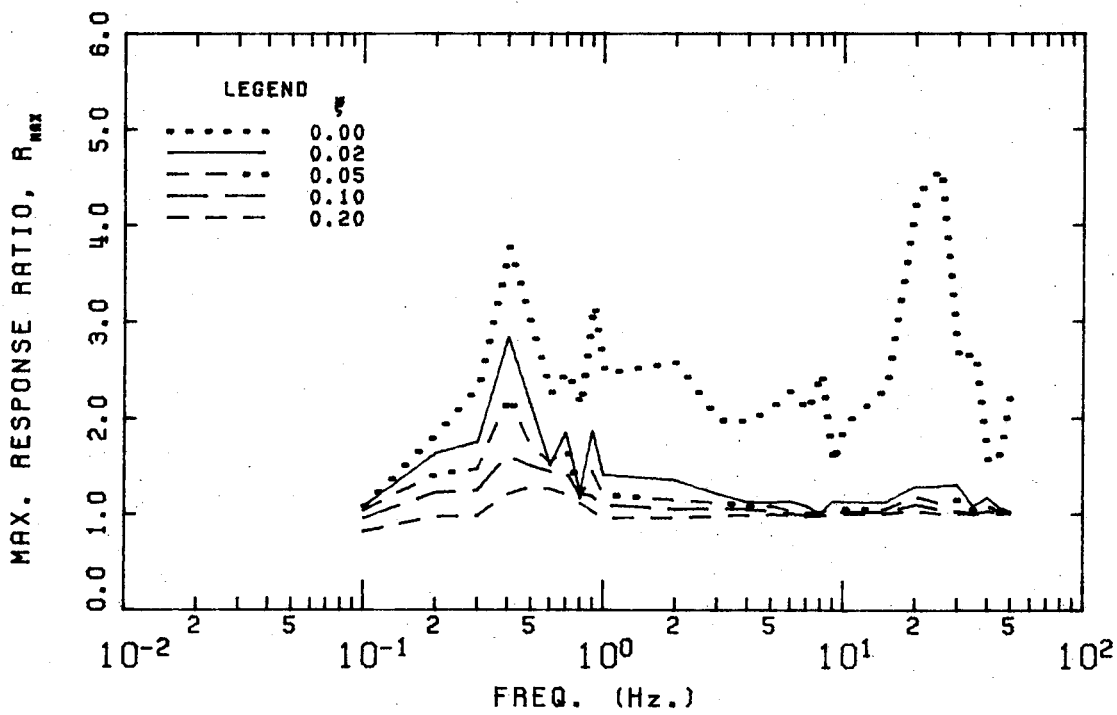

FIGURE B.52 HONDO 26 APRIL 1979 16H 47M 59S

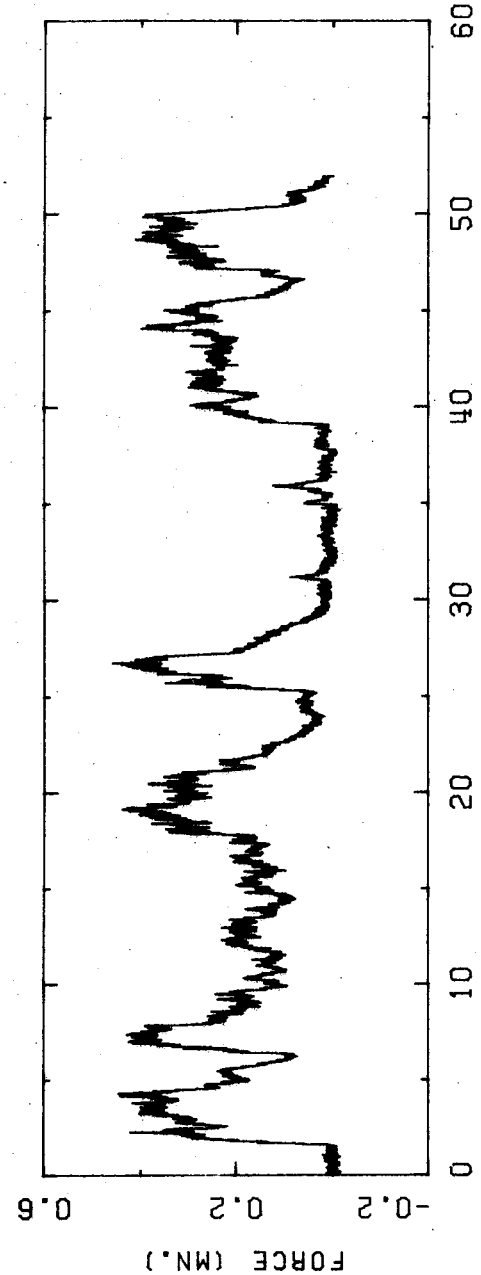

FIGURE B.53 HONDO 26 APRIL 1979 16H 50M 54S

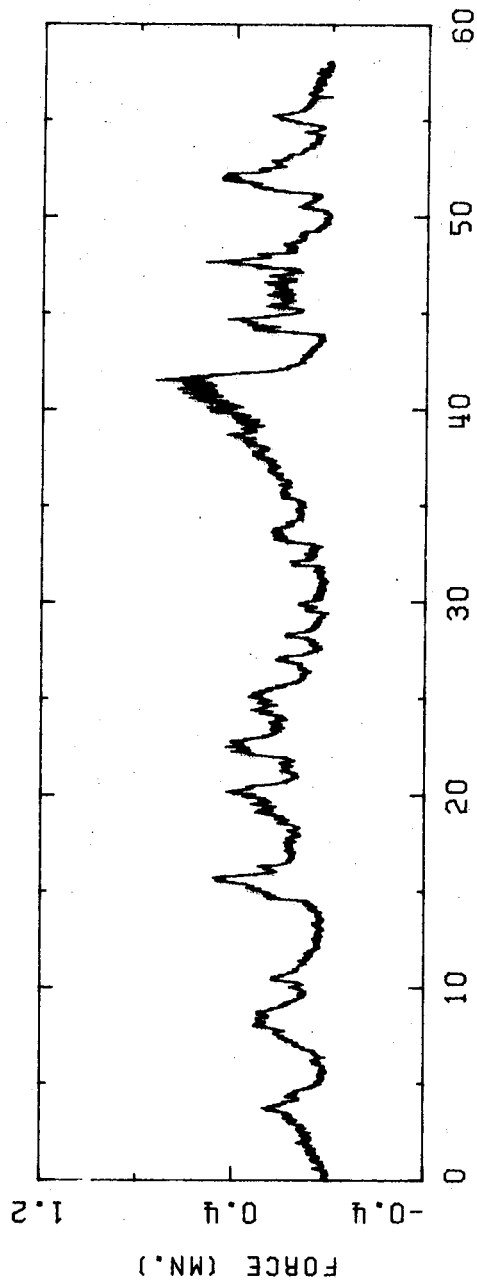

FIGURE B.54 HONDO 26 APRIL 1979 16H 55M 57S

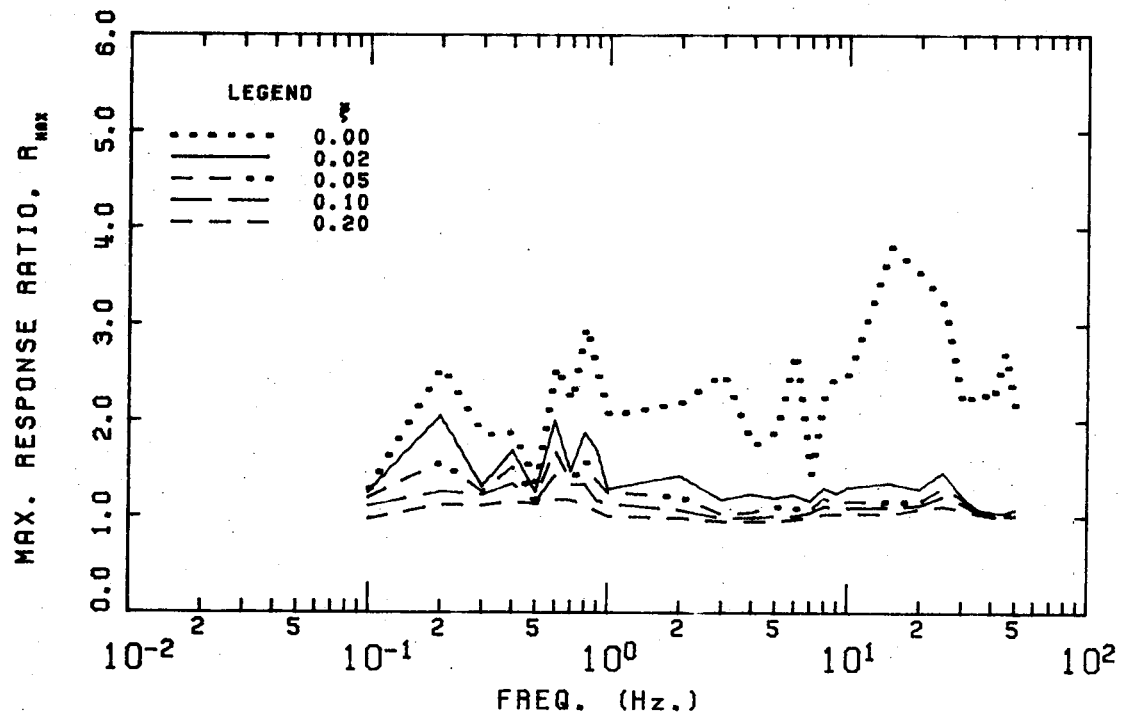

FIGURE B.55 HONDO 26 APRIL 1979 16H 50M 54S

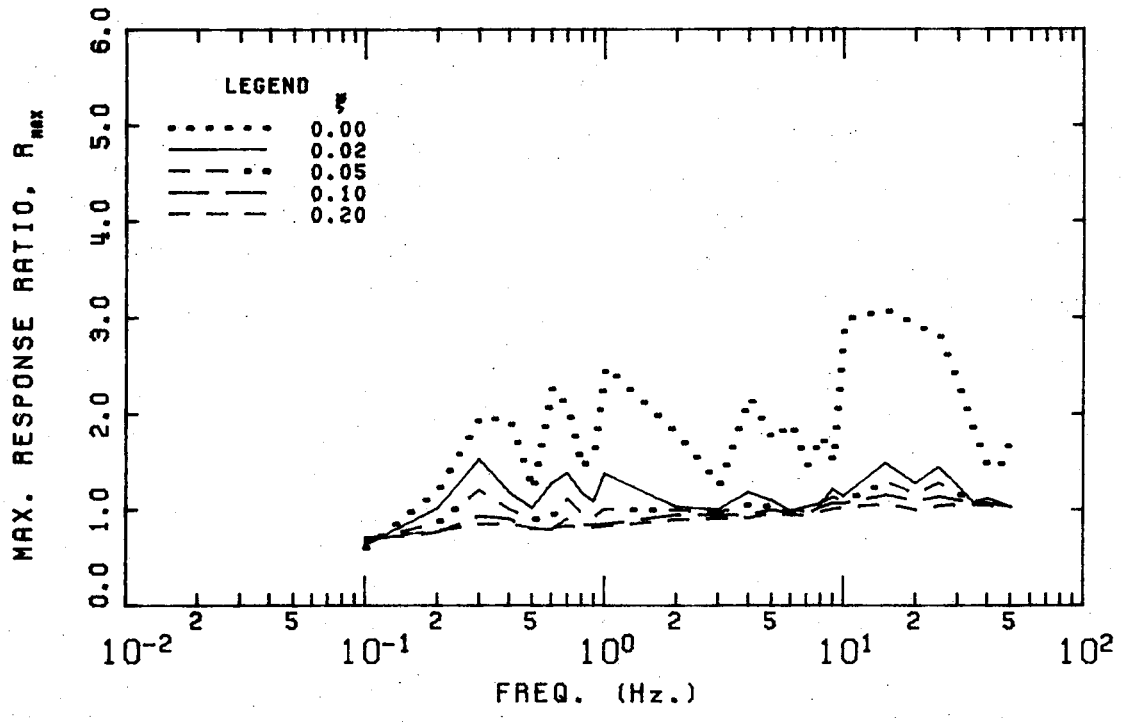

FIGURE B.56 HONDO 26 APRIL 1979 16H 55M 57S

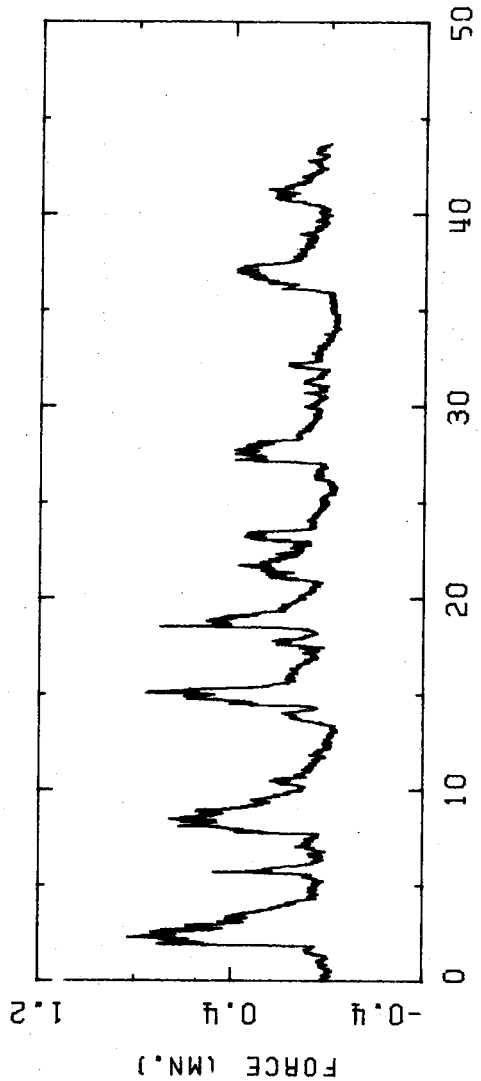

FIGURE B.57 HONDO 26 APRIL 1979 16H 59M 03S

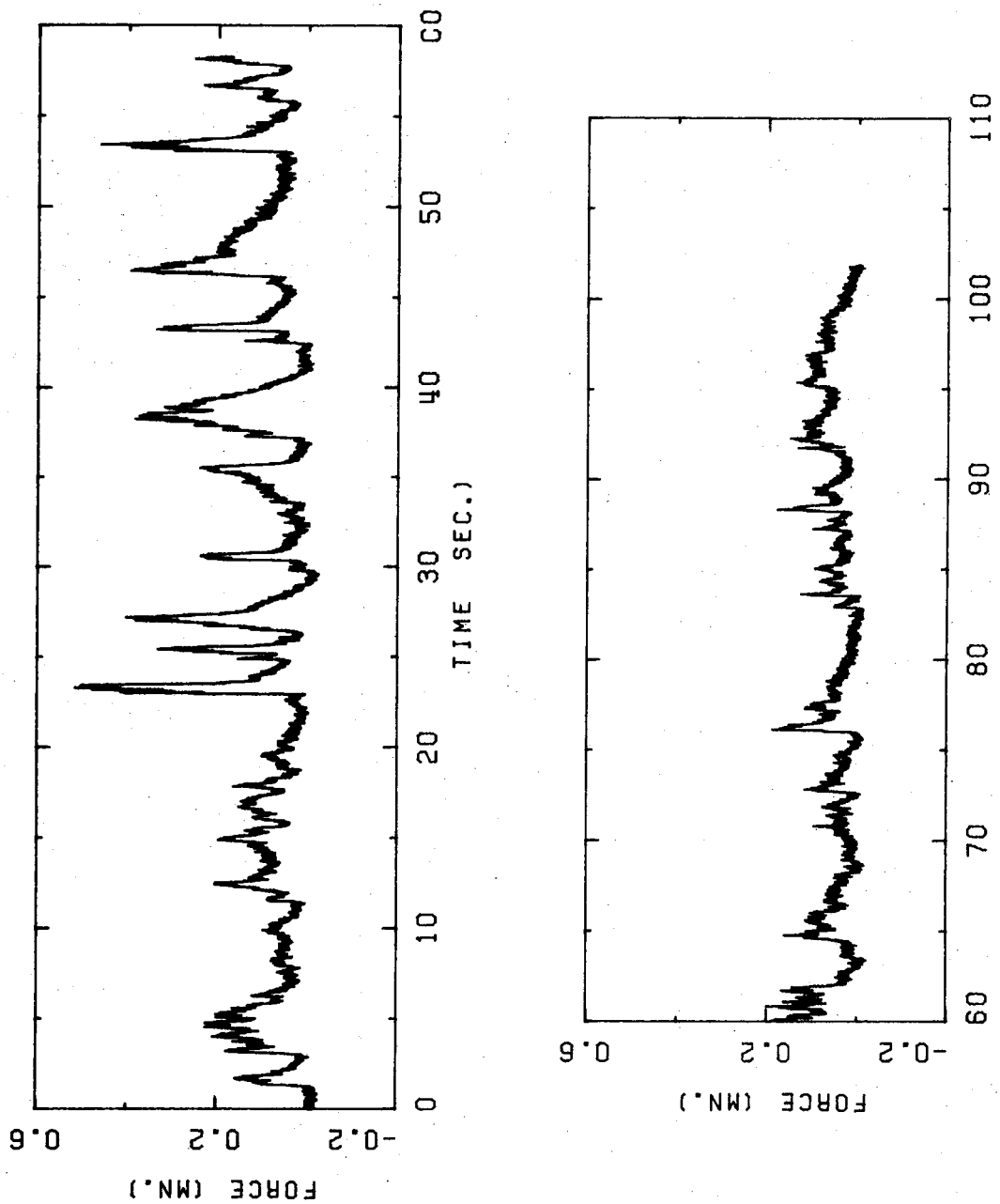

FIGURE B.58 HONDO 26 APRIL 1979 17H 04M 37S

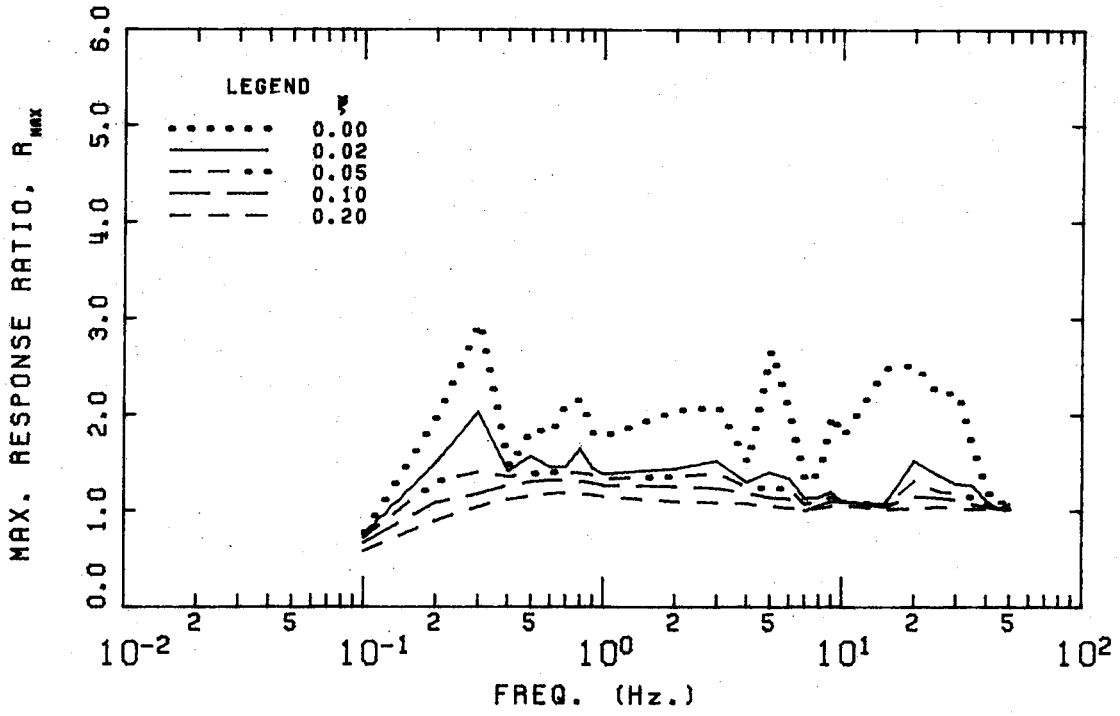

FIGURE B.59 HONDO 26 APRIL 1979 16H 59M 03S

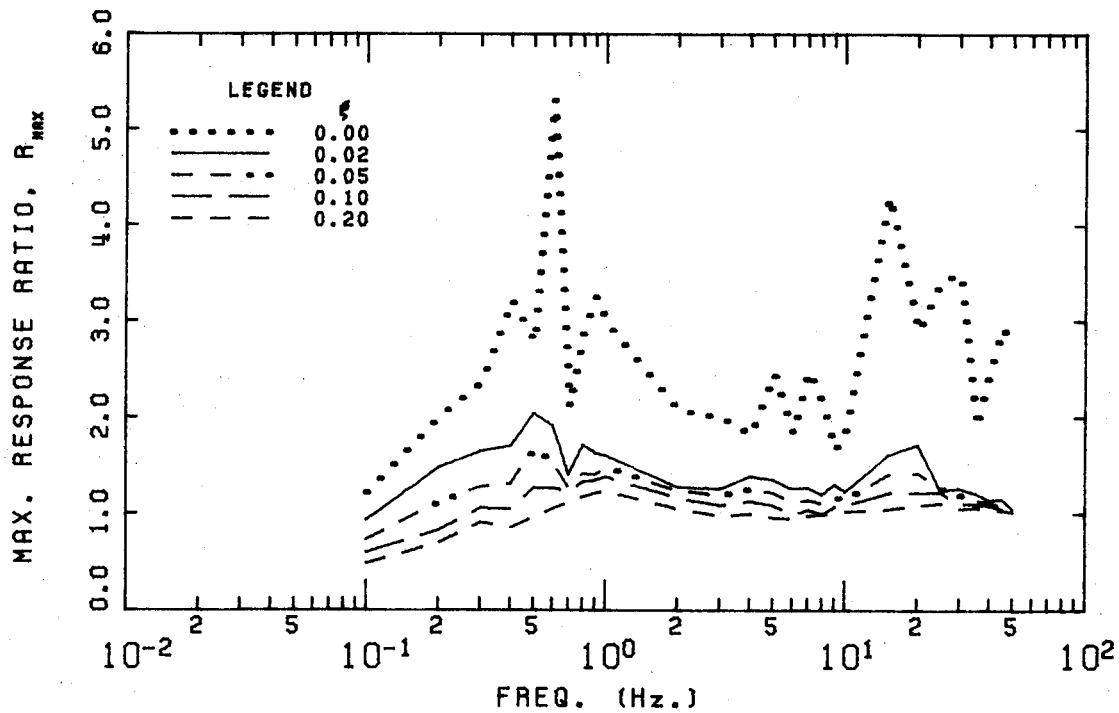

FIGURE B.60 HONDO 26 APRIL 1979 17H 04M 37S

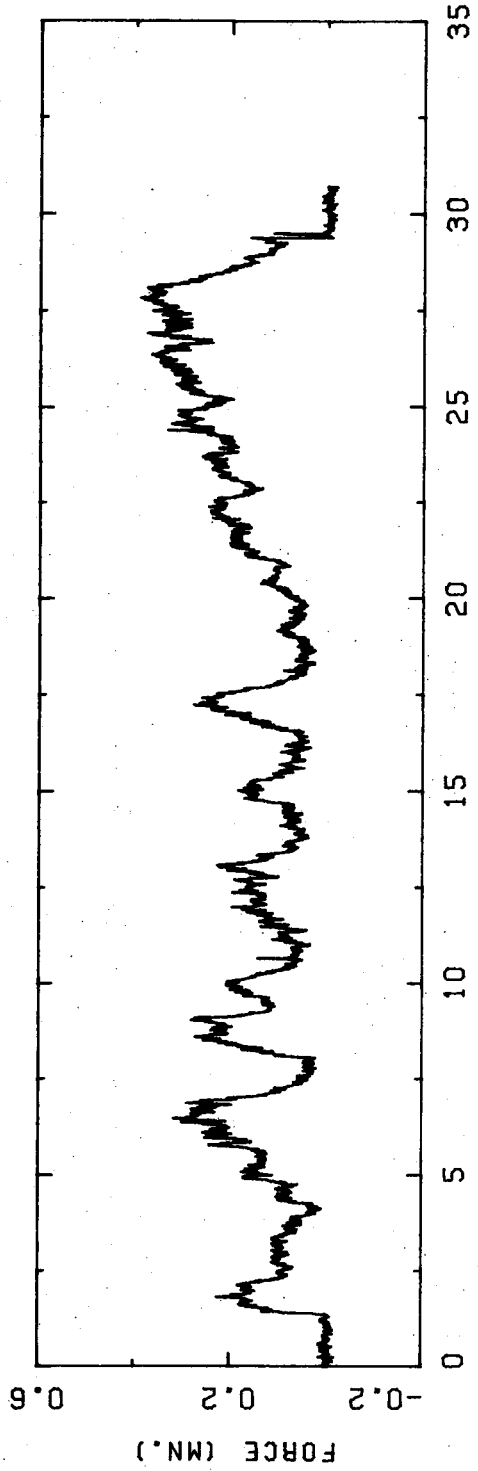

FIGURE B.61 HONDO 26 APRIL 1979 17H 08M 54S.

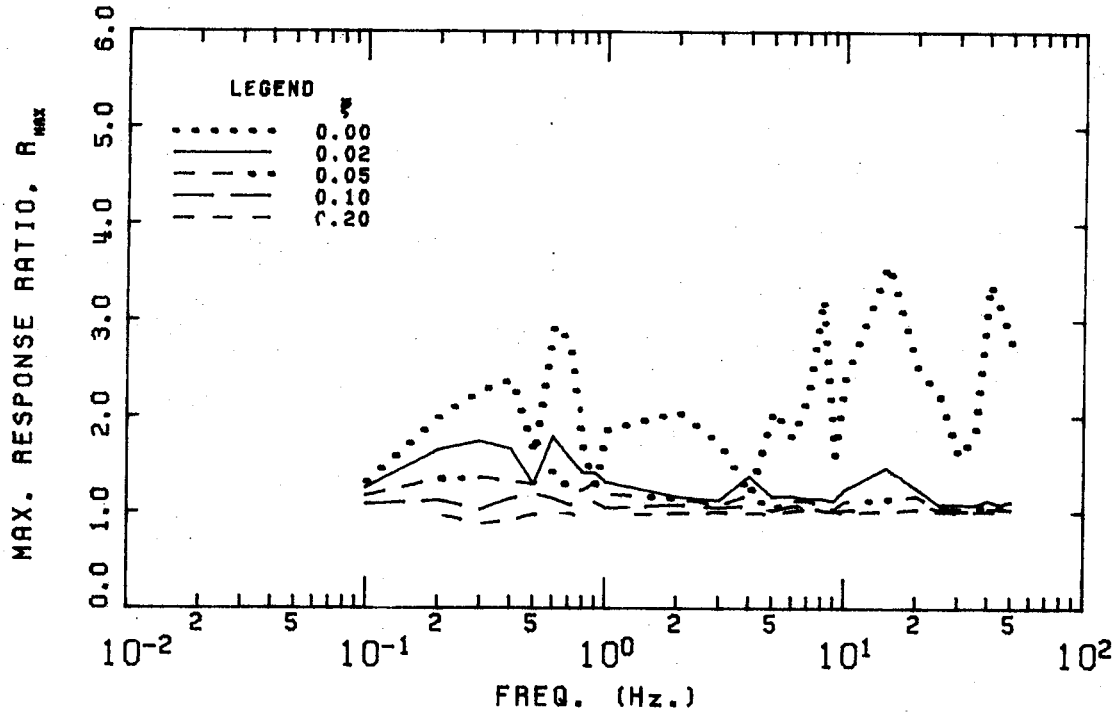

FIGURE B.62 HONDO 26 APRIL 1979 17H 08M 54S

B.3 Crushing Failure Load Histories and Response Spectra - Hondo

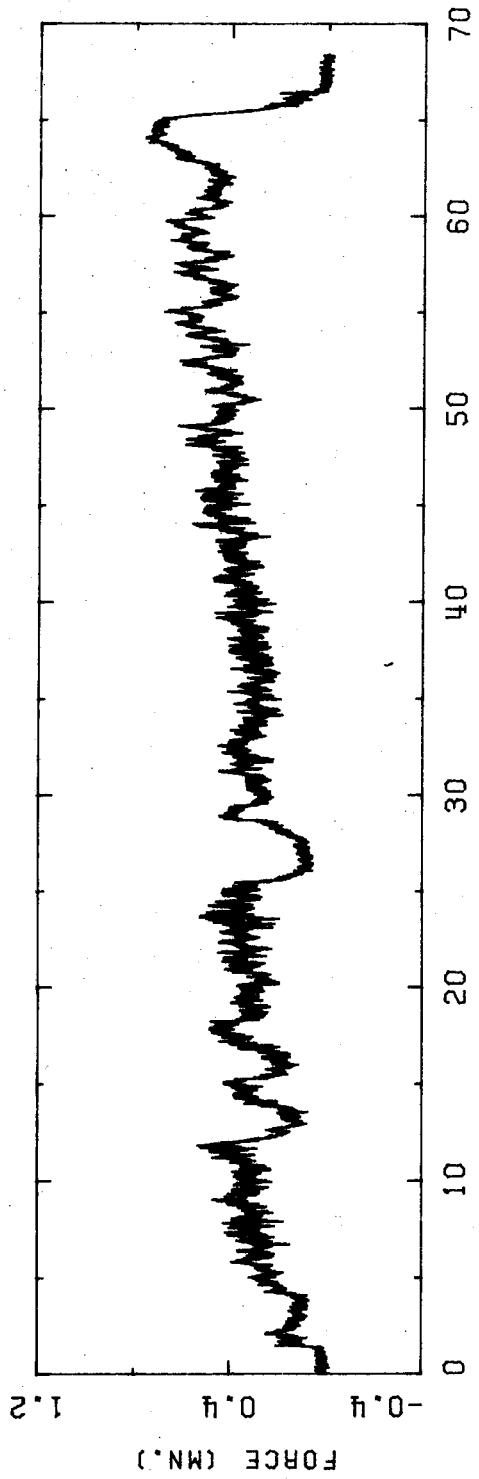

FIGURE B.63 HONDO 10 APRIL 1976 18H 42M 35S

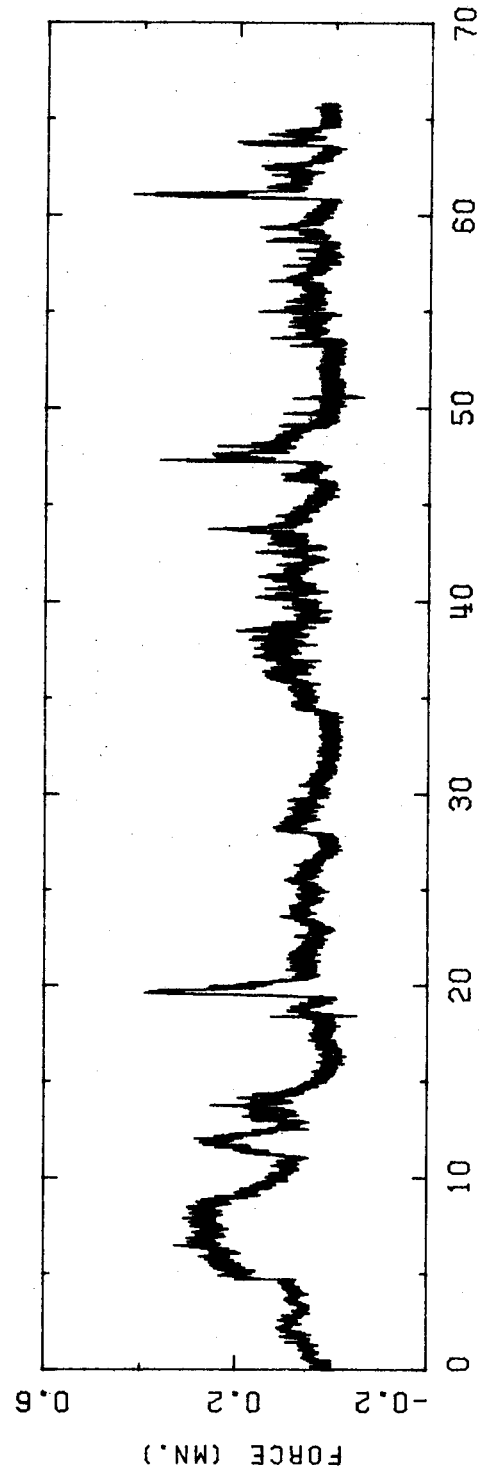

FIGURE B.64 HONDO 10 APRIL 1976 21H 13M 11S

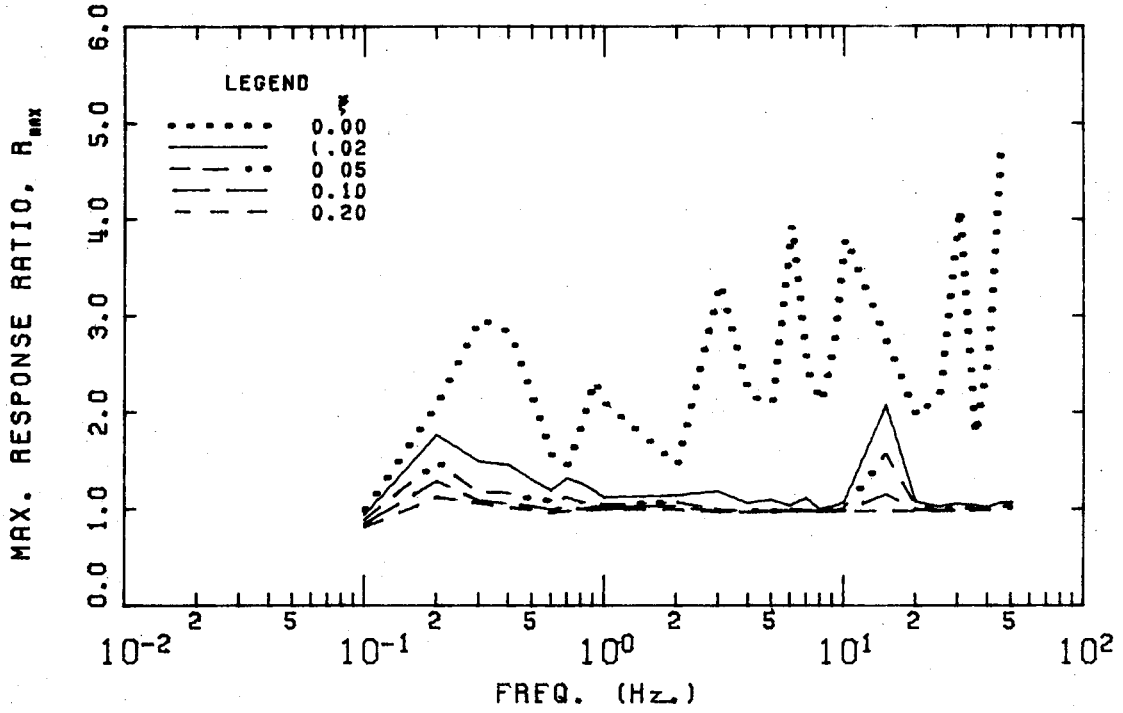

FIGURE B.65 HONDO 10 APRIL 1976 18H 42M 35S

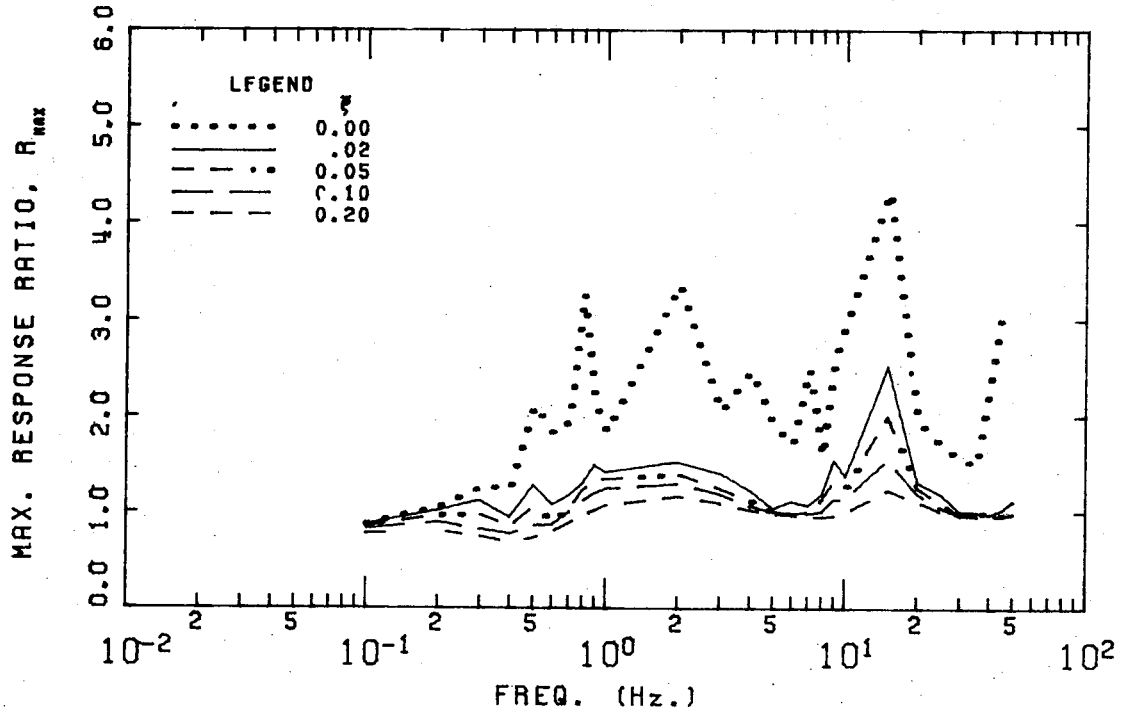

FIGURE B.66 HONDO 10 APRIL 1976 21H 13M 11S

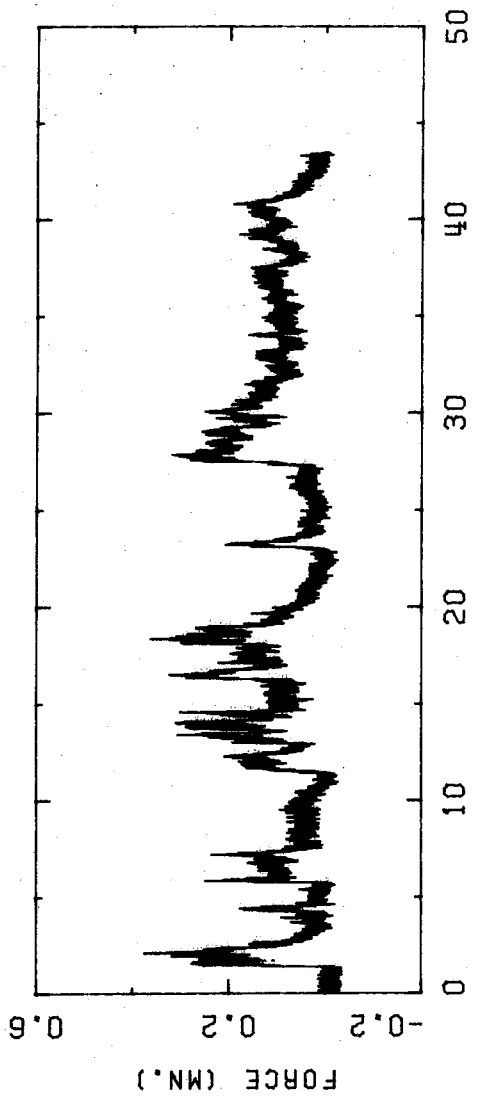

FIGURE B.67 HONDO 10 APRIL 1976 21H 13M 28S

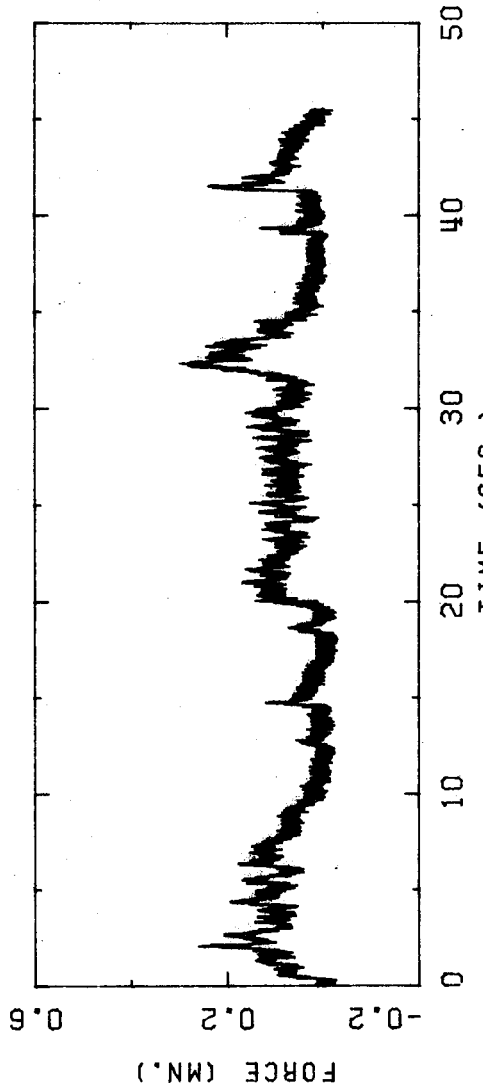

FIGURE B.68 HONDO 10 APRIL 1976 21H 14M 47S

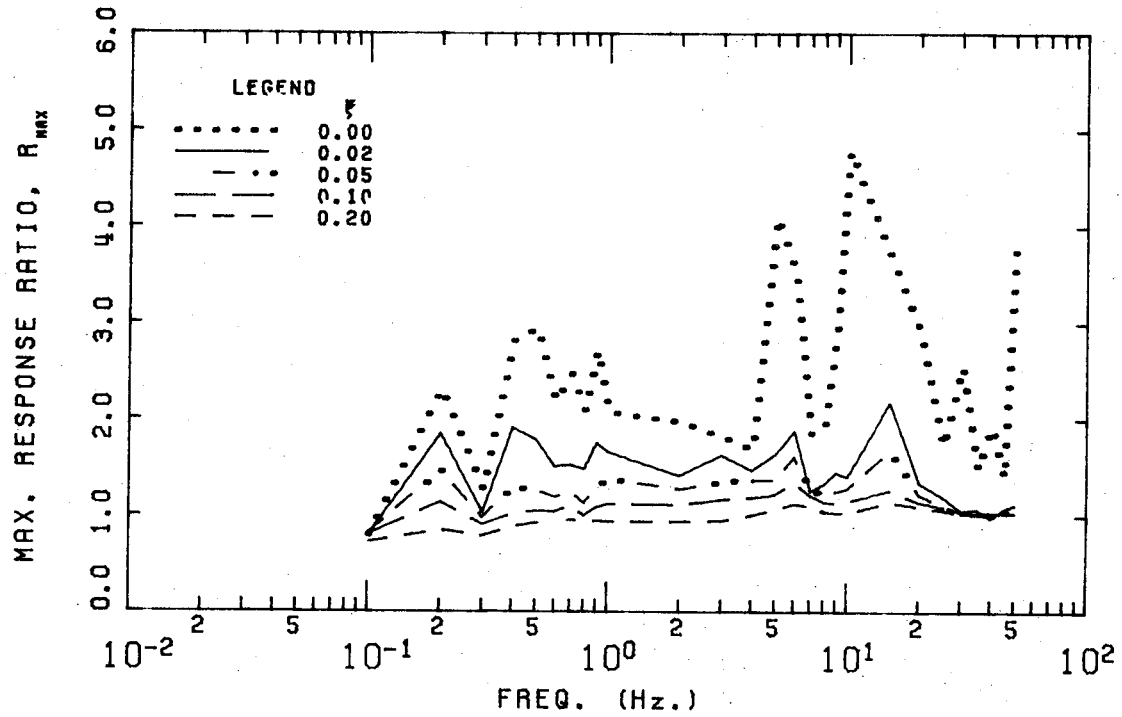

FIGURE B.69 HONDO 10 APRIL 1976 21H 13M 28S

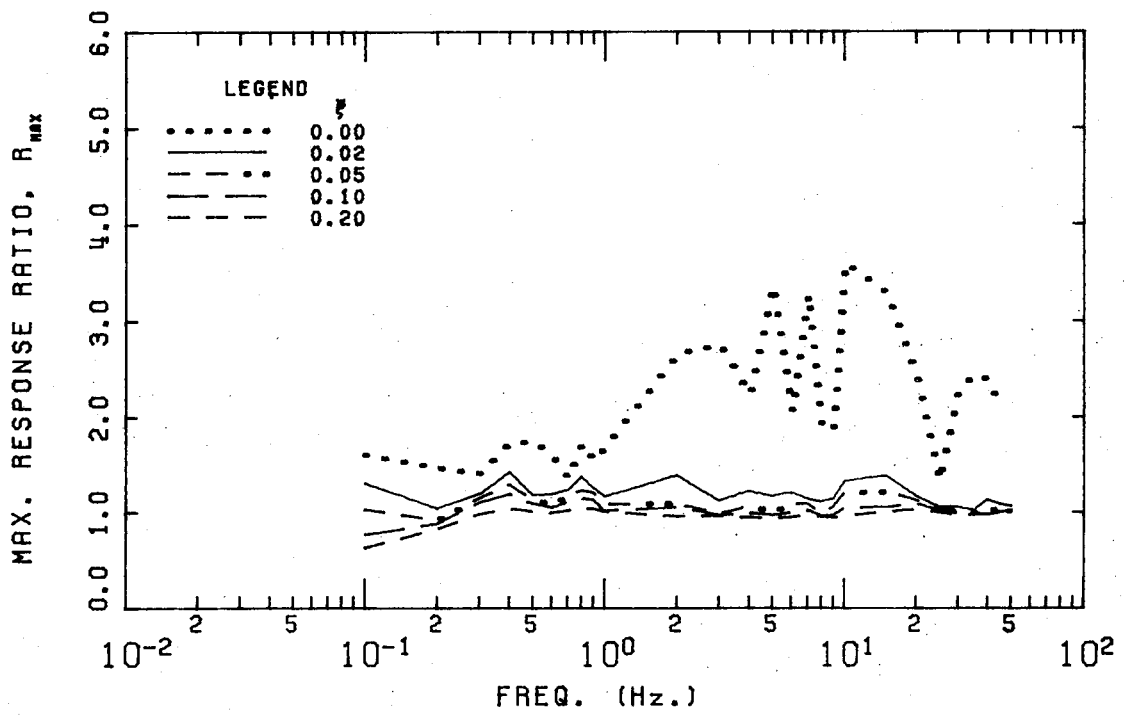

FIGURE B.70 HONDO 10 APRIL 1976 21H 14M 47S

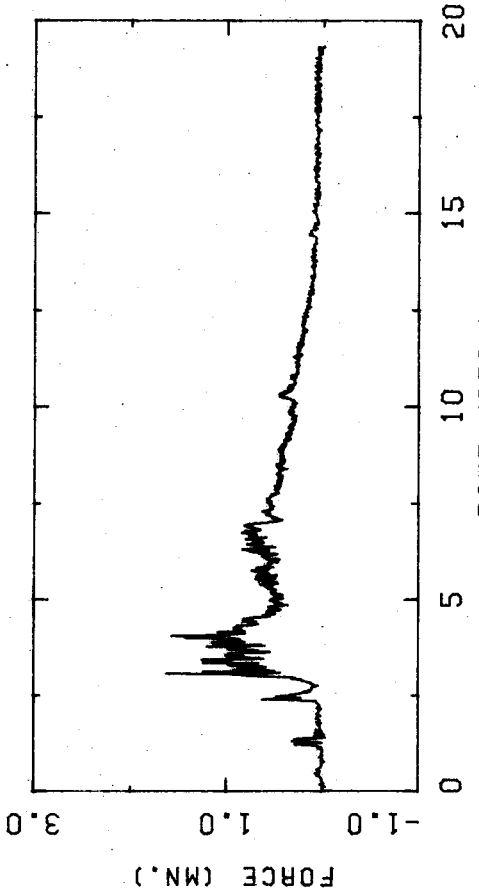

FIGURE B.71 HONDO 12 APRIL 1976 16H 13M 12S

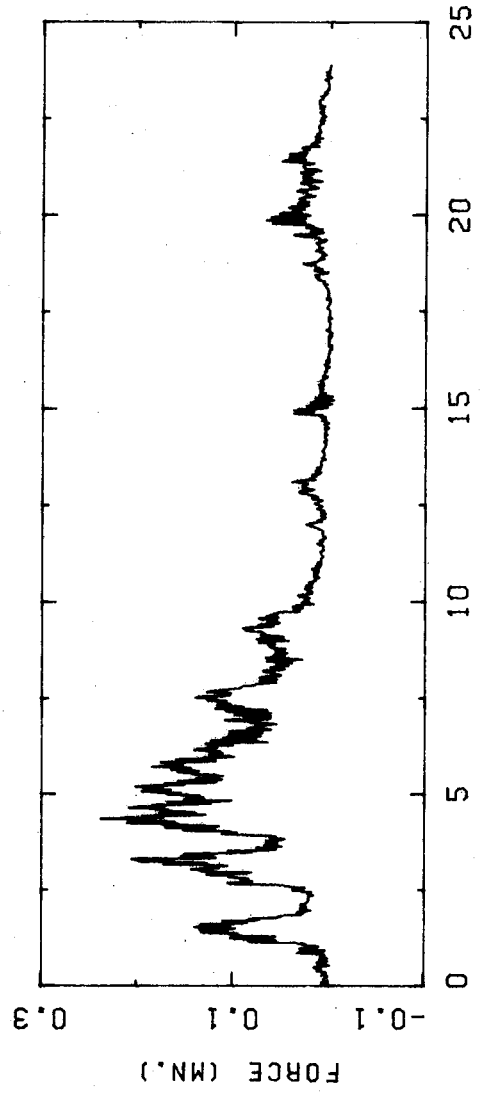

FIGURE B.72 HONDO 11 APRIL 1977 17H 37M 31S

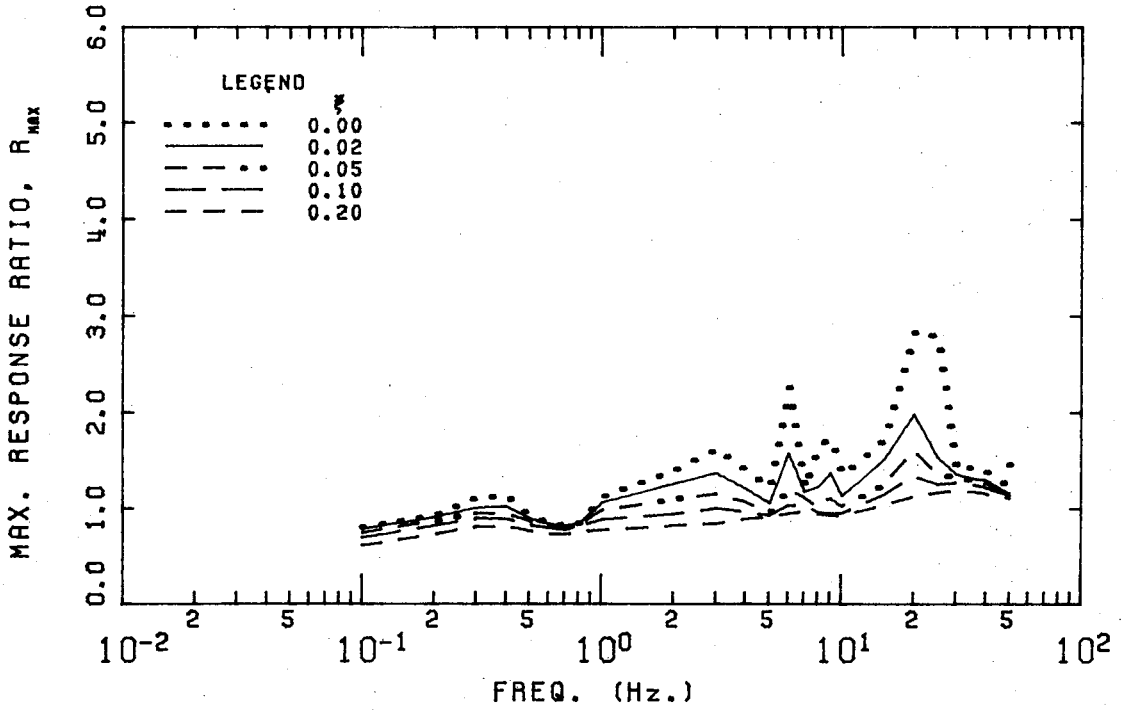

FIGURE B.73 HONDO 12 APRIL 1976 16H 13M 12S

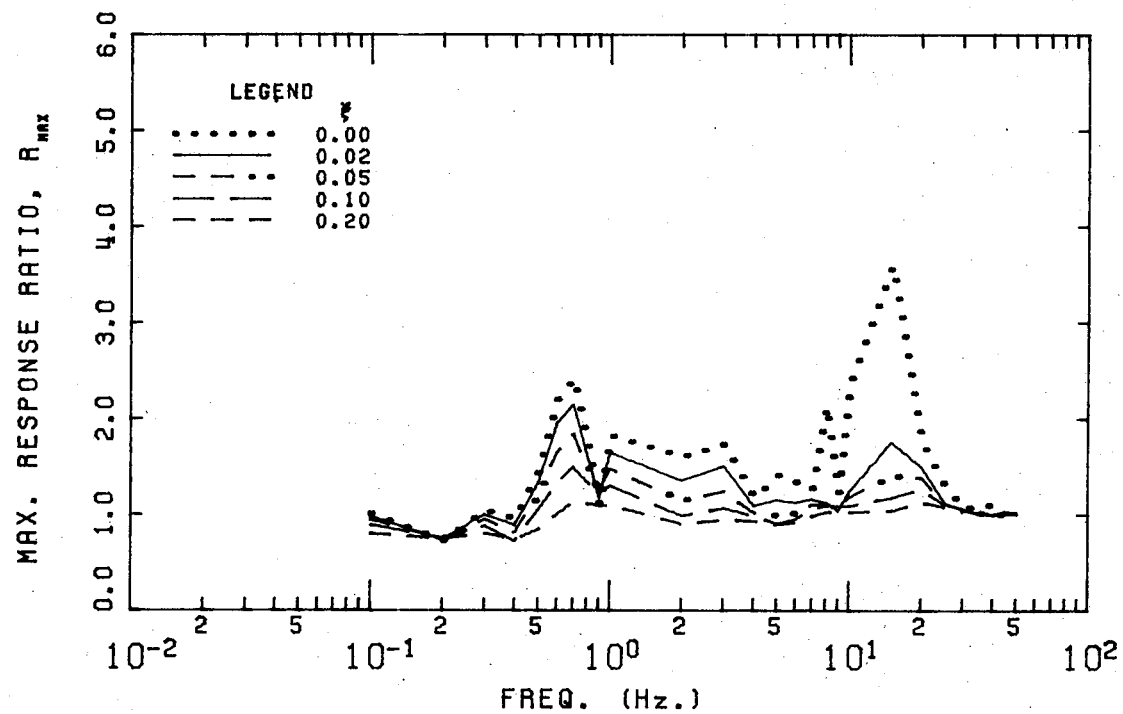

FIGURE B.74 HONDO 11 APRIL 1977 17H 37M 31S

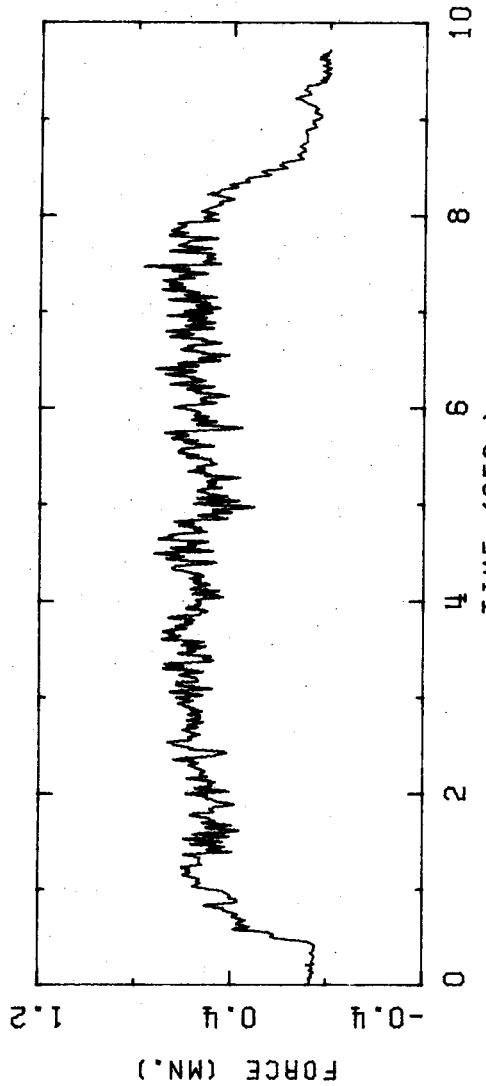

FIGURE B.75 HONDO 12 APRIL 1977 03H 46M 17S

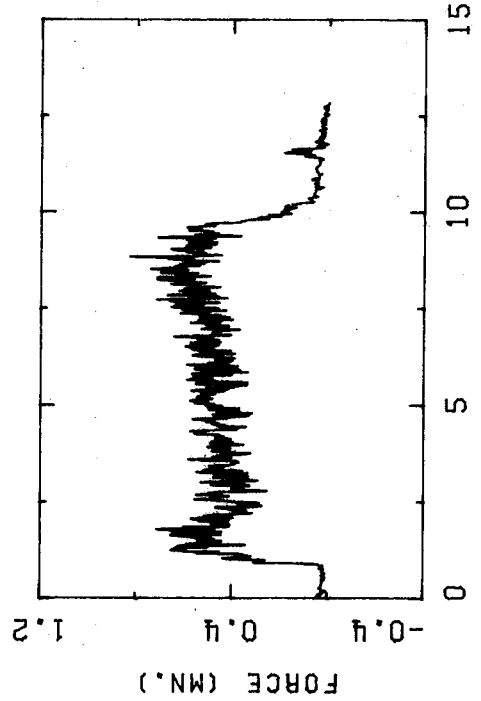

FIGURE B.76 HONDO 12 APRIL 1977 03H 47M 16S

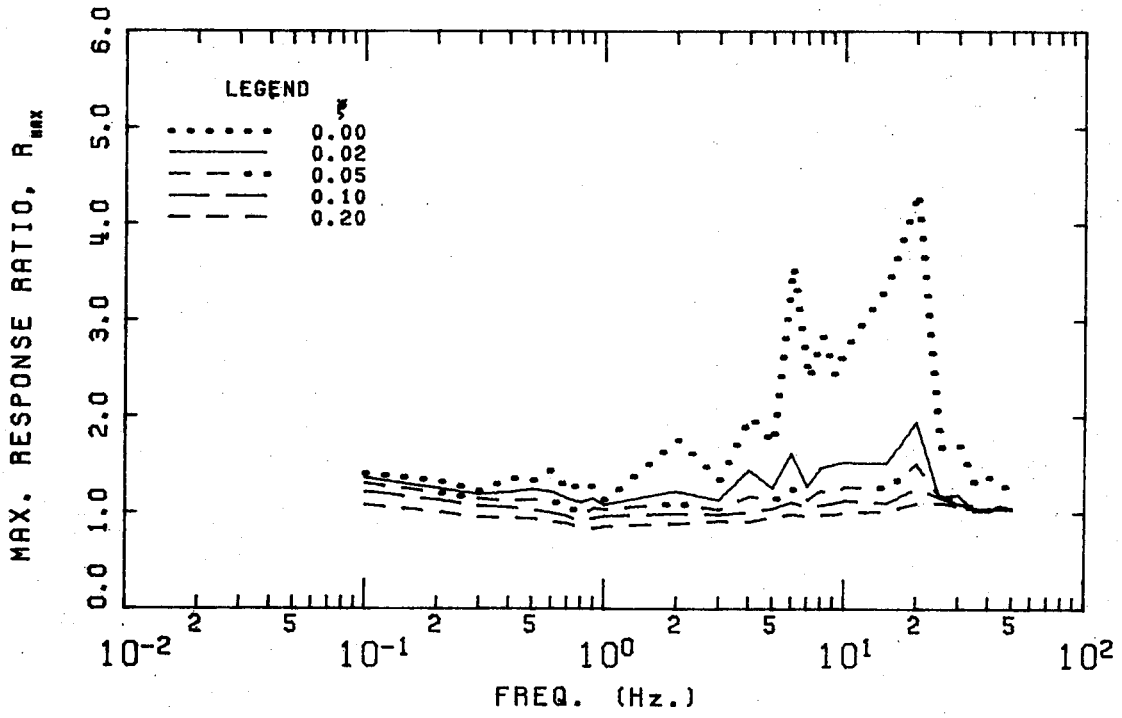

FIGURE B.77 HONDO 12 APRIL 1979 03H 46M 17S

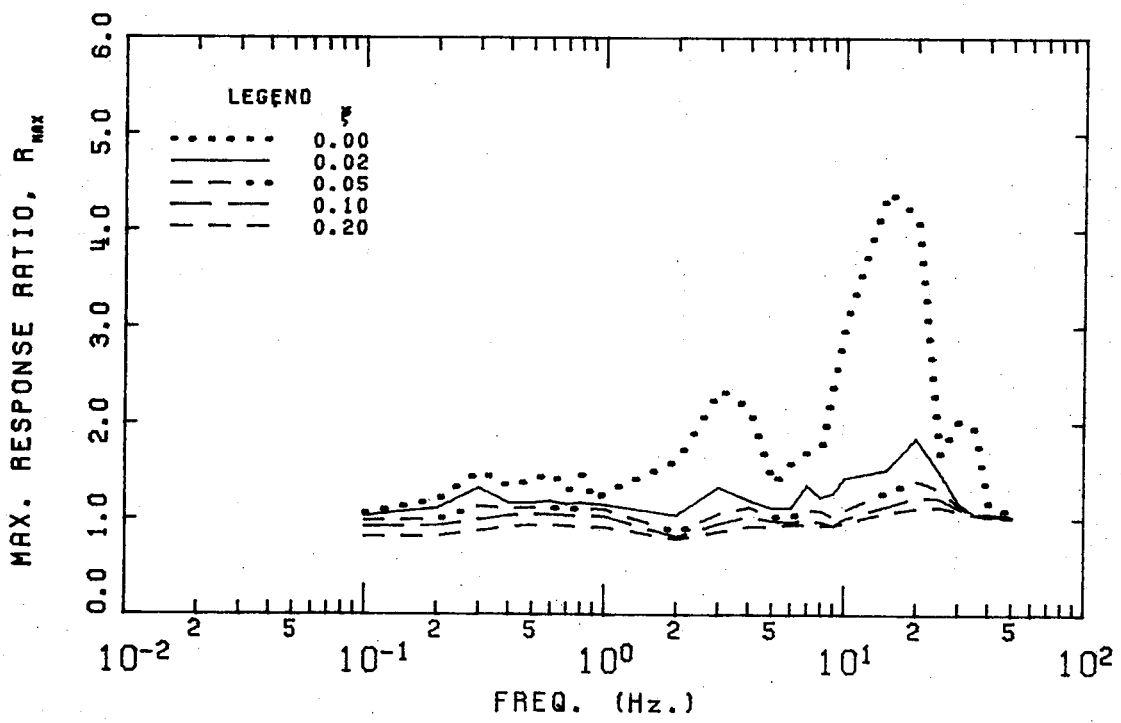

FIGURE B.78 HONDO 12 APRIL 1977 03H 47M 16S

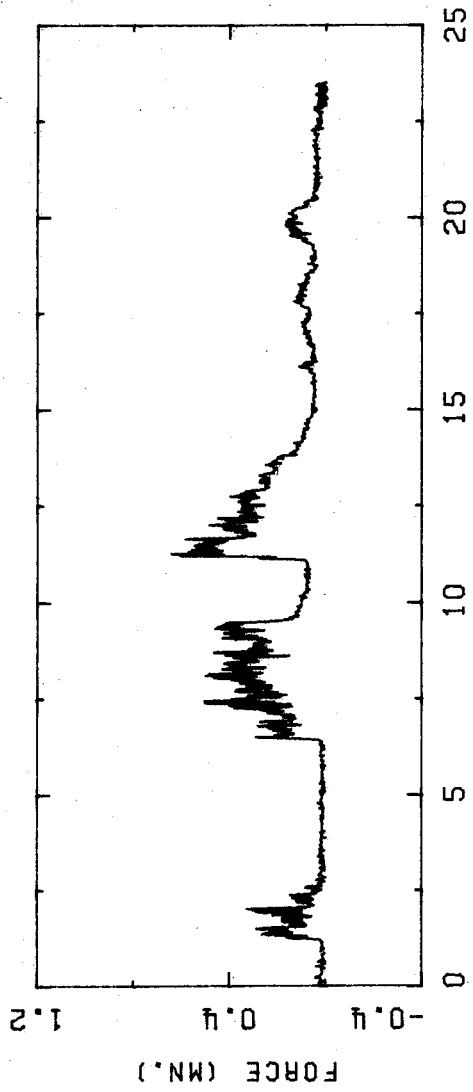

FIGURE B.79 HONDO 12 APRIL 1977 03H 56M 50S

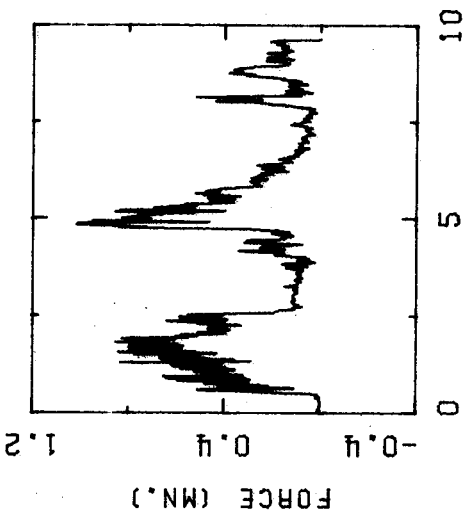

FIGURE B.80 HONDO 12 APRIL 1977 04H 00M 13S

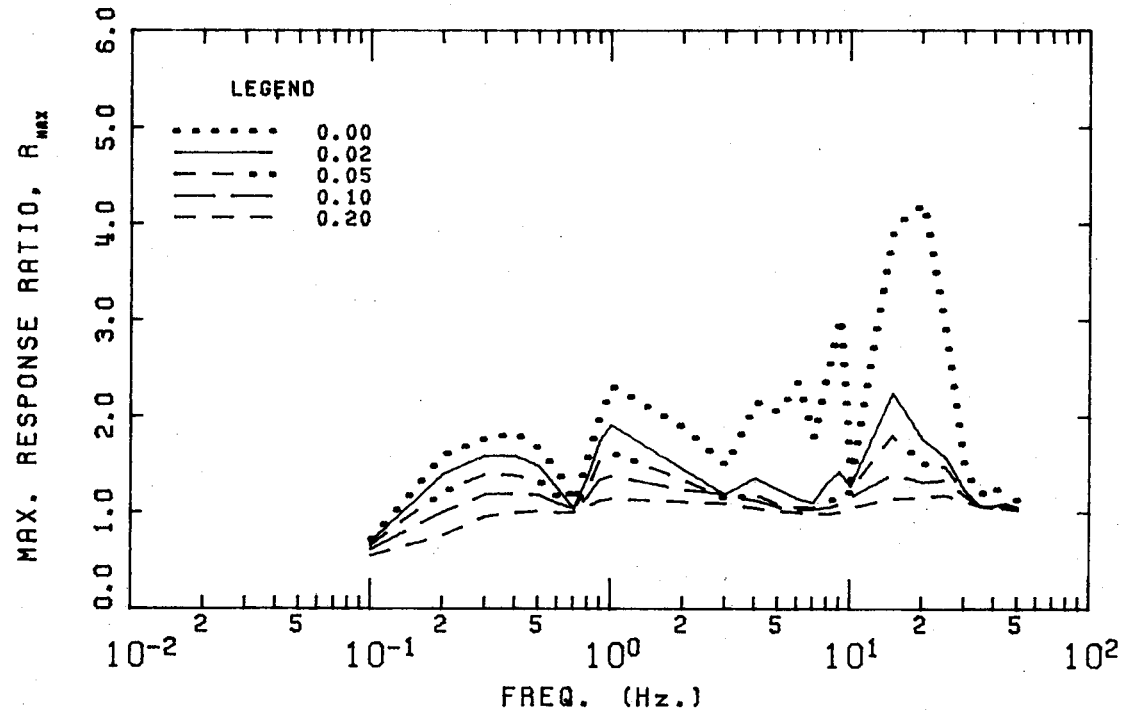

FIGURE B.81 HONDO 12 APRIL 1977 03H 56M 50S

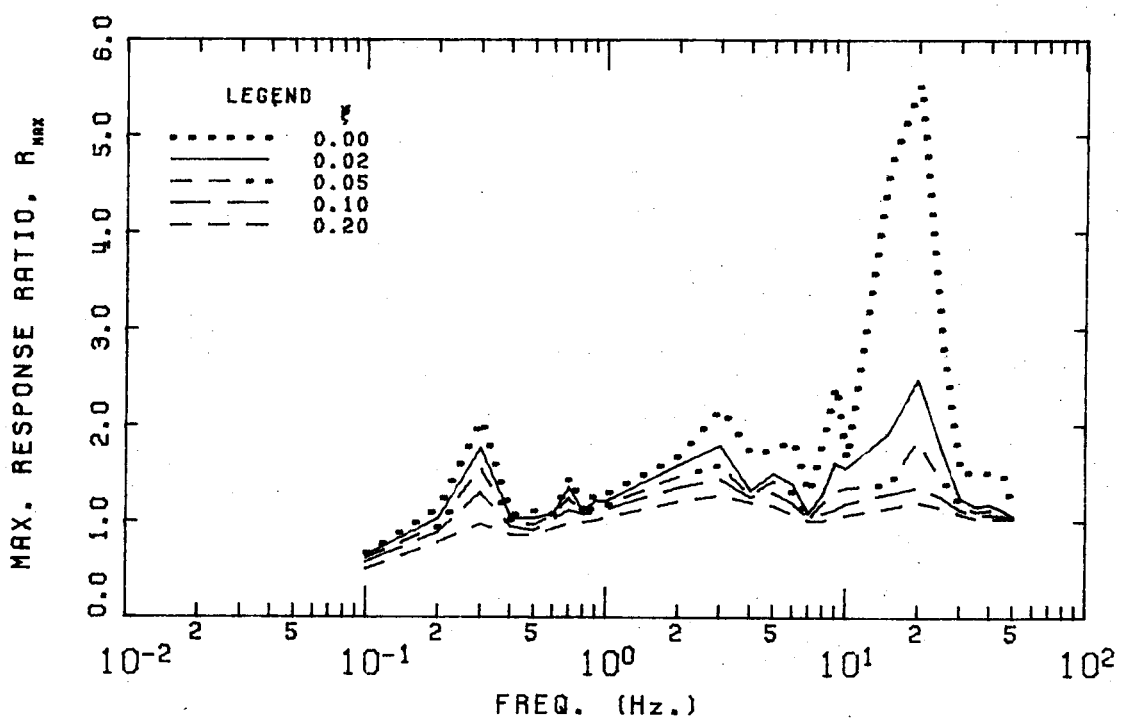

FIGURE B.82 HONDO 12 APRIL 1977 04H 00M 13S

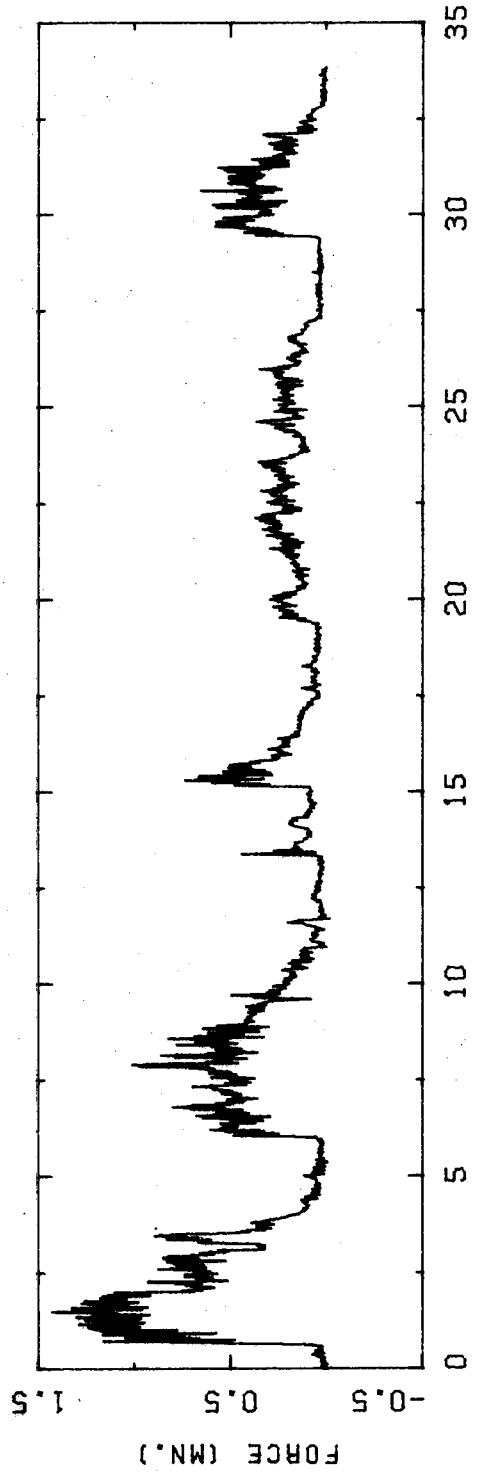

FIGURE B.83 HONDO 12 APRIL 1977 04H 03M 20S

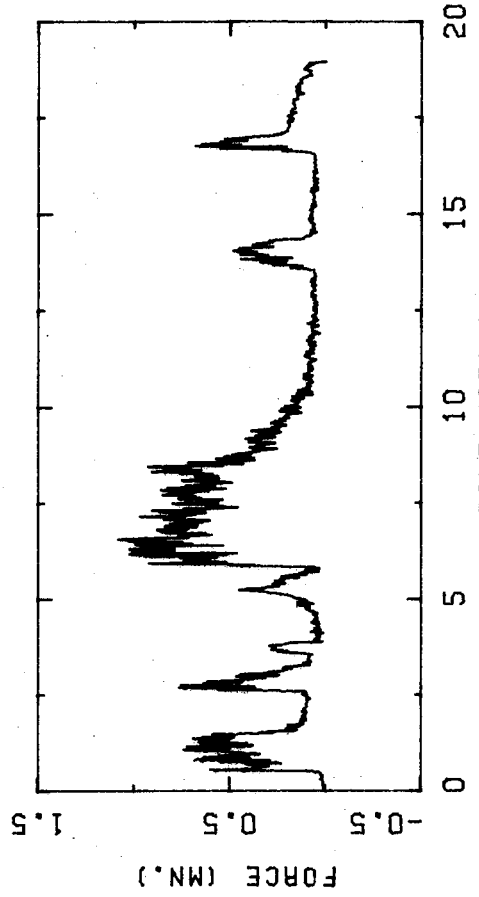

FIGURE B.84 HONDO 12 APRIL 1977 05H 02M 32S

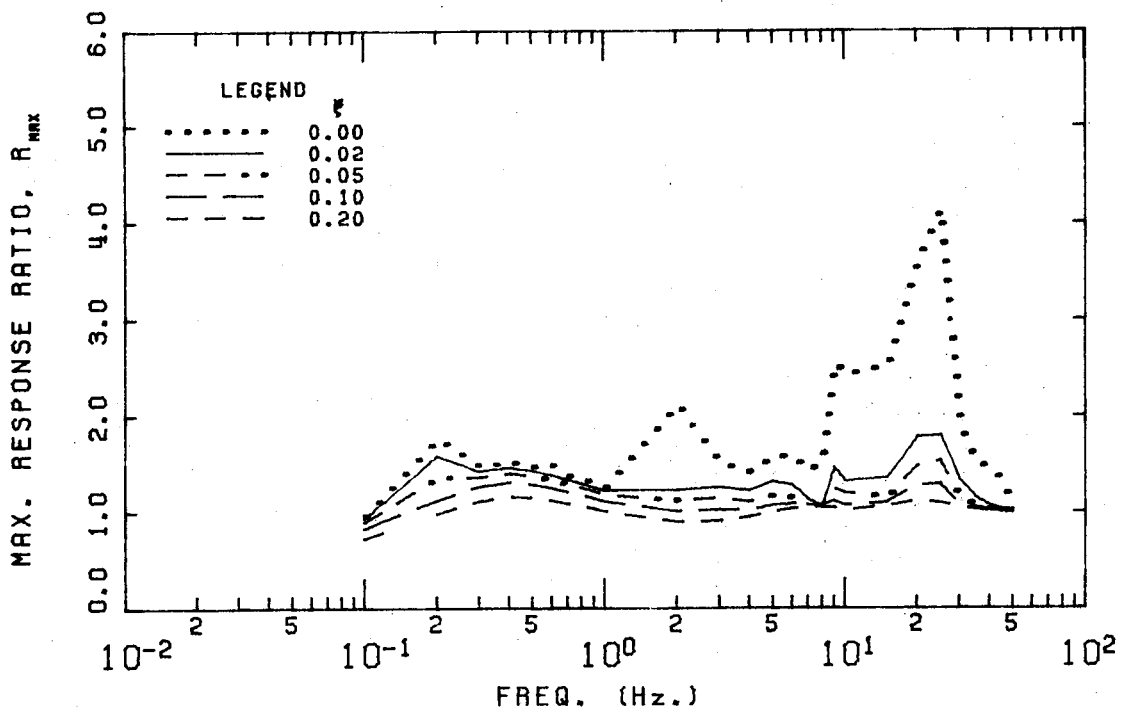

FIGURE B.85 HONDO 12 APRIL 1977 04H 03M 20S

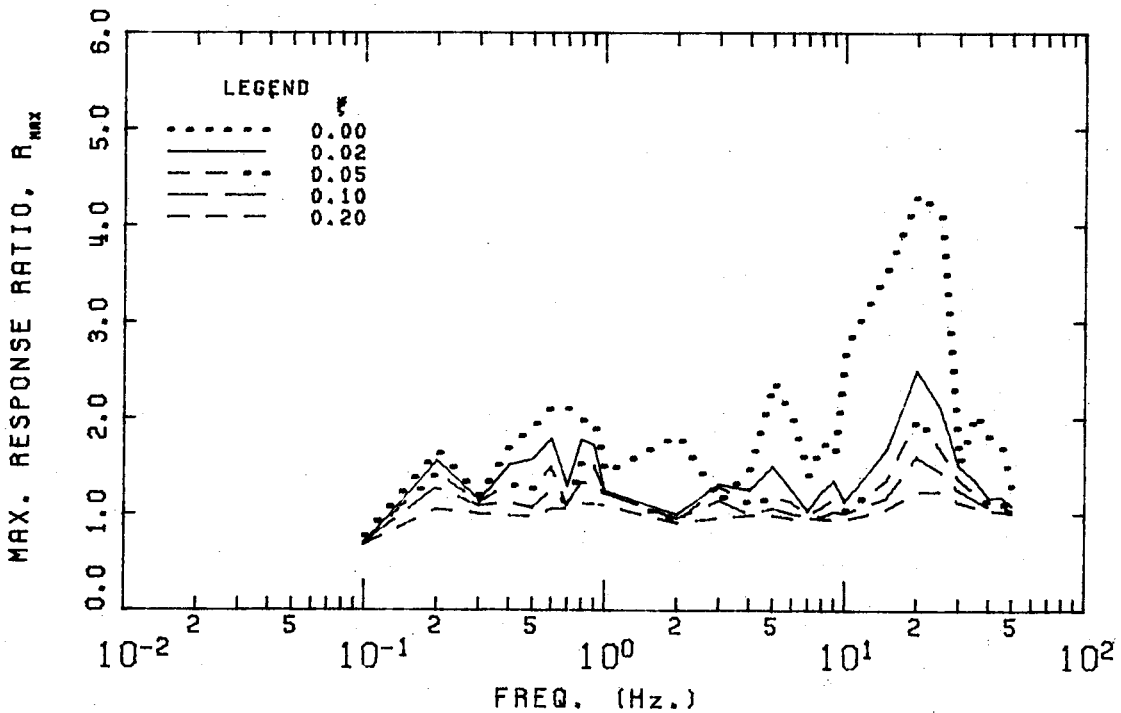

FIGURE B.86 HONDO 12 APRIL 1977 05H 02M 32S

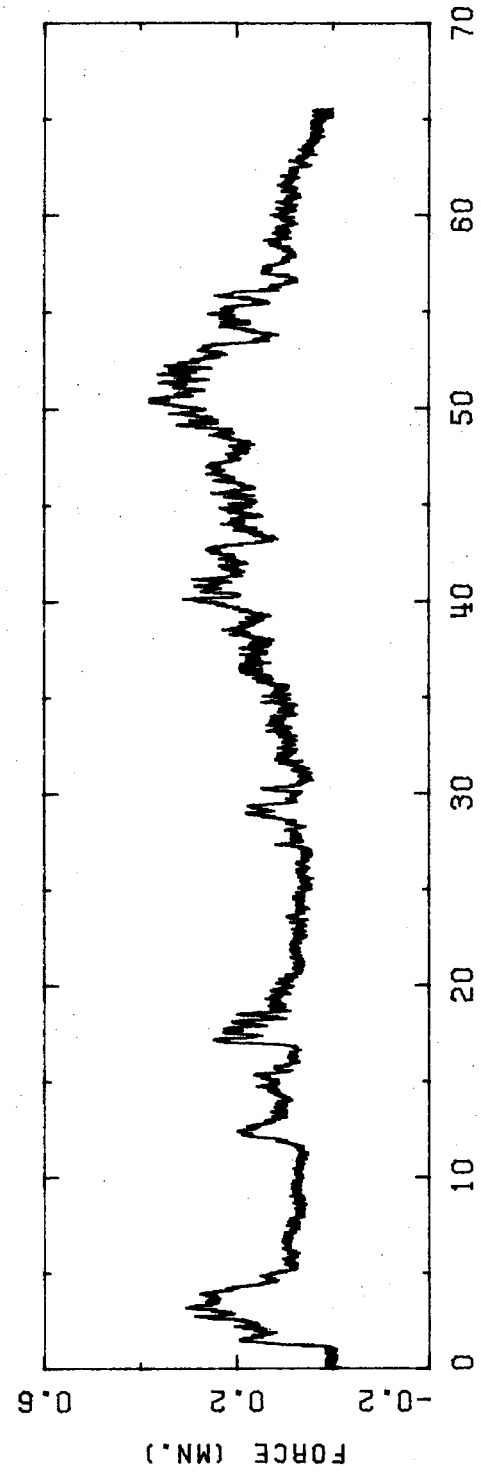

FIGURE B.87 HONDO 25 APRIL 1979 16H 54M 09S

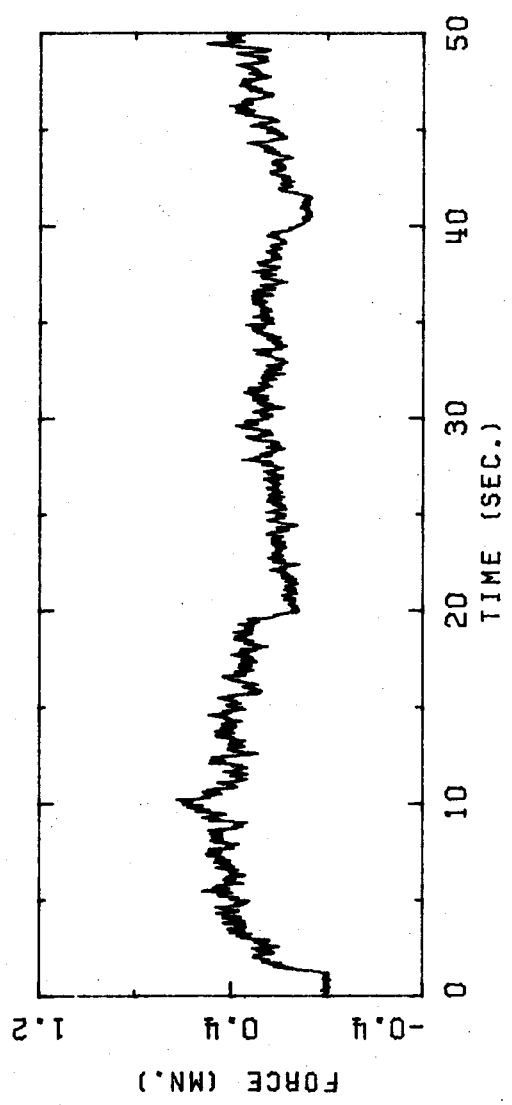

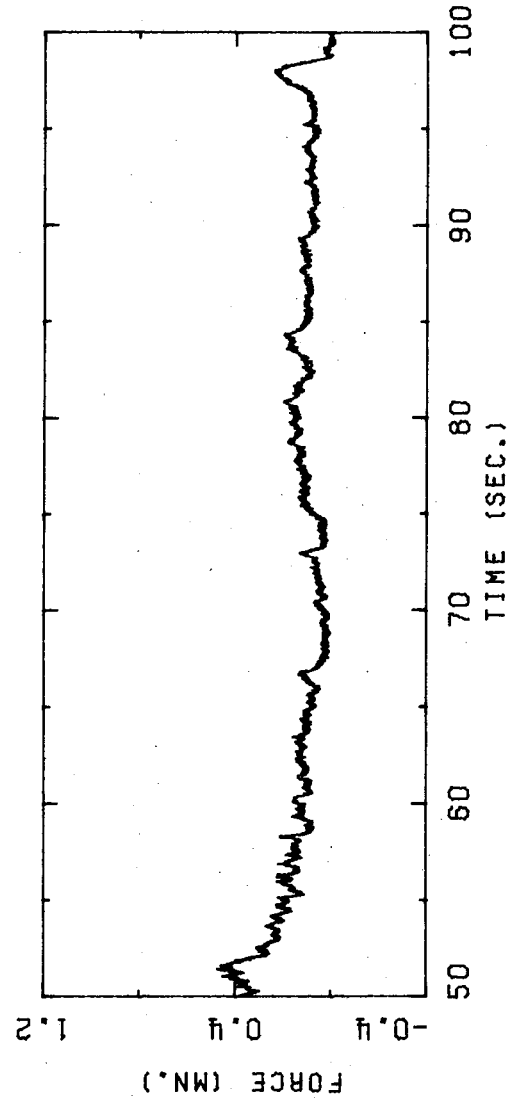

FIGURE B.88 HONDO 25 APRIL 1979 16H 54M 51S

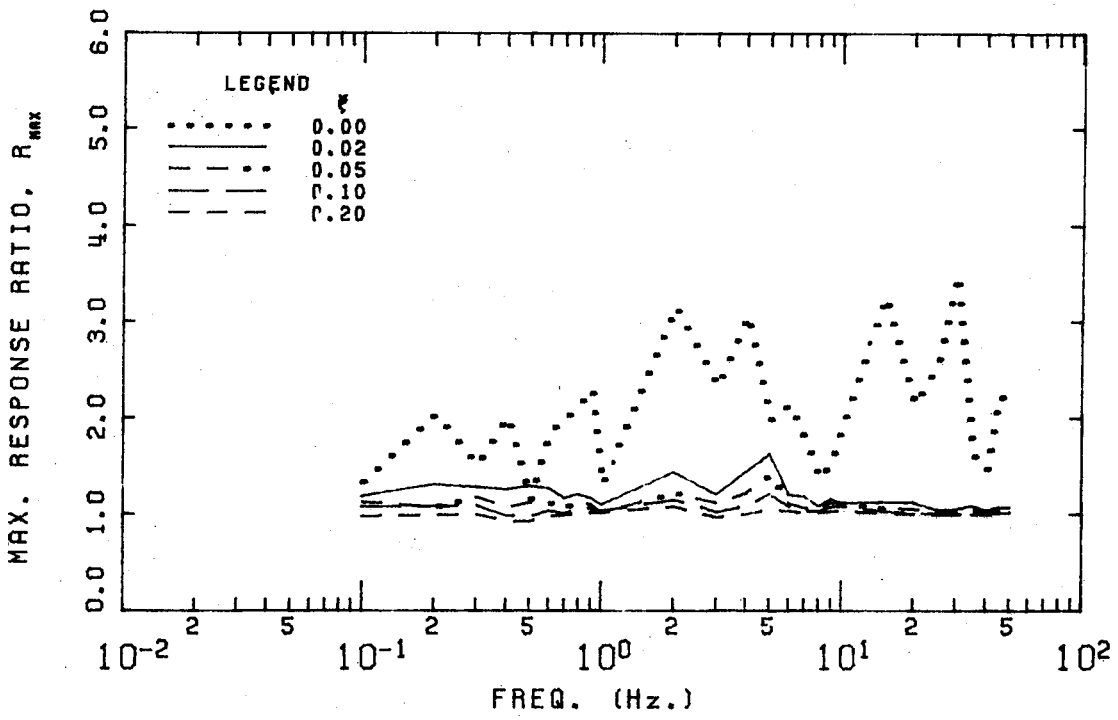

FIGURE B.89 HONDO 25 APRIL 1979 16H 54M 09S

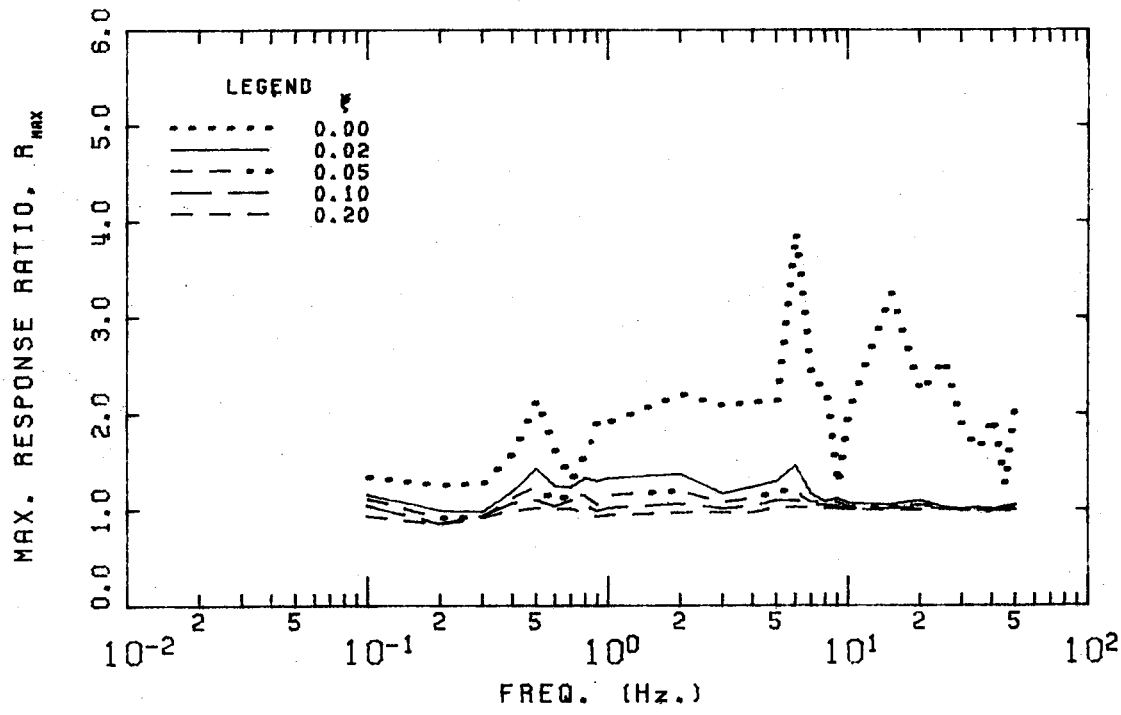

FIGURE B.90 HONDO 25 APRIL 1979 16H 54M 51S

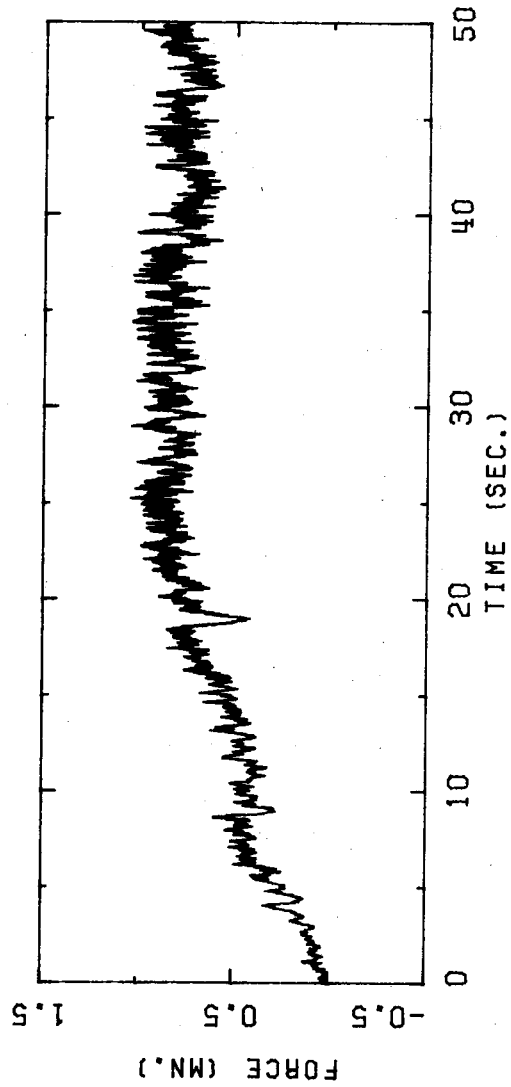

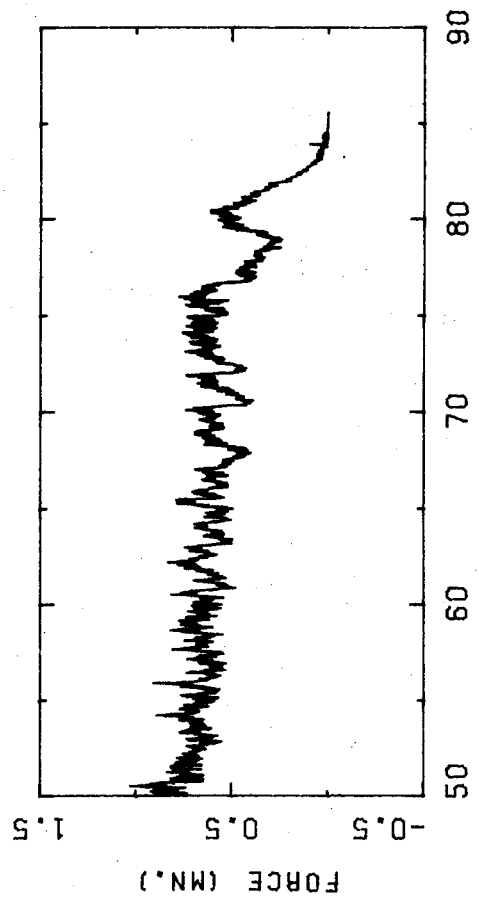

FIGURE B.91 HONDO 26 APRIL 1979 16H 49M 19S

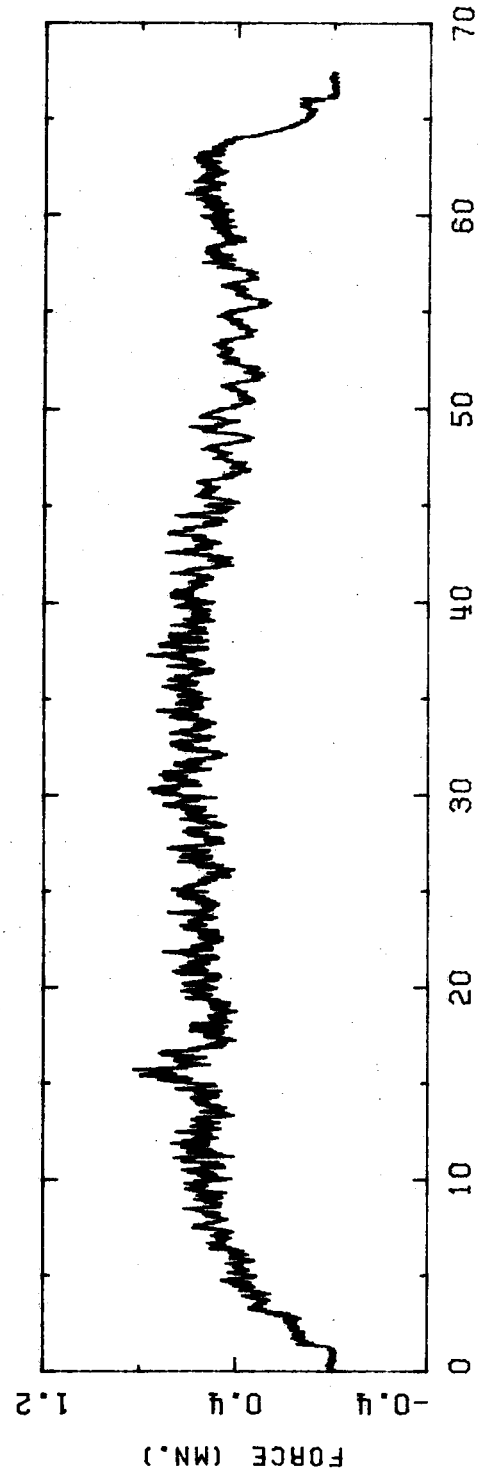

FIGURE B.92 HONDO 26 APRIL 1979 16H 51M 41S

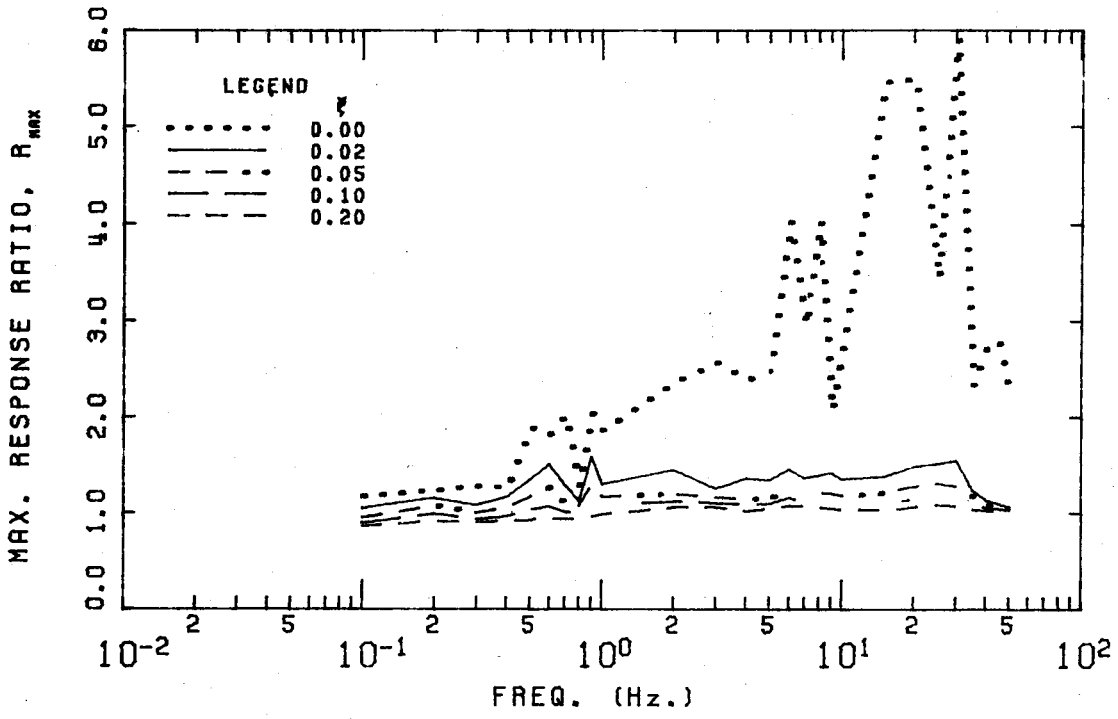

FIGURE B.93 HONDO 26 APRIL 1979 16H 49M 19S

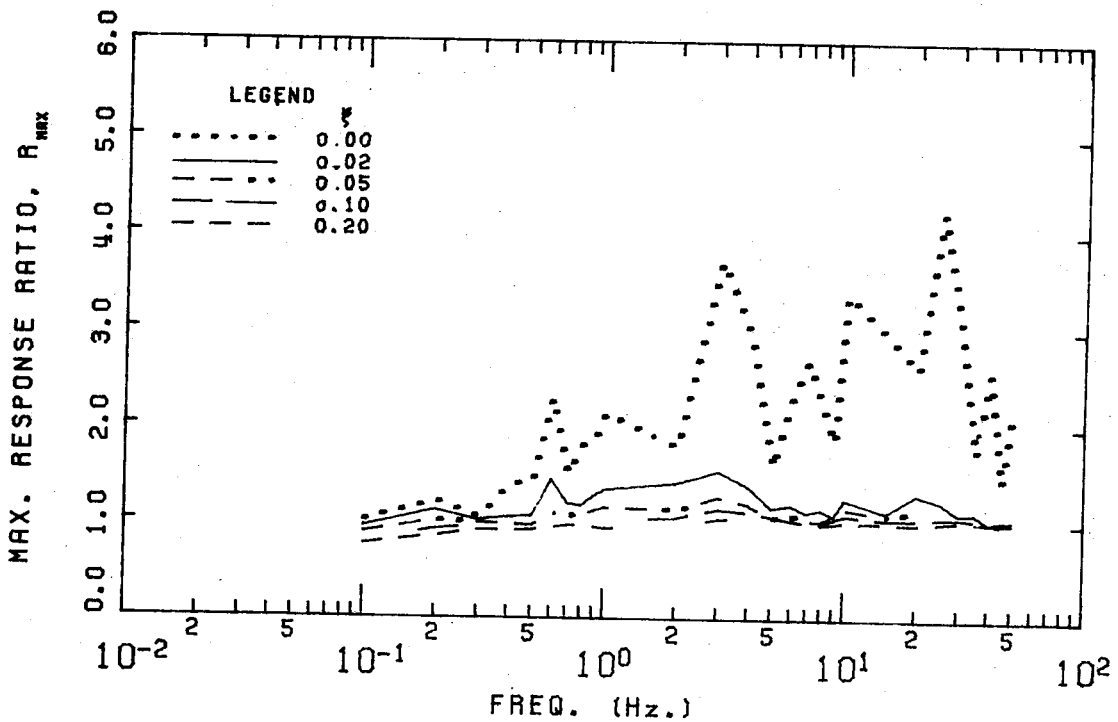

FIGURE B.94 HONDO 26 APRIL 1979 16H 51M 41S

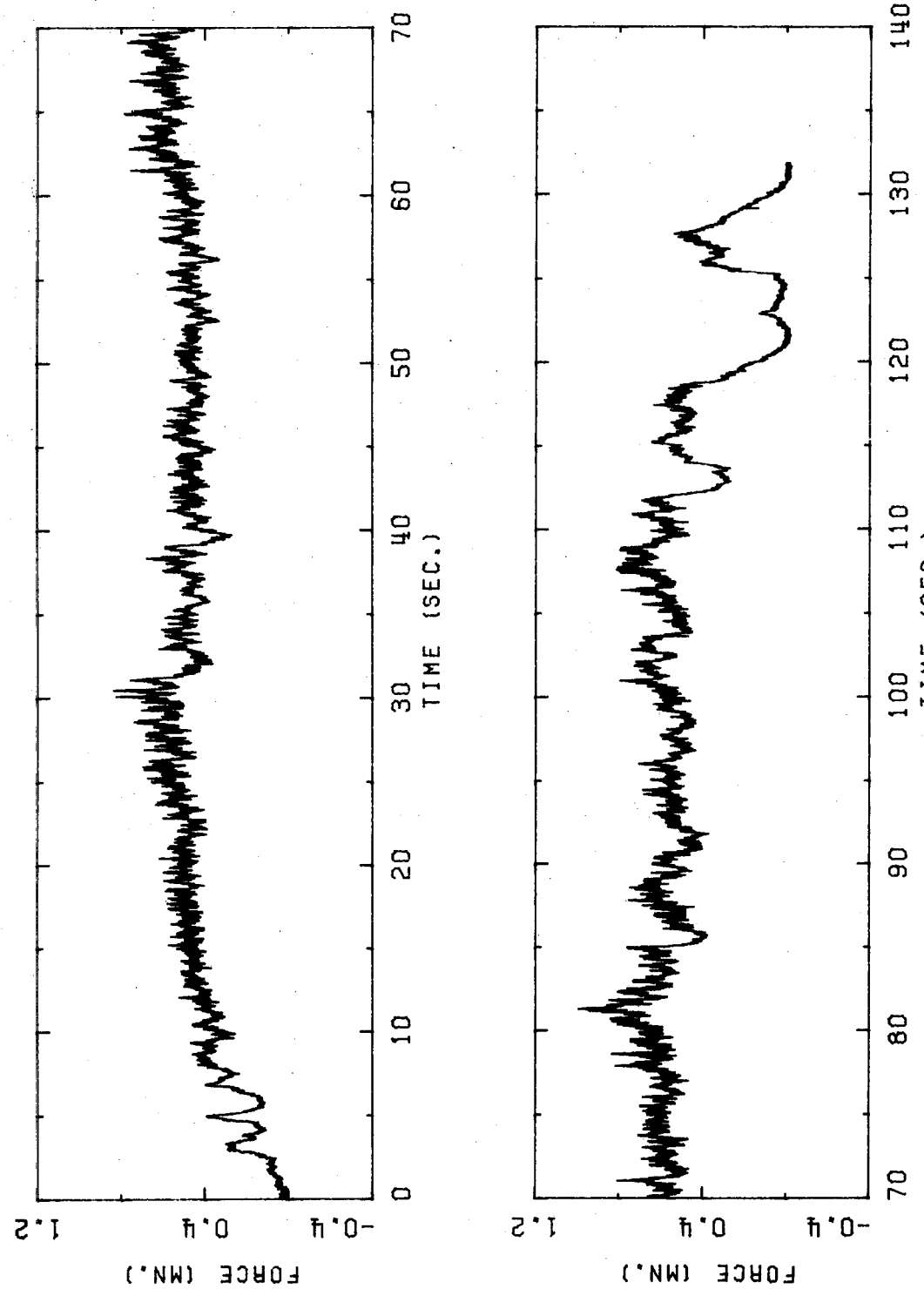

FIGURE B.95 HONDO 26 APRIL 1979 16H 54M 16S

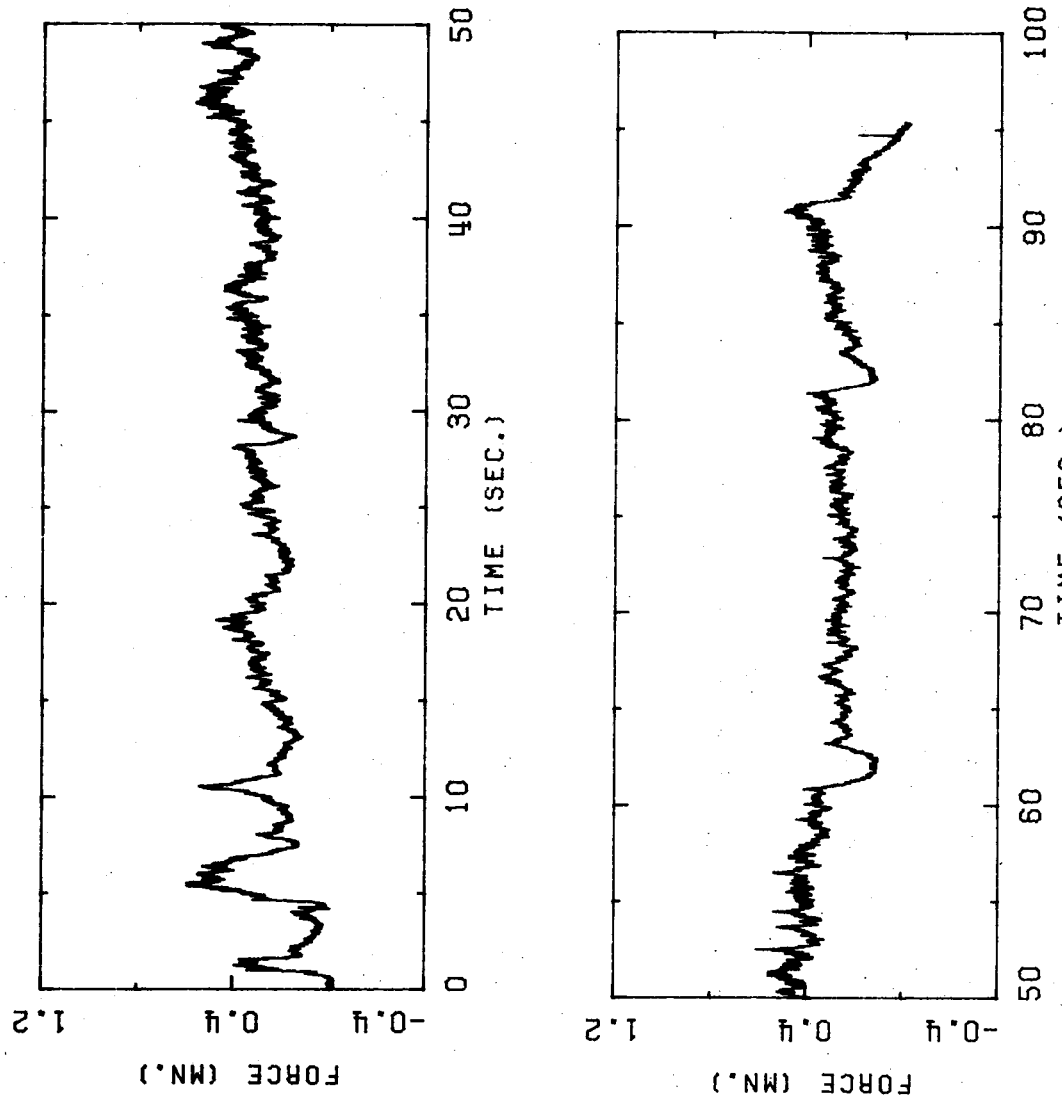

FIGURE B.96 HONDO 26 APRIL 1979 16H 56M 17S

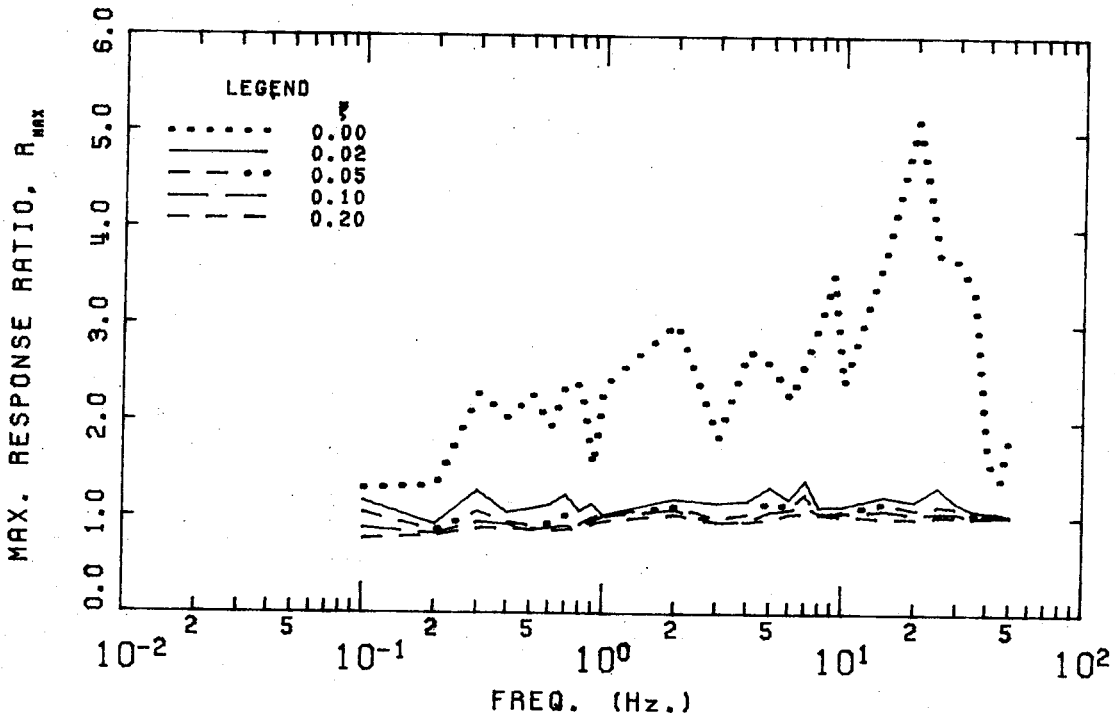

FIGURE B.97 HONDO 26 APRIL 1979 16H 54M 16S

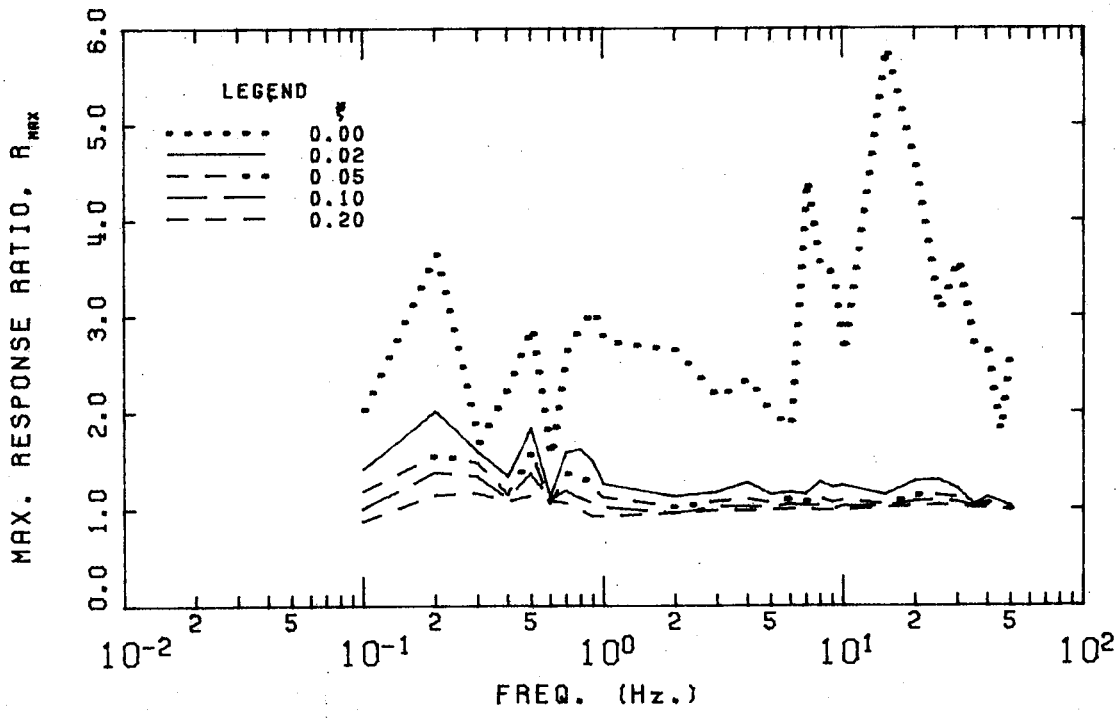

FIGURE B.98 HONDO 26 APRIL 1979 16H 56M 17S

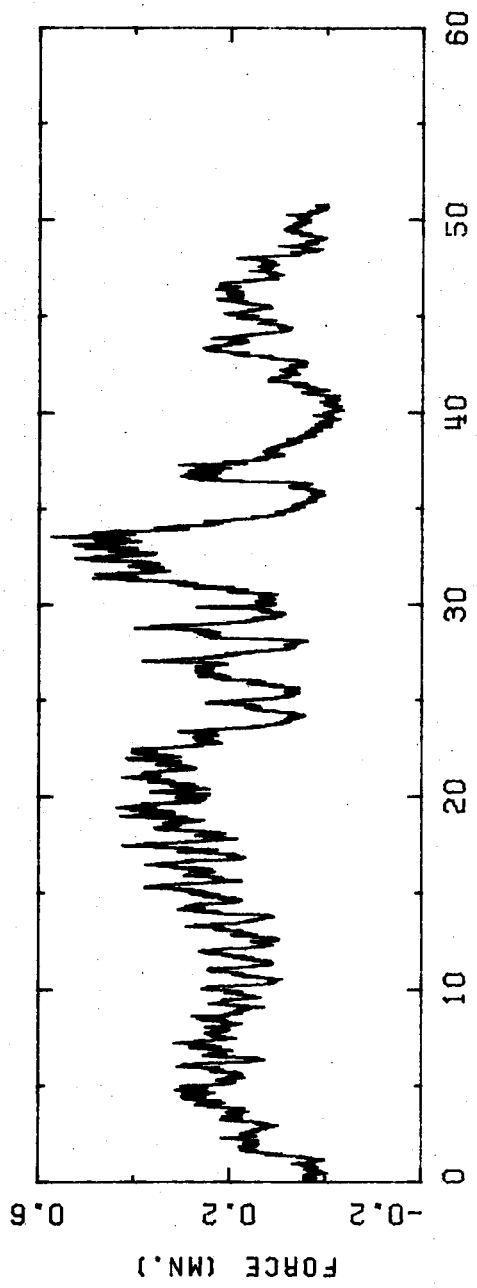

FIGURE B.99 HONDO 26 APRIL 1979 17H 00M 17S

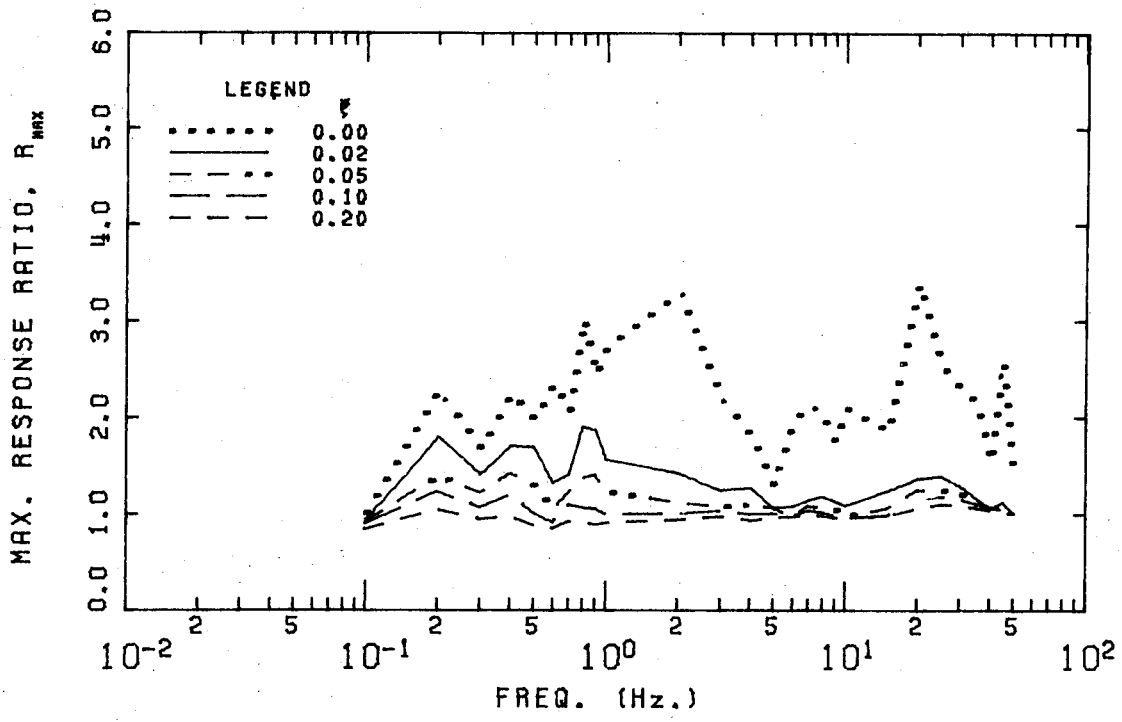

FIGURE B.100 HONDO 26 APRIL 1979 17H 00M 17S

B.4 Splitting Failure Load Histories and Response Spectra - Hondo

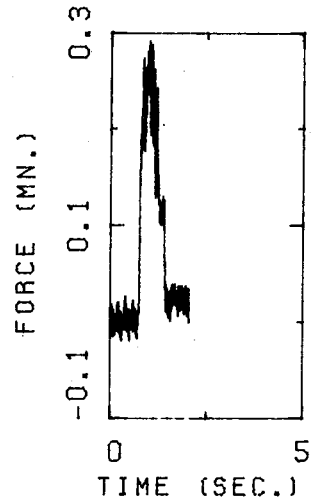

FIGURE B.101 HONDO 10 APRIL 1976 21H 18M 21S

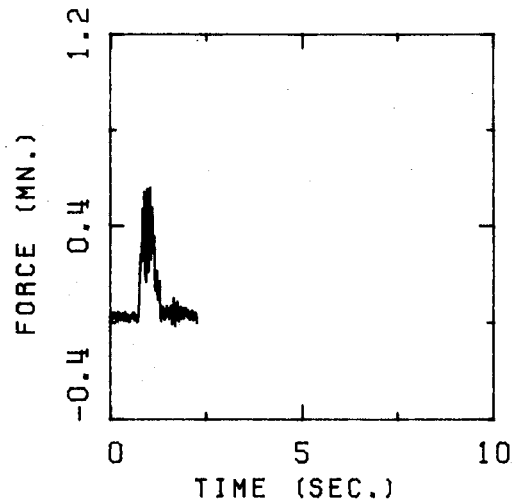

FIGURE B.102 HONDO 10 APRIL 1976 21H 18M 22S

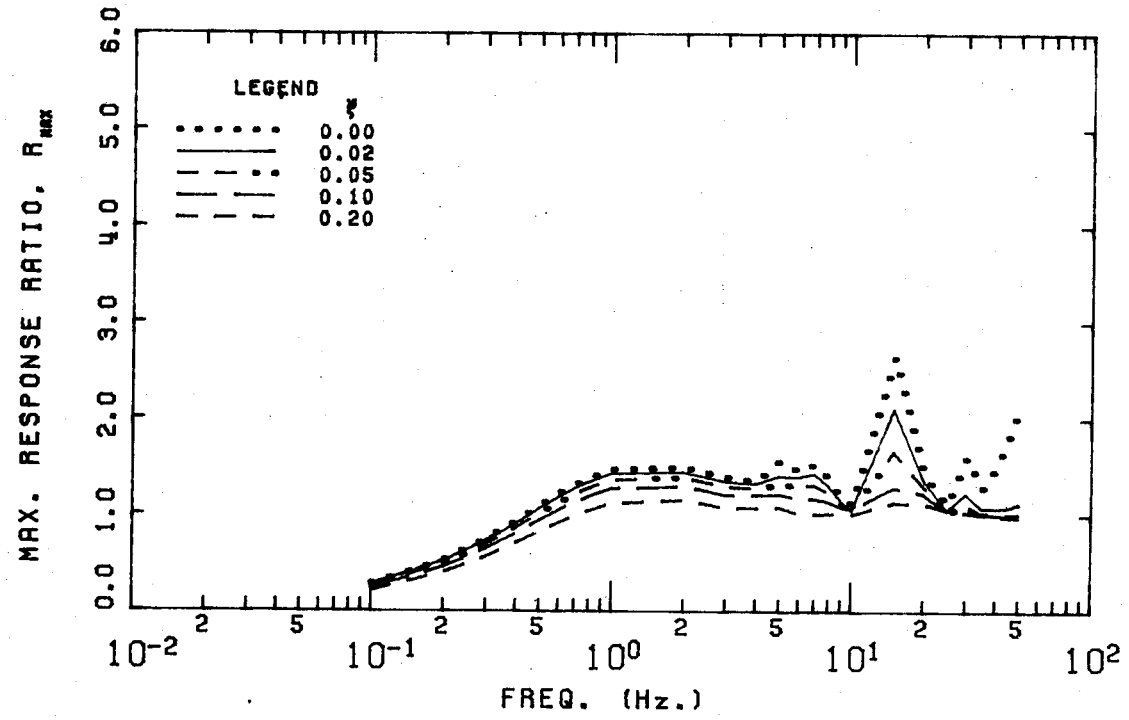

FIGURE B.103 HONDO 10 APRIL 1976 21H 18M 21S

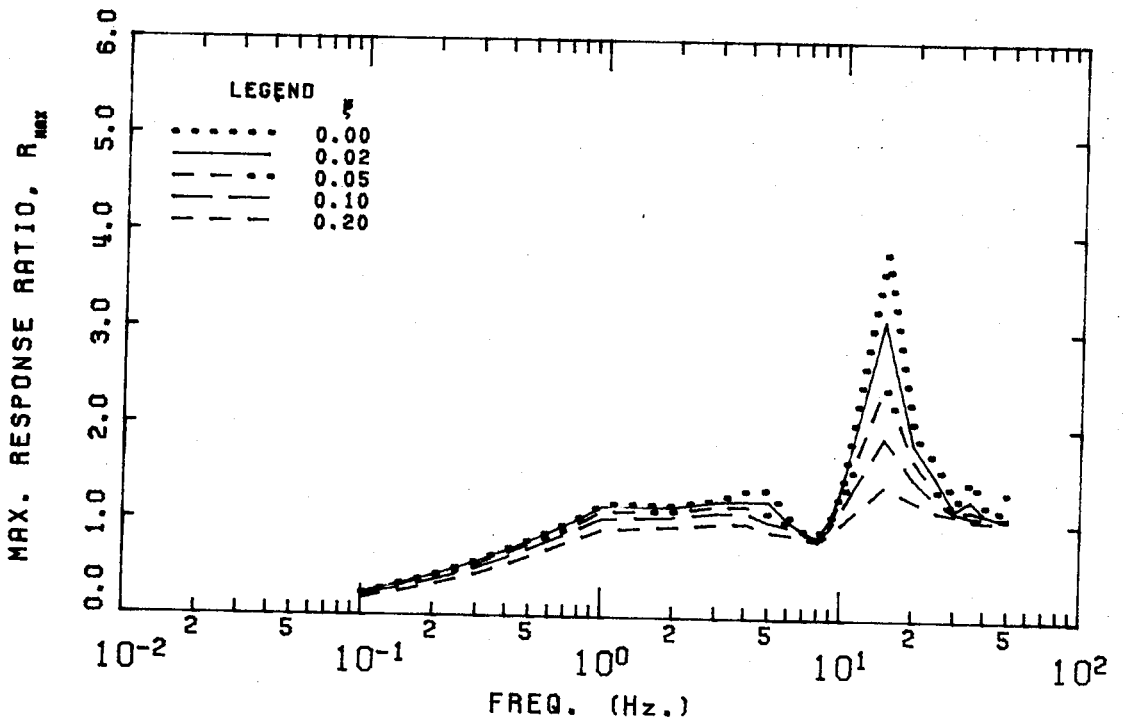

FIGURE B.104 HONDO 10 APRIL 1976 21H 18M 22S

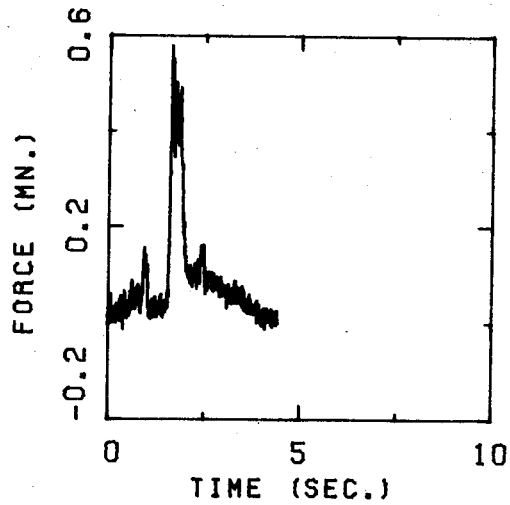

FIGURE B.105 HONDO 10 APRIL 1976 21H 18M 26S

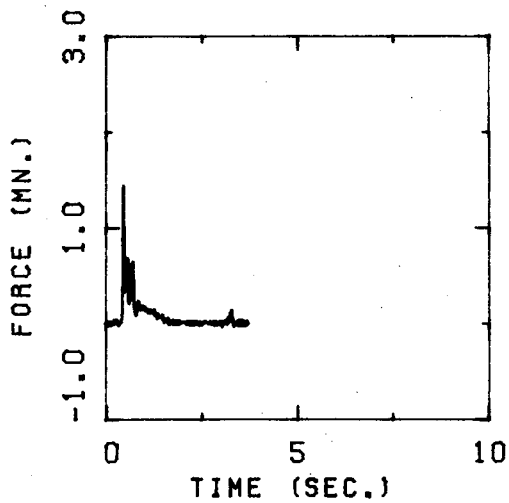

FIGURE B.106 HONDO 12 APRIL 1976 15H 59M 33S

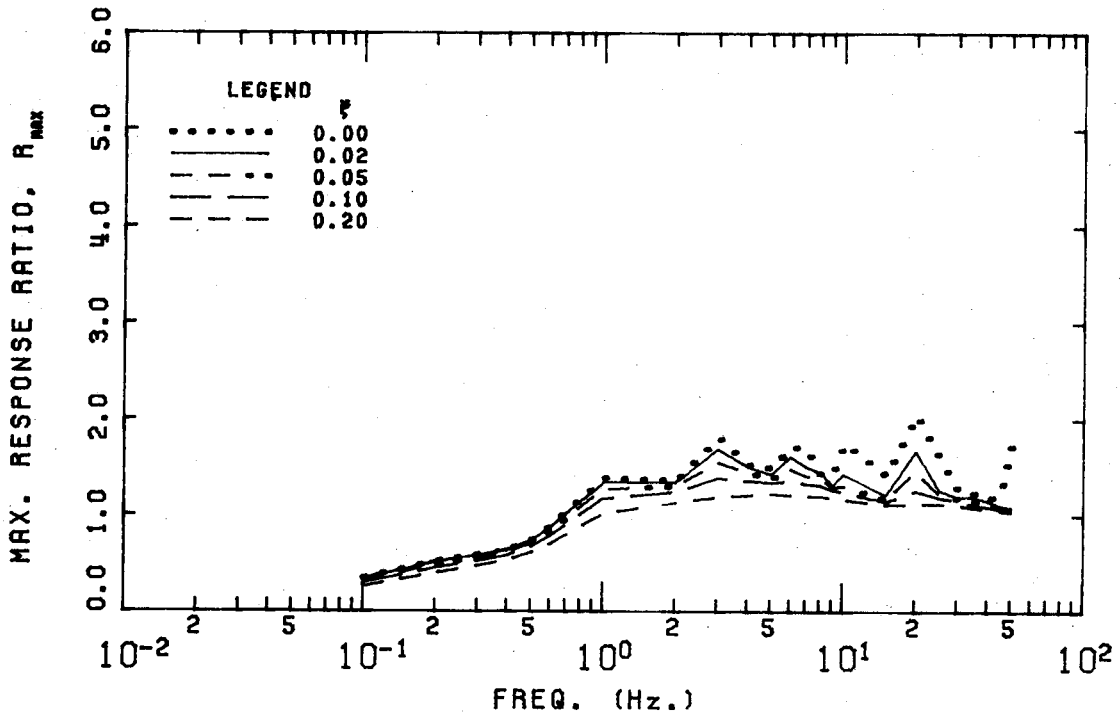

FIGURE B.107 HONDO 10 APRIL 1976 21H 18M 26S

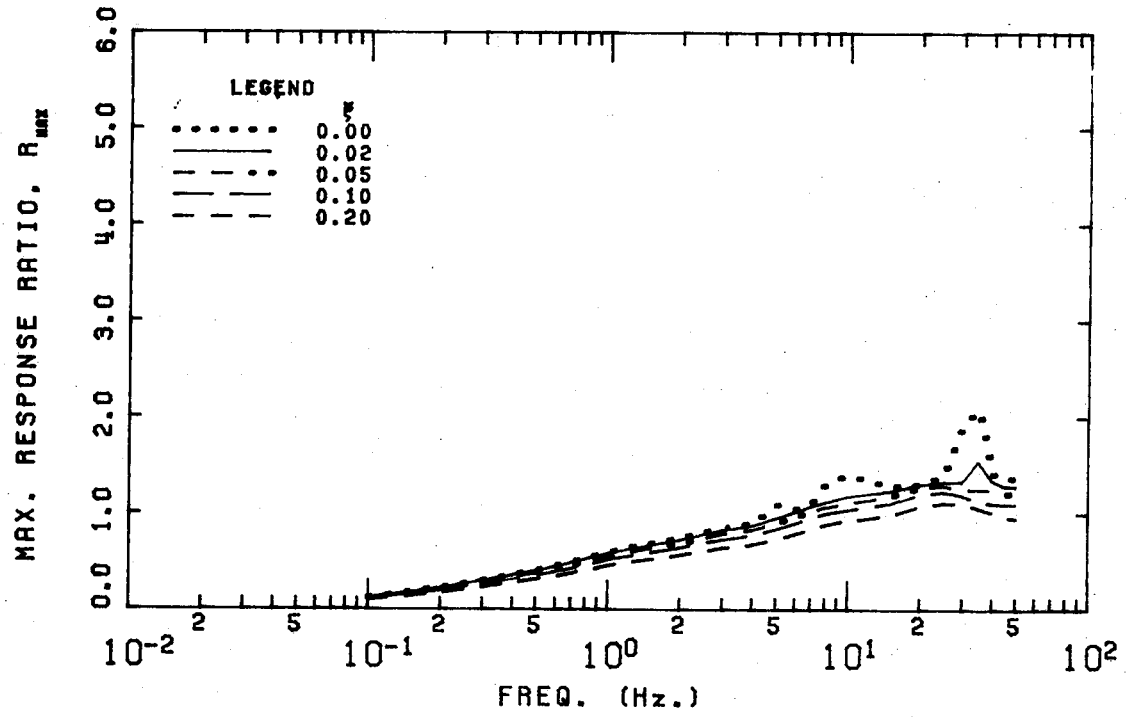

FIGURE B.108 HONDO 12 APRIL 1976 15H 59M 33S

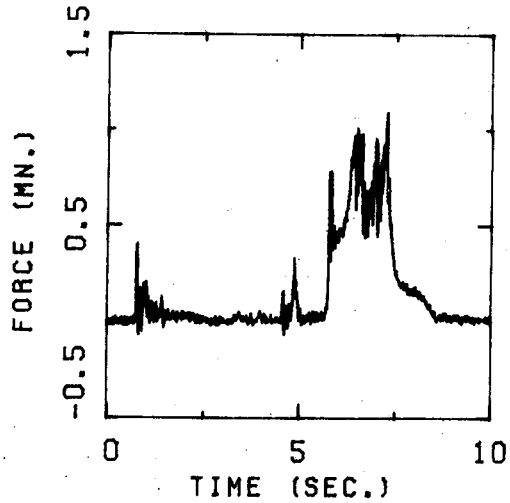

FIGURE B.109 HONDO 12 APRIL 1976 16H 08M 37S

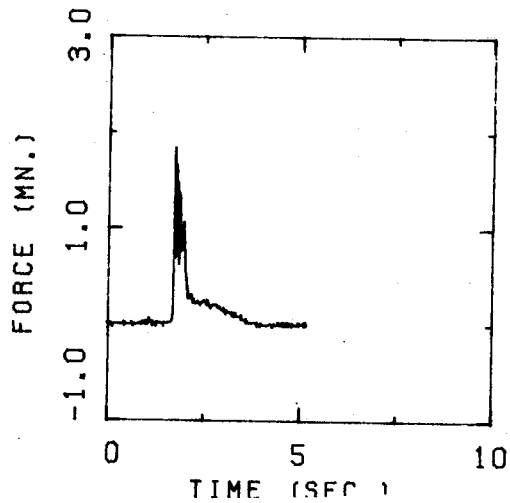

FIGURE B.110 HONDO 12 APRIL 1976 16H 12M 02S

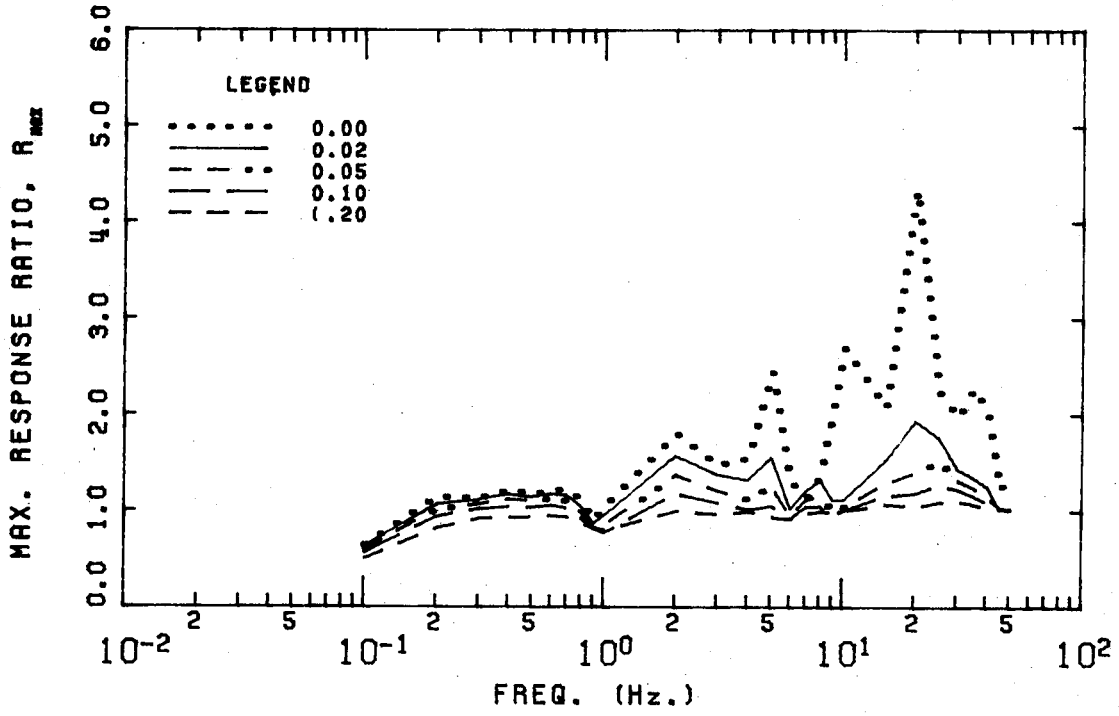

FIGURE B.111 HONDO 12 APRIL 1976 16H 08M 37S

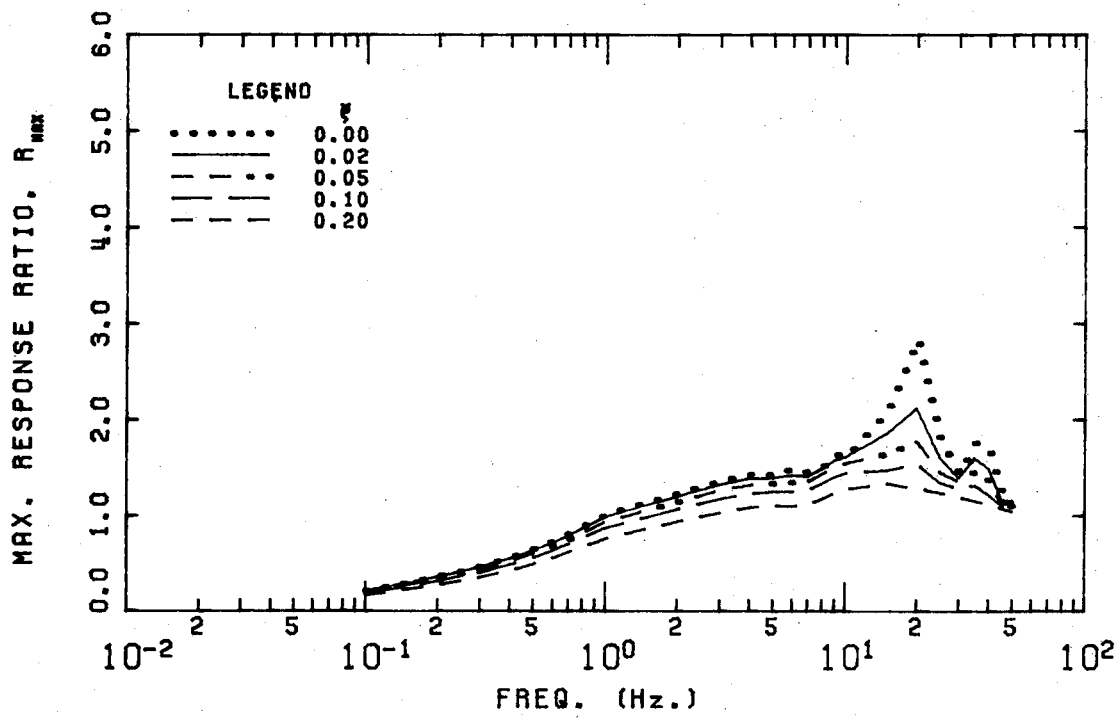

FIGURE B.112 HONDO 12 APRIL 1976 16H 12M 02S

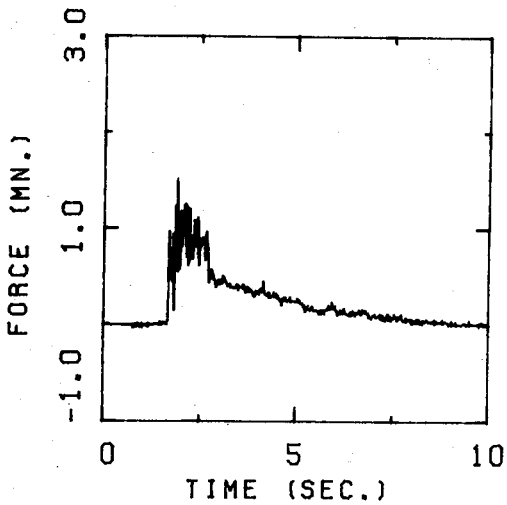

FIGURE B.113 HONDO 12 APRIL 1976 16H 12M 34S

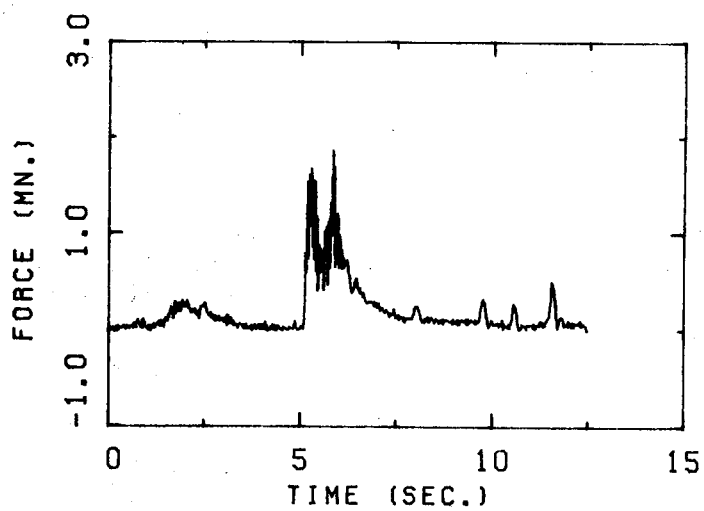

FIGURE B.114 HONDO 12 APRIL 1976 16H 14M 19S

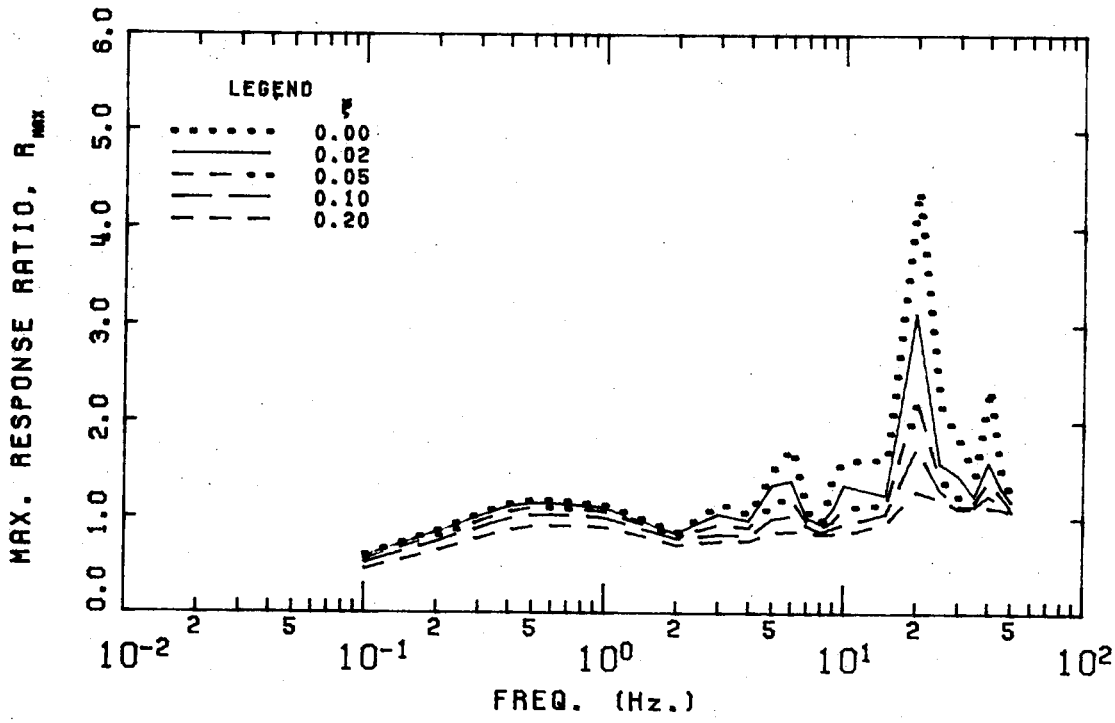

FIGURE B.115 HONDO 12 APRIL 1976 16H 12M 34S

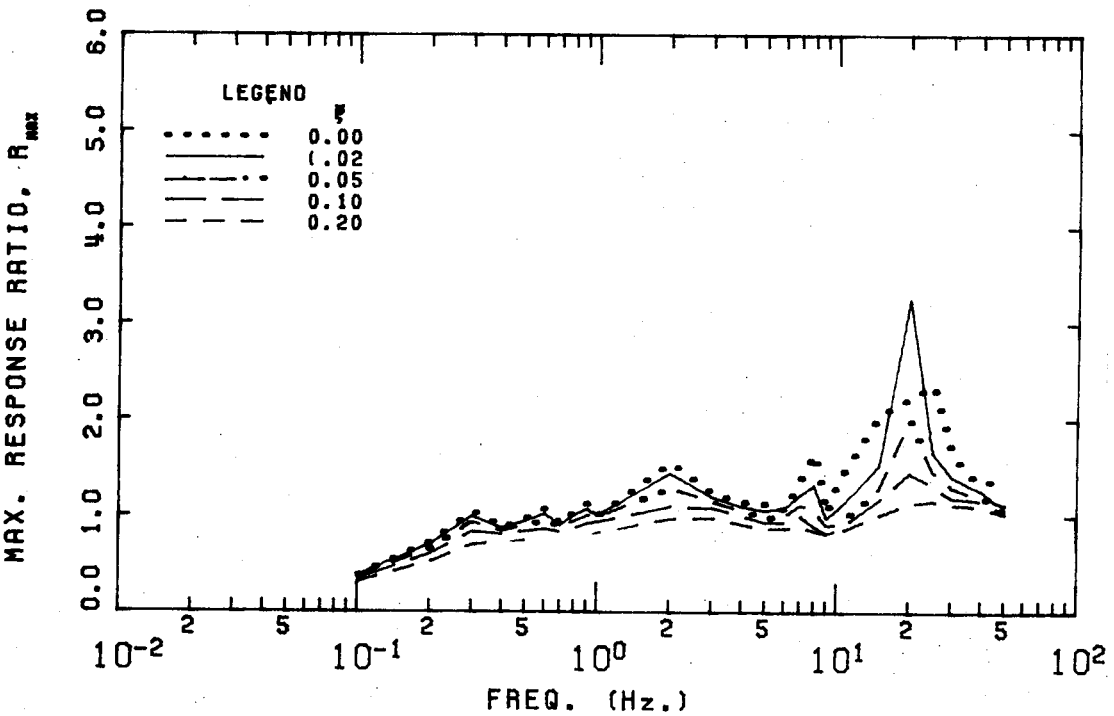

FIGURE B.116 HONDO 12 APRIL 1976 16H 14M 19S

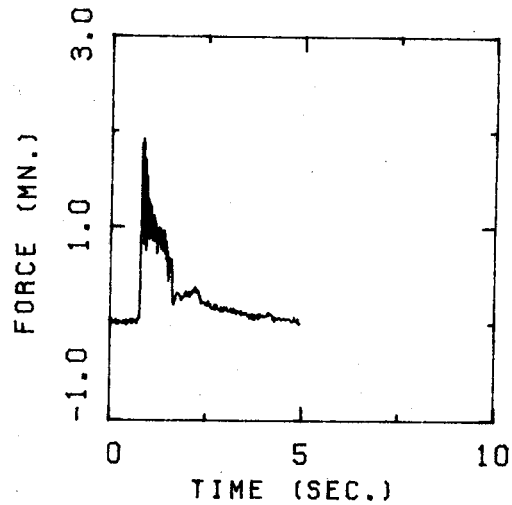

FIGURE B.117 HONDO 12 APRIL 1976 16H 21M 38S

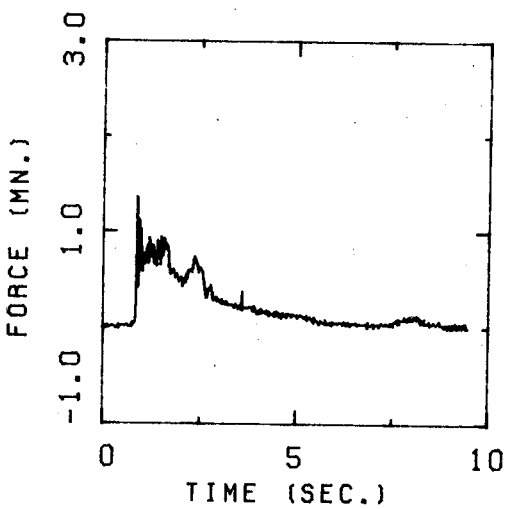

FIGURE B.118 HONDO 12 APRIL 1976 16H 22M 20S

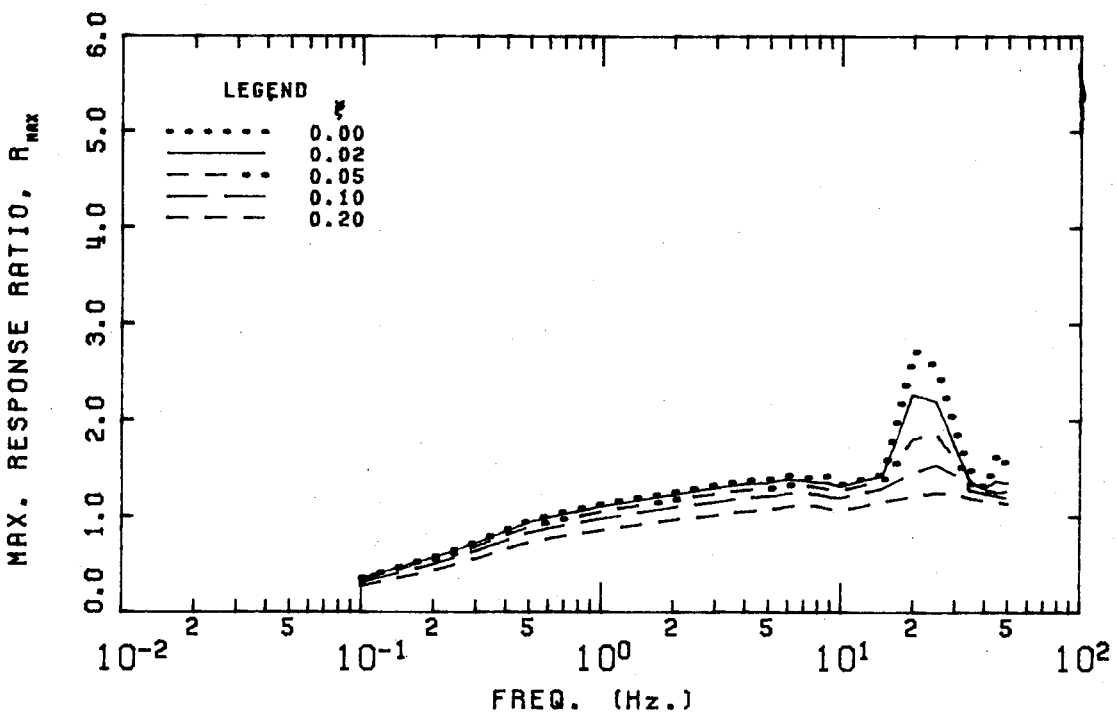

FIGURE B.119 HONDO 12 APRIL 1976 16H 21M 38S

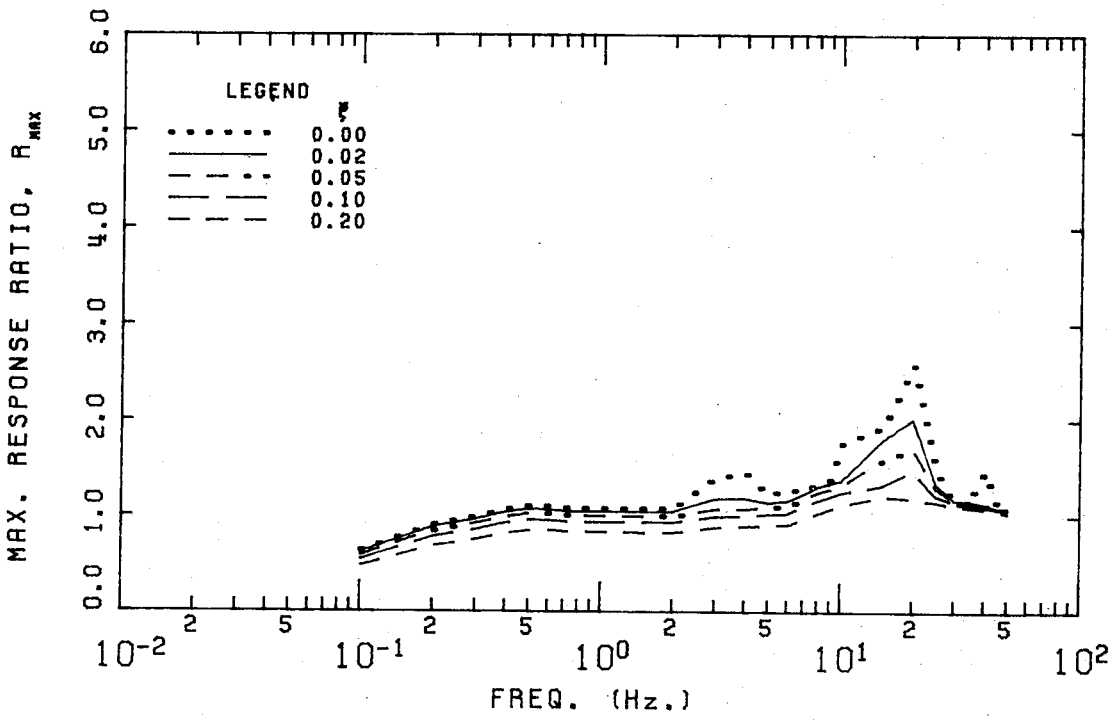

FIGURE B.120 HONDO 12 APRIL 1976 16H 22M 20S

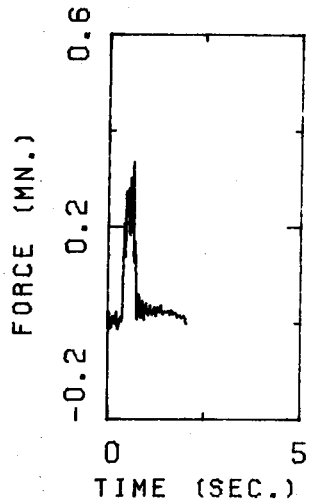

FIGURE B.121 HONDO 11 APRIL 1977 17H 55M 15S

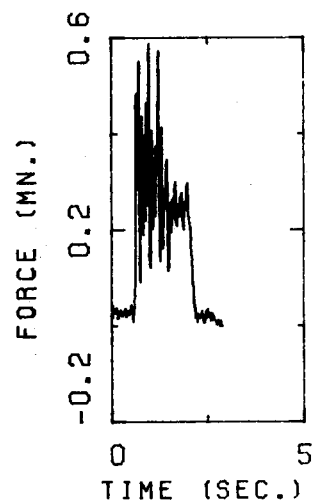

FIGURE B.122 HONDO 12 APRIL 1977 03H 57M 13S

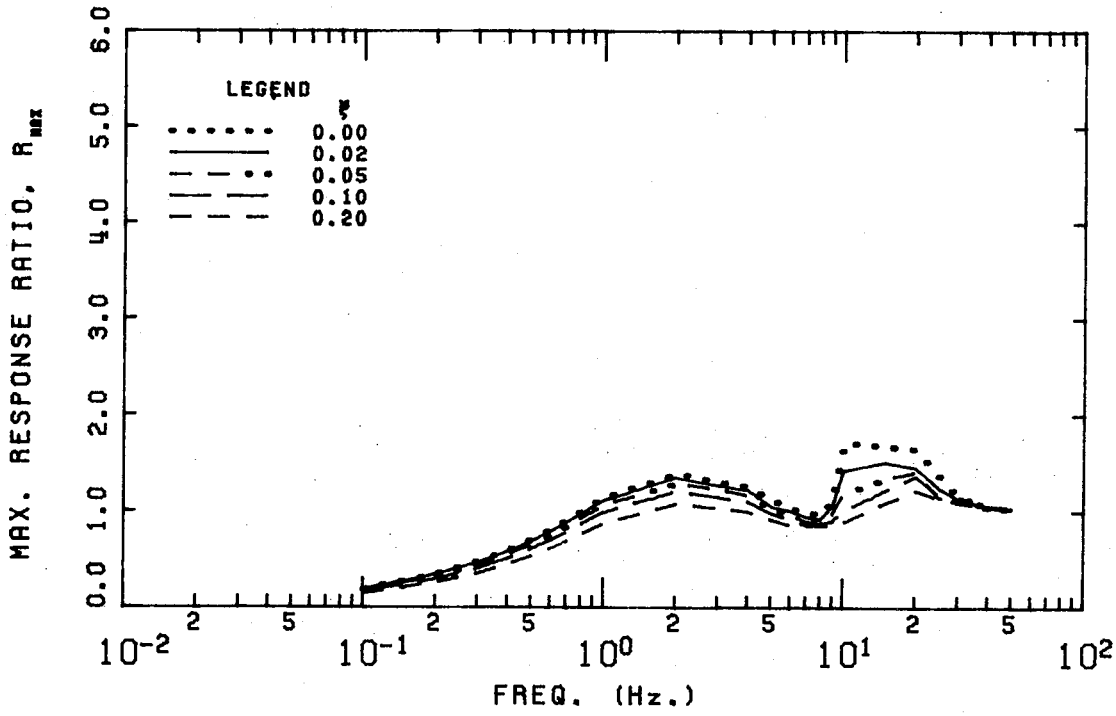

FIGURE B.123 HONDO 11 APRIL 1977 17H 55M 15S

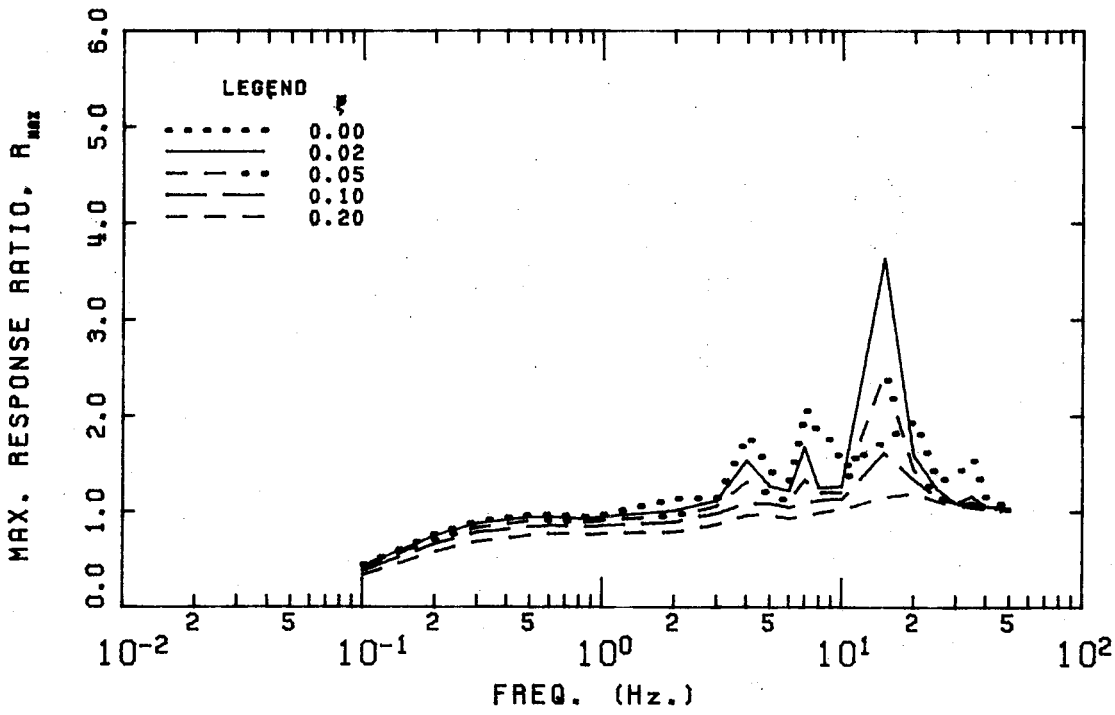

FIGURE B.124 HONDO 12 APRIL 1977 03H 57M 13S

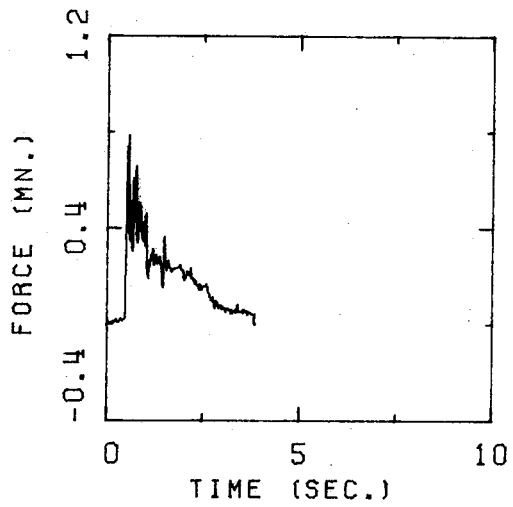

FIGURE B.125 HONDO 12 APRIL 1977 04H 06M 07S

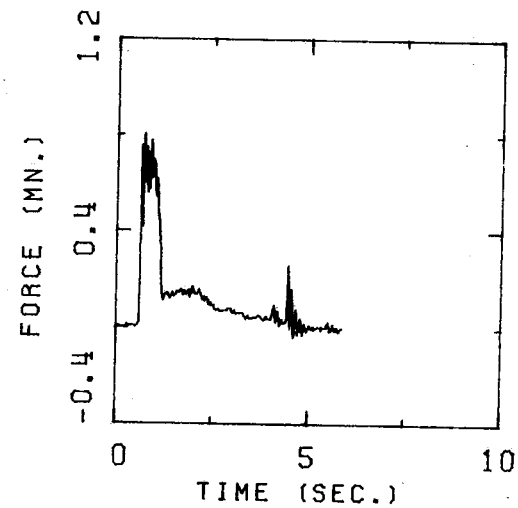

FIGURE B.126 HONDO 12 APRIL 1977 06H 18M 07S

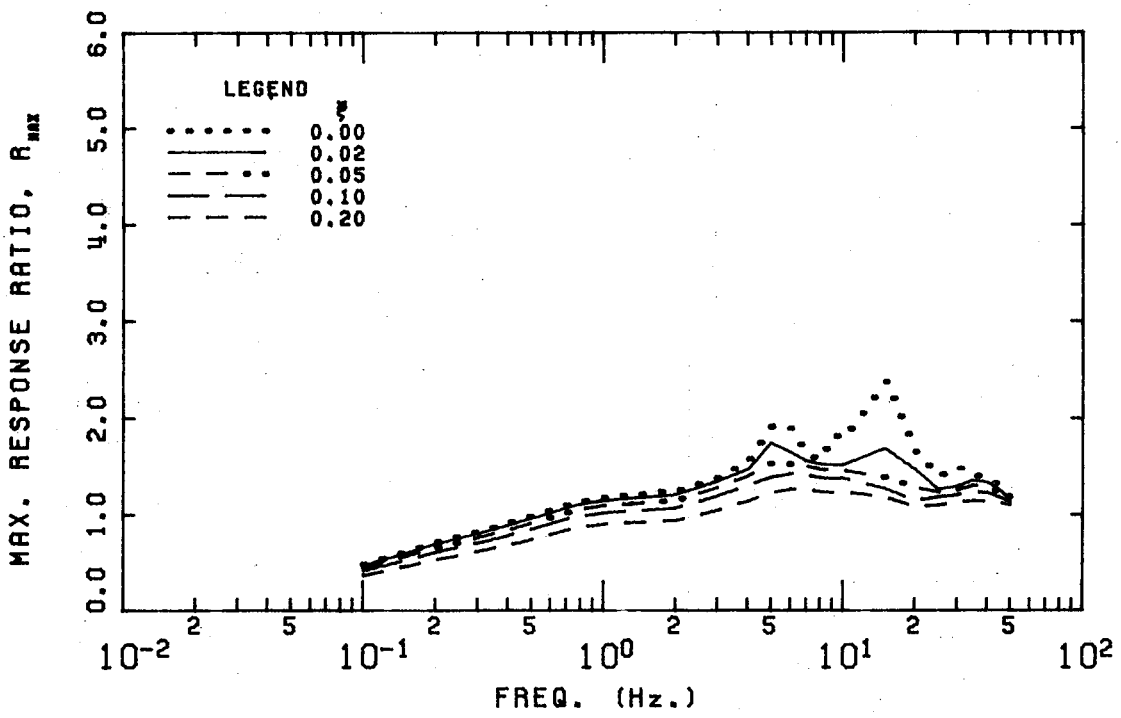

FIGURE B.127 HONDO 12 APRIL 1977 04H 06M 07S

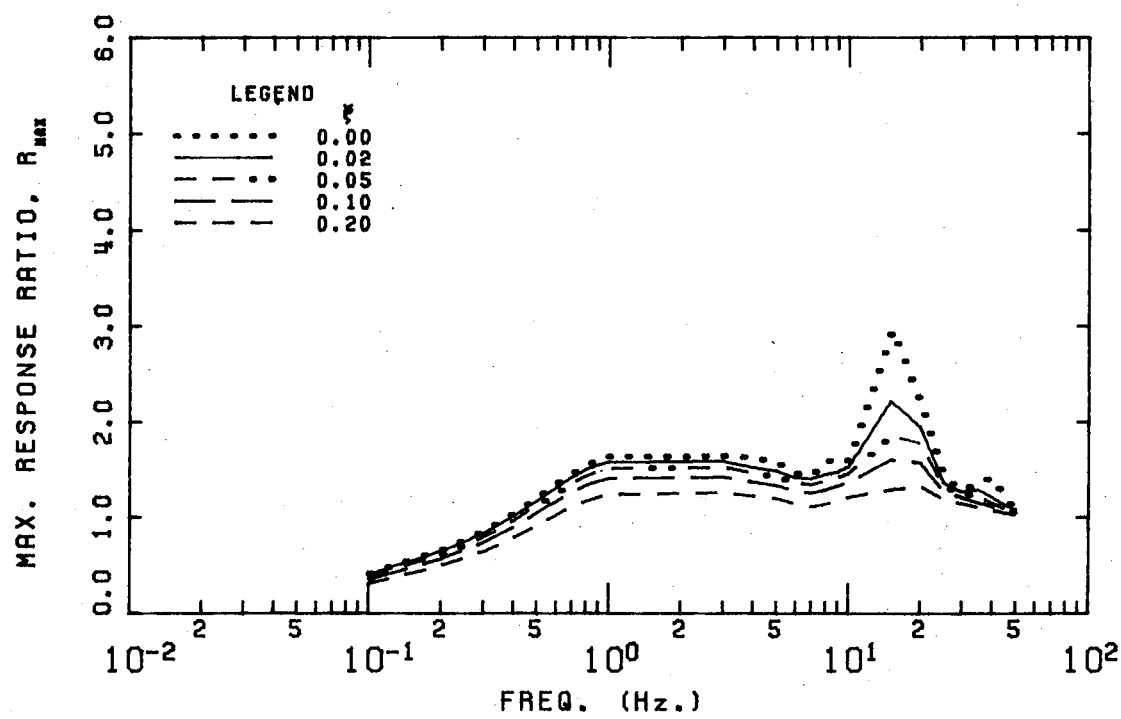

FIGURE B.128 HONDO 12 APRIL 1977 06H 18M 07S

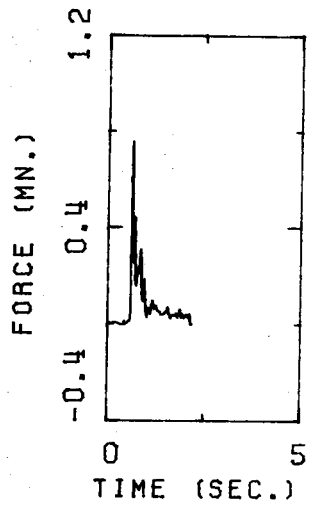

FIGURE B.129 HONDO 12 APRIL 1977 06H 18M 39S

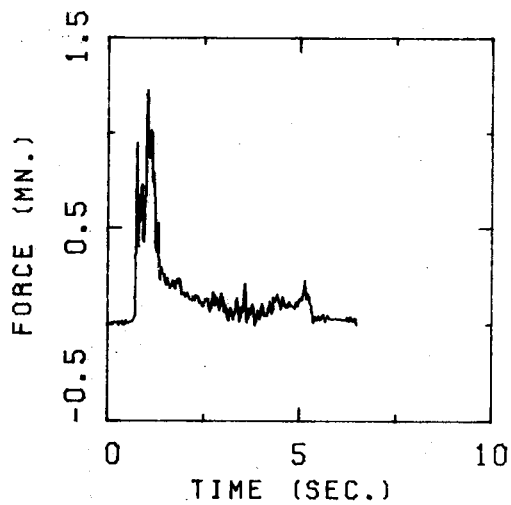

FIGURE B.130 HONDO 12 APRIL 1977 06H 19M 48S

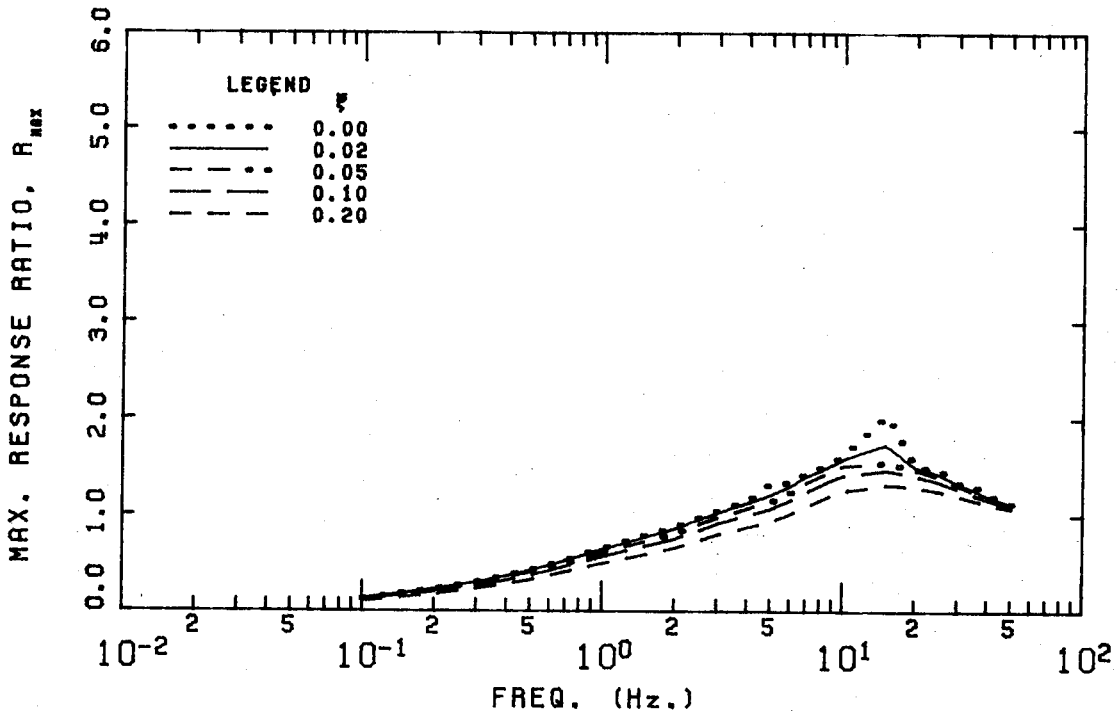

FIGURE B.131 HONDO 12 APRIL 1977 06H 18M 39S

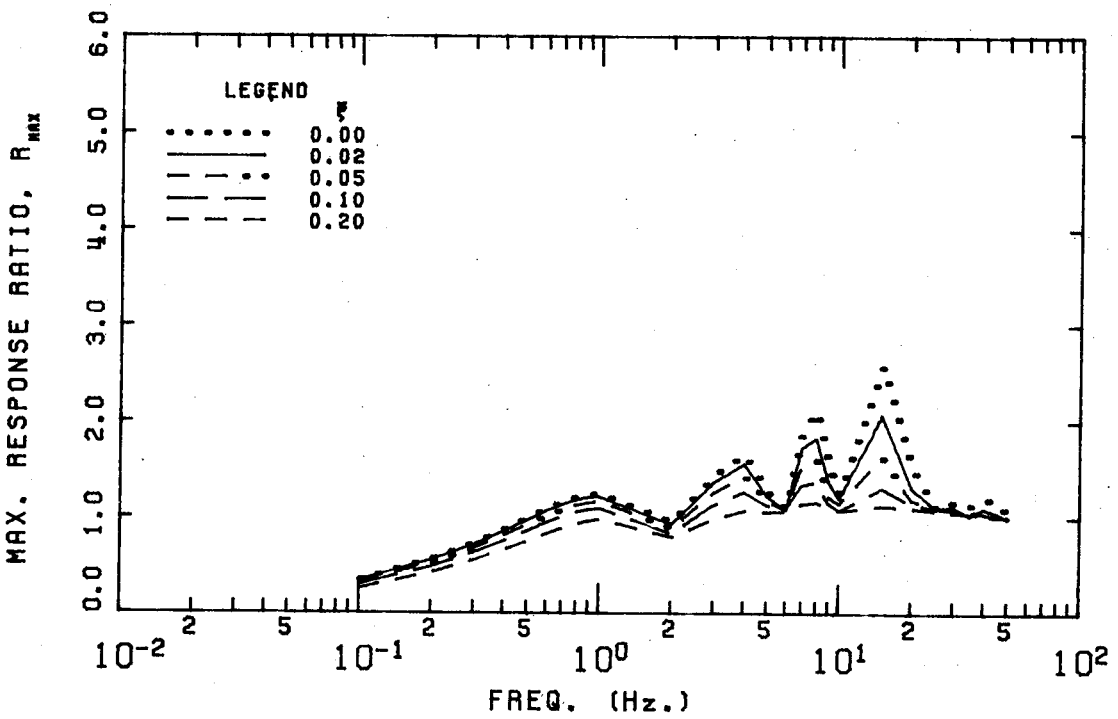

FIGURE B.132 HONDO 12 APRIL 1977 06H 19M 48S

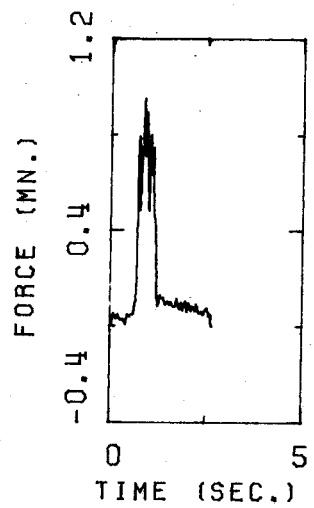

FIGURE B.133 HONDO 12 APRIL 1977 06H 40M 40S

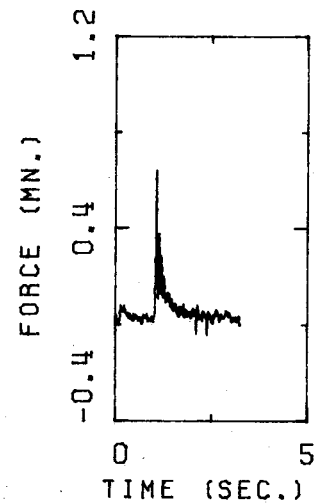

FIGURE B.134 HONDO 27 APRIL 1979 12H 51M 48S

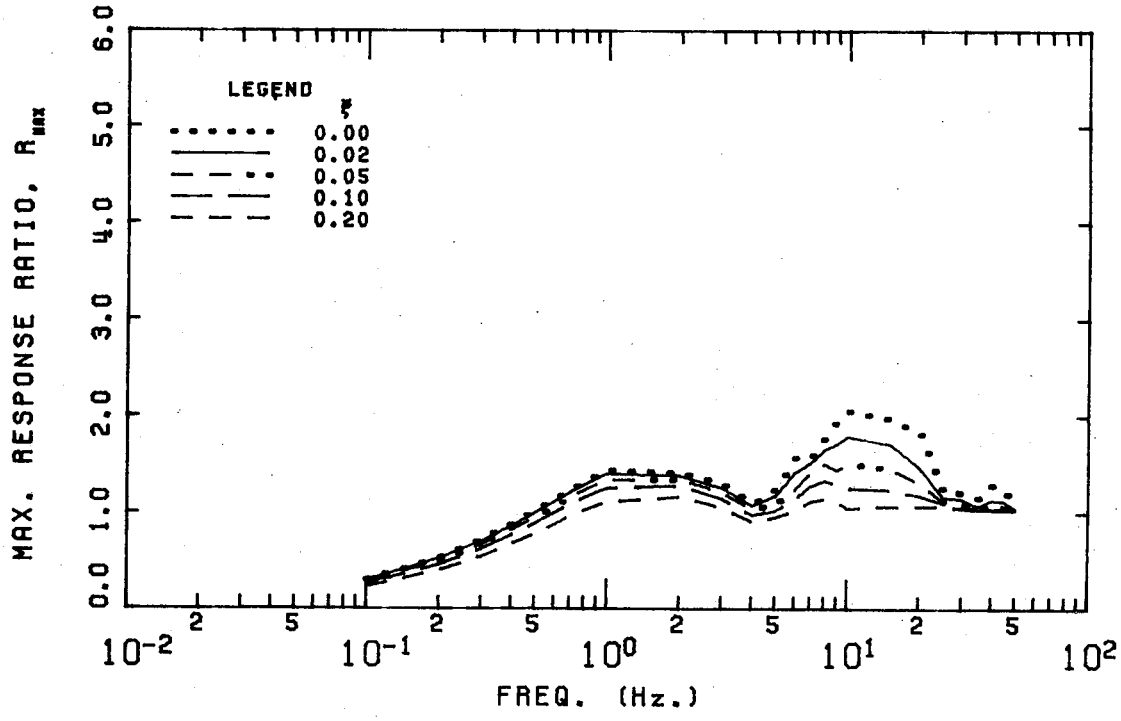

FIGURE B.135 HONDO 12 APRIL 1977 06H 40M 40S

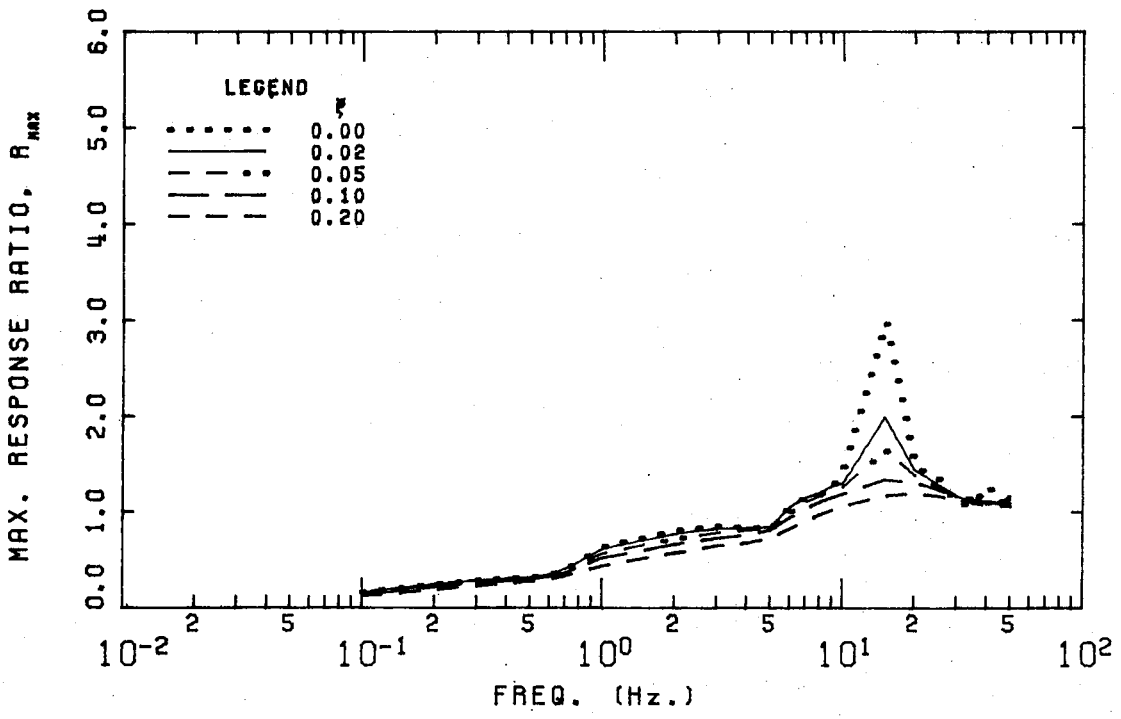

FIGURE B.136 HONDO 27 APRIL 1979 12H 51M 48S

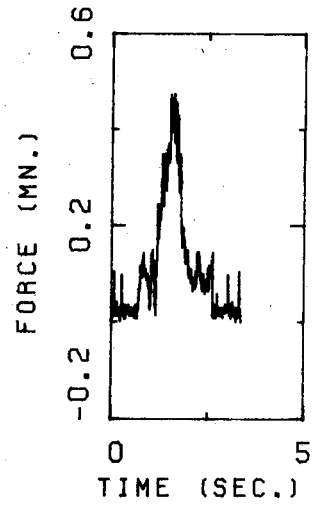

FIGURE B.137 HONDO 27 APRIL 1979 13H 29M 53S

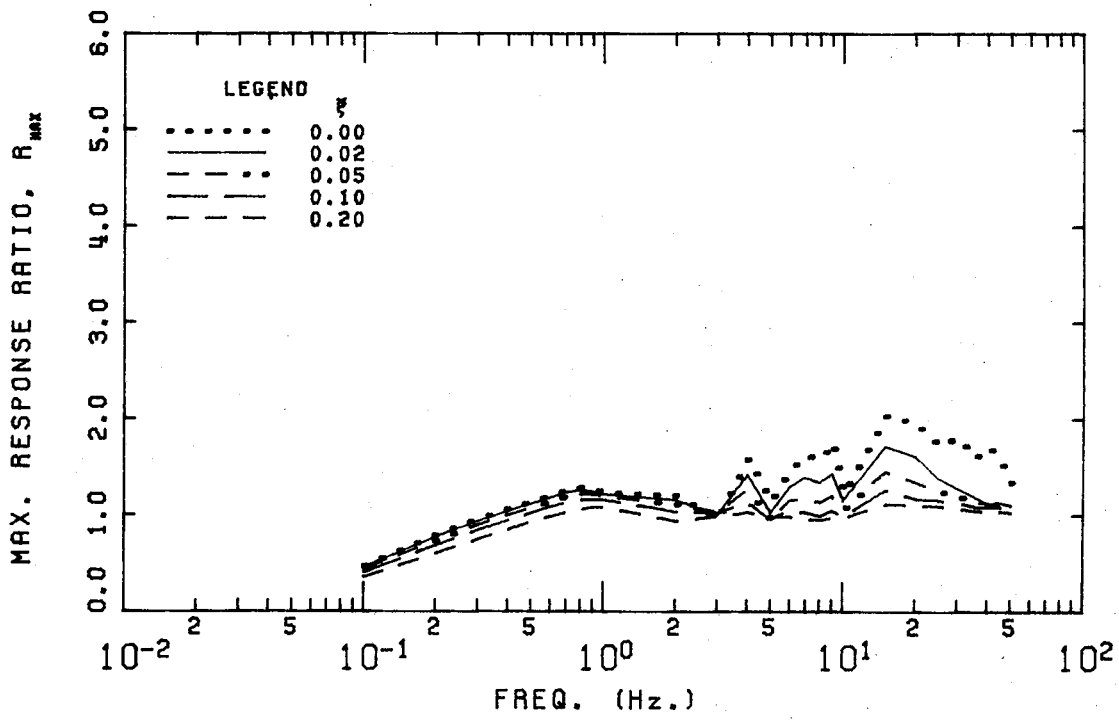

FIGURE B.138 HONDO 27 APRIL 1979 13H 29M 53S

B.5 Load Histories and Response Spectra - Pembridge

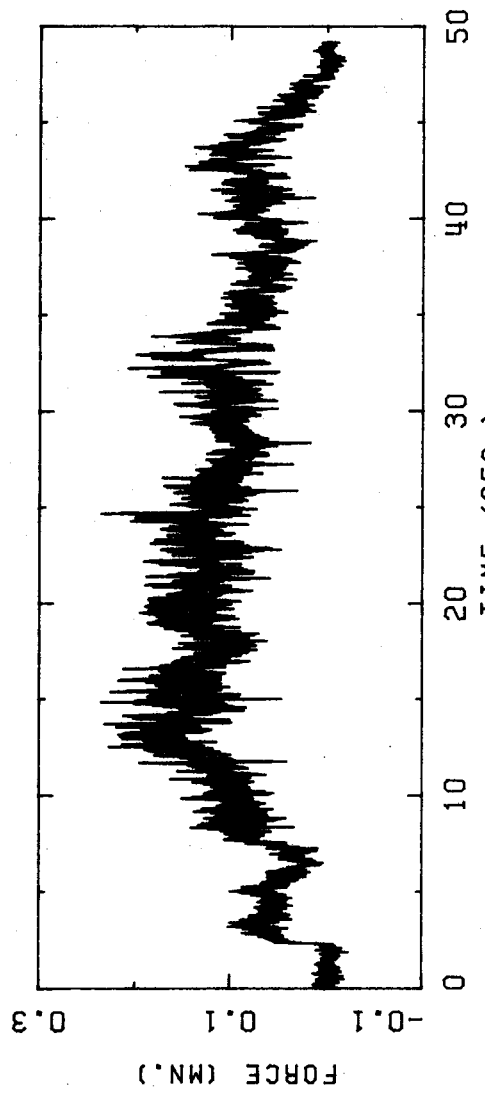

FIGURE B.139 PEMBRIDGE 17 APRIL 1974 22H 07M 28S

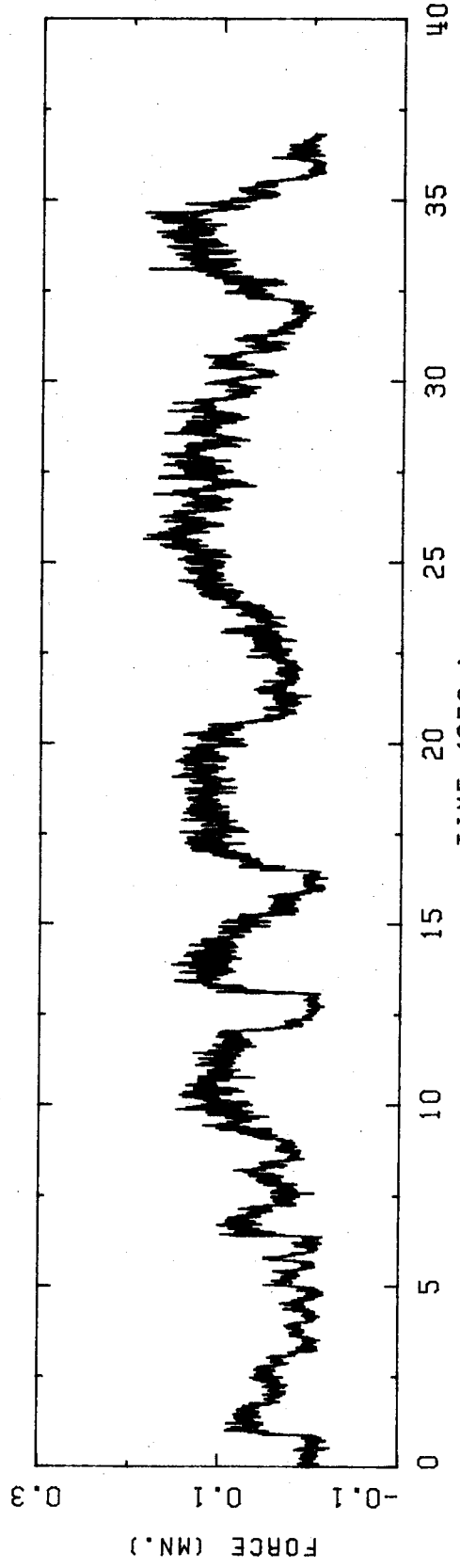

FIGURE B.140 PEMBRIDGE 17 APRIL 1974 22H 09M 46S

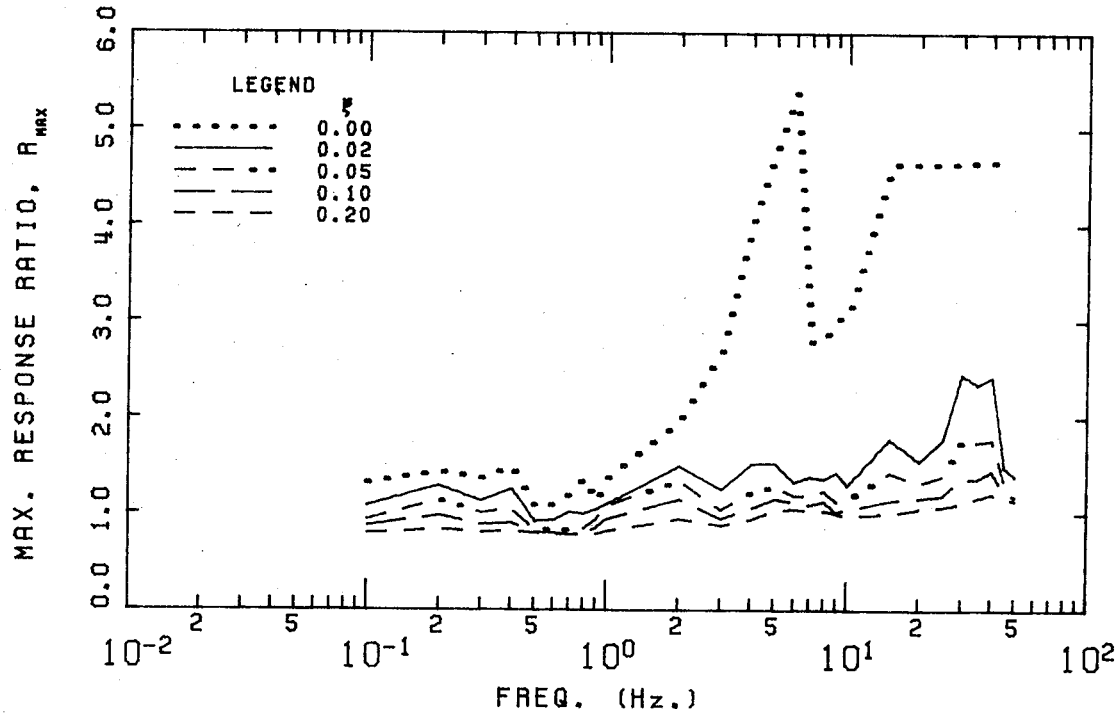

FIGURE B.141 PEMBRIDGE 17 APRIL 1974 22H 07M 28S

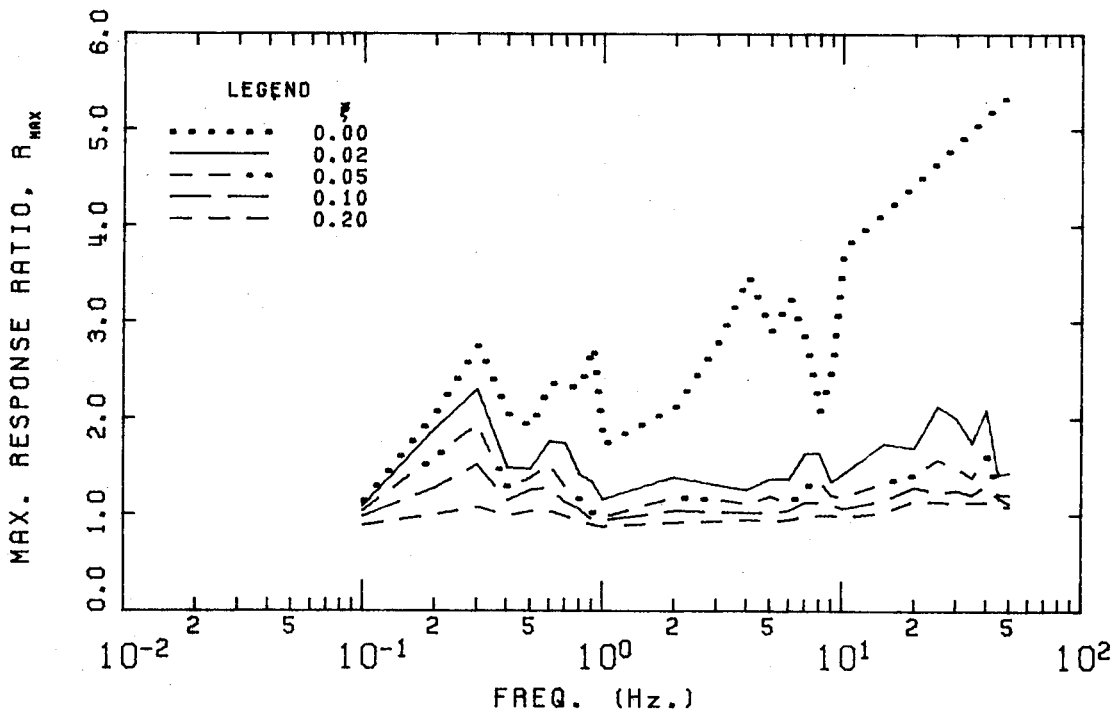

FIGURE B.142 PEMBRIDGE 17 APRIL 1974 22H 09M 46S

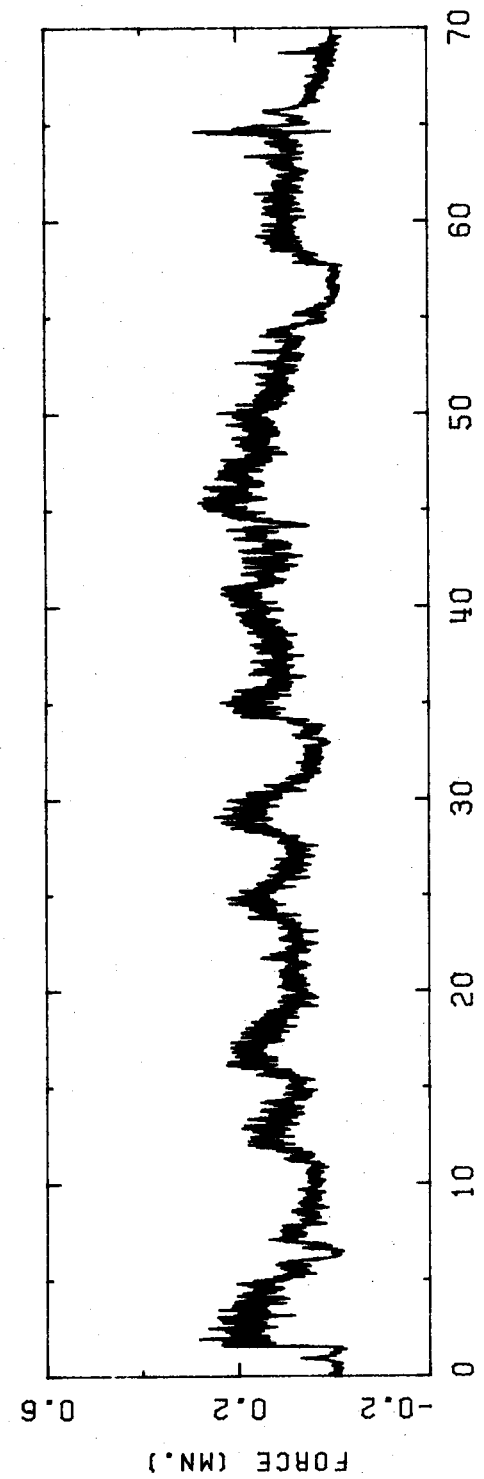

FIGURE B.143 PEMBRIDGE 17 APRIL 1974 22H 13M 07S

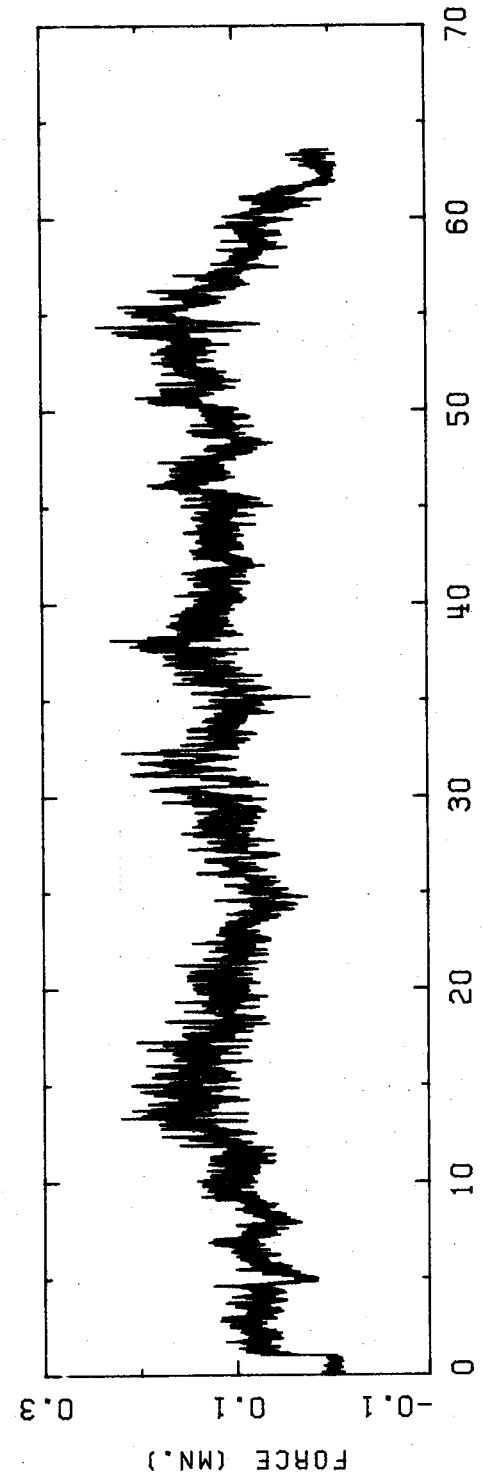

FIGURE B.144 PEMBRIDGE 17 APRIL 1974 22H 15M 31S

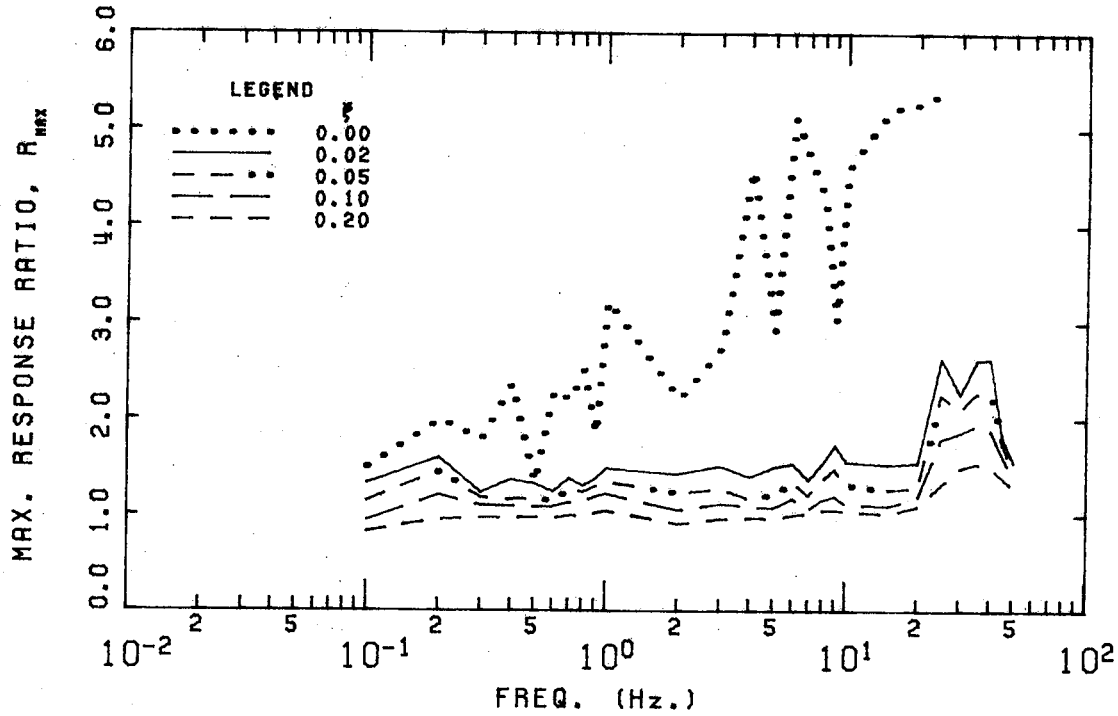

FIGURE B.145 PEMBRIDGE 17 APRIL 1974 22H 13M 07S

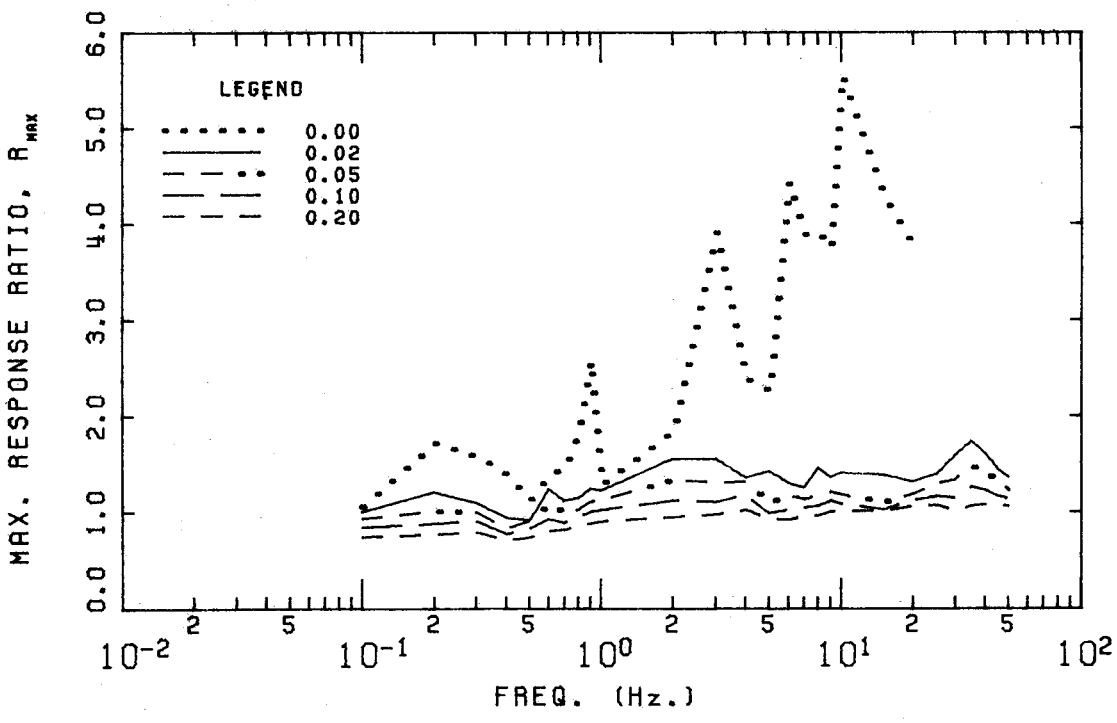

FIGURE B.146 PEMBRIDGE 17 APRIL 1974 22H 15M 31S

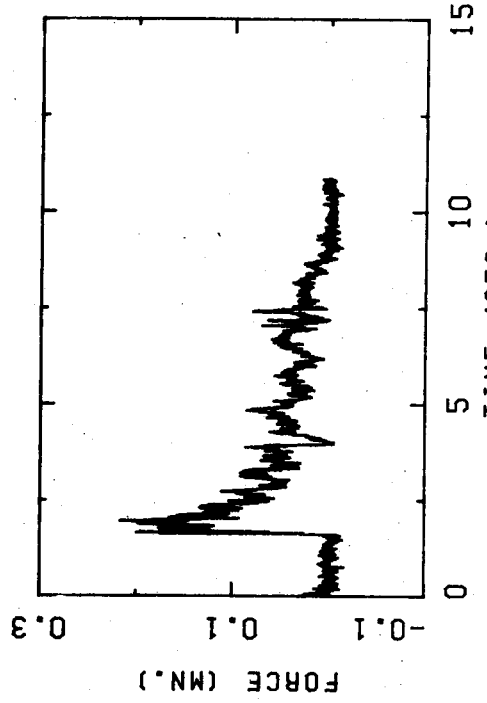

FIGURE B.147 PEMBRIDGE 17 APRIL 1974 22H 15M 61S

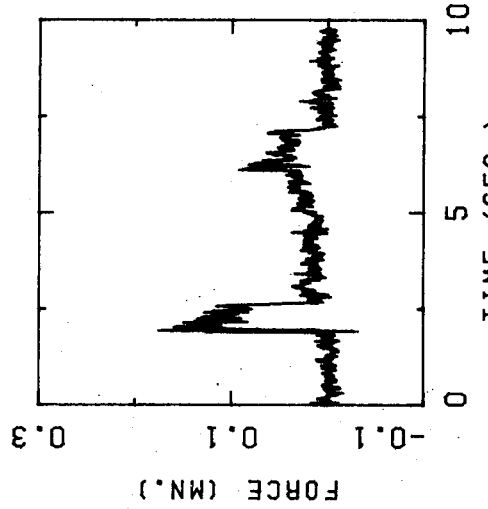

FIGURE B.148 PEMBRIDGE 17 APRIL 1974 22H 16M 14S

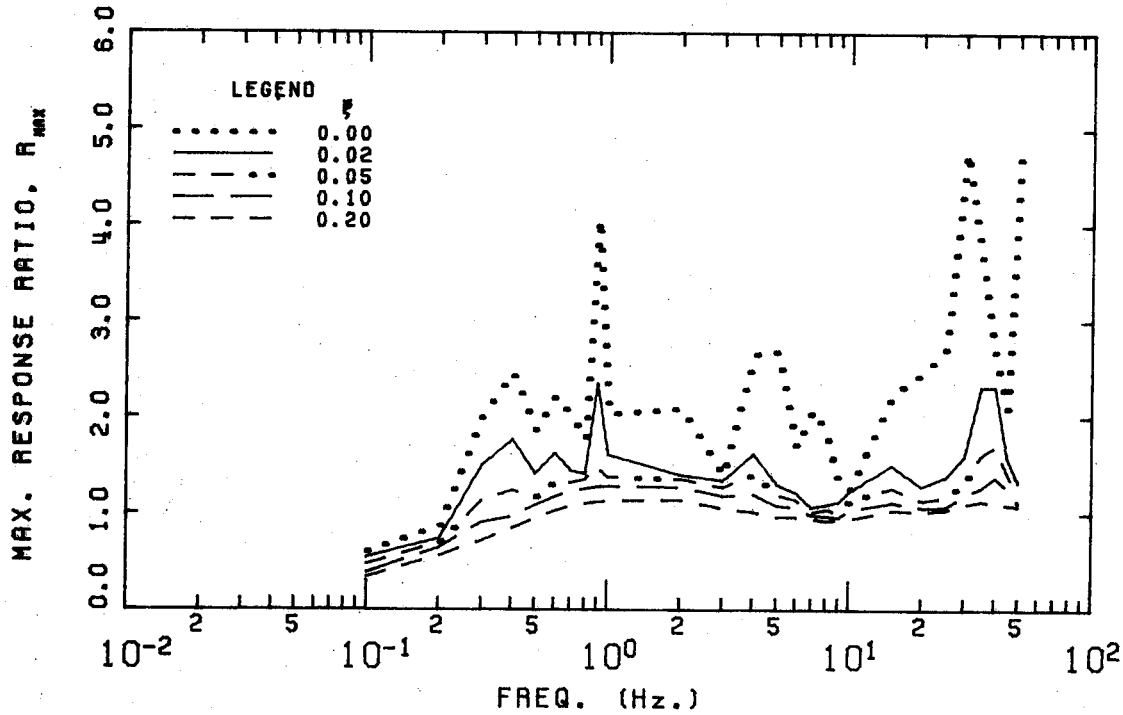

FIGURE B.157 PEMBRIDGE 17 APRIL 1974 22H 41M 50S

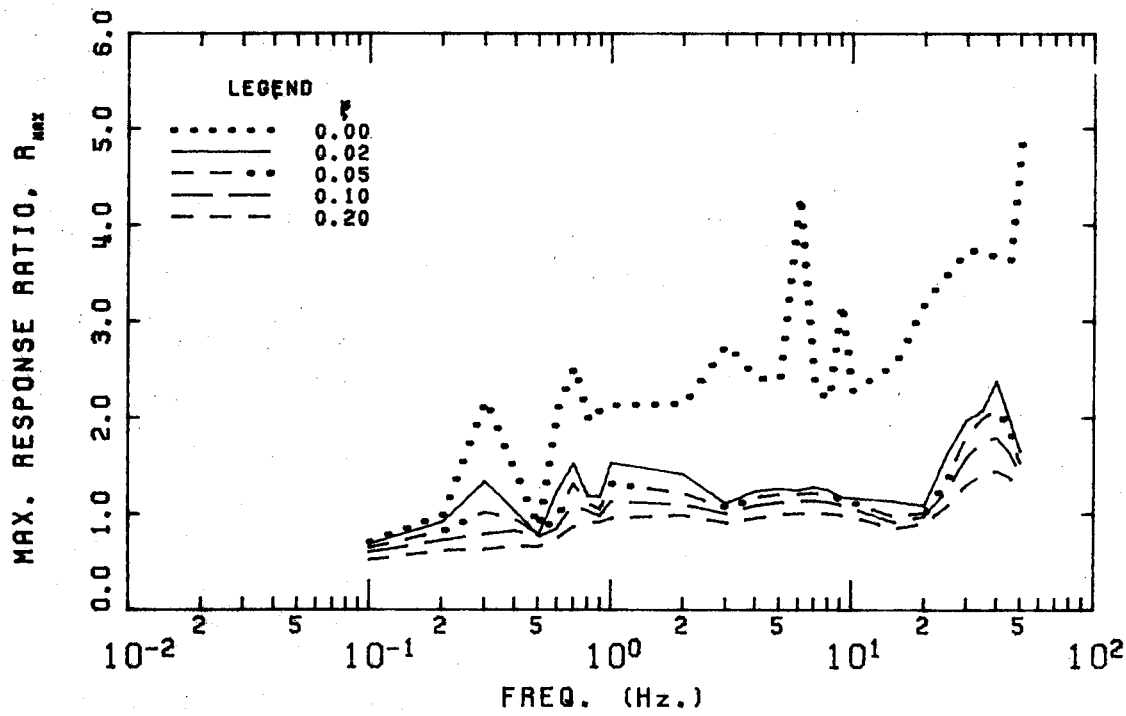

FIGURE B.158 PEMBRIDGE 17 APRIL 1974 22H 42M 38S

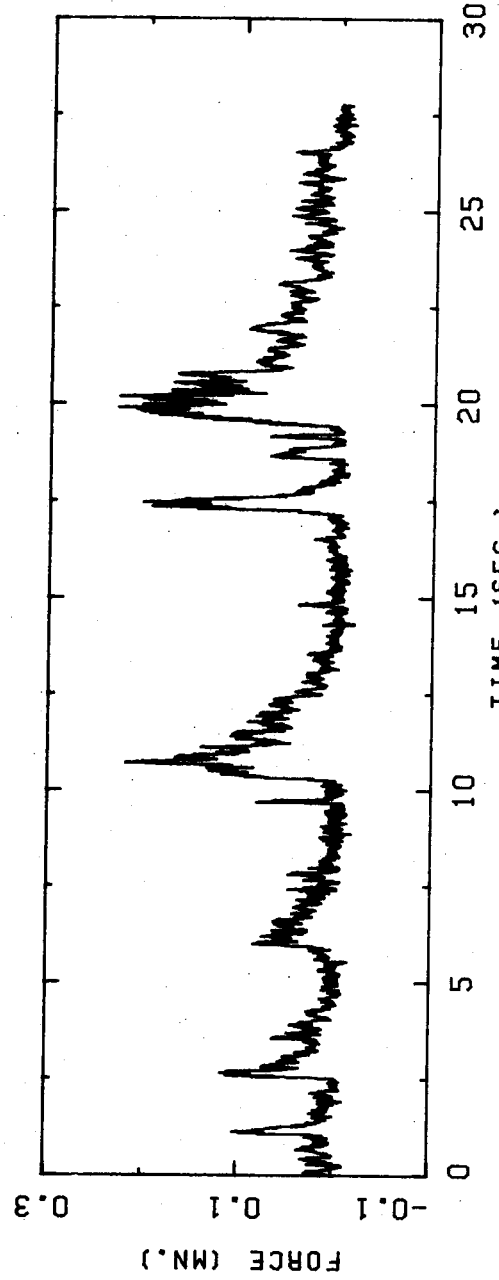

FIGURE B.159 PEMBRIDGE 17 APRIL 1974 22H 43M 20S

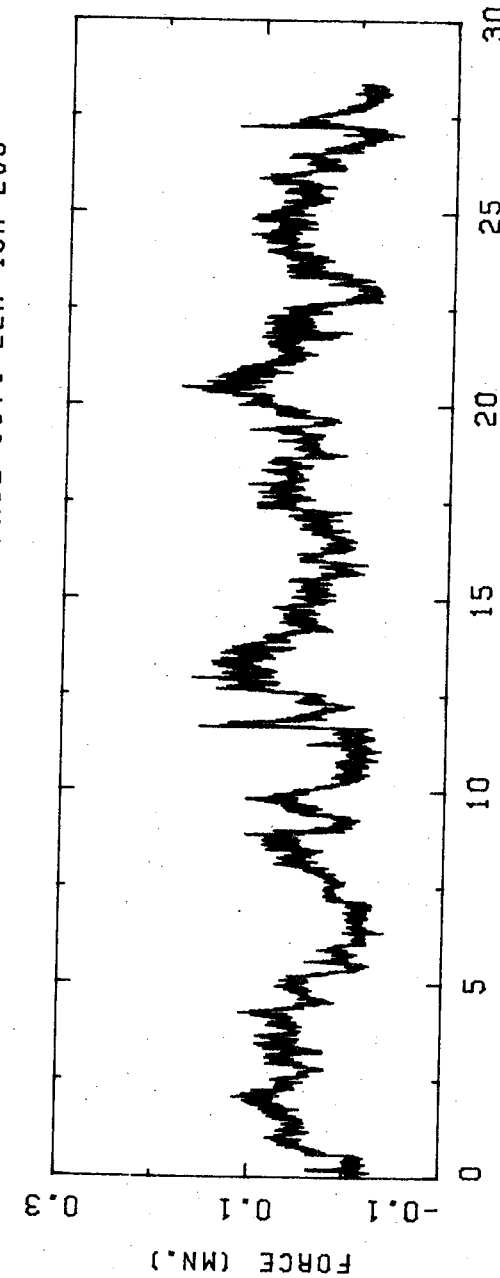

FIGURE B.160 PEMBRIDGE 17 APRIL 1974 23H 00M 46S

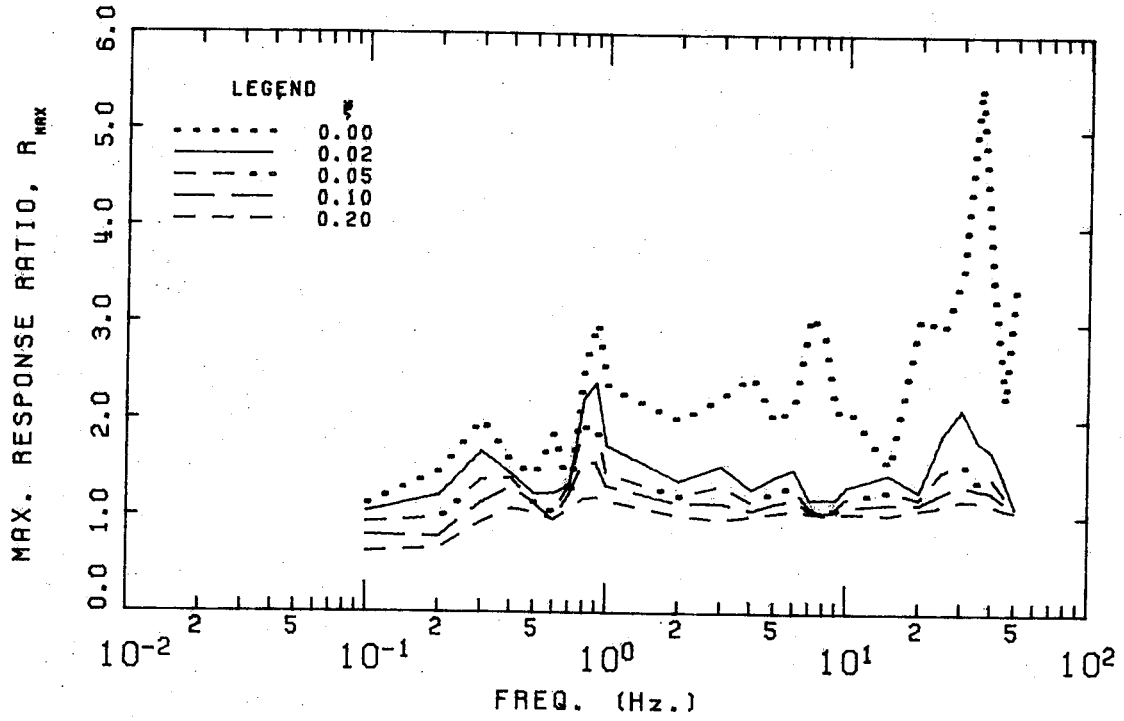

FIGURE B.161 PEMBRIDGE 17 APRIL 1974 22H 43M 20S

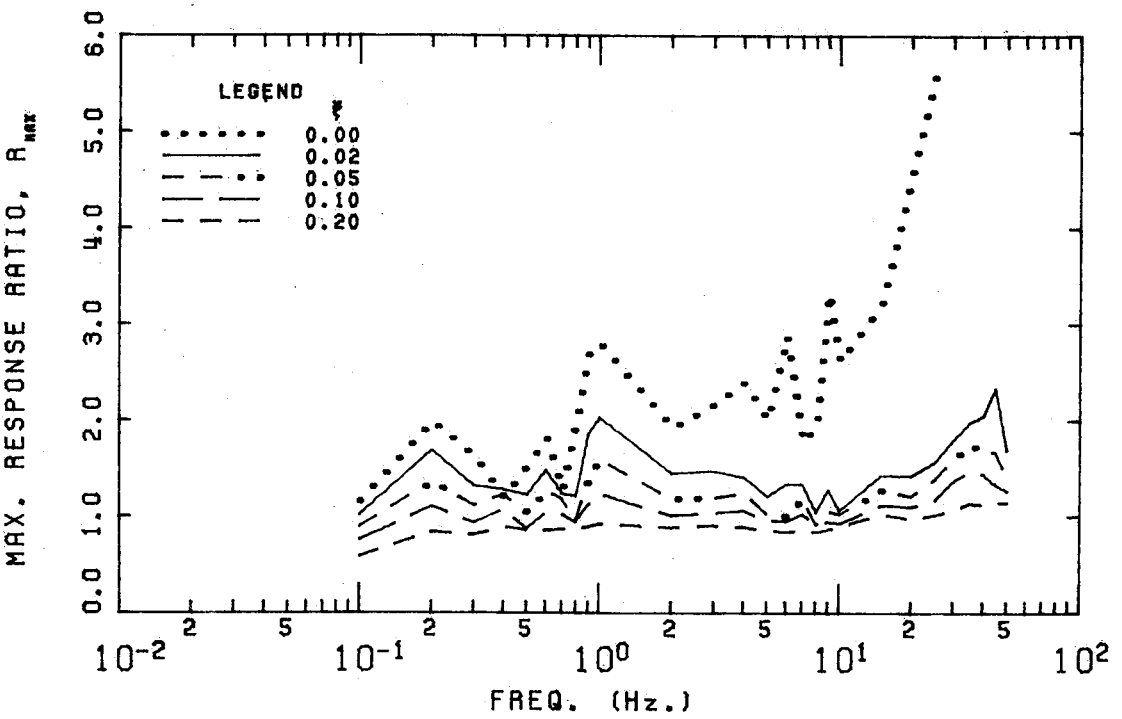

FIGURE B.162 PEMBRIDGE 17 APRIL 1974 23H 00M 46S

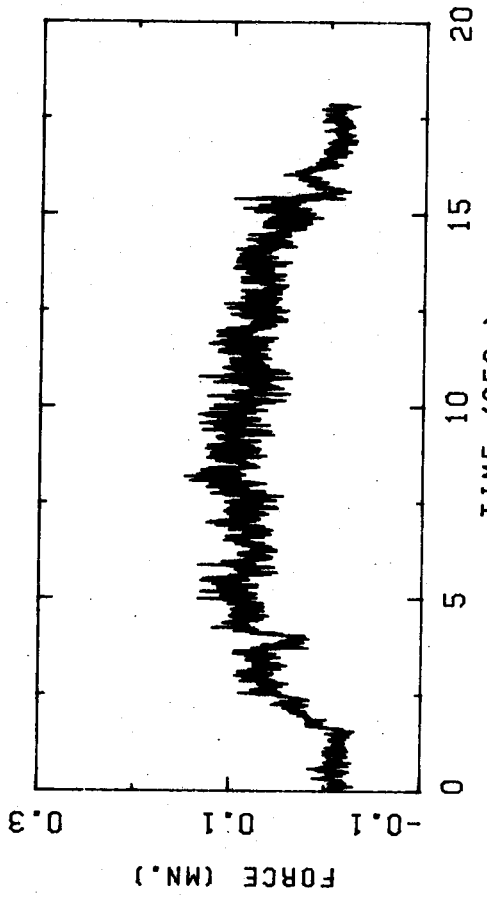

FIGURE B.163 PEMBRIDGE 17 APRIL 1974 23H 01M 13S

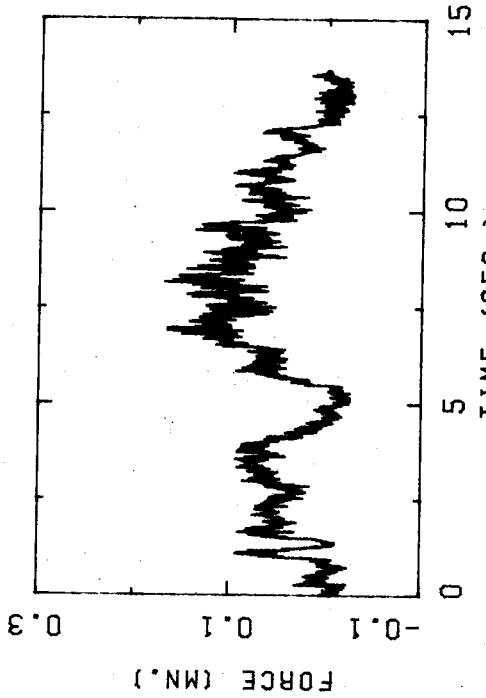

FIGURE B.164 PEMBRIDGE 17 APRIL 1974 23H 01M36S

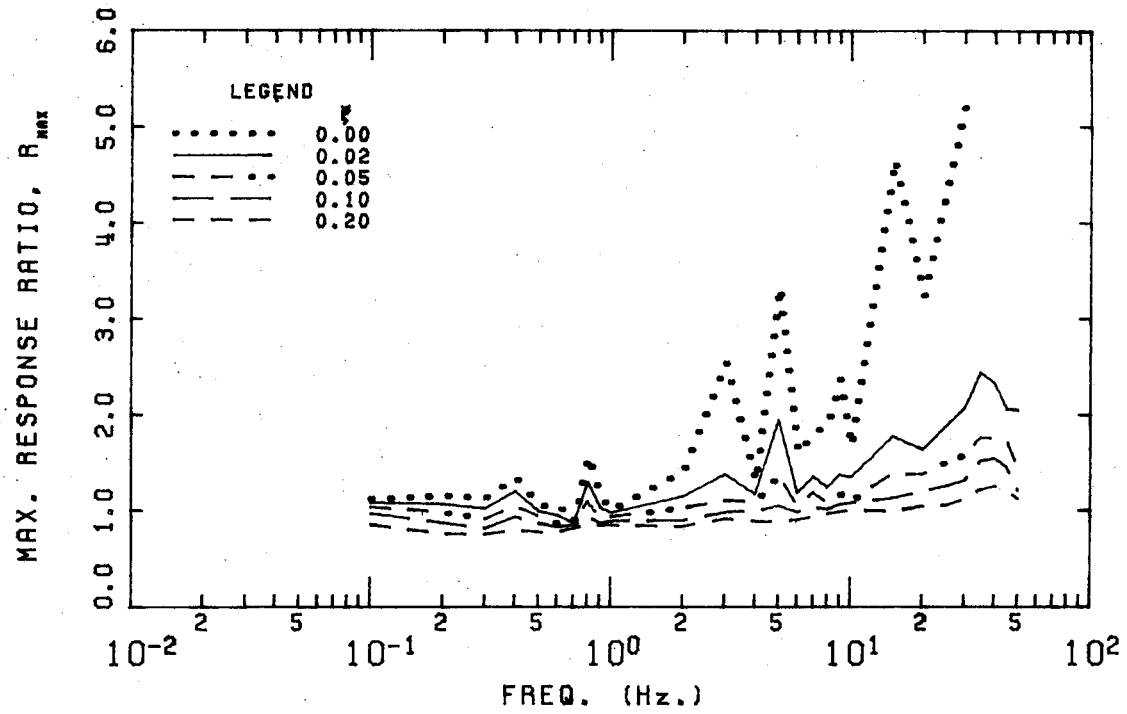

FIGURE B.165 PEMBRIDGE 17 APRIL 1974 23H 01M 13S

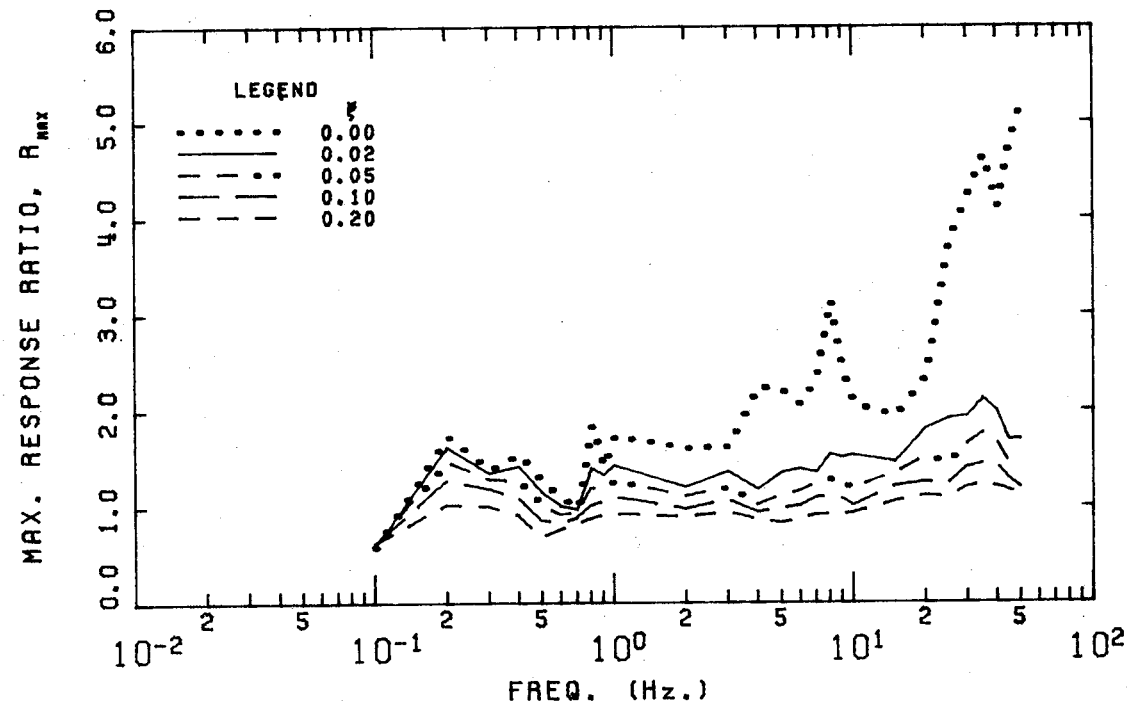

FIGURE B.166 PEMBRIDGE 17 APRIL 1974 23H 01M 36S

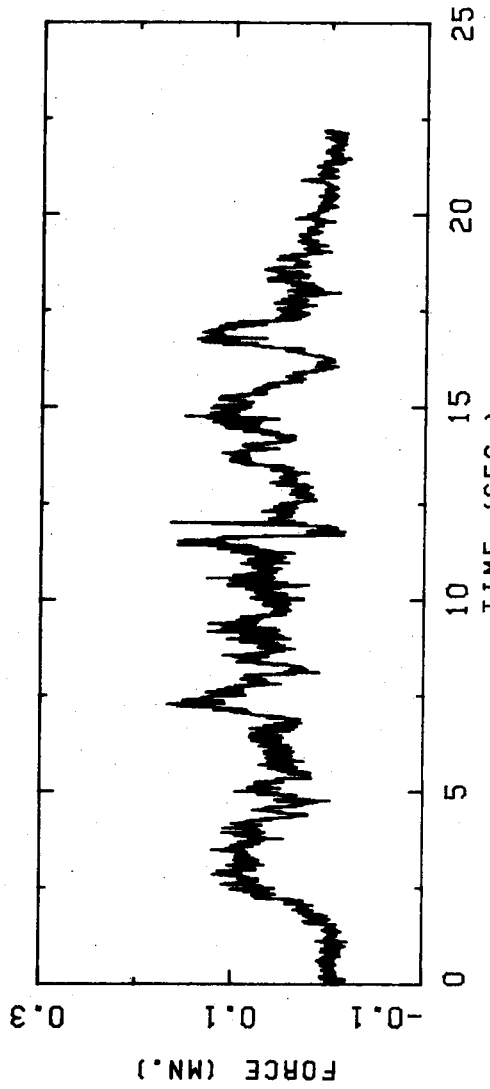

FIGURE B.167 PEMBRIDGE 17 APRIL 1974 23H 09M 49S

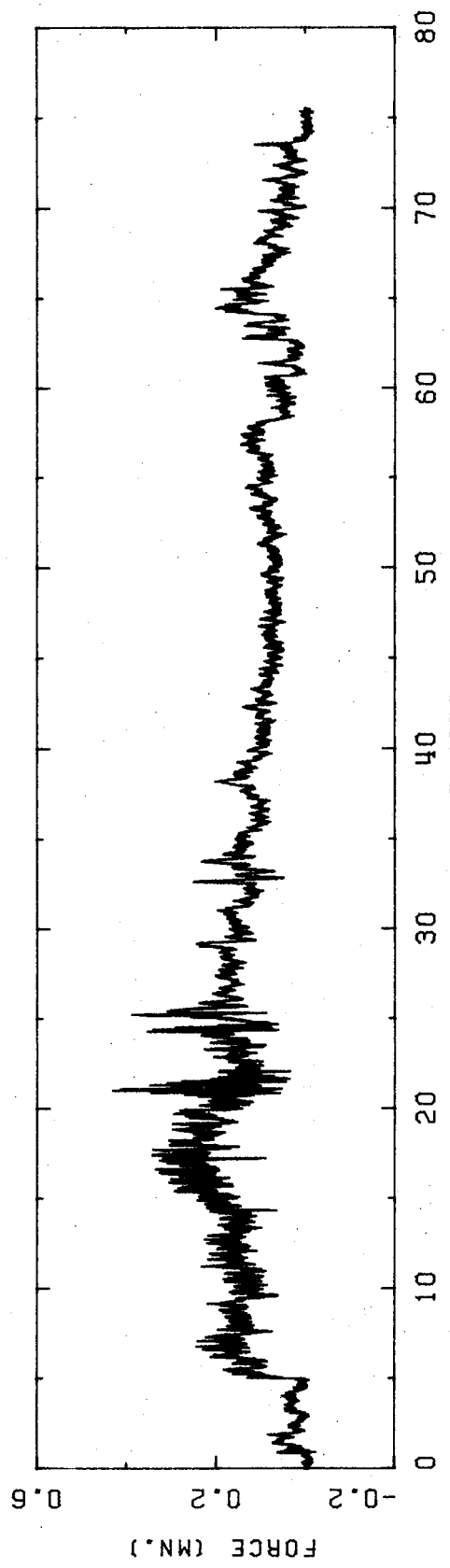

FIGURE B.168 PEMBRIDGE 17 APRIL 1974 22H 10M 16S

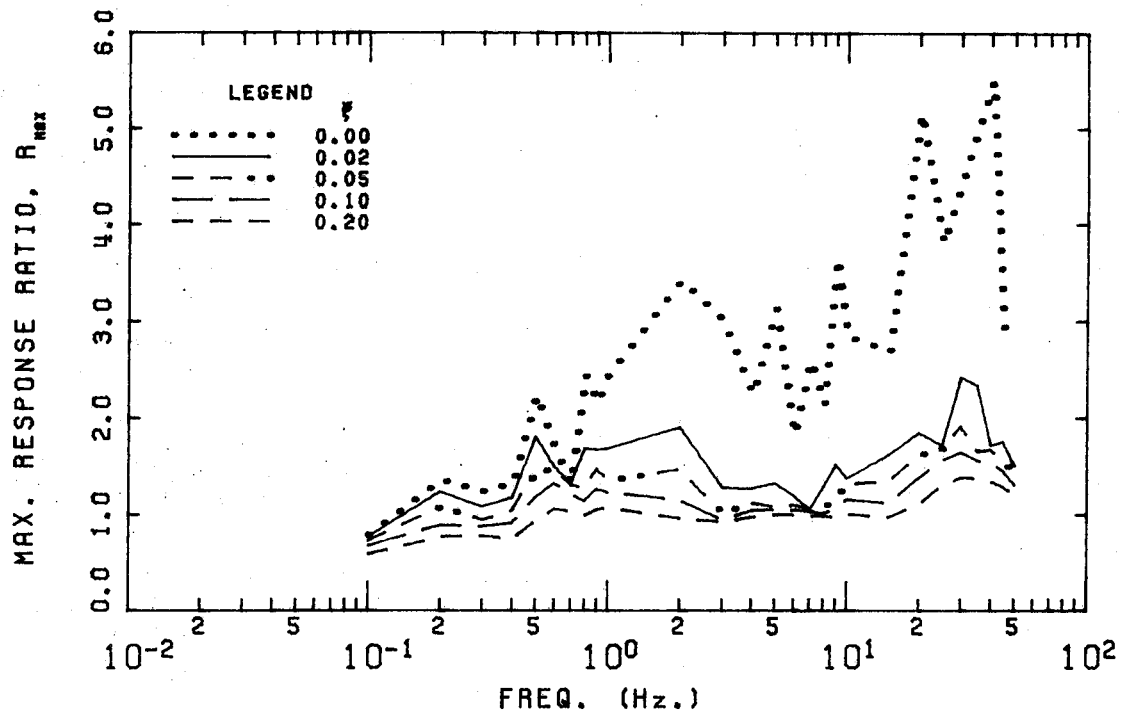

FIGURE B.169 PEMBRIDGE 17 APRIL 1974 23H 09M 49S

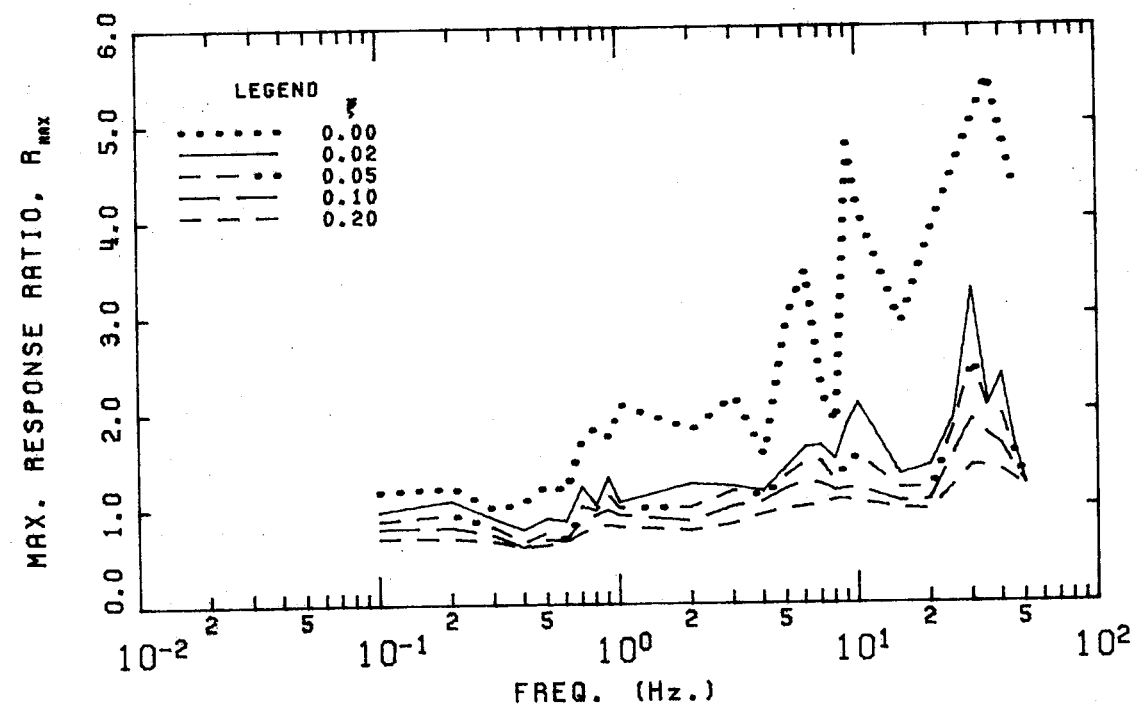

FIGURE B.170 PEMBRIDGE 17 APRIL 1974 22H 10M 16S

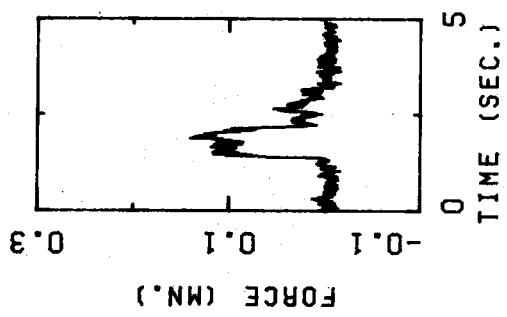

FIGURE B.171 PEMBRIDGE 17 APRIL 1974 23H 10M 19S

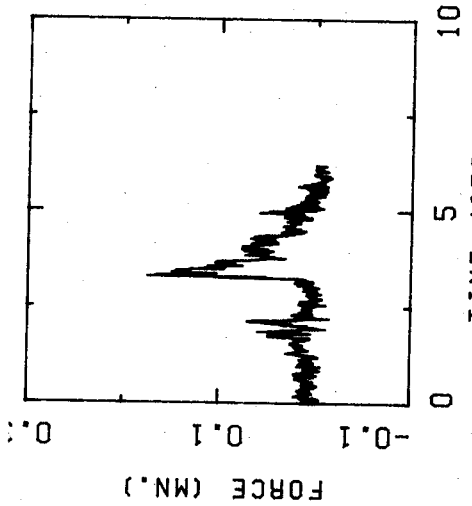

FIGURE B.172 PEMBRIDGE 17 APRIL 1974 23H 10M 29S

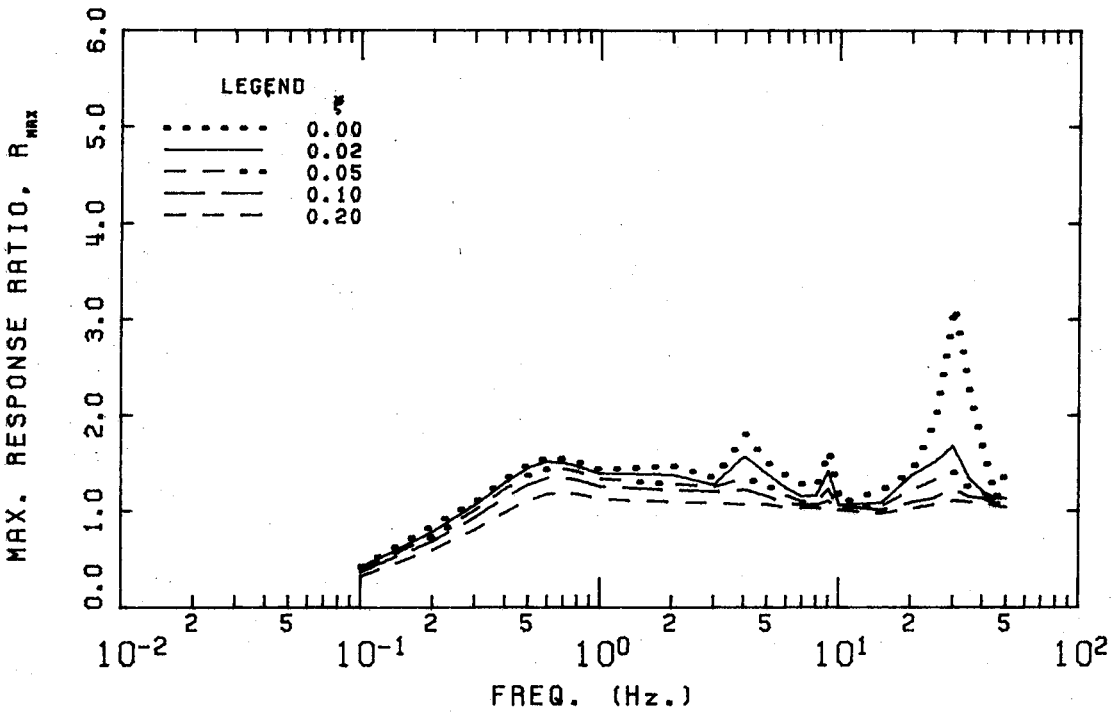

FIGURE B.173 PEMBRIDGE 17 APRIL 1974 23H 10M 19S

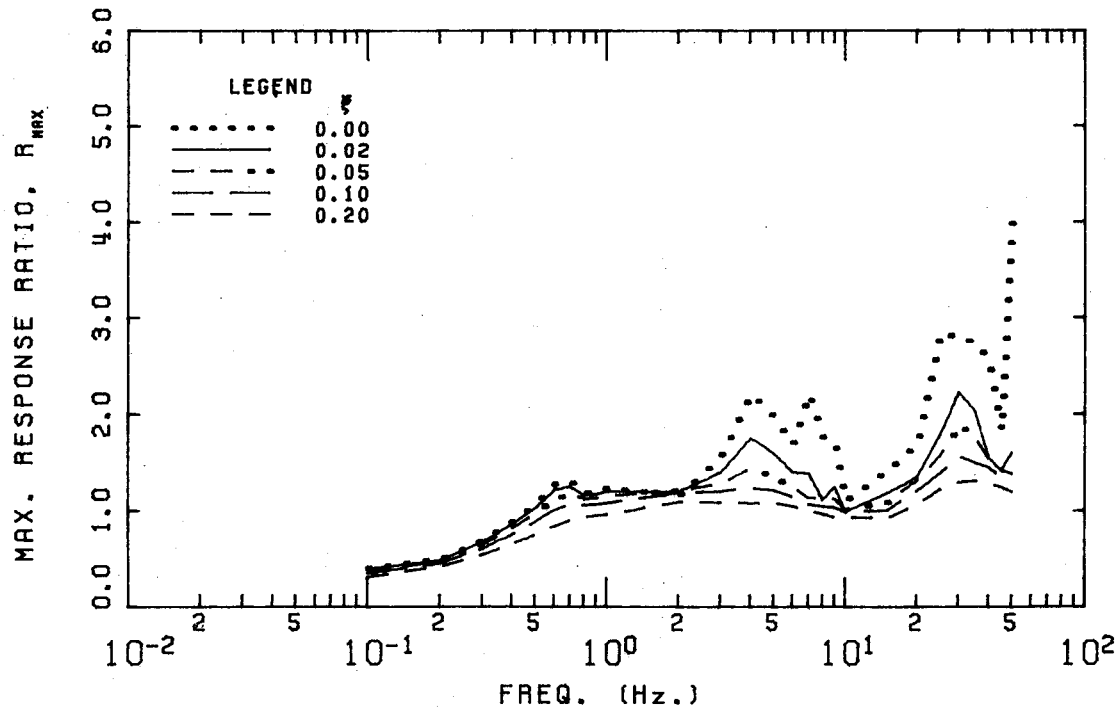

FIGURE B.174 PEMBRIDGE 17 APRIL 1974 23H 10M 29S

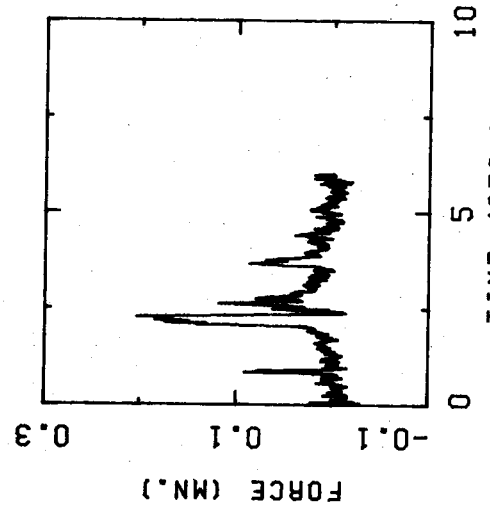

FIGURE B.175 PEMBRIDGE 17 APRIL 1974 23H 10M 39S

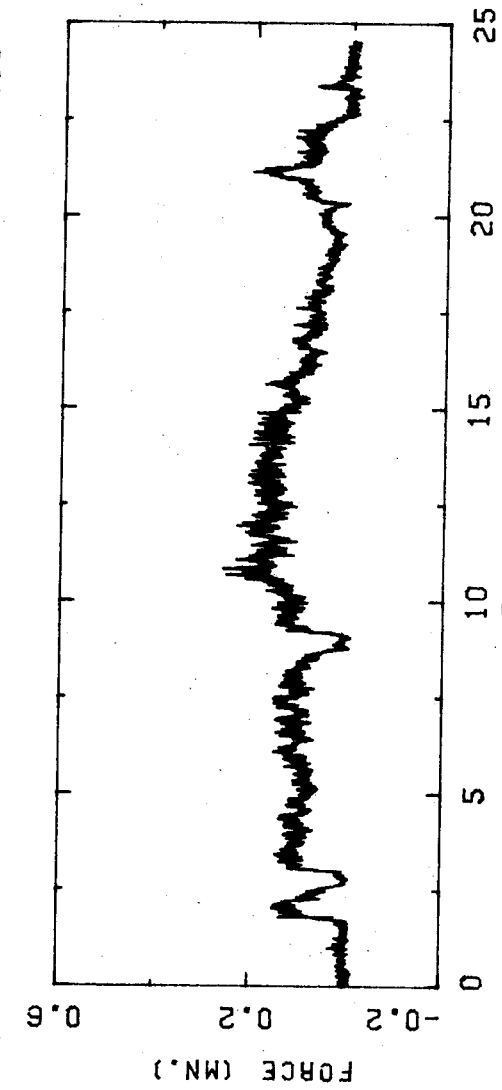

FIGURE B.176 PEMBRIDGE 17 APRIL 1974 23H 11M 36S

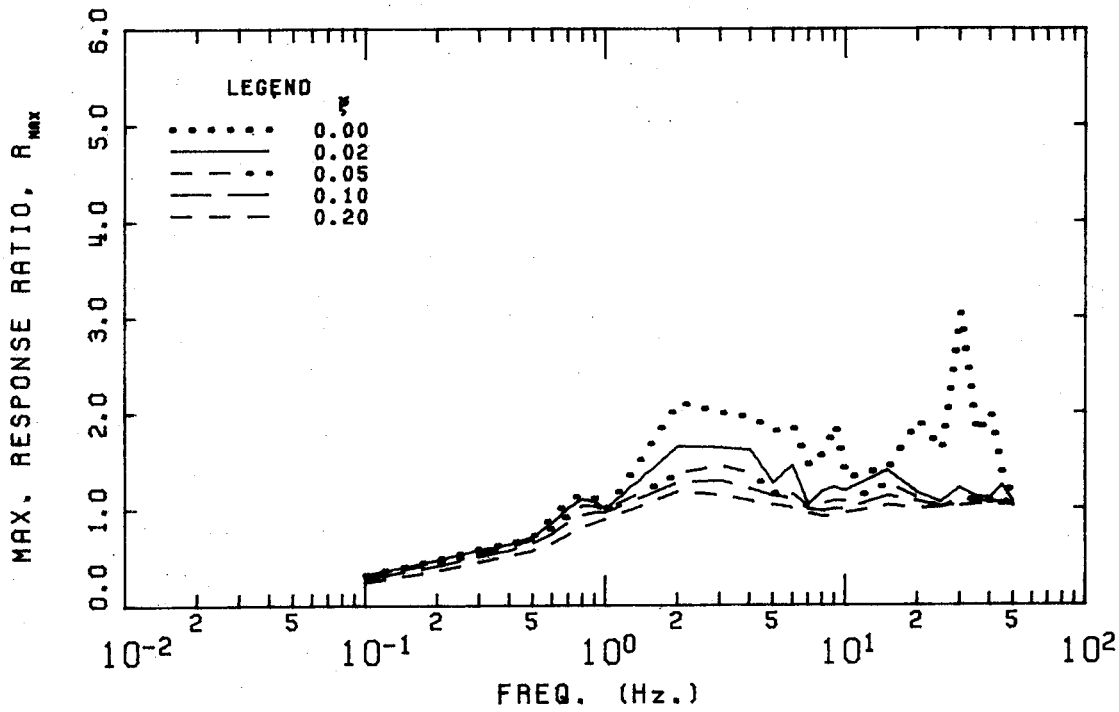

FIGURE B.177 PEMBRIDGE 17 APRIL 1974 23H 10M 39S

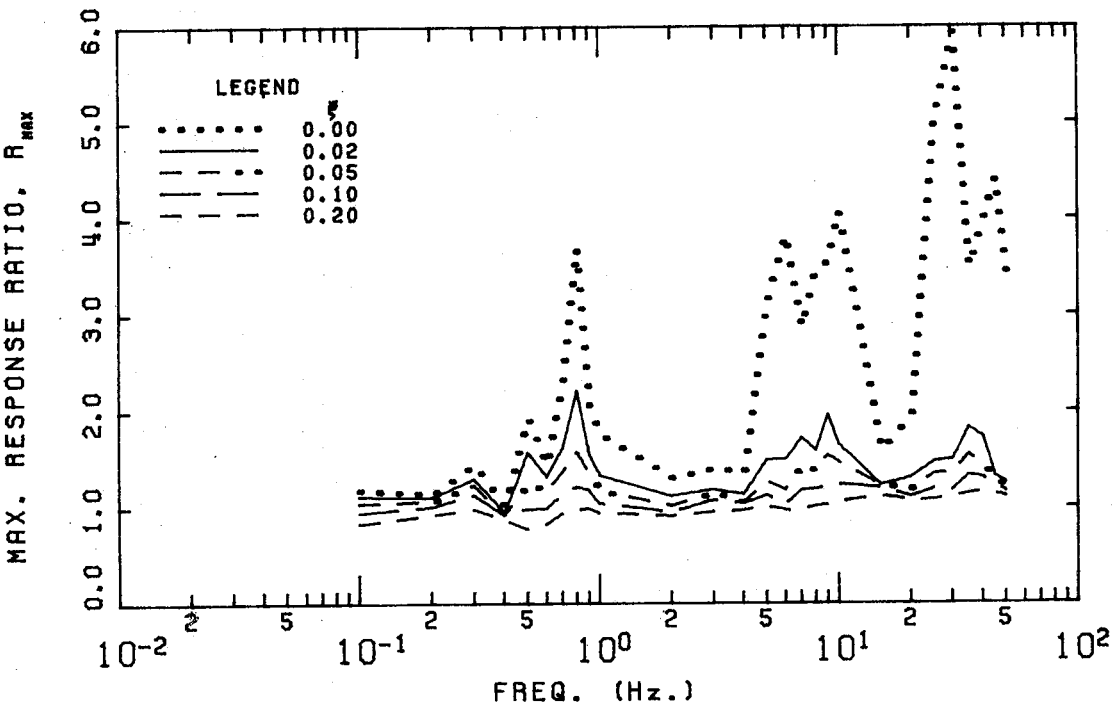

FIGURE B.178 PEMBRIDGE 17 APRIL 1974 23H 11M 36S

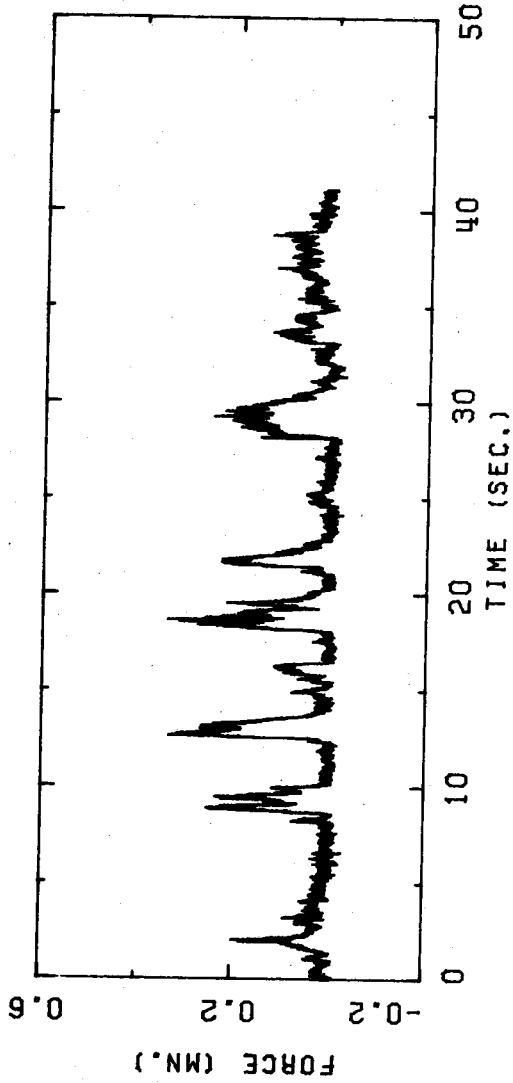

FIGURE B.179 PEMBRIDGE 17 APRIL 1974 23H 12M 01S

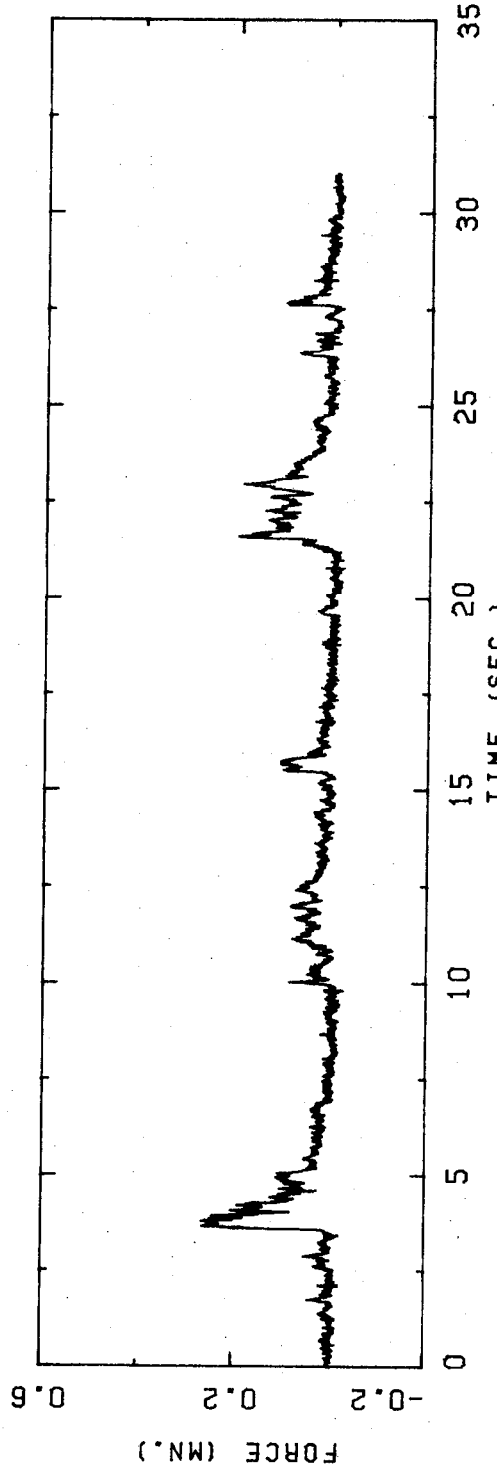

FIGURE B.180 PEMBRIDGE 17 APRIL 1974 23H 13M 54S

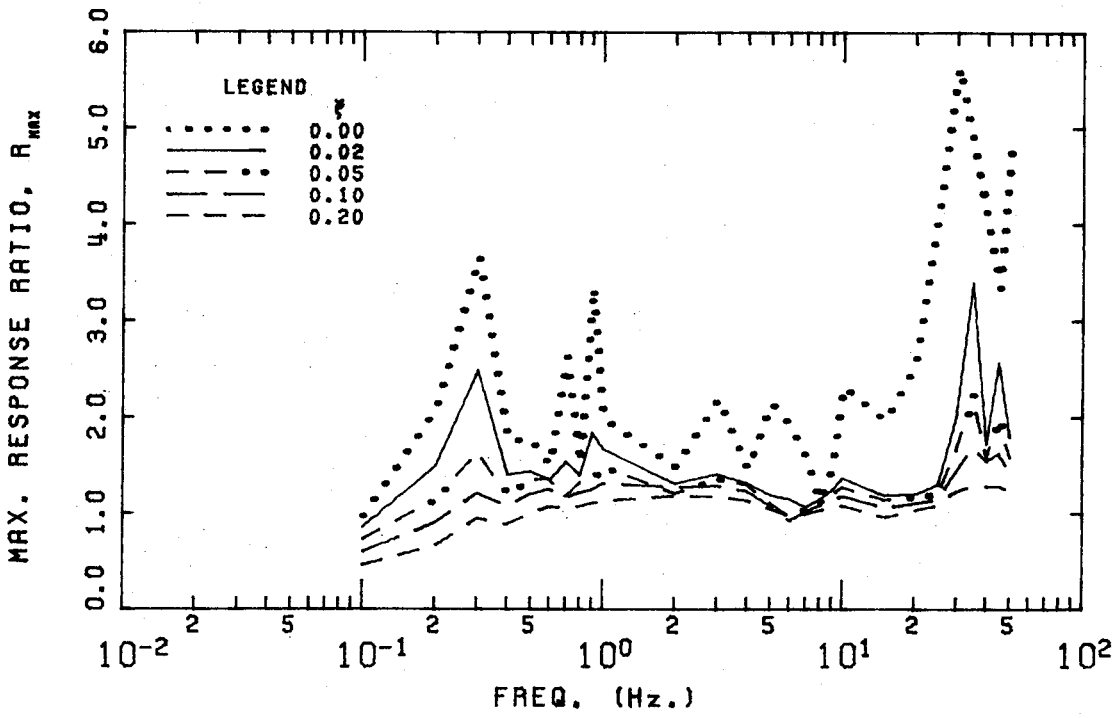

FIGURE B.181 PEMBRIDGE 17 APRIL 1974 23H 12M 01S

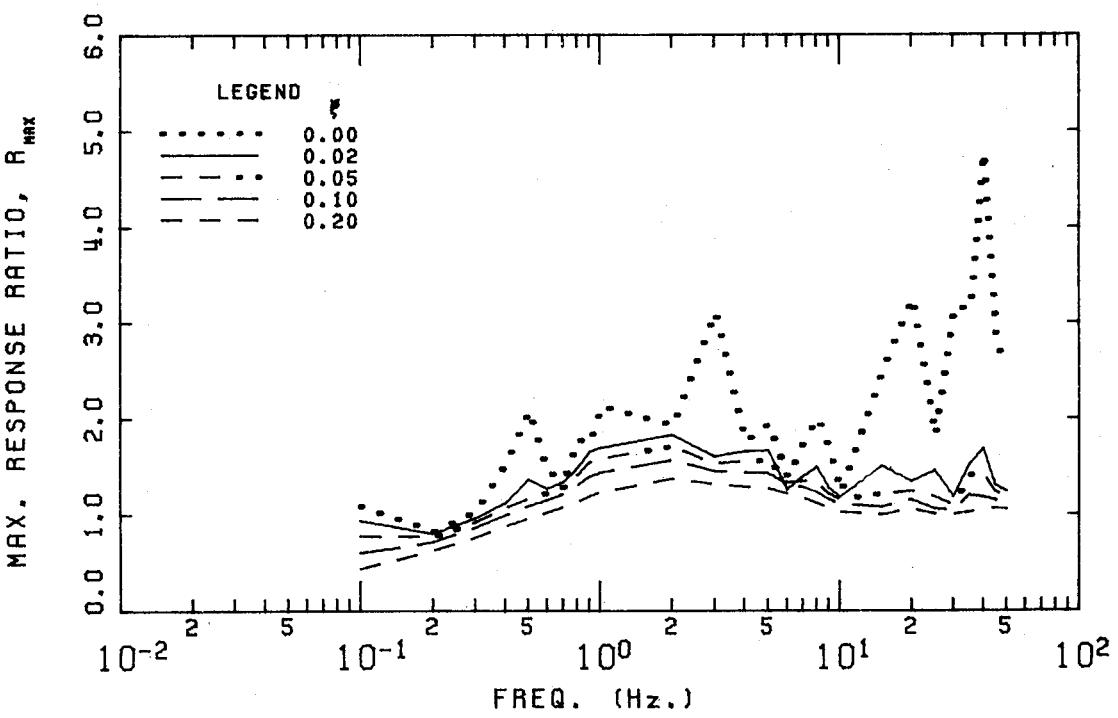

FIGURE B.182 PEMBRIDGE 17 APRIL 1974 23H 13M 54S

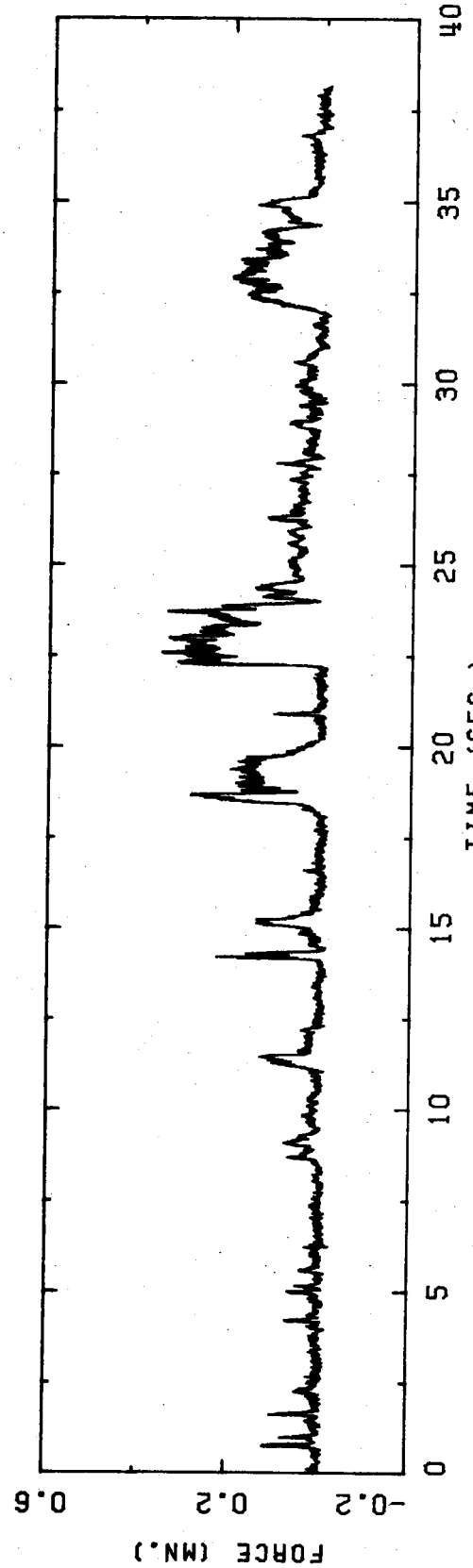

FIGURE B.183 PEMBRIDGE 17 APRIL 1974 23H 14M 24S

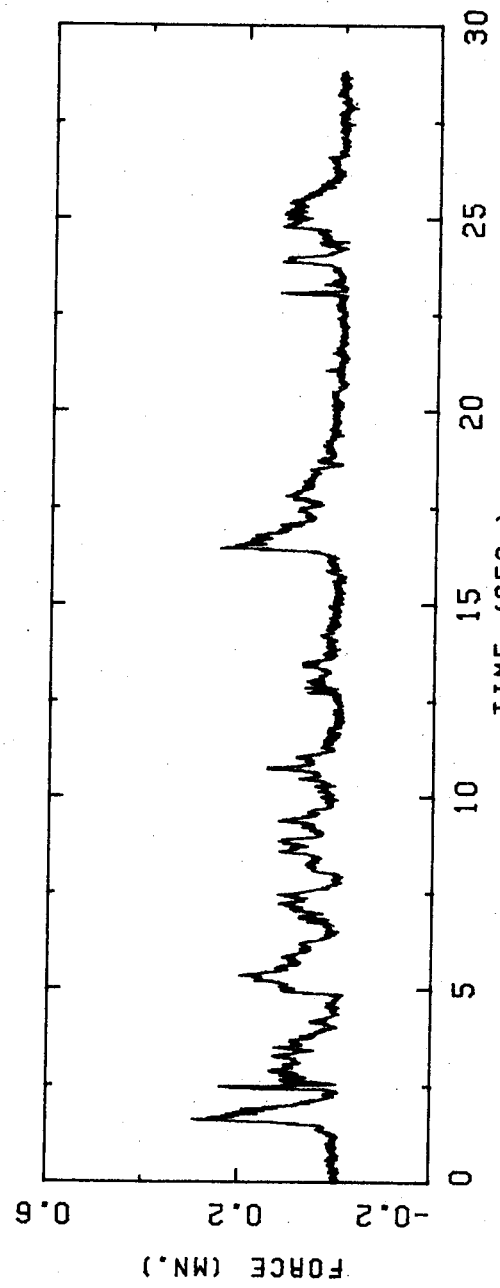

FIGURE B.184 PEMBRIDGE 17 APRIL 1974 23H 14M 46S

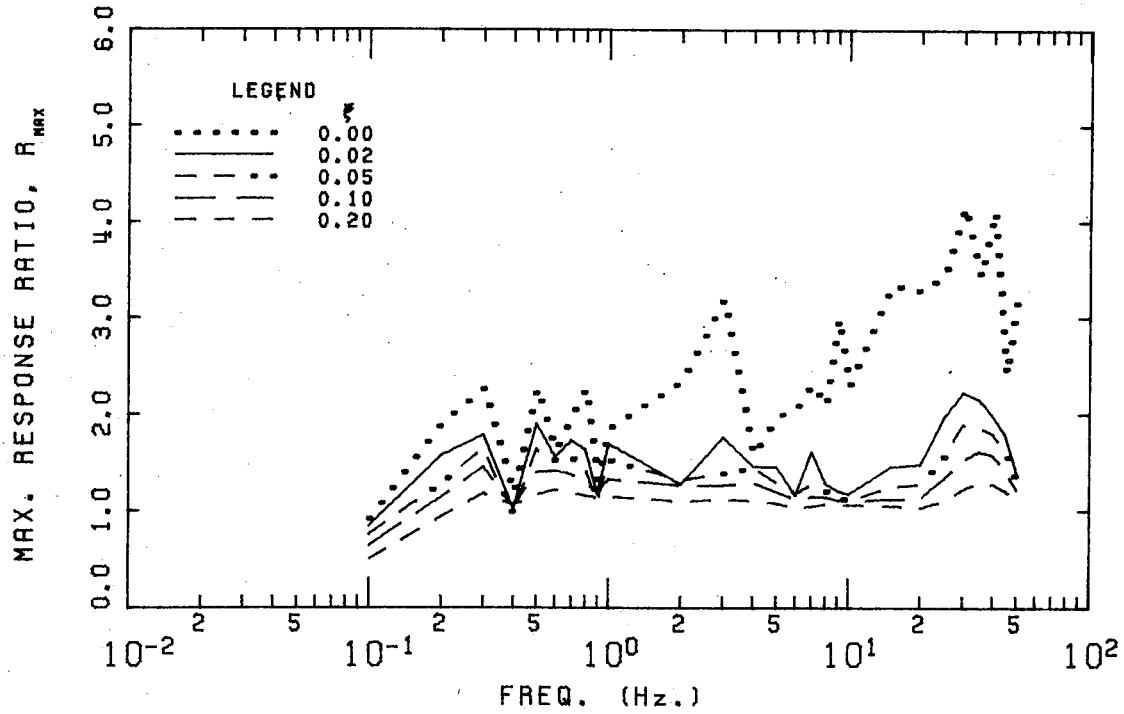

FIGURE B.185 PEMBRIDGE 17 APRIL 1974 23H 14M 24S

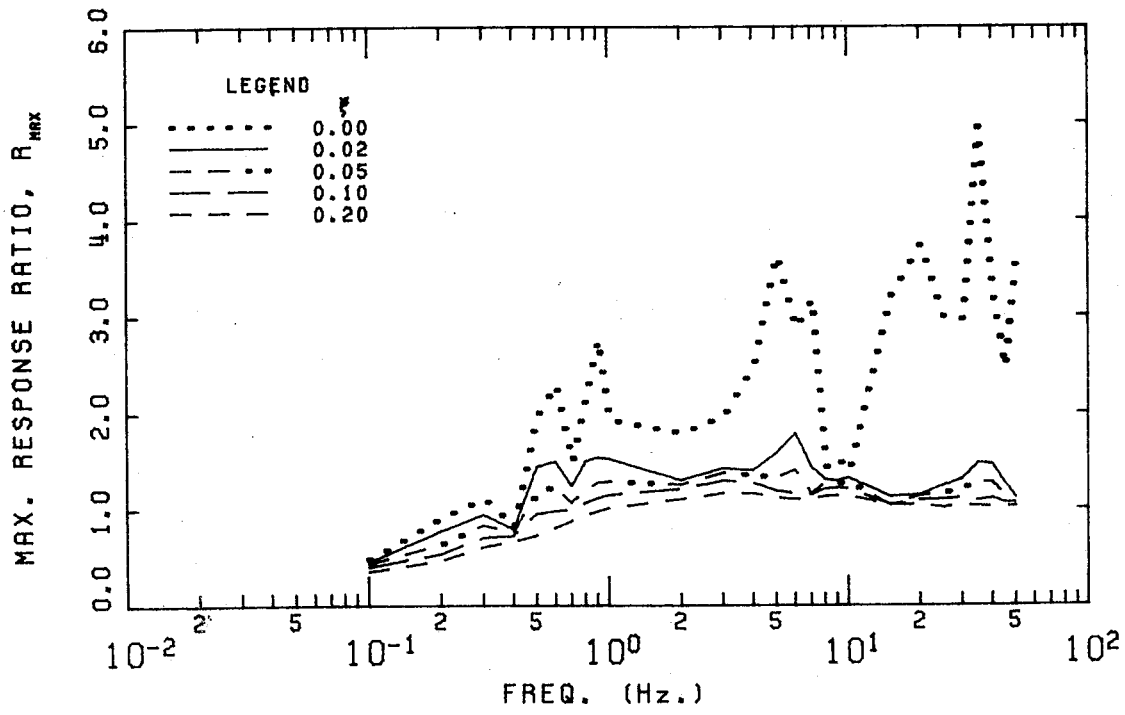

FIGURE B.186 PEMBRIDGE 17 APRIL 1974 23H 14M 46S

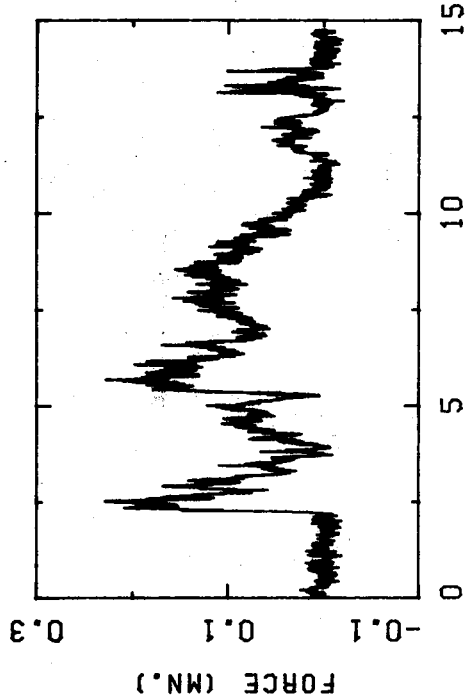

FIGURE B.187 PEMBRIDGE 17 APRIL 1974 23H 17M 34S

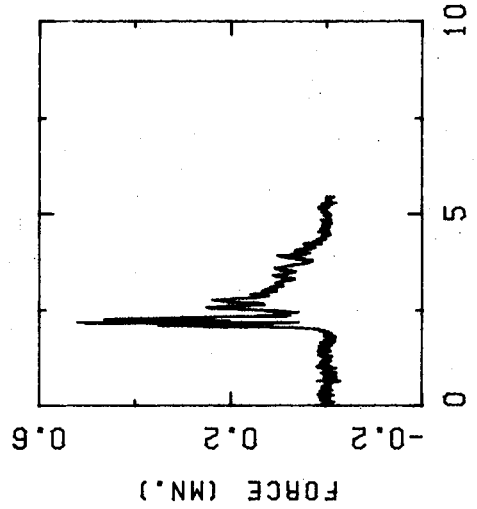

FIGURE B.188 PEMBRIDGE 17 APRIL 1974 23H 17M 50S

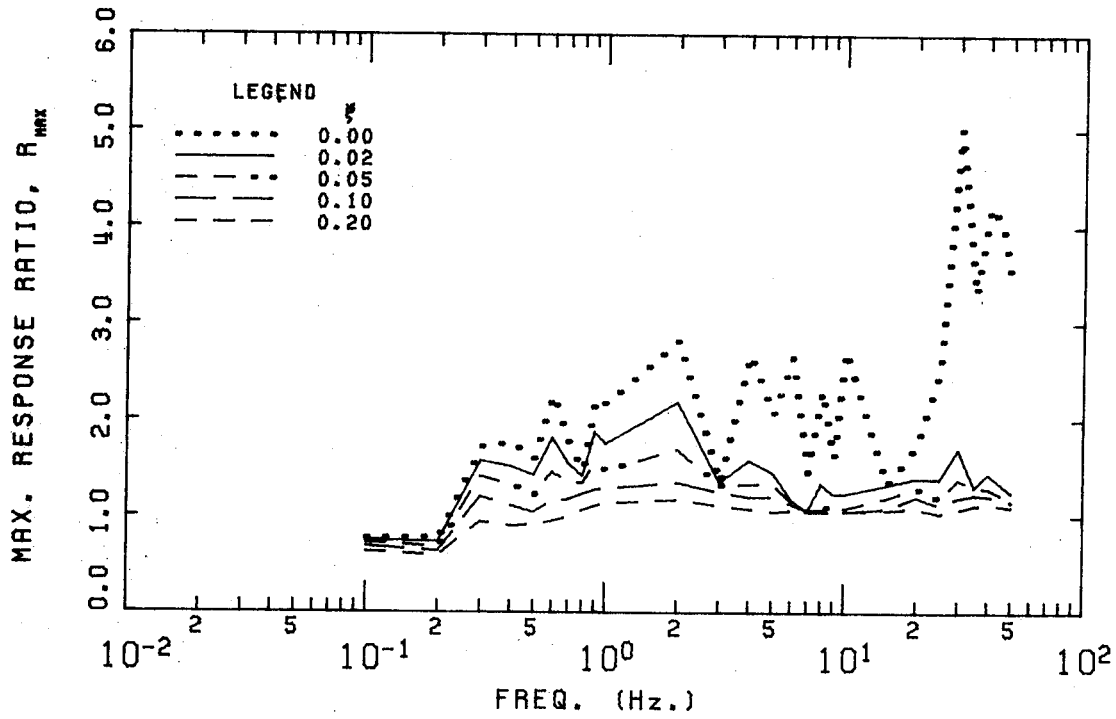

FIGURE B.189 PEMBRIDGE 17 APRIL 1974 23H 17M 34S

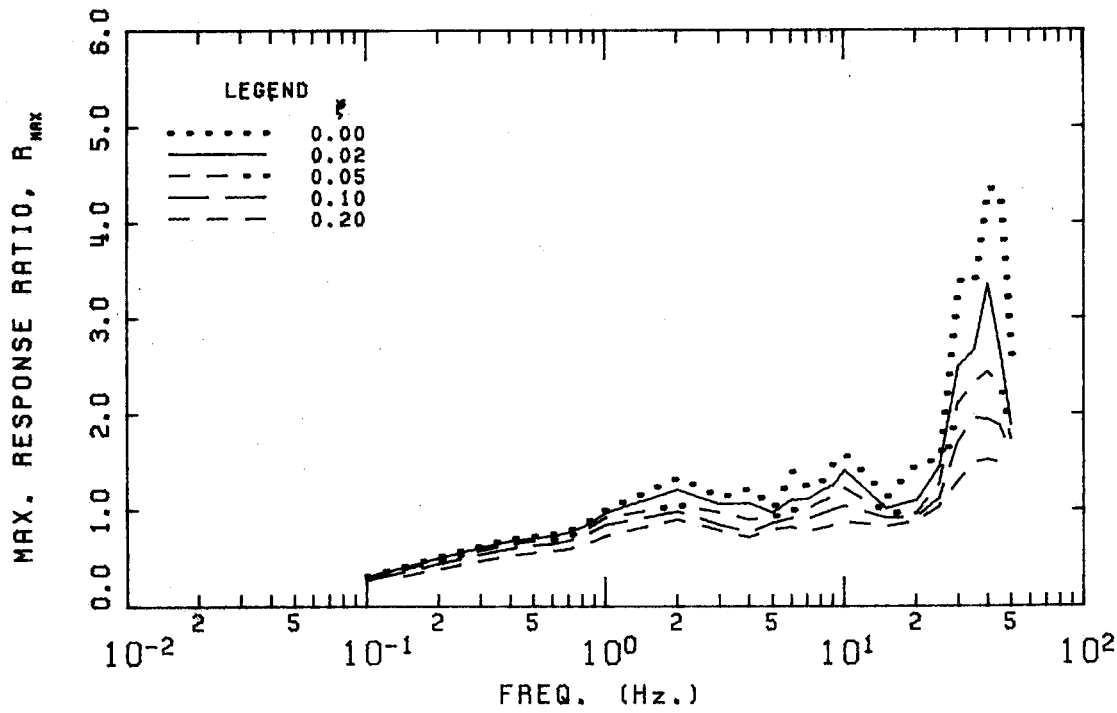

FIGURE B.190 PEMBRIDGE 17 APRIL 1974 23H 17M 50S

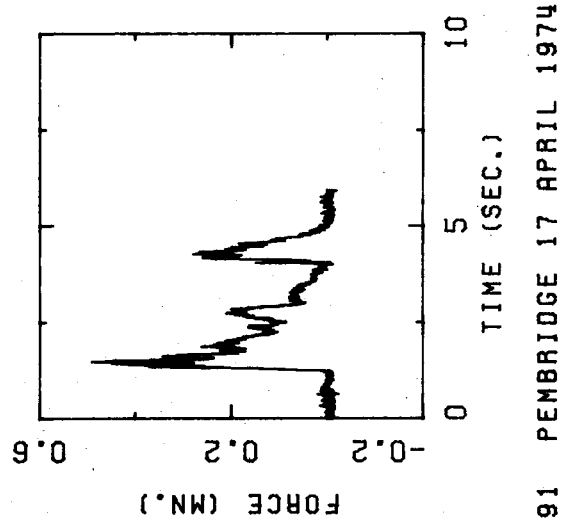

FIGURE B.191 PEMBRIDGE 17 APRIL 1974 23H 18M 04S

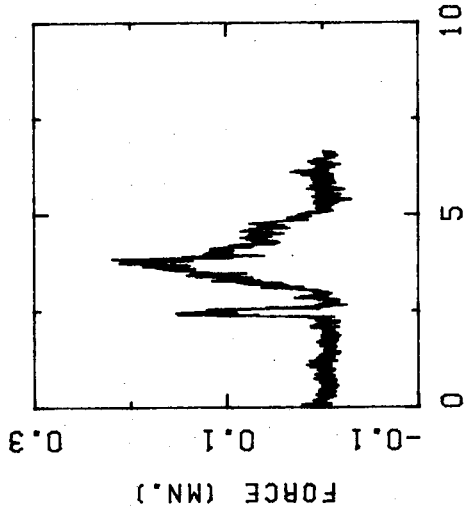

FIGURE B.192 PEMBRIDGE 17 APRIL 1974 23H 18M 12S

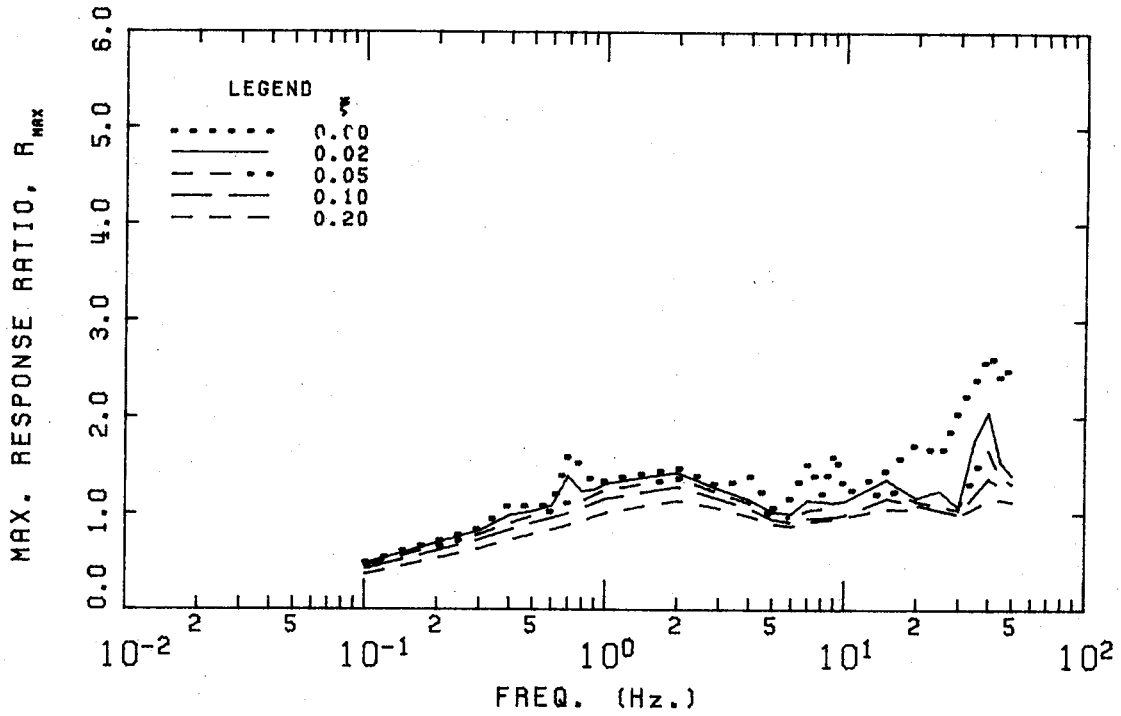

FIGURE B.193 PEMBRIDGE 17 APRIL 1974 23H 18M 04S

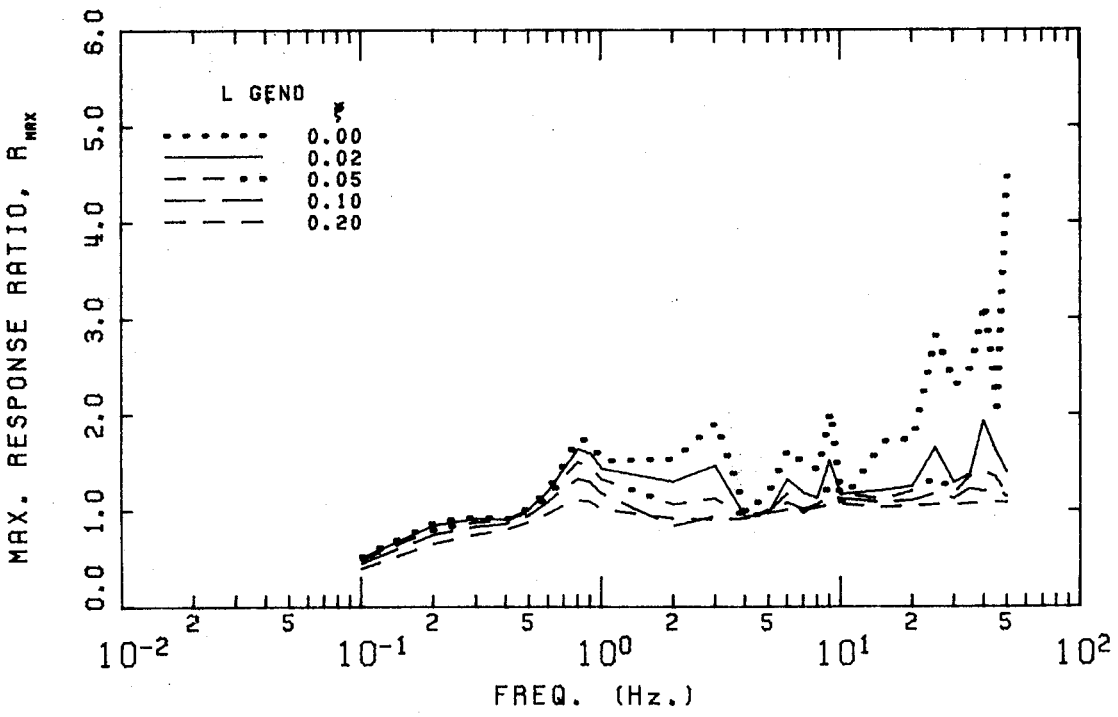

FIGURE B.194 PEMBRIDGE 17 APRIL 1974 23H 18M 12S

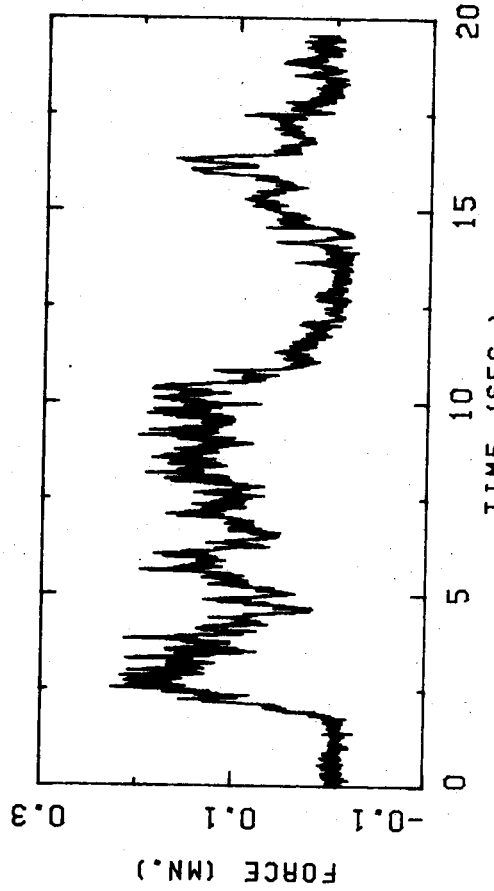

FIGURE B.195 PEMBRIDGE 17 APRIL 1974 23H 54M 48S

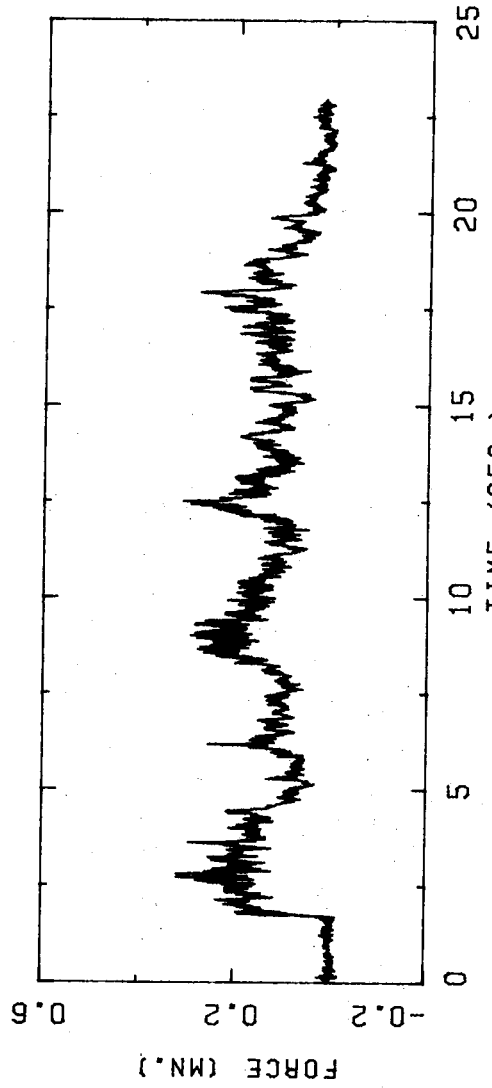

FIGURE B.196 PEMBRIDGE 18 APRIL 1974 00H 00M 11S

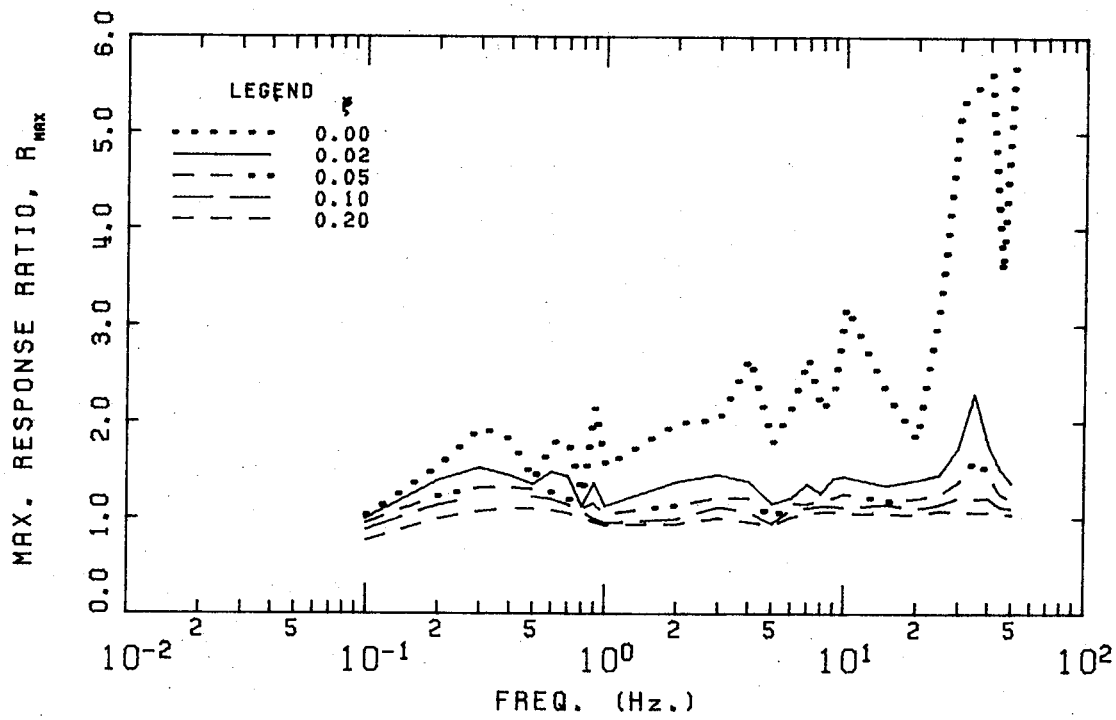

FIGURE B.197 PEMBRIDGE 17 APRIL 1974 23H 54M 48S

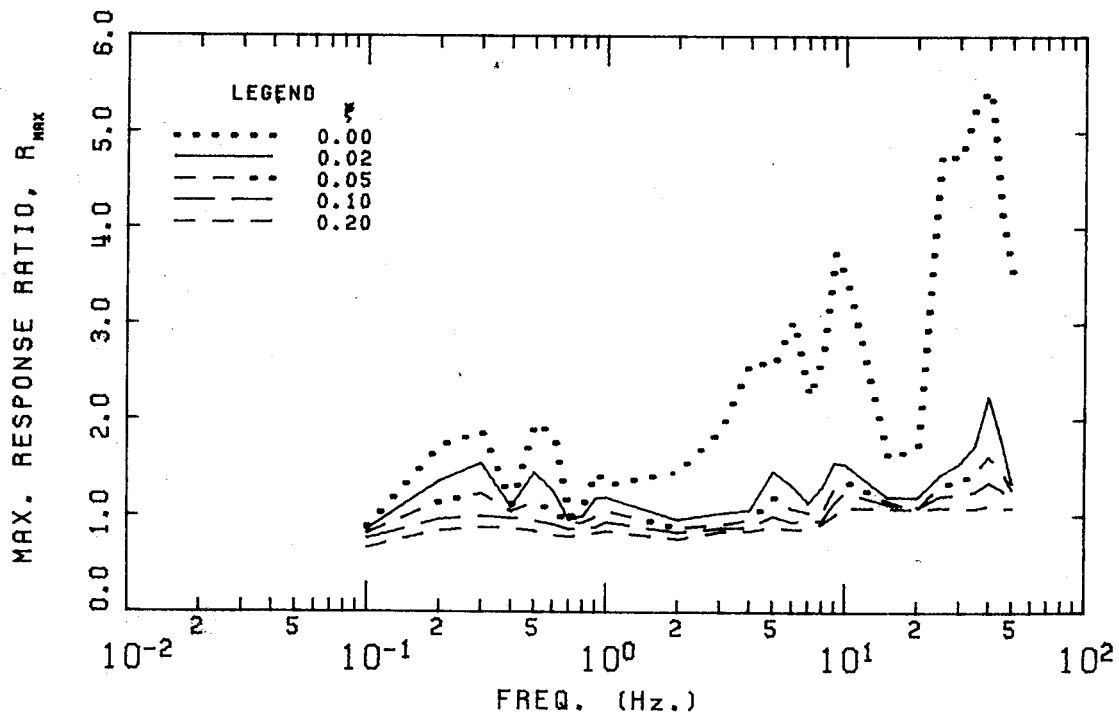

FIGURE B.198 PEMBRIDGE 18 APRIL 1974 00H 00M 11S

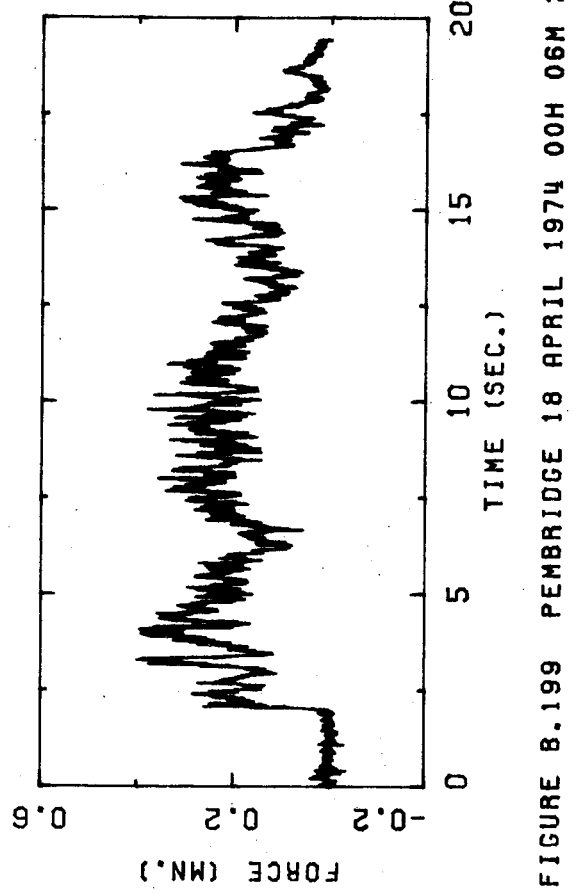

FIGURE B.199 PEMBRIDGE 18 APRIL 1974 00H 06M 29S

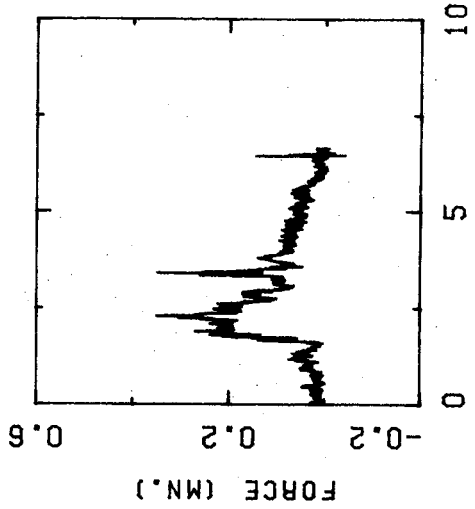

FIGURE B.200 PEMBRIDGE 18 APRIL 1974 00H 06M 47S

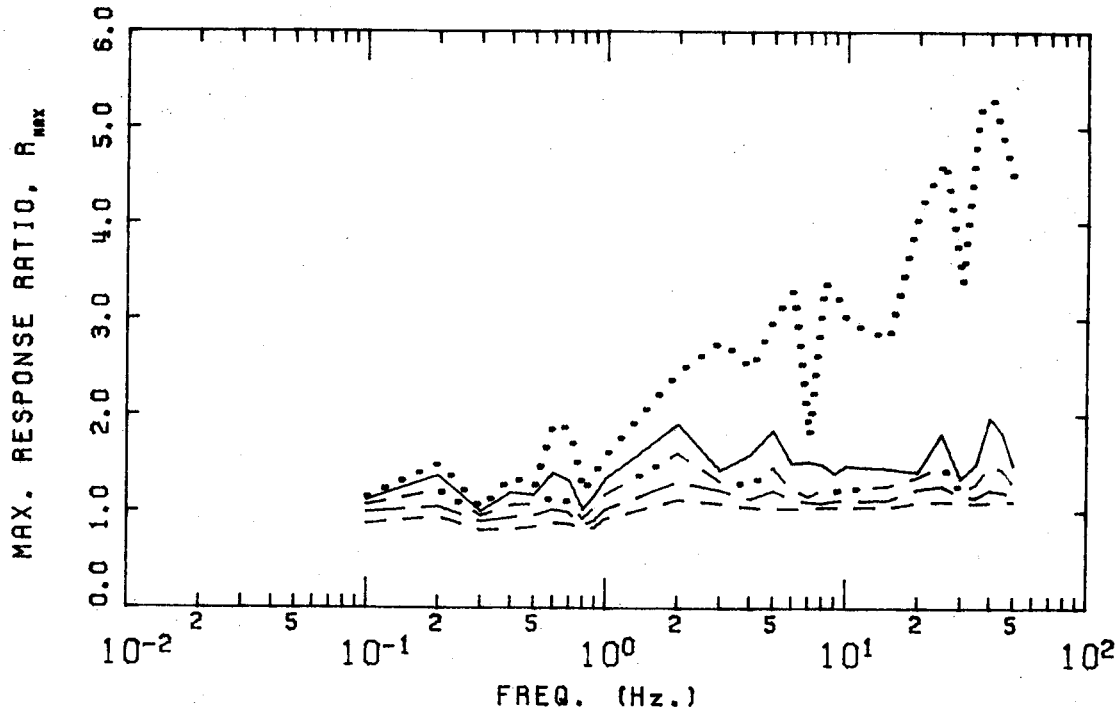

FIGURE B.201 PEMBRIDGE 18 APRIL 1974 00H 06M 29S

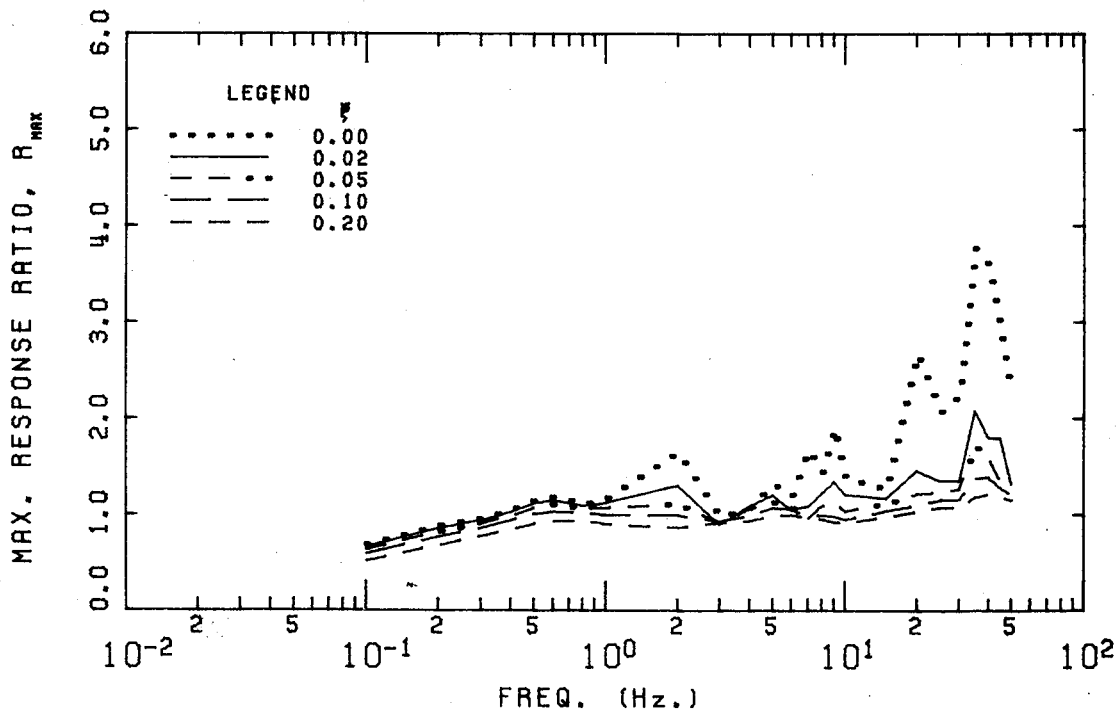

FIGURE B.202 PEMBRIDGE 18 APRIL 1974 00H 06M 47S

RECENT STRUCTURAL ENGINEERING REPORTS

Department of Civil Engineering

University of Alberta

65. *Strength and Behavior of Cold-Formed HSS Columns* by Reidar Bjorhovde, December 1977.

66. *Some Elementary Mechanics of Explosive and Brittle Failure Modes in Prestressed Containments* by D.W. Murray, June 1978.

67. *Inelastic Analysis of Prestressed Concrete Secondary Containments* by D.W. Murray, L. Chitnuyanondh, C. Wong and K.Y. Rijub-Agha, July 1978.

68. *Strength of Variability of Bonded Prestressed Concrete Beams* by D.K. Kikuchi, S.A. Mirza and J.G. MacGregor, August 1978.

69. *Numerical Analysis of General Shells of Revolution Subjected to Arbitrary Loading* by A.M. Shazly, S.H. Simmonds and D.W. Murray, September 1978.

70. *Concrete Masonry Walls* by M. Hatzinikolas, J. Longworth and J. Warwaruk, September 1978.

71. *Experimental Data for Concrete Masonry Walls* by M. Hatzinikolas, J. Longworth and J. Warwaruk, September 1978.

72. *Fatigue Behaviour of Steel Beams with Welded Details* by G.R. Bardell and G.L. Kulak, September 1978.

73. *Double Angle Beam-Column Connections* by R.M. Lasby and Reidar Bjorhovde, April 1979.

74. *An Effective Uniaxial Tensile Stress-Strain Relationship for Prestressed Concrete* by L. Chitnuyanondh, S. Rizkalla, D.W. Murray and J.G. MacGregor, February 1979.

75. *Interaction Diagrams for Reinforced Masonry* by C. Feeg and J. Warwaruk, April 1979.

76. *Effects of Reinforcement Detailing for Concrete Masonry Columns* by C. Feeg, J. Longworth, and J. Warwaruk, May 1979.

77. *Interaction of Concrete Masonry Bearing Walls and Concrete Floor Slabs* by N. Ferguson, J. Longworth and J. Warwaruk, May 1979.

78. *Analysis of Prestressed Concrete Wall Segments* by B.D.P. Koziak and D.W. Murray, June 1979.

79. *Fatigue Strength of Welded Steel Elements* by M.P. Comeau and G.L. Kulak, October 1979.

80. *Leakage Tests of Wall Segments of Reactor Containments* by S.K. Rizkalla, S.H. Simmonds and J.G. MacGregor, October 1979.

81. *Tests of Wall Segments from Reactor Containments* by S.H. Simmonds, S.H. Rizkalla and J.G. MacGregor, October 1979.

82. *Cracking of Reinforced and Prestressed Concrete Wall Segments* by J.G. MacGregor, S.H. Rizkalla and S.H. Simmonds, October 1979.

83. *Inelastic Behavior of Multistory Steel Frames* by M. El Zanaty, D.W. Murray and R. Bjorhovde, April 1980.

84. *Finite Element Programs for Frame Analysis* by M. El Zanaty and D.W. Murray, April 1980.

85. *Test of a Prestressed Concrete Secondary Containment Structure* by J.G. MacGregor, S.H. Simmonds and S.H. Rizkalla, April 1980.

86. *An Inelastic Analysis of the Gentilly-2 Secondary Containment Structure* by D.W. Murray, C. Wong, S.H. Simmonds and J.G. MacGregor, April 1980.

87. *Nonlinear Analysis of Axisymmetric Reinforced Concrete Structures* by A.A. Elwi and D.W. Murray, May 1980.

88. *Behavior of Prestressed Concrete Containment Structures - A Summary of Findings* by J.G. MacGregor, D.W. Murray, S.H. Simmonds, April 1980.

89. *Deflection of Composite Beams at Service Load* by L. Samantaraya and J. Longworth, June 1980.

90. *Analysis and Design of Stub-Girders* by T.J.E. Zimmerman and R. Bjorhovde, August 1980.

91. *An Investigation of Reinforced Concrete Block Masonry Columns* by G.R. Sturgeon, J. Longworth and J. Warwaruk, September 1980.

92. *An Investigation of Concrete Masonry Wall and Concrete Slab Interaction* by R.M. Pacholok, J. Warwaruk, and J. Longworth, October 1980.

93. FEPARCS5 - *A Finite Element Program for the Analysis of Axisymmetric Reinforced Concrete Structures - Users Manual* by A. Elwi and D.W. Murray, November 1980.

94. *Plastic Design of Reinforced Concrete Slabs* by D.M. Rogowsky and S.H. Simmonds, November 1980.

95. *Local Buckling of W Shaped Used as Columns, Beams, and Beam-Columns* by J.L. Dawe and G.L. Kulak, March 1981.

96. *Dynamic Response of Bridge Piers to Ice Forces*, by E.W. Gordon and C.J. Montgomery, May 1981.